Environmentally friendly hybrid coatings for corrosion protection: silane based pre-treatments and nanostructured waterborne coatings

Michele Fedel
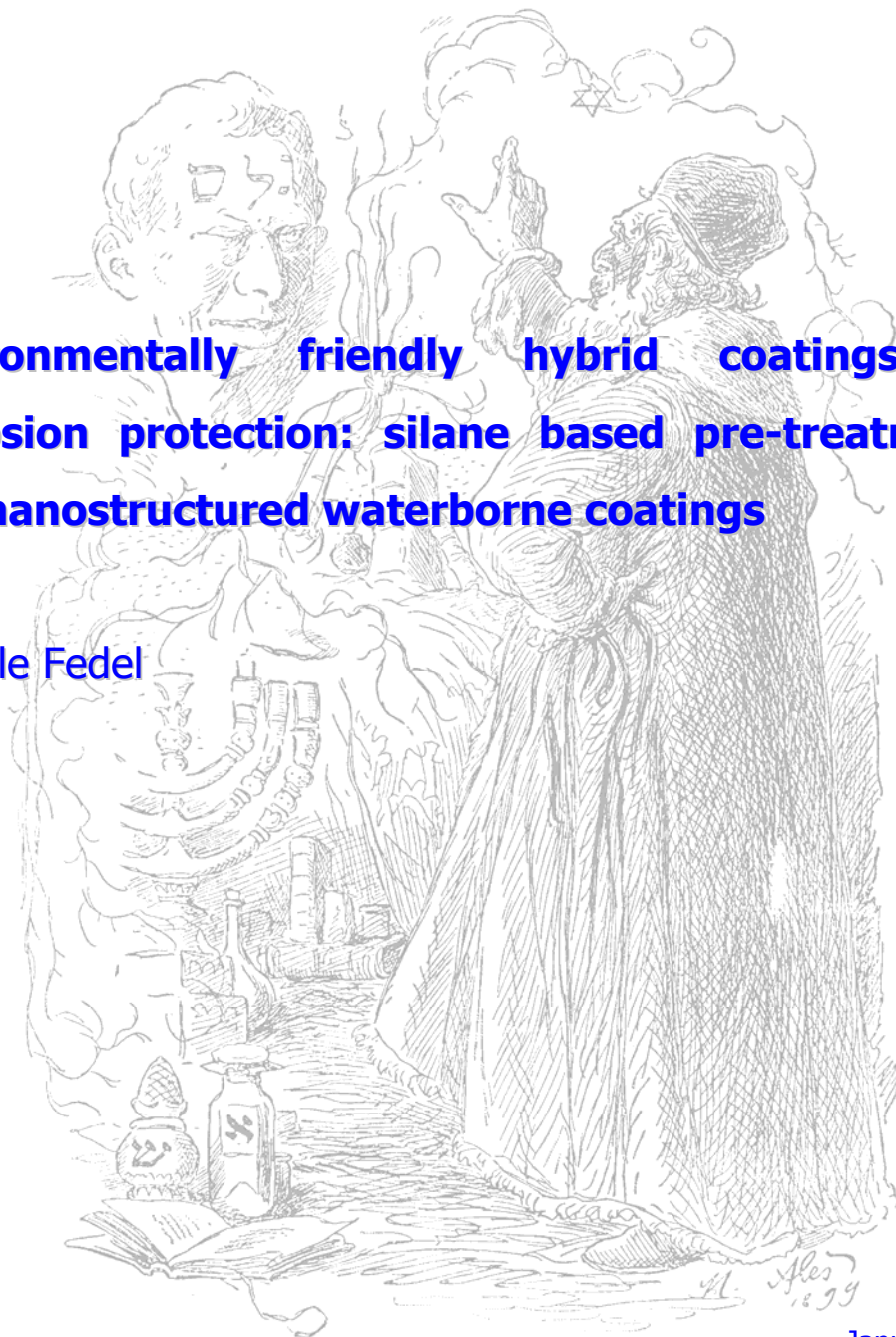
January 2010

"Objectivity cannot be equated with mental blankness; rather, objectivity resides in recognizing your preferences and then subjecting them to especially harsh scrutiny - and also in a willingness to revise or abandon your theories when the tests fail (as they usually do)."

Stephen Jay Gould *"Capturing the Center"* Natural History 107 (1998) 18

Abstract

This thesis considers a nanotechnology approach based on the production of metals pre-treatments and organic coatings (a complete protection system at all) designed from the nanoscale. The final aim is to develop protection systems with improved corrosion protection properties and a low environmental impact. In particular, multifunctional silane hybrid molecules were used to design sol-gel pre-treatments for metals and to modify the inner structure of UV curable waterborne organic coatings. In the first part of this thesis thin (hundreds of nanometers) sol-gel films consisting of an experimental mixture of hybrid silicon alkoxides molecules were applied onto aluminium and hot dip galvanized (HDG) steel for the development of effective and environmentally friendly corrosion protection systems A chemical and electrochemical characterization of the sol-gel films highlighted their good corrosion protection properties both for aluminium and HDG steel. To test the effectiveness of the sol-gel coatings as coupling agent between metallic substrates and organic coatings (paints) both a powder coating paint and a cataphoretic coating paint were applied on the silane pre-treated substrates. The electrochemical measurements and the accelerated tests carried out on these protection systems proved the capability of these sol-gel conversion coatings to improve the corrosion protection properties of the traditional protective cycles. The

performance of the silane pre-treatments was also compared to commonly used surface conversion coatings for metals. The result of this comparison evidenced that the corrosion protection properties ensured by the sol-gel conversion treatment is comparable or higher than most of the commonly used pre-treatments.

A study about the incorporation of inorganic nanoparticles into these sol-gel films gave evidences of an improved corrosion resistance due to the addition of certain amount of montmorillonite nanoparticles in the sol-gel matrix. The same hybrid silicon alkoxide molecules used to perform the pre-treatments were used modify the inner structure of UV curable waterborne coatings in order to improve the corrosion protection properties maintaining the environmental compatibility of the protecting system. The design, application and characterisation of urethane, acrylic and epoxy waterborne UV curing coatings modified with the hybrid silicon molecules in order to obtain nano-structured waterborne films with improved corrosion resistance and thermo-mechanical properties were studied. The characterization proved the great potential of the silicon alkoxide molecules as a tool to modify the properties of the organic matrix of the paint: silicon alkoxides can promote the self assembly of inorganic nanoparticles into the matrix or can act as an effective coupling agent between inorganic nanoparticles and the polymeric matrix. Silicon alkoxide molecules were proved to be an efficient tool to design a protection system from the nanoscale leading to the prospective of an accurate control of the overall properties of the macroscopic systems.

Acknowledgments

Contents

Preface

This work summarizes the experimental research activity performed during my Ph.D. studies in Materials Engineering. Chapter 1 is a bibliographic research work devoted to the analysis of the environmental concerns related to traditional solutions for corrosion protection and to the explanation of some basic theoretical concepts useful to appreciate the experimental sections, Chapters 2 and 3. Chapter 2 is devoted to the analysis of the potential of experimental mixtures of hybrid silicon alkoxides molecules as sol-gel pre-treatments for the development of ecological protection systems. An extension of this work has been published in [a]. Part of the work presented in Chapter 2 was performed in collaboration with the University of Mons (Belgium), and it has been object of publication in [b]. This collaboration led to other publications, which will appear in [c] and [d]. Chapter 3 introduces a contribution to the development of hybrid silane molecules modified UV curable water-borne coatings carried out in collaboration with the Polytechnic of Milan (Italy) and the Polytechnic of Turin (Italy) as a part of a project founded by the Italian Ministry of Research (PRIN 2005 no. 2005099532). An extension of this work has been published in [e] and [f].

[a] F. Deflorian, S. Rossi, <u>M. Fedel</u>, Corrosion Engineering, Science and Technology (2009) In press.

[b] <u>M. Fedel</u>, M. Olivier, M. Poelman, F. Deflorian, S. Rossi, M.-E. Druart, Prog. Org. Coat., 66 (2009) 118

[c] <u>M.Fedel</u>, M.-E. Druart, M. Olivier, M. Poelman, F. Deflorian, S. Rossi, Prog. Org. Coat., Submitted (2009)

[d] F. Deflorian, S. Rossi, <u>M. Fedel</u>, C. Motte, Prog. Org. Coat., Submitted (2009)

[e] F. Deflorian, <u>M. Fedel</u>, A. Di Gianni, R. Bongiovanni, S. Turri, Corrosion Engineering, Science and Technology, 43 (2008) 81

[f] G. Malucelli, A. Di Gianni, F. Deflorian, <u>M. Fedel</u>, R. Bongiovanni, Corros. Sci., 51 (2009) 1762

Introduction

Corrosion protection of metallic manufactures through improved environmentally friendly surface treatment and organic coatings are becoming more and more critical needs. In fact, in the last few years, the restrictions on the use of traditional pre-treatments and organic coating for corrosion protection have been strictly limited due to both human health and environmental concerns. The thresholds values for the dangerous and hazardous substances involved in the production and application of some of the most common pre-treatments and organic coatings of proved corrosion protection efficiency are becoming more and more stringent year by year. The need of alternatives to conventional protection systems promoted a huge number of studies and investigations aiming at the development of innovative and effective solutions with low environmental impact. In this sense, nanotechnology attracted considerable interest. The likelihood to design a protection system from the nanoscale leads to the prospective of an accurate control of the overall macroscopic properties. This potential aroused great interest, especially in the last decades, and lot of work was done to develop commercial available metal pre-treatments and organic coatings based on a nanotechnology approach. In this context, this thesis considers a nanotechnology approach based on the production of metals pre-treatments and

organic coatings (a complete protection system at all) designed from the nanoscale. By means of multifunctional silane hybrid molecules it is possible to design the final properties of pre-treatments and organic coatings.

In particular, the hybrid silicon alkoxides molecules technology was chosen for the development of effective and environmentally friendly protection systems against corrosion. In other words, in this work the potential of hybrid silicon base molecules as multifunctional materials to produce efficient pre-treatments and organic coatings to protect metals against corrosion was investigated. In particular, the development of hybrid silane sol-gel pre-treatments containing nanoparticles and UV cured water-bone coatings conveniently modified with hybrid silicon molecules and nanoparticles will be discussed in this thesis. The hybrid molecules consist of hybrid silicon alkoxides and organically modified hybrid silicon alkoxides molecules while the above mentioned nanoparticles consist of montmorillonite nanoparticles.

The final aim is to develop protection system with improved corrosion protection properties and a low environmental impact. In this framework, this thesis is a contribution to the efforts of other many research groups for the replacement of traditional approaches to corrosion protection by creating new materials and new processing solutions.

1 Preliminary remarks

In this chapter same environmental issues dealing with traditional and innovative solution for metal pre-treatments and corrosion protection by means of organic coatings are discussed. In particular, the most relevant aspects of the application of silanes based sol-gel coating onto metal substrates and the radiation curing of waterborne organic coatings are briefly discussed. To complete the theoretical remarks, the chemistry of the hybrid alkoxysilane molecules as well as the photochemistry of the UV photo-initiators are thoroughly analysed.

1.1 On some environmental concerns about corrosion protection through organic coatings

Commonly, metals surfaces are pre-treated prior the application of an organic coating: thus, the overall properties of the complete protection system improve remarkably [1]. For many decades, chromium conversion treatments involving the use of chromic acid containing Cr^{6+} species have been used for their corrosion protection and adhesion promotion performances [2]. Their success

was due to the formation of a few decades of nanometers of complex mixture of chromium compounds as a consequence of Cr^{6+} reduction, to the reduction of either water, hydrogen ion or dissolved oxygen to form hydroxyl ions at the metal surface and to the presence of oxidising Cr^{6+} species, responsible of the self-healing potential in presence of defects [3]. Moreover, the chromate conversion coatings promote a very good initial adhesion with paint, lacquer, and organic finishes [4]. However, in the early nineties, the restrictions on the use of Cr^{6+} based conversion treatments became more and more stringent owing to the health and environmental issues related to the use of these kinds of metal finishing [5]. In fact, it was proved that hexavalent chromium can cause lung cancer in humans as a result of inhalation exposure in certain occupational settings. Hexavalent chromium was recognised as a known carcinogen by the World Health Organisation (WHO) and by the U.S. Environmental Protection Agency (EPA) but it is also toxic and it can lead to allergic contact dermatitis as a result of direct skin exposure to powders or liquids containing hexavalent chromium [6,7]. In addition, Cr^{6+} has a high oxidizing potential and, thus, it is also dangerous for the environment. Aiming at the replacement of chromate conversion treatment in the metal finishing industry, in the last two decades several different "environmental friendly" pre-treatments were studied. Among them, a lot of studies deal with:

✓ Pre-treatments with protecting mechanism similar to Cr^{6+}, acting as passivating agents, such as molybdates, permanganates, vanadates, and tungstates [8,9];

✓ Rare earth based conversion treatment, mainly based on cerium and lanthanium salts [10-12];

✓ Cr^{3+} conversion layers which do not contain oxidising Cr^{6+} species, responsible of the self-healing of flaws [13];

✓ Fluo-titanate and fluo-zirconate conversion treatment, obtained using acidic compounds of titanium and zirconium oxides [14];

✓ Phosphate conversion treatment which lead to the formation of phosphate compound on metals surface [15,16];

✓ Metal alkoxides and/or organically modified metal alkoxides, applied onto the metal substrates via sol-gel route [17,18];

In this panorama, in the last few decades, thin sol-gel films from hybrid silicon alkoxides precursors are of growing interest as efficient pre-treatments to promote the adhesion between organic coatings and metal surfaces addressing the environmental issues [19]. In particular, in the very last few years, the development of water based silicon alkoxides sol-gel pre-treatments promoted a great diffusion of these conversion layers as a "green" technology [20].

As far as the organic coating itself is concerned, volatile organic compounds (VOCs) are among the most common pollutants emitted by paints industries dealing with processing of chemicals such as solvents, thinners, degreasers and

cleaners [21]. In the past, solvent-borne organic coatings were the most widespread sort of painting system. Due to their volatility, compounds coming from the solvent used in paints, varnishes and vehicle refinishing are emitted directly into the atmosphere, after having undergone physical or chemical transformation [22]. The presence of organic compounds deriving from organic solvents lead to the formation of ozone in the troposphere as a consequence of the photochemical reactions of VOCs with atmospheric nitrogen oxides (NO_x) [21]. This concern with regard to tropospheric ozone pollution has given rise to a number of initiatives to reduce emissions of the precursors which lead to ozone formation [23]. In 1999, the Gothenburg Protocol set new restrictive emission thresholds (to be reached, at least, in 2010) for abating acidification, eutrophication and ground-level ozone, for four types of pollutants, including VOCs. It is expected that 2010 will see further changes of VOCs limits concerning organic coatings [24]. In addition, VOCs have been perceived as a contributor to global warming [25]. These drawbacks of using solvent-borne organic coatings led to an increasing interest, over the recent years, in research and development activities towards reducing the VOCs within the legal ceilings in a way that is both technically feasible and economically viable [26] without losing the corrosion protection properties of solvent-borne coatings. A few different solutions were proposed:

✓ High solid coatings (solvent about 20% by volume), obtained lowering the molecular weight of resins and simultaneously increasing their

molecular branching [27]: highly branched structure in the polymer backbone are obtained using multifunctional monomers or building blocks [28];

✓ Powder coating, consisting in the sintering of powders of the organic coating to apply on the substrate (no solvent is present) containing binder, hardener pigments and additives: melting, flow, gel point and cure completion are the different phases in film formation of powder coatings [29,30];

✓ Water-borne coatings, consisting of aqueous compositions with only a small amount of organic solvent (water reducible coatings) or no organic solvent at all (water soluble polymers and latexes), where water is the only solvent present [31,32];

Despite the difficulties related to the formulation, the needs of specific additives, the critical control of wetting properties and the complexity of the thermodynamic concerns [33,34], water-borne coating are a very promising solution for the replacement of solvent-borne coatings. Moreover, the environmental impact of waterborne coatings can be even improved combining the potential of water based coating technology with the UV curing process. UV irradiation curing have a lot of advantages over traditional thermal curing, such as rapid polymerization, high efficiency, very low energy, consumption [35] in addition to low temperature operation, application versatility, good viscosity control, high cross-linking density and, consequently, superior mechanical and

thermal properties [36]. It was proved that, compared to conventional curing methods, UV curing processes use only 5-50% of energy [37]. Thus, concerning the environmental impact of UV curing process, this technology has a relevant impact in the lowering of the energy consumption for the curing of an organic coating.

In the previously discussed overture on the new environmental friendly solution for metals pre-treatment and protection through organic coatings, two innovative solutions were highlighted: silicon alkoxides sol-gel pre-treatments and UV curable waterborne coatings.

The corrosion protection properties of these low environmental impact very promising materials can be further increased conveniently modifying their structure by using hybrid silane molecules and nanoparticles, or, more in general, by applying the chemical nanotechnology to design coatings with special corrosion protection related properties. An improvement in corrosion protection properties can lead to both ecological and economical beneficial effects, related to the higher service life and the lower material consumption to ensure a sufficient protection level.

Nanotechnology is likely to be the answer to the need of efficient and definitive solution for the development of new effective environmental friendly protection systems, as stated a few years ago by D. R. Baer et al. [38]:

> *"Coatings and coating processes will play a major role in the future of nanotechnology regardless of the directions in which*

they will be taken. Because nanostructured materials, in whatever form they are produced, will be incorporated into larger mesoscopic and macroscopic systems, coating processes will play a critical role in the success of nanotechnology in many different applications."

1.2 Hybrid silane sol-gel coatings

In the last two decades, the potential of organofunctional silane molecules for the replacement of chrome conversion treatments has been the topic of a huge number of studies [39-46]. Silanes have been widely studied as coupling agents between inorganic and organic materials since the first works of E. P. Pueddlemann [47]. Concerning corrosion science, a lot of efforts have been made to apply these materials as adhesion promoters between metallic substrates and the organic coatings used for protection against corrosion phenomena [48-50]. The chemistry of silanes and the mechanism of interaction of these molecules with a metallic substrate and an organic coating have been widely explained and are reported elsewhere in literature [51-53]. Silanes molecules are applied onto metal surfaces by means of the sol-gel process. The deposition of hybrid silane sol-gel coatings generally occurs in four stages [54]:

1. Hydrolysis of the silicon alkoxides molecules;

2. Condensation reactions and polymerization of monomers to form chains and particles;

3. Growth of the particles (or chains);

4. Agglomeration of the polymer structures followed by the formation of a network;

The hydrolysis occurs in presence of water. Alkoxy-silanes molecules generate Si-OH groups from Si-OR groups (where R is an organic group) following approximately the steps schematically reported in Figure 1.1 [55]. Notice that alcohols are by-products produced by the hydrolysis reaction. Without going into details, it is worthy to highlight that hydrolysis reactions are affected by a huge number of parameters, such as temperature, pH, nature of the alkoxides, age of the solution, etc. [38-43,56] that can affect and modify the reaction kinetics.
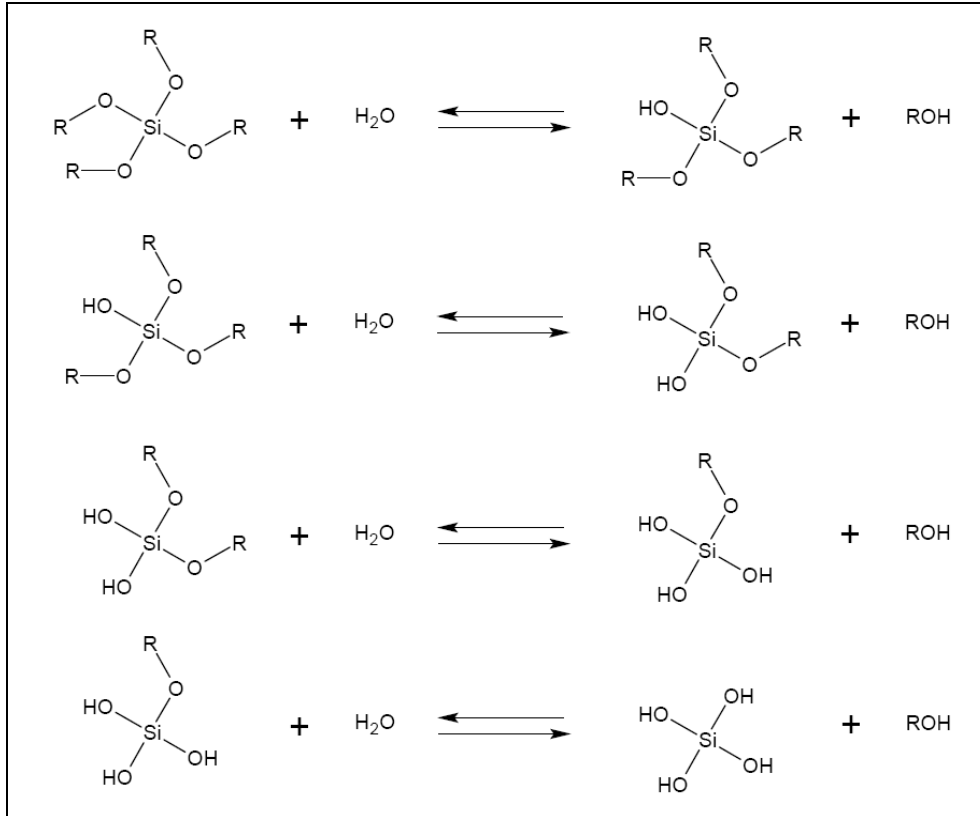
Figure 1.1 Hydrolysis reactions for a silicon tetralkoxide: different steps

As far as the application of silane sol-gel films onto metal is concerned, the hydrolysis of the alkoxy-silanes has a dramatic effect on the final properties of the sol-gel film. In fact, it is necessary to have sufficient number of silanol (Si-OH) groups to interact with the metal substrate [49], because only the hydrolyzed species can lead to the formation of strong covalent bonds with the metal substrate. After the hydrolysis, the condensation reactions among the different silanol groups takes place [57]. Usually, silanes molecules are applied

onto the substrate via dipping or spraying of the hydrolyzed silane solution [58]. In this way, the silane solution of hydrolysed molecules is in contact with the hydroxyl groups in equilibrium with the oxide on the metal surface. Thus, the silanol groups can interact, not only among themselves, but also with the hydroxyl groups in equilibrium on metal substrate. This is a critical point for the deposition of silane sol-gel films. The metal surface has to be rich in hydroxyl groups to permit the adsorption of the silanols to occur, according to the mechanism depicted in Figure 1.2 [59-61].
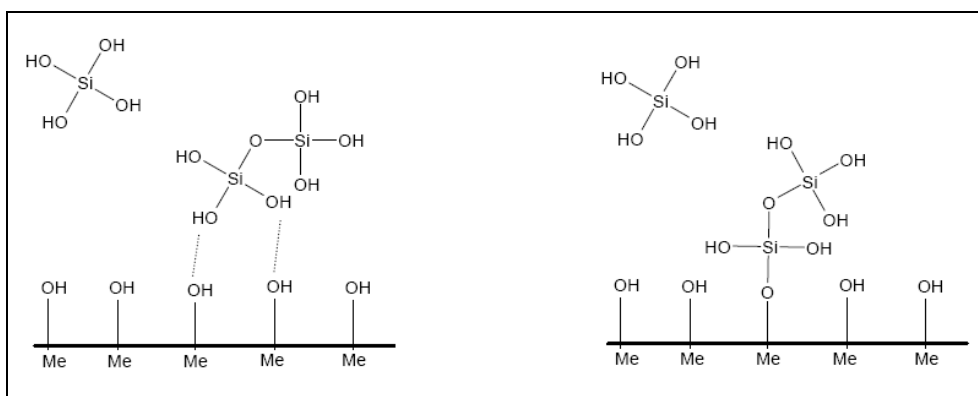
Figure 1.2 Schematic representation of hydrolysis (on the left) and condensation (on the right) reactions onto metal surface.

Considering the interaction between silane molecules and metal hydroxides, first of all, the formation of weak hydrogen bonds between the hydroxyl groups in equilibrium on metal surface and silanol groups takes place (Figure 1.2, on the left). Upon drying, condensation reactions occur between the Si-OH groups of the silanol and the M-OH hydroxides of the metal, leading to the formation

of covalent metal-siloxane bonds (M-O-Si), according to the mechanism depicted in Figure 1.2 on the right and the following reaction (silanization reaction) [62].

$$Si - OH_{(solution)} + M - OH_{(surface)} \rightleftharpoons Si - O - M_{(interface)} + H_2O$$
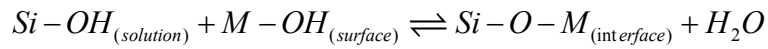
If the rate of hydrolysis is sufficiently high compared to the condensation between silanols groups, many Si-O-M bonds can be formed between small-sized silanols and the metal. On the other hand, if the rate of hydrolysis is relatively low compared to the condensation between silanols groups, few Si-O-M bonds are formed between large-sized hindered silanols and the substrate [57,63].

In fact, the silanization reaction occurs in competition with the condensation reaction of the silanol groups which interact among themselves, according to:

$$Si - OH_{(solution)} + Si - OH_{(solution)} \rightleftharpoons Si - O - Si_{(solution\_or\_film)} + H_2O$$
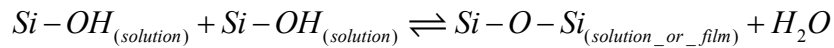
As a result of the hydrolysis and, consequently, the condensation reactions of the alkoxy groups linked to the silicon atom, a sol-gel film is formed [64]. The structure of the film is strongly related to the chemistry of the silane molecules involved, the deposition condition and the properties of the silane diluted solution.

However, the final structure can be schematically represented as depicted in Figure 1.3, where *M* represents the metal substrate.
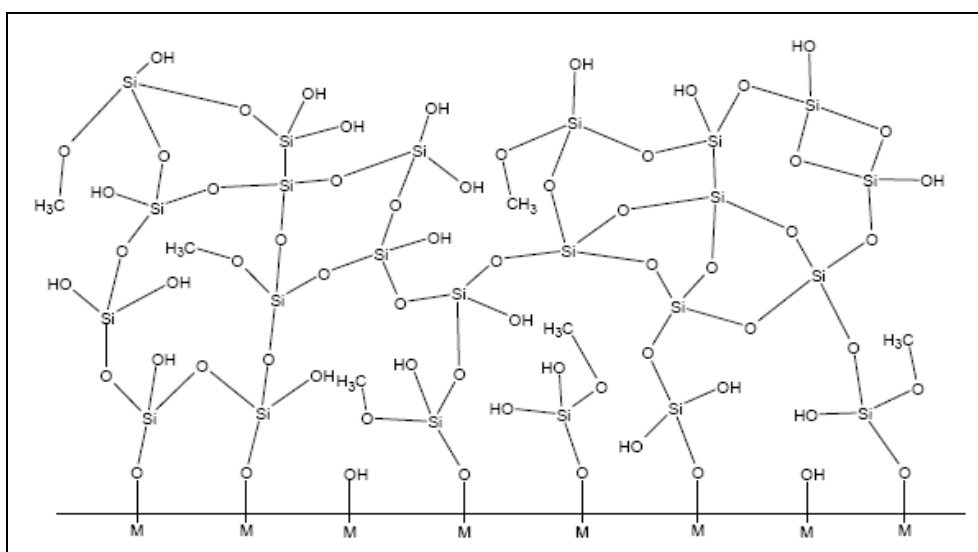
Figure 1.3 Two-dimension schematic representation of the structure of a silane sol-gel film bonded onto a metal (*M*) substrate

Considering Figure 1.3, notice that the number of hydroxyls groups depends on the curing process: higher the temperature and/or longer the heat treatment, lower the number of uncondensed Si-OH bonds.

As far as organofunctional alkoxy-silanes are concerned, the mechanism of film formation is very similar. Organofunctional alkoxy-silanes are hybrid molecules containing one or more non-hydrolysable substituent linked to the silicon atom. The structure of this kind of molecules is approximately:

$$(R-O)_{4-n} SiR_n^*$$
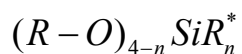
where $4 - n$ alkoxy groups (R-O) and n non hydrolysable substituent (R*) are present [65]. The R* group is carbon chain containing a functional group (amino, urethanic, epoxy, etc.). The silicon/carbon bond is not hydrolysable [66], and, therefore, it is stable in water at room temperature. Figure 1.4 shows, for example, the corresponding hydrolysis reaction for a trialkoxy-silane molecule.
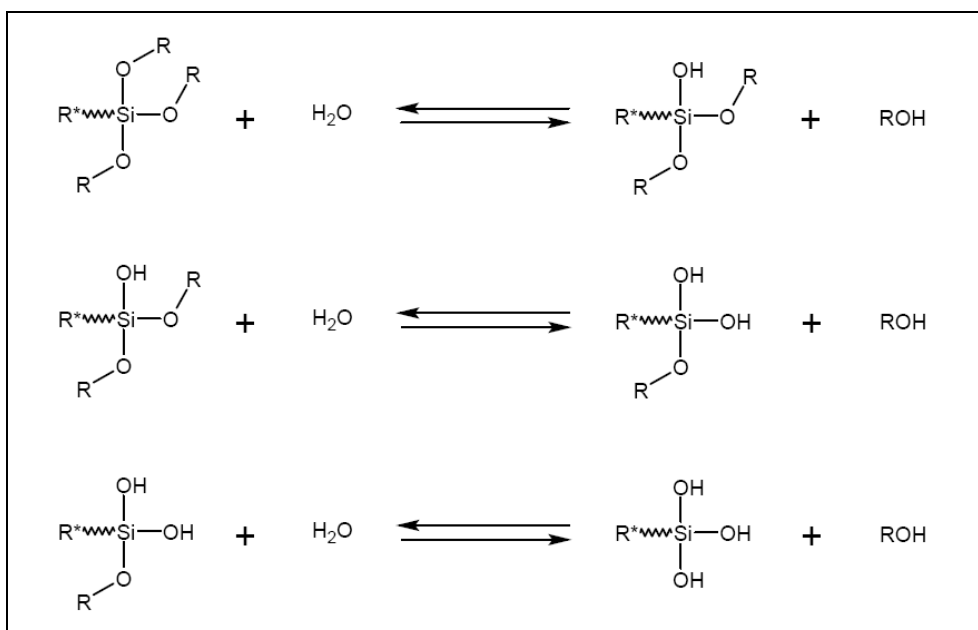
Figure 1.4 Hydrolysis reactions for an organically modified alkoxide: different steps

These kinds of molecules usually contains one organically modified group (stable in water) which ensures a second step polymerization if either thermal or photochemical curing are carried out [64]. Moreover, the organic functionalization of the alkoxy-silane molecules with organic groups allows the sol-gel film to chemically interact with organic molecules, such as polymers. A sol gel film made up of organofunctional molecules contains organic chemical groups able to interact with an organic coating. In this sense, it is possible to design sol-gel film with organically modified silane molecules which can act as coupling agent between metallic inorganic substrates and an organic coating [67]. In fact, organofunctional silane molecules contains both alkoxide groups, which hydrolyse reacting with water, generate the sol-gel network and bond to the metal substrate, and organic functionalities which are embedded in the silane film and can polymerize and chemically interact with an organic coating. This latter mechanism of interaction is schematically represented in Figure 1.5. The organic group linked to the silicon atom can be properly designed to chemically interact with the organic coating to form covalent bonds between the hybrid organically modified sol-gel film and the polymer itself.
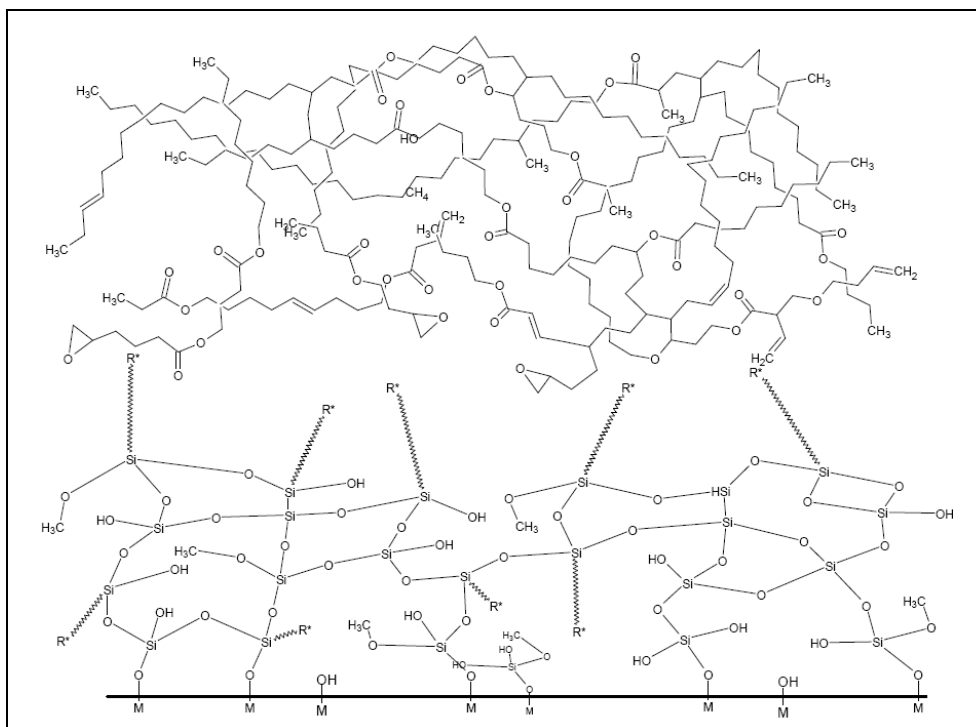
Figure 1.5 Two-dimension schematic representation of the interaction between a silane sol-gel film bonded onto a metal (M) and an organic coating

Silane sol-gel films not only ensure the adhesion between metal substrates and organic coatings but they also provide a thin, but efficient, barrier against oxygen diffusion to the metal [68]. Compared to the traditional chromate conversion treatments (the carcinogenic pre-treatment silanes are thought to replace) the only drawback of silanes is that they do not provide an active protection to the metallic substrate [69-71]. In fact, when water and aggressive ions reach the surface of the metal, silane layers are not able to ensure an active inhibition of the corrosion process as well as chromates compounds [72].

For this reason, and in general to improve the protection properties of the silane layers, several attempts were made adding corrosion inhibitors such as cerium and lanthanum salts [73-75] or CeO_2 and LaO_2 nanopowders [76] to the silane sol-gel films. In addition, the performances of silane layers filled with silica particles were also evaluated [77-80], aiming at an improvement of the barrier properties of the sol-gel film itself.

1.3 UV curable waterborne coatings

More and more national and international scientific communities are moving towards the development of sustainable and low impact chemical technologies. In this respect the issue of environmentally friendly organic coatings is very important. Reduction or elimination of toxic anticorrosive pigments and organic solvents are among the main targets. Together with high solid and powder coatings, waterborne coatings represent an interesting solution to address the present ecological issues. Water based paints offer significant advantages especially for in field applications, where the problem of solvent emission of volatile organic compounds (VOC) is really stringent since no recycling process is feasible. UV curing coatings cross-link by reaction initiated by radiation, rather than heat: these coatings are indefinitely stable when stored in absence of radiation, while after UV application, cross-linking occurs rapidly, also at room temperature [81]. Thus, owing the UV curable coatings do not

need, in principle, thermal energy to crosslink, the ultra-violet curing process can be considered "environmentally friendly". A waterborne UV curable coating can be considered is a low environmental impact technology, owing to both the absence of organic solvents and, therefore, the restriction related to VOCs and the replacement of the heat treatment with a curing procedure at room temperature. Concerning the UV curing process, a molecule which contains unsaturations that are capable of reacting with other unsaturated molecules when subjected to UV light energy is necessary in the UV curable mixture [82]. Thus, exposing the polymeric mixture to a suitable UV light source it is possible to produce a solid coherent film. The waterborne UV-curable resins usually consists of a mixture of a photoinitiator, a functionalized oligomer and a low vapour pressure monomer serving as a reactive diluent to meet the formulation viscosity requirements [83]. Two different types of photo-polymerization or photo-crosslinking process can be employed:

- Free radical chain process;
- Ionic (commonly cationic) chain process;

The free radical chain process consist in the photogeneration (obtained by irradiation with a UV source) of a radical which initiate the polymerization by adding to vinyl double bonds. The mechanism by which the initiator molecules generate the free radicals that initiate the polymerization or crosslinking is

depicted in Figure 1.6, where hydroxyl-phenyl-ketone (Darocur 1173®) molecule is considered for example.
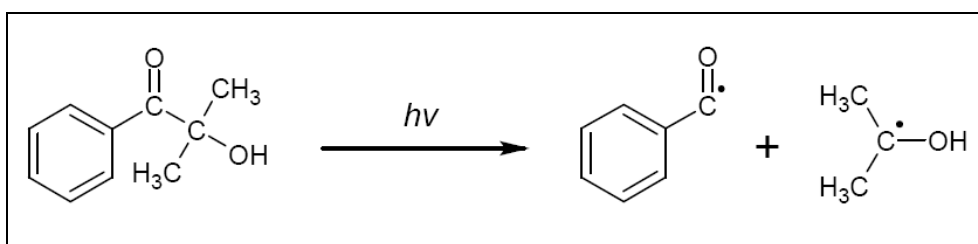
Figure 1.6 Schematic representation of the mechanism by which hydroxyl-phenyl-ketone generates the radicals

As far as Figure 1.6 is concerned, a hydroxyl-phenyl-ketone was used to generate the free radicals which are able to initiate the polymerization or crosslinking of the monomer. The photo-cleavage of this molecule produces a benzoyl radical and a hydroxyalkyl radical, both of which are capable to react with the acrylate double bond [84]. The photo-initiators that undergo the above mentioned mechanism to form radicals are named *type I* or *first class* radical photo-initiators. In fact, photo-cleavage is not the unique mechanisms for a molecule to generate radicals: there is another class of photo-initiator, the so-called *type II* or *second class* photo-initiators [82]. The mechanism by which these kinds of initiators generate the free radicals that initiate the polymerization or crosslinking is depicted in Figure 1.7, where benzophenone molecule is considered for example.
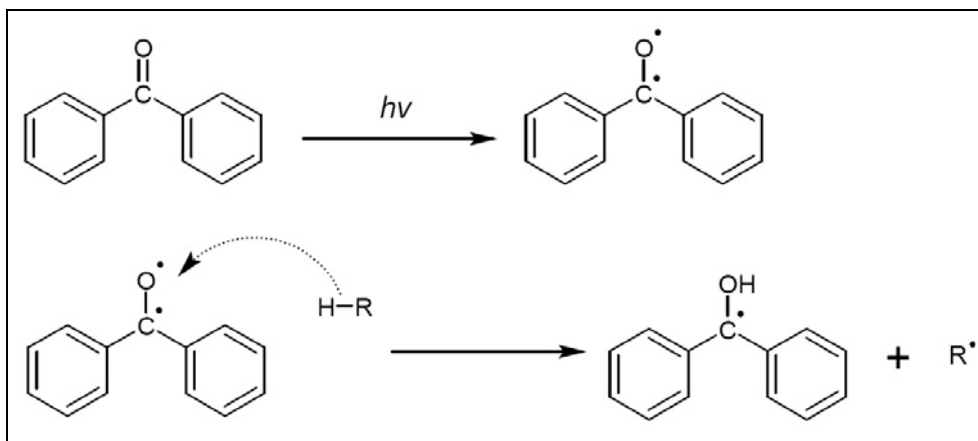
Figure 1.7 Schematic representation of the mechanism by which benzophenone generates the free radicals

Notice that the excitation of the carbonyl group in the benzophenone molecule by UV light leads to the lowest triplet state which can be described as a bi-radical (Figure 1.7). By abstraction of a hydrogen atom from the polymer backbone or from the environment, a ketyl ($Ar_2C\cdot OH$) and a carbon radical ($R\cdot$) are formed [85].

The cationic chain process consists in the photo-generation of strong acids to initiate the polymerization or the crosslinking. Actually, in principle the cationic photo-initiator can produce either Lewis acids or Brönsted acids. However, cationic photo-initiators are generally onium salts of very strong acids [81]. The photo-generated protonic acid induces the chain reaction and, consequently, the polymerization or crosslinking [86].

The mechanism by which the cationic photo-initiator molecule generate the strong acid that initiate the polymerization or crosslinking is depicted in Figure

1.8, where phosphate tri-arylsulphonium salt molecule is considered for example.
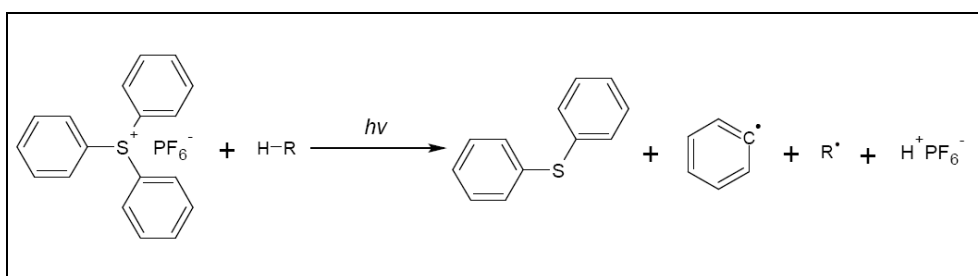
Figure 1.8 Schematic representation of the mechanism by which phosphate tri-arylsulphonium salt generates the strong cationic acid that initiate the polymerization or crosslinking

Considering Figure 1.8, the photolysis of the initiator yields strong protonic acids ($H^+PF_6^-$). A hydrogen atom from the polymer backbone or from the environment took part in the reaction that lead to the formation of the Brönsted acid, the diphenyl-sulphide molecule and the two radicals (Ar· and R·) [87]. The protonic acid obtained from the above mentioned reaction (see Figure 1.8) provides the polymerization or crosslinking by reacting with the monomer.

2 Silane sol-gel pre-treatments

In literature there is a huge number of studies concerning the potential of organofunctional silane molecules as adhesion promoters between metallic substrates and organic coatings used for protection against corrosion phenomena [39-52]. Besides being one of the most interesting way to replace chromate conversion treatments it has been widely demonstrated that silane sol-gel coatings are also environmentally friendly. The silanes molecules used in the field of corrosion protection are hybrid molecules designed to bond at the same time with a metallic substrate and with an organic coating. As anticipated in the previous chapter, silane sol-gel films ensure not only the adhesion between metal substrates and organic coatings but they also provide a certain corrosion protection. In this chapter, several experimental silane based films applied on aluminium and hot dip galvanized steel were evaluated. A preliminary study of the performance and the potential of silane sol-gel pre-treatment for the development of improved duplex systems is carried out. A duplex system consist in the combination of two different coating to protect the steel substrate: metallic zinc/zinc alloy coating (galvanization) applied on the metallic substrate and an organic coating (paint) applied the galvanization. The performances of two different environmentally friendly complete duplex protection systems were evaluated. In fact, two different painting systems were

applied on the silane pre-treated galvanized steel: an electro-coated epoxy cataphoretic paint and an epoxy-polyester powder coating paint were applied. Notice that these protection systems are designed to be completely environmentally friendly. In fact the organic coating does not contain solvents, the cataphoretic coating and the sol–gel pre-treatment are water based and the galvanization of the HDG steel used in this study is lead free. Remark that lead is a heavy metal, dangerous for both human health and the environment. In this sense, the restrictions on the use of this metal are becoming more and more stringent. Eventually, some attempts were made to modify the inner structure of the sol-gel film by embedding montmorillonite nanoparticles into the hybrid films. A complete corrosion testing was carried out on the different protection system, in order to deeply investigate the potential of the different protecting system with high environmental compatibility.

2.1 Synthesis and application of silane sol-gel films

2.1.1 Silanes mixture: properties & preparation

The diluted silane solution consists of an experimental mix of three different silanes molecules: γGlycidil-oxypropil-triethoxy-silane (γGPS), Tetraethoxy-silane (TEOS) and Methyl–triethoxy-silane (MTES).

γGPS (depicted in Figure 2.1) is an organo-functional silane composed of a short carbon backbone of 3 carbon atoms with an epoxy functionalized *tail* and a silicon atom substituted with 3 (–O-CH$_2$-CH$_3$) groups as *head*. The main organic fraction of the hybrid sol-gel coating is carried into the film by this molecule.
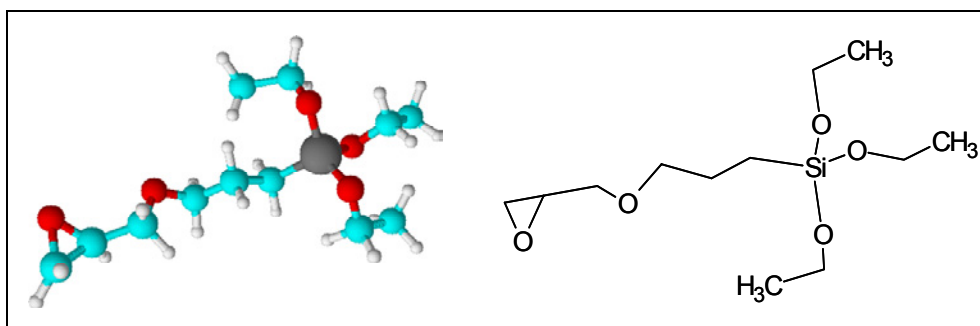
Figure 2.1 Schematic representation of γGlycidil-oxypropil-trimethoxy-silane

The silicon – oxygen bonds can hydrolyze in presence of water, leading to the formation of Si-OH bonds, following the reactions discussed in the previous chapter. The hydroxyl groups are responsible for the chemical bonding to metal substrate, by means of condensation reaction with the hydroxides present on metal substrates.

The silicon – carbon bond is not susceptible to hydrolysis and is stable in water. Due to the presence of the epoxy group this molecule ensures an active interaction with the organic coating. Under proper conditions, i.e. adding thermal energy, the epoxy ring opens and leads to the formation of covalent bonds with an organic coating. This molecule contributes to the formation of the inorganic network as well as acts as an effective coupling agent with

polymers. The stability and the efficiency of the organic coating/sol-gel film interface depend mainly on the interaction between this hybrid molecule and the macromolecules or polymer chains of the organic coating. In order to ensure a chemical compatibility between the sol-gel film and the organic coating, in this study only epoxy functionalized polymers have been used. In fact, pure epoxy polymers or epoxy-polyesters copolymer have been used as coating for the evaluation of the performances of the silane sol-gel film as a coupling agent between metallic substrate and the organic coating.

TEOS (depicted in Figure 2.2) is a very simple molecule composed of a silicon atom bonded to four ($-$O-CH_2-CH_3) groups.
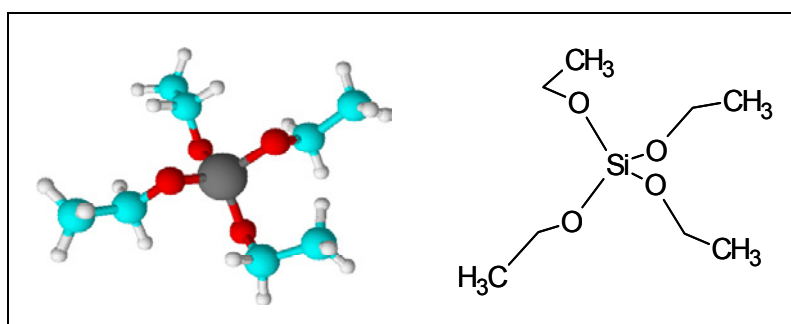
Figure 2.2 Schematic representation of Tetraethoxy-silane

As a function of the hydrolysis condition, all the Si–O-(CH_2-CH_3) bonds can, potentially, hydrolyze and form Si–OH bonds. For this reason, TEOS is a sort of *network former*, owing to it promotes the formation of an inorganic network and inorganic domains of silica. The inorganic phase is likely to be responsible of the improved barrier properties of the silane sol-gel films. In addition, the

hydroxyl groups can interact with the metal substrate, leading to the formation of covalent bonds after hydrolysis (as well as the γGPS molecules).

MTES (depicted in Figure 2.3) is quite similar to TEOS, except for the methyl group bonded to the silicon atom in place of one of the (–O-CH$_2$-CH$_3$) group.
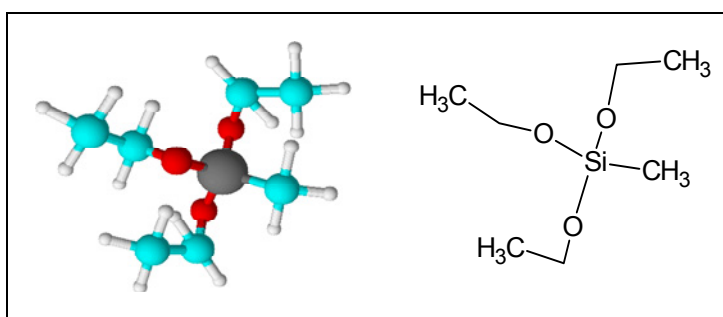
Figure 2.3 Schematic representation of Methyl-triethoxy-silane

The silicon - methyl bond is stable in water, while the other three Si–O-(CH$_2$-CH$_3$) groups are susceptible to hydrolysis reactions and thus can lead to the formation of Si-OH bonds. The function of this molecule is to promote the formation of the inorganic network. The presence of a methyl group lead to a decrease of the density of intermolecular bonding among the condensed species. The presence of this kind of molecule provides a certain control of the densification of the silane film. In fact, high density silane films have to be avoided because of a high degree of intermolecular bonds lead to the formation of brittle films.

The different properties of these three different silane molecules were combined in order to obtain a sol-gel film with improved properties.

In order to achieve the hydrolysis of the silane molecules, a water based solution was prepared to dilute the neat molecules. The mixture diluted in water consists of an equal weight percentage of each one of the three silane molecules. The silane solution was prepared dissolving 10w/w% of the silane mixture in deionised water. In this work, the hydrolysis was performed in acidic condition, modifying the natural pH of the solution by adding hydrochloric acid. The acid conditions act as a catalyst, promoting the hydrolysis reactions. In particular, the pH was always adjusted to 3.5. Under these conditions, the hydrolysis takes place mainly following the steps schematically presented in Figure 2.4 [88].
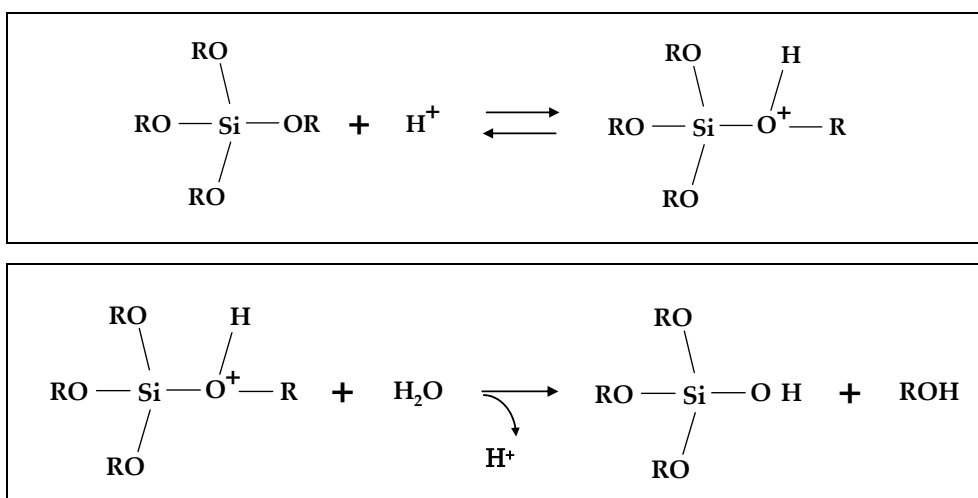
Figure 2.4 Schematic representation of hydrolysis reactions in acidic conditions

The silane molecules were added all together to the previously acidified de-ionized water. The solution was vigorously stirred for 1 hour in order to achieve

the optimal degree of hydrolysis. After this lapse of time, the solution is ready for the application onto the metal substrates.

2.1.2 Pre-treatment of the substrates

In spite of the different nature of the treated metal sample, prior the application of the sol-gel film, the samples were pre-treated approximately in compliance with the following procedure. Figure 2.5 depicts schematically the different stages of the pre-treating procedure.
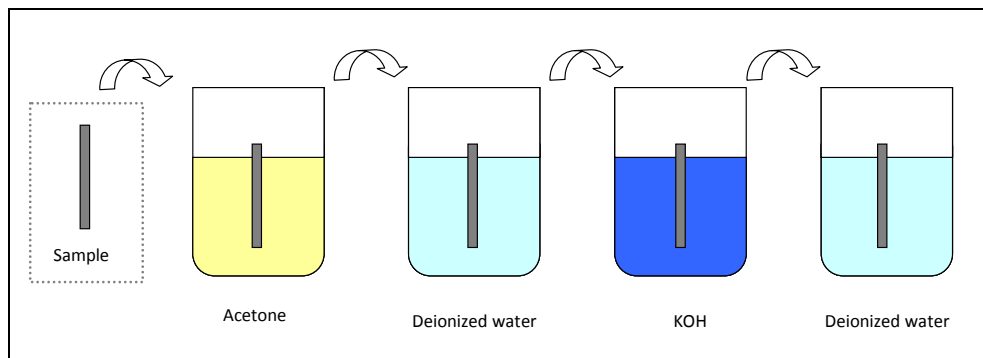
Figure 2.5 Different stages of the pre-treating procedure

Before the immersion in the silane solution the metal substrates were ultrasonically degreased in acetone for 15 minutes. Afterwards they were cleaned in an alkaline solution containing KOH (Gardoclean®, supplied by Chemetall) for 10 minutes at 50°C. This treatment provides an alkaline etching

and a chemical activation of the surface. The alkaline treatment leads to the formation of a high surface density of hydroxyl groups on the metal sample. The presence of M-OH bonds (were "M" stands for "metal") is responsible for the subsequent interaction between the metal surface and the hydrolyzed silane molecules [89]. In fact, as described in the previous chapter, the condensation reactions occur at the metal interface between the metal hydroxides and the silane molecules. After this treatment, followed a rinse in tap water and then in de-ionized water.

2.1.3 Application and curing of the sol-gel films

The application of the silane molecules onto the metal substrates, as well as the pre-treatments, was carried out by dipping. The film deposition was performed by withdrawing a substrate from a bath with solution. Figure 2.6 schematically represents the dipping procedure [90].
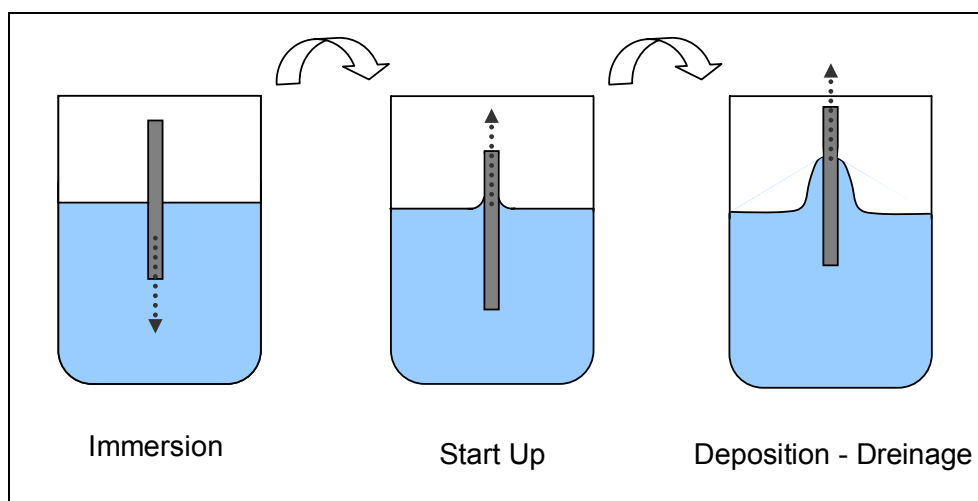
Figure 2.6 Schematic representation of the dipping procedure

The rheological properties of the solution (related to the physical properties of the fluid, i.e. fluid density and viscosity), the surface tension and the withdrawal speed influence the thickness of the final sol-gel coating [91]. In particular, the higher is the viscosity and the withdrawal speed, the higher is the thickness of the final sol-gel coating [92]. Figure 2.7 [93] shows what happens during the extraction of a sample from a diluted solution like the one used in this study. It is possible to see that evaporation of the solvent and gelation occurs during the extraction from the diluted solution. In this work, the physical properties of the fluid are maintained always constant because of the type and concentration of the silane molecules and hydrolysis temperature are always the same.
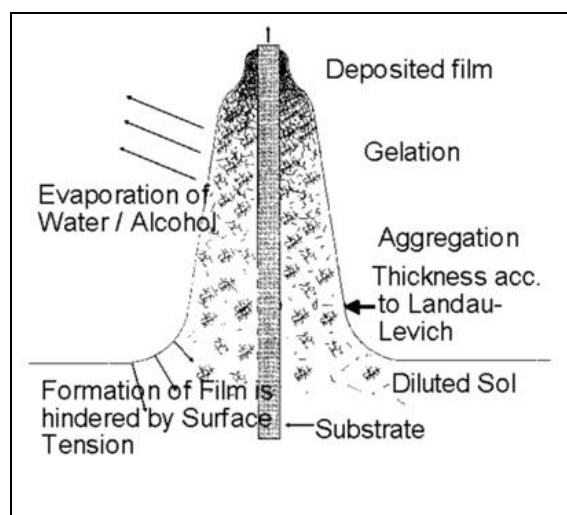
Figure 2.7 Schematic representation of evaporation and gelation [93]

The metal samples were maintained into the dilute silane solution for about 2 minutes. During this lapse of time, the formation of weak hydrogen bonds takes place and the molecules self-organize themselves onto the surface of the metal. After the withdrawing, a heat treatment in oven followed the layers deposition. Figure 2.8 schematically depicts these two last stages of the deposition of the sol-gel layer. The heat treatment provides to the sol-gel coating the thermal energy for the condensation reactions.
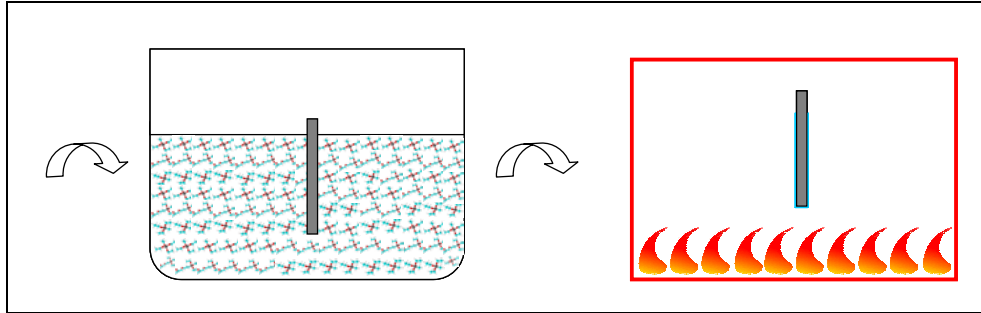
Figure 2.8 Last stages of sol-gel deposition: dipping and curing

According to the mechanisms discussed in the previous chapter, the condensation reactions occur both between the different hydrolyzed molecules and between the metal hydroxide and the silane hydrolyzed molecules. In this work, the effect of the curing temperature was investigated by analyzing the effect of different curing temperature (in a range from 120°C to 180°C) on the properties of the final silane sol-gel film.

2.2 Silane sol-gel films as pre-treatment for aluminium

The potential and the real effectiveness of the silane sol-gel film produced following the previously discussed procedure was checked applying the hybrid coatings on an innovative aluminium alloy designed for marine application. The aluminium alloy consists of AlSi7Mg alloy produced by casting.

The performance of the silane sol-gel film as coupling agent as well as barrier against corrosion was compared to traditional pre-treatments [94]. Traditionally, to reduce the corrosion rate of aluminium alloys, chemical conversion layers based on CrVI, able to increase the passivation tendency of the alloys (chromating) were used [95]. This is probably the most effective pre-treatment for aluminium alloys, because of this treatment is also effective for improving the adhesion of organic coatings deposited on the metal surface. However, as previously stated, nowadays there are strong restrictions in the use of these compounds due to the environmental protection legislation. In this chapter the performances of the experimental silane sol-gel layer are compared with other traditional pre-treatment, such as CrIII chemical conversion layer, CrVI chemical conversion layer, and a fluorotitanate/zirconate acid based conversion treatment. The electrochemical properties of the pre-treatments for the aluminium samples and their corrosion protection properties were analyzed. Eventually, an organic coating was applied onto the pre-treated samples, in order to test the effectiveness of the pre-treatment to improve the adhesion and the corrosion protection properties of the whole protection system. This allows us to test the potential of the silane sol gel film as a coupling agent for the enhancement of the adhesion between the metal substrates and the organic coating. The samples were characterised by electrochemical techniques (mainly EIS measurements), electron microscopy observations, adhesion tests, anodic polarisation test and exposure in the salt spray chamber.

2.2.1 Materials and experimental procedure

The exact chemical composition of the aluminium alloy used as substrate is reported in Table 2.1.

Table 2.1 Composition of the aluminium alloy

Al	Si	Mg	Fe	Cu	Zn	Ti	Mn	P	Ca
Bal.	6.5-7.5	0.3-0.5	0.1	0.03	0.03	0.2	0.03	0.0015	0.002

After the cleaning of the aluminium surface performed following the procedure described in the previous chapter, the samples were pre-treated using the following chemical treatments:

✓ *CrVI*, typical chromium VI conversion layer: a mixture of 50–60% CrO_3, 20–30% KBF_4, 10–15% $K_3Fe(CN)_6$, 5–10% K_2ZrF_6, 5–10% NaF, temperature deposition about 35°C.

✓ *CrIII,* chromium III conversion layer: slightly acidic solution (pH 3.8 – 3.9) containing nitric acid, 0.1 M Cr^{3+} salts and additives, temperature deposition 40°C.

✓ *ZTF*, chromium free chemical conversion layer obtained by dipping in a fluorotitanate/zirconate acid based solution at room temperature.

✓   *Silane,* hybrid silicon based sol-gel film applied following the previously described standard procedure: deposition temperature about 20°C and curing temperature at 120°C.

Finally, an organic coating was applied onto the differently pre-treated samples. The organic coating consist of a 100 µm thickness epoxy-polyester powder coating, cured at about 200°C for about 15 minutes. Table 2.2 summarizes the different samples object of the study.

Table 2.2 Different samples object of the study

	Name of the sample	
Pre-treatment	Uncoated	Coated
Untreated	Bare	PW
CrVI pre-treatment	CrVI	CrVI-PW
CrIII pre-treatment	CrIII	CrIII-PW
Fluorotitanate/zirconate pre-treatment	ZTF	ZTF-PW
Silane sol-gel layer	Silane	Silane-PW

2.2.2 Experimental results and discussion

Prior the investigation of the complete protection systems, the pre-treatments were characterized in order to analyse their different properties and to correlate

the final performances of the protection cycle to the characteristics of the pre-treatments.

Pre-treated aluminium alloy samples

The environmental scanning electron microscope (ESEM) observations of the surface morphology and appearance of the different pre-treatments are presented in Figure 2.9.
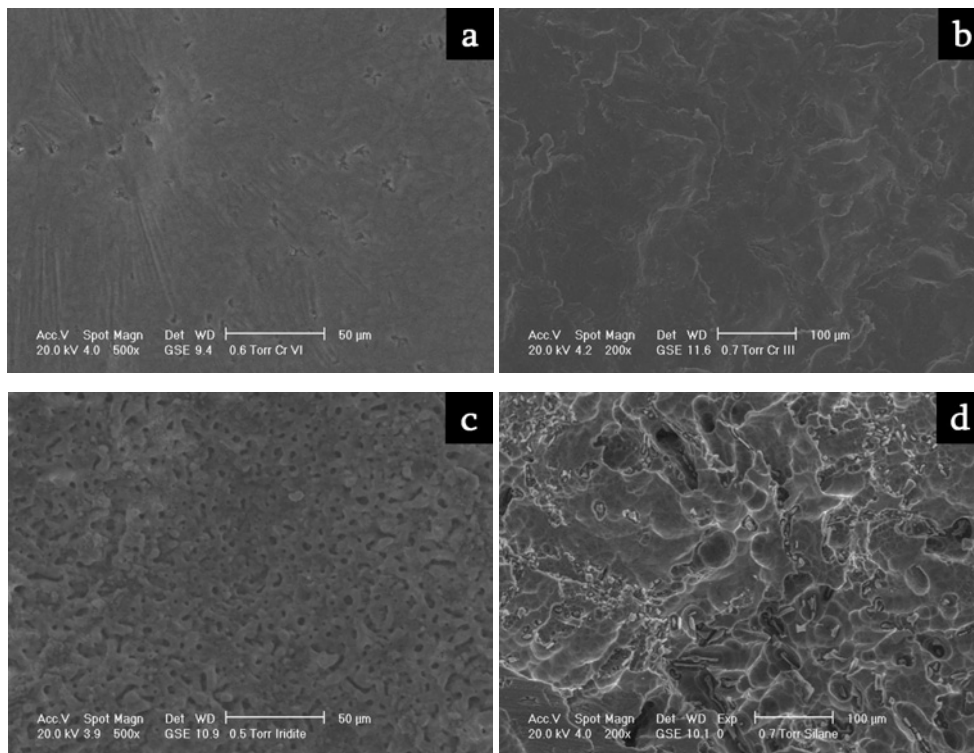

Figure 2.9 ESEM images of the surface of CrVI sample (a), CrIII sample (b), ZTF sample (c) and Silane samples (d)

The samples pre-treated with chromium baths (CrVI, Figure 2.9a, and CrIII, Figure 2.9b) show a surface morphology without any evident features, because of the very limited thickness of the conversion layer. The only visible heterogeneities are related to the aluminium surface roughness. Different is the appearance of the other two pre-treatments. The ZTF pre-treatment (Figure 2.9c) shows a rough and apparently porous surface as consequence of the conversion layer deposition which is able to modify the surface morphology. Also the silane pre-treatment (Figure 2.9d) modify the surface appearance due to the presence of the hybrid sol gel film. The silane layer is very thin (hundreds on nano-meters) and it complies with the surface roughness. However, a sort of globular structure is observable.

More important is to verify if the pre-treatment is able to give sufficient protection properties. For this purpose, electrochemical impedance spectroscopy measurements were performed. A classical three electrodes arrangement was used. An Ag/AgCl (+0.207 V vs SHE) electrode and a platinum ring were used as reference and counter electrode, respectively. The frequency range used for these measurements was from 100 kHz to 10 mHz, while the signal amplitude was 5 mV. The immersed area was about 15 cm^2 and the testing solution was 3.5w/w% NaCl.

Figure 2.10 shows the free corrosion potential trends for the pre-treated samples and the just cleaned material. After the first few hours of immersion the differences are very limited and therefore it is possible to conclude that the pre-treatments do not change significantly the nature of the electrochemical reaction influencing the free corrosion potential.
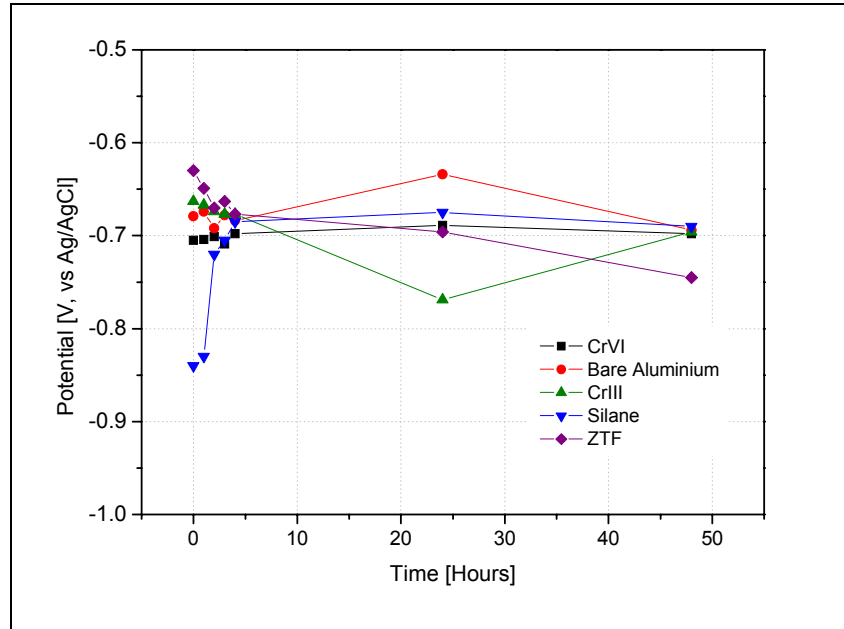
Figure 2.10 Free corrosion potential trends for the pre-treated samples

More interesting is the analysis of the EIS spectra. For the pre-treated samples, it was possible to model the EIS data using an equivalent electrical circuit with two times constant: the first one, at higher frequencies, is related to the surface layer contribution (i.e. the contribution to the total impedance due to the conversion layer or silane layer) together with the presence of possible corrosion products [96]. The second one, at lower frequencies, can be attributed to the corrosion reaction (the electrochemical reaction at the metal surface can be modelled using a resistance, the charge transfer resistance and a capacitance, the double layer capacitance) [97].

The capacitance of the conversion layer is shown in Figure 2.11. Increasing the pre-treatment thickness d, the capacitance per unit of area C decreases, considering the equation (Eq. 1.1):

$$C = \frac{\varepsilon \cdot \varepsilon_0}{d} \qquad \text{(Eq. 1.1)}$$

Where ε is the dielectric constant of the medium and ε_0 the vacuum permittivity and ε is the relative permittivity [98].
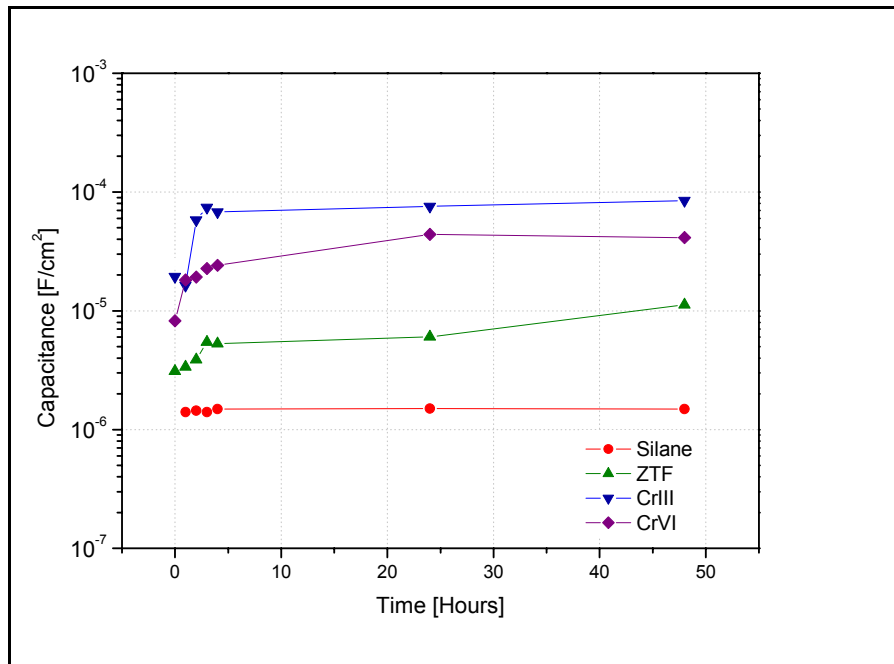
Figure 2.11 The capacitance of the conversion layer with immersion time

The pre-treatments with the supposed higher thickness are the silane pre-treatment and the conversion layer ZTF (see also the microstructure in Figure 2.9). These pre-treatments shows the lower capacitance values, while the CrIII and CrVI pre-treatments show capacitance values quite close to bare metal, proving the presence of a very thin conversion layer. In the literature the typical thickness of these layers is a few decade of nanometres [99], while in the case of silane layer the thickness is at least hundred of nanometres [100].

The pre-treatment resistance, which can be related to the barrier properties of the chemical conversion layer, is shown in Figure 2.12.
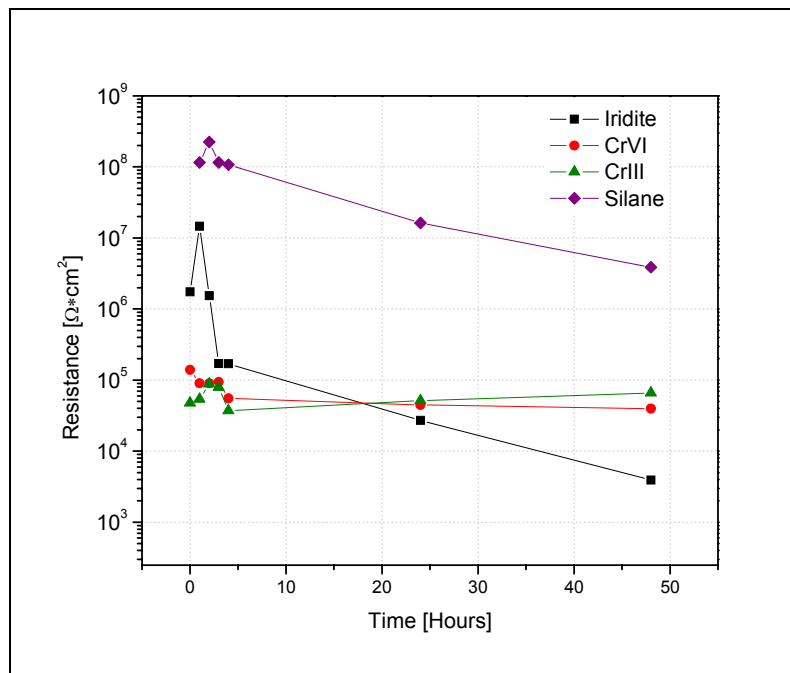
Figure 2.12 The pre-treatment resistance with immersion time

The behaviour of all the pre-treatments, not considering the silane layer, is very similar. Only the pre-treatment ZTF, probably because of the layer thickness and microstructure, shows relevant temporary barrier properties just for short immersion time. On the contrary, the silane layer shows important barrier properties, reducing with the immersion time. The coating resistance of the silane pre-treatment reaches about 10^7 $\Omega \cdot cm^2$ after 2 days of immersion in the testing solution.

The conclusion of this preliminary pre-treatments characterisation is that silane layer shows the better corrosion protection performances respect to the other pre-treatments. It has to be underlined that the silane sol-gel coating is really thicker than the other pre-treatments, but, however, the protection performances of this conversion treatment remains very interesting in the light of the high absolute values of the resistance (showed in Figure 2.12). The sol-gel film provides the metal with an efficient barrier against water and ions, dramatically slowing down the corrosion rate.

Pre-treated aluminium alloy covered with the organic coating

The samples covered with the organic coating were investigated by means of electrochemical impedance spectroscopy. All the studied complete protective cycles showed very high impedance values (higher than 10^{10} $\Omega \cdot cm^2$) because of the very good barrier properties of the organic coating systems and the high thickness. The degradation time for these systems is, therefore, very long in our testing conditions. In order to obtain earlier corrosion information accelerating

the degradation process and in order to better highlight the pre-treatment influence, we produced an artificial defect (scratch) in the coating, promoting the system degradation [101]. In particular, it is possible to monitor the delamination of the coating starting from the defect and quantify the interface stability induced by the pre-treatment. The measurements arrangement of the electrodes as well as the electrolyte were the same used for the surface conversion treatments. The experimental spectra were acquired and modelled in order to determine the suitable electrochemical data.

The equivalent electrical circuit for the modelling of our system is shown in Figure 2.13 where, in addition to the coating capacitance Q_c and the coating resistance R_p (the contribution of the organic coatings to the total impedance which is in this case very low because of the artificial defect), a second time constant related to the faradic reaction is visible with the double layer capacitance Q_{dl} and charge transfer resistance R_{ct} [102].
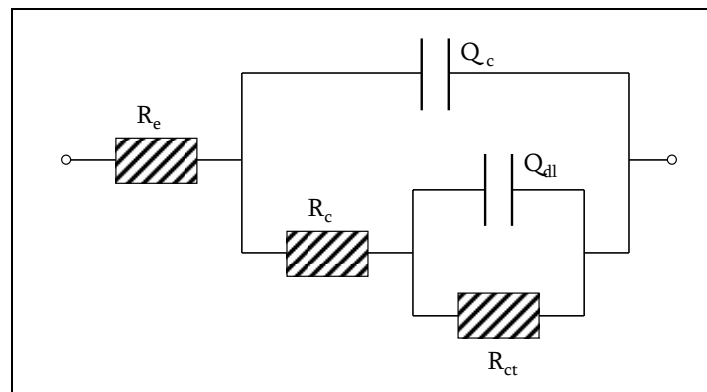
Figure 2.13 Equivalent electrical circuit used for the modelling of the experimental spectra

Because of the artificial defect, damaging also the surface pre-treatment, the chemical conversion layer and the silane sol-gel pre-treatment are not detectable any more in the EIS data and, therefore, they are not included in the equivalent electrical model.

Figure 2.14 shows the trends of the charge transfer resistance as a function of the time of immersion in the aggressive solution.
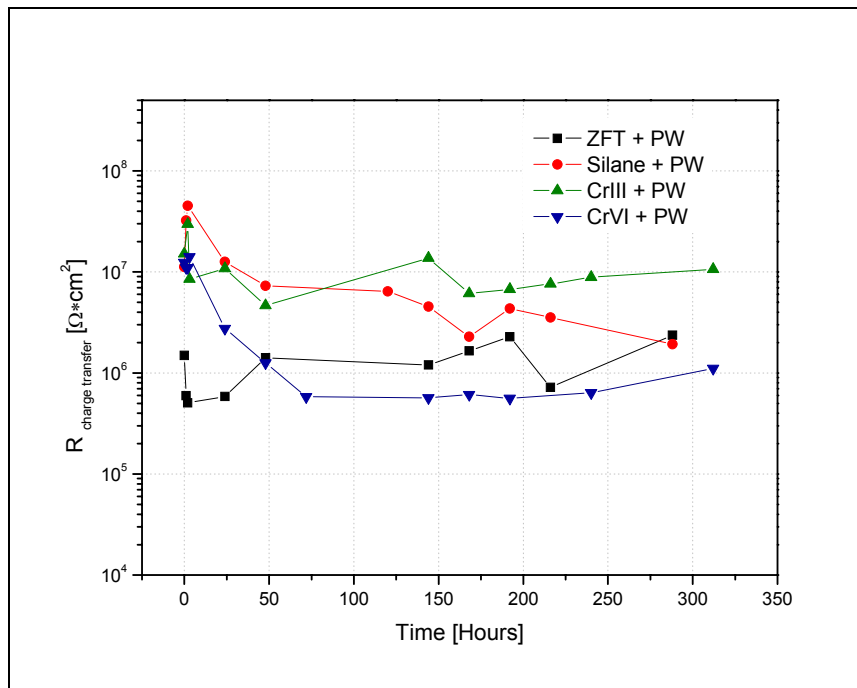
Figure 2.14 Charge transfer resistance vs. immersion time

Considering the trends reported in Figure 2.14, it is possible to observe that the values of R_{ct} show a decrease for samples *Silane+PW* (*PW* stands for powder

coating)and *CrVI+PW* while samples *CrIII+PW* and *ZTF+PW* maintain a stable value of this parameter.

After the initial scattering (about 50 hours of testing) of the experimental data of the R_{ct} values due to the activation of the corrosion reaction, an almost stationary condition is reached. The highest R_{ct} values, related to lower corrosion rate, are measured on CrIII and silane pre-treatments, while the highest corrosion rate is measured on CrVI samples despite the corrosion inhibition action of these kinds of materials. The silane sol-gel pre-treatment shows the higher starting values of the charge transfer resistance, which is inversely proportional to the corrosion rate [103]. More interesting to discriminate the different effectiveness of the pre-treatments is the analysis of the double layer capacitance (Q_{dl}). This parameter is directly proportional to the extent of the metal surface in contact with the electrolyte. Thus, the double layer capacitance can be considered as an indicator for monitoring the stability of the metal-coating interface. In fact, as a consequence of the corrosion reactions, the coating can delaminate from the scratch, allowing the electrolyte to wet the metal surface. The ratio between the double layer capacitance after a certain time of immersion (Q_{dlx}) and the initial double layer capacitance (Q_{dl0}) is an indication of the increase of wetted metal surface and therefore it measures the loss of adhesion of the coating [104].

Figure 2.15 shows the trend of this parameter as a function of the time of immersion in the 3.5w/w% NaCl solution.
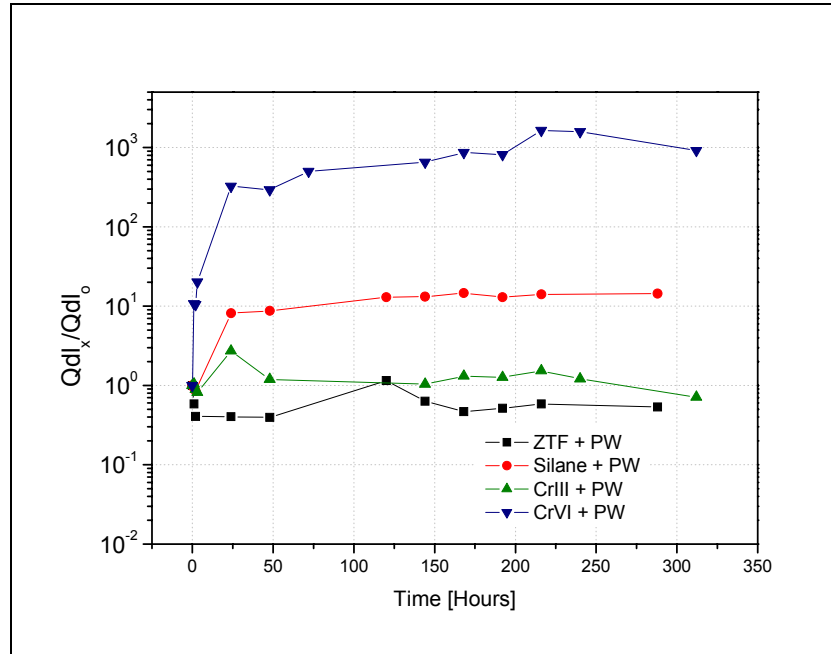
Figure 2.15 Q_x/Q_0 with time of immersion

CrIII and *ZTF* pre-treatments show a very high adhesion stability being the delamination process almost negligible. A very limited delamination was measured in the case of silane layers, while the only pre-treatment showing a relevant delamination is the pre-treatment *CrVI*. It is important to remember that the pre-treatments based on chromates (CrVI) have certain solubility for leaching the Cr^{6+} ions able to favour the surface passivation and therefore they are intrinsically less stable in aqueous solutions. However, the values of the double layer capacitance for the CrVI treated sample are quite high for this kind of pre-treatment. It is likely that the conversion layer is particularly thin compared to the other pre-treatments and, consequently, less efficient.

To complete the characterisation, data concerning the mechanical adhesion of the coatings with the substrate (pull-off test) were also collected in compliance with ASTM D4541 standard. This test aim at investigating the potential of the silane sol-gel film as a coupling agent between the aluminium alloy and the organic coating. The data of the pull-off stress are reported, for each sample, in Figure 2.16. The values of the measured adhesion are quite similar among the differently pre-treated samples. With respect to the coated bare aluminium (reported in Figure 2.16 as PW), all the pre-treatments improve the adhesion between the metal and the organic coating.
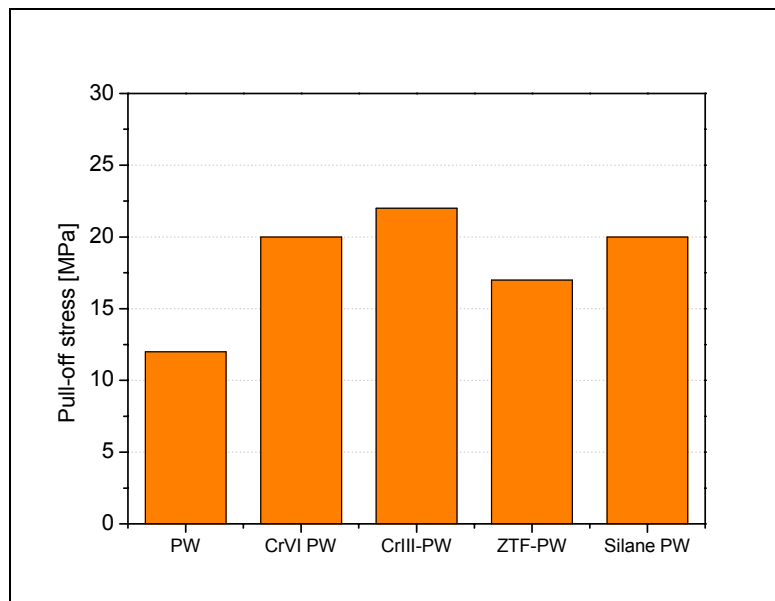

Figure 2.16 Experimental results of the pull-off test

CrIII, *CrVI* and *Silane* pre-treatments show high and very comparable values of the adhesion, while *ZTF* pre-treatment shows a lower value. However, in general the adhesion values are quite good for all the materials, being not lower than 10 MPa.

Observe that great difference between the results of the interfacial stability during corrosion process (Figure 2.15) and the values of the dry adhesion (Figure 2.16). The differences in pull-off measurements are very limited and the pronounced differences among the samples visible in Figure 2.15 are not reproduced (*CrVI* pull-off values are actually higher than the values of *ZTF* pre-treatment). This fact is not unusual, proving that the two experimental approaches are different, being the dry adhesion test different from the adhesion stability evaluated in wet environments. It is possible to conclude that the dry pull-off measurements are not sufficient to characterise the adhesion stability.

A further way to test the stability of the polymer/metal interface (the adhesion of the organic coating in wet condition and under active electrochemical reaction), is the anodic delamination. The application of an anodic potential increases the aluminium substrate activity (corrosion) promoting the anodic undermining process [105]. In practice, a 25mm long scratch was performed on the intact samples. Also in this case, the electrolyte and the arrangement were the same discussed for EIS measurement. The samples were polarized at -200 mV vs. Ag/AgCl (+207 vs. SHE) for 240 hours. This particular value of the potential can represent a real situation when a galvanic coupling of the aluminium component with a nobler metal (such as stainless steel) occurs in

service. In fact, in this case the corrosion process is forced by the coupling of the two metals with different potential. After the polarization period, the extent of the produced defect was measured for each sample. For example, Figure 2.17 (a,b) shows the appearance of the sample *ZTF+PW* (a) and *Silane+PW* (b) after 240 hours of anodic polarisation.
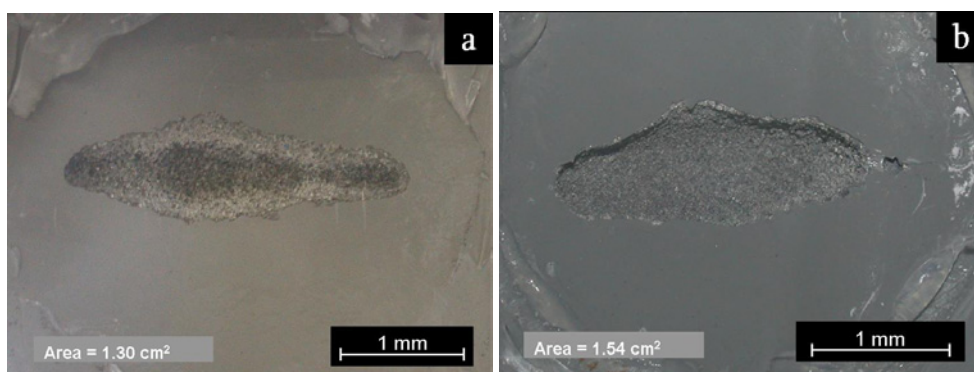
Figure 2.17 . *ZTF+PW* (a) and *Silane+PW* (b) after 240 hours of anodic polarisation @ -200mV (vs. Ag/AgCl)

The coating and metal degradation around the defect is evident, showing the delaminated area which can be measured. The extent of the delaminated areas is reported, for each sample, in Figure 2.18.
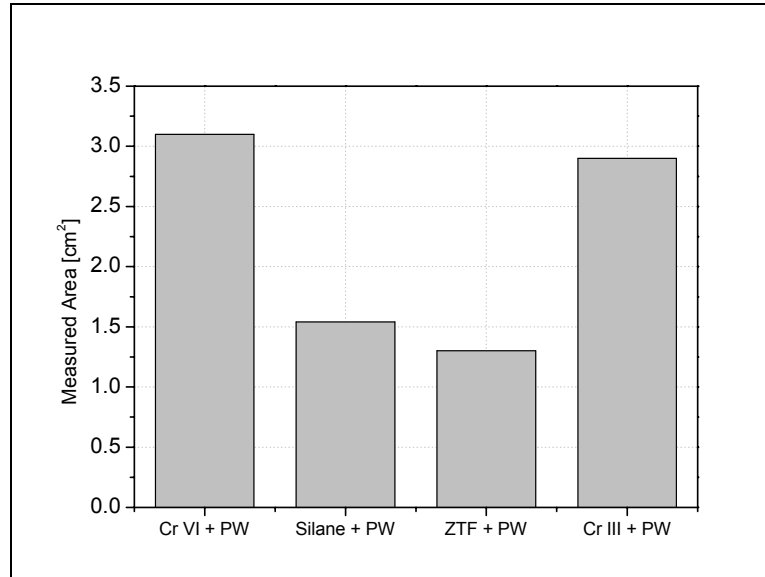
Figure 2.18 . The extent of the delaminated areas after 240 hours of anodic polarisation @ -200mV (vs. Ag/AgCl)

The lowest delamination is shown by the samples pre-treated with *ZTF* or *Silane* layers, while a higher, even if limited, delamination was measured for the Cr based pre-treatments. The corrosion properties of the differently pre-treated aluminium samples were finally evaluated by means of exposure in the salt spray chamber, performed in compliance with the ASTM B117 standard. The aim of this test is to obtain experimental data easy to compare with other materials characterisation and to confirm, using an industrial test, the corrosion performance of the studied systems obtained by the previously discussed electrochemical tests. Scratched samples were exposed in the salt spray chamber and the samples were considered deteriorated when the average linear detachment of the coating from the scratch was about 5 mm. Table 2.3

summarizes the experimental results of the resistance in the salt spray chamber. In order to quantitatively estimate the wet adhesion, the threshold of 5 mm of disbonding (starting from the artificial defect) was set to consider no more protective the coating.

Table 2.3 Salt spray chamber results

Sample	Resistance (hours)
CrVI+PW	>2500
CrIII+PW	1500
ZTF+PW	1500
Silane+PW	2200

All the different samples show a good resistance in the salt spray chamber. The sample pre-treated with the CrVI conversion treatment shows the higher resistance, followed by the silane sol-gel treated sample. CrIII and ZTF treated samples shows the lowest resistances among the different samples, despite the absolute values are, actually, high.

2.2.3 Comments

The aim of this chapter was to compare the effectiveness of the sol-gel film produced starting from an innovative and experimental mixture of silane molecules with other traditional pre-treatments. For this purpose, the corrosion

protection properties and the potential as coupling agent of the experimental silane sol-gel film was compared with other traditional pre-treatments for aluminium. The tests performed on the aluminium alloy samples investigated a few properties of the different combination of pre-treatment and coating, such as adhesion, stability of the interface and barrier properties. The experimental measurements proved that silane sol-gel films provide a good corrosion protection of the substrate, even in the absence of the organic coating, in consideration of the fact that it is just a few hundreds of nanometers thick. In addition, the experimental measurements highlighted that they act as a coupling agent. In fact, the silane sol-gel coating provide good adhesion properties between the metal and the organic coating both in dry (see pull-off test, Figure 2.16) and wet (see salt spray test, Table 2.3) conditions.

2.3 Development of silane sol-gel films for duplex systems

In the previous section the efficiency of the silane sol-gel film produced from the experimental mixture was proved to be comparable or higher than other traditional pre-treatment on an aluminium alloy. In this chapter, this same silane sol-gel layer (of proved effectiveness) was investigated as a pre-treatment for the development of high performance duplex systems for the protection of steel structure. A duplex system consists of a fine combination of a zinc metallic

coating, a galvanization, to protect the steel and an organic coating to protect the whole structure. In particular, the corrosion performances of hot dip galvanized steel treated with silane molecules and covered with an organic coating were analyzed. The aim is to develop a corrosion resistant protection system consisting of only "environmentally friendly" elements.

For this purpose, besides using silanes pre-treatments instead of chromates, galvanization bath contains no lead, considered dangerous for human health and the environment [106]. The organic coating was applied on the galvanized and pre-treated by means of two different environmentally friendly techniques which prevent problems due to volatile organic compounds (VOCs). As anticipated in the previous section, these techniques are powder coating painting and cataphoretic coating painting. As cited many times, the silane solution is completely water based and, therefore, no organic solvent is present.

Because of the experimental nature of the silane mixture, a commercial water based silane pre-treatment was used for comparison. In addition, a common industrial pre-treatment such as fluozirconate conversion treatment was applied for a further comparison, in order to have a complete overview of the different performances of the different pre-treatments.

In the first part of chapter the properties of the silane sol-gel layers applied onto galvanized steel surfaces were investigated. In the second part the analysis and characterization of the complete protection system considering the two different organic coatings were carried out. Concerning the cataphoretic electrodeposition, a preliminary study on the compatibility between the

electrodeposition process and the silane film was performed and it is reported for comprehensiveness.

The characterization of the corrosion protection performances of the complete protection system and the analysis of the silane pre-treatment as neat were performed by means of chemical and electrochemical techniques (FT-IR, ToF-Sims, XPS, EIS, potentiodynamic polarization), accelerated laboratory tests (salt spray chamber, cathodic polarization) and observations with environmental scanning electron microscope (ESEM). The properties of the different silane layers were underlined and the corrosion protection properties of the complete system were analyzed and discussed.

2.3.1 Materials and experimental procedure

Hot dip galvanized steel sheets (Zn alloy: 0.25 w/w% Al, supplied by Arcelor Mittal, Belgium) with a mean roughness of 1.59 µm were used as substrate for the development of the duplex systems.

After the cleaning of the galvanized steel substrate performed following the previously discussed procedure, the samples were pre-treated using the following chemical treatments:

✓ Silane mixture sol-gel film applied following the standard procedure at about 20°C and 40% r.h.. The effect of the curing temperature was

investigated: the fresh films were cured at two different temperatures, 120 and 180°C, for about 20 minutes.

✓ A commercial water-based silane, SIVO® silane (supplied by Degussa), whose composition is patented. The dilution is 10 w/w% in water. No modification of the pH of the solution was performed (product specification). Also this solution was stirred for 1 hour before the dipping of the galvanized samples. The heat treatment was performed at 120°C for 15 minutes in compliance with the product specification.

✓ A fluozirconate treatment obtained by dipping the galvanized sample into a solution containing an acid solution of HF and ZrO_2 compounds at room temperature. This treatment provides the formation of a protective film of hydrated compounds of fluorine, zinc, zirconium and oxygen on the zinc surface.

Two kinds of organic coatings were applied onto the pre-treated samples:

✓ an about 70 μm thick epoxy-polyester powder coating (supplied by Pintarelli s.r.l., Italy) cured at about 210°C for 15 minutes;

✓ an about 20 μm thick lead free epoxy cataphoretic electro-coating (supplied by PPG, France) obtained applying 180V for 3 minutes between the target and a stainless steel electrode at a bath temperature of 30°C.

Eventually, the electro-coated samples were cured for 25 minutes at 175°C.

2.3.2 Experimental results and discussion

Similarly to the previous section, the properties of the experimental silane sol-gel coatings were investigated prior the study of the complete protection system. In the light of the experimental results obtained in the previous paragraph concerning the pre-treatments, in this case only the silane based pre-treatment were characterized. In fact, despite being very thin, silane sol-gel films are a coating with a thickness noticeably higher than any chemical surface conversion treatment. This fact could lead to misunderstandings or misconceptions if silanes sol-gel films are compared to other pre-treatments, because of the different nature of these treatments lead to hardly comparable results.

Pre-treated galvanized steel samples

Table 2.4 summarizes the different pre-treated samples which will be analyzed in following of the chapter. Table 2.4 provides also the names used to refer to the different samples.

Table 2.4 Summary of the pre-treated samples

Name of the sample	Surface treatment	Heat treatment (15 minutes)
Galvanized steel	-	-
Silane HT120	Silane mix	120°C
Silane HT180	Silane mix	180°C
Commercial silane	SIVO®	120°C
FZT	HF + ZrO$_2$ conversion	-

Figure 2.19 (a, b, c and d) shows the ESEM images obtained by using the gaseous secondary electron (GSE) detector for the bare galvanized sample and the silane coated samples. Because their very low thickness, the silane films (Figure 2.19 b, c and d) do not modify the roughness of the surface and they approximately comply with the morphology of the galvanized surface (Figure 2.19a).
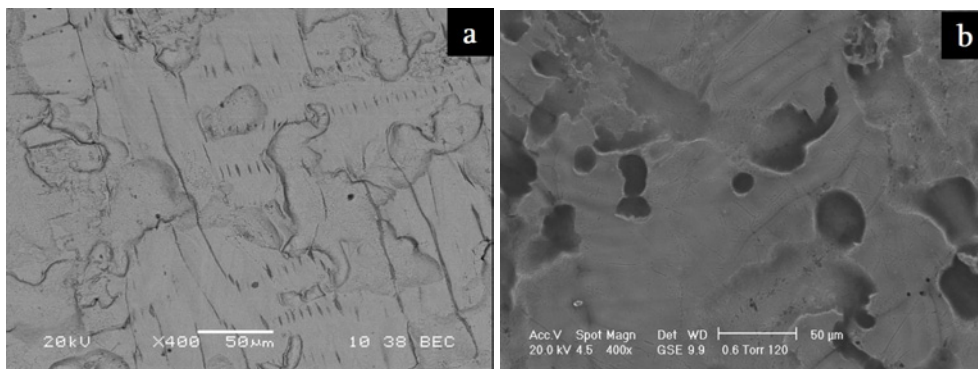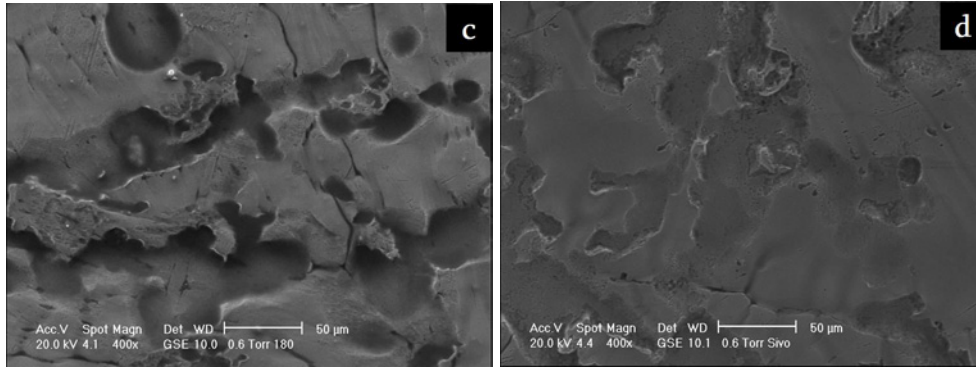
Figure 2.19 ESEM images of the differently treated surface: Bare galvanized steel (a), Silane HT120 (b), Silane HT180 (c) and Commercial Silane (d)

The three different layers seem to be quite homogeneous and there are no clearly visible differences among them. Figure 2.20 (a, b and c) depicts the same samples analyzed by using the back scattering electron (BSE) detector of the ESEM. Considering the pictures showed in Figure 2.20, different areas are observable. In fact there are white "islands" with a sort of black contour.

A localized energy dispersive X-ray microanalysis (EDXS) demonstrates that the dark portions of the pictures are richer in silane (highlighted by the higher intensity of the peak corresponding to the silicon) than the bright areas.

It is likely that the different sol-gel films are not homogeneous over the HDG steel surfaces:
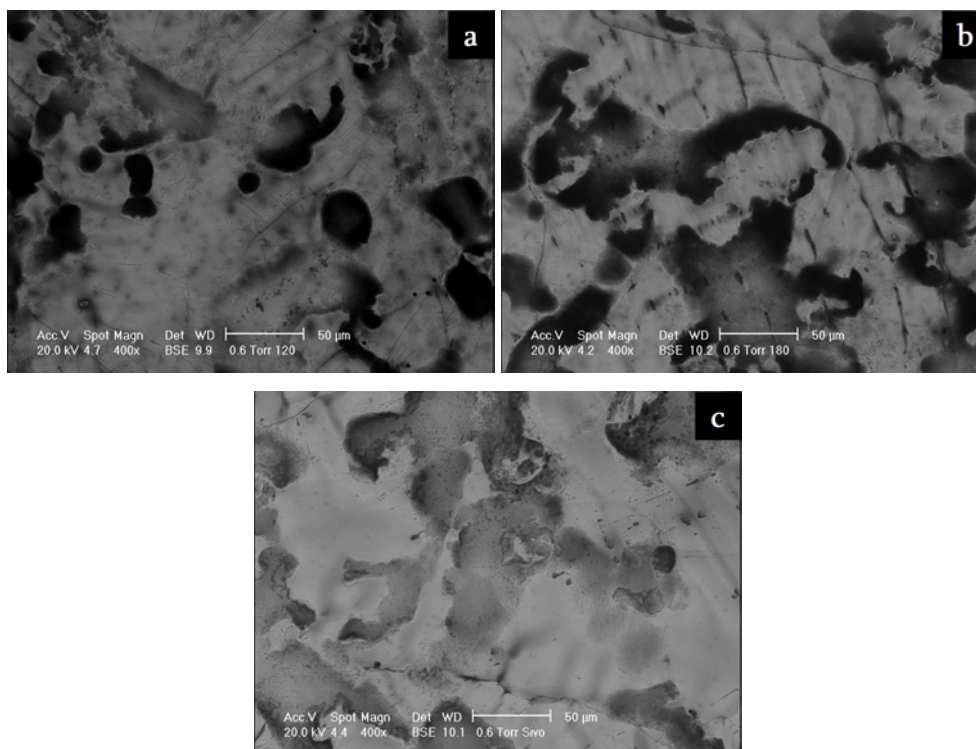
Figure 2.20 ESEM images of the differently treated surface: Silane HT120 (a), Silane HT180 (b) and Commercial Silane (c)

Despite the film is present over the whole surface, probably there are several accumulations of silane molecules, in particular areas of the surface of the sample where several hollows are observable.

The thickness of the hybrid coupling films was measured by means of the ToF-Sims (Time of Flight – Secondary ions mass spectroscopy). Figure 2.21 shows an example of ToF-Sims profile showing the increase of the Al and Zn signal and the decrease of carbon and silicon compounds, due to the silane layer, for Silane HT120 sample.
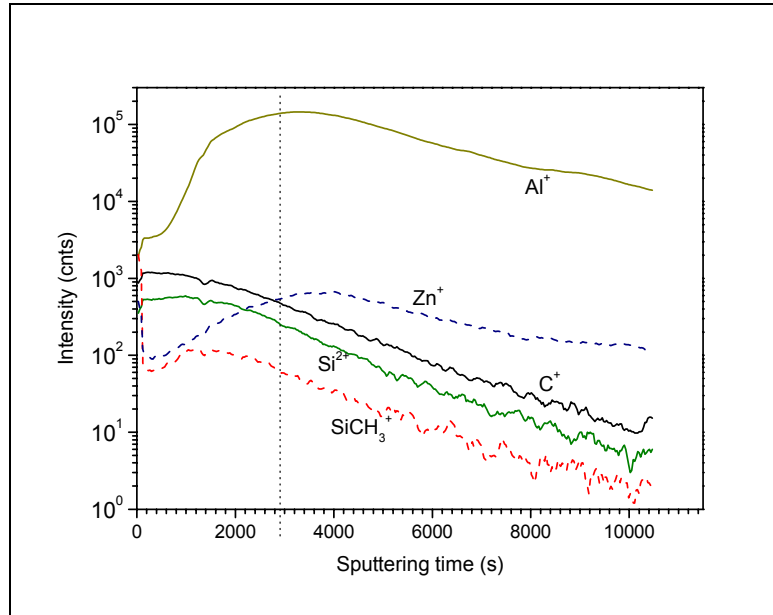
Figure 2.21 ToF-Sims profile on the surface of sample Silane HT120

The layer thickness was estimated from the sputtering time. The value of the sputtering time corresponding to the metal/film interface is highlighted by the dotted line in Figure 2.21. Table 2.5 summarizes the corresponding calculated numerical values and some additional information provided by the experimental analysis.

Table 2.5 Thicknesses of the different sol-gel coatings

Sample	Thickness (Å)	Additional information
Silane HT120	3000	
Silane HT180	1000	High reticulation
Commercial silane	2200	

The film obtained curing the silane mixture at 180°C is thinner and denser compared to the film cured at 120°C. This can be explained by the fact that condensation reactions are promoted by heat. Thus, the film cured at 180°C is characterized by a highly reticulated Si-O-Si network. This denser reticulation, confirmed by ToF-Sims measurements, was observed on the Fourier transform infra-red spectroscopy (FT-IR) spectra. Indeed, by means of the infra-red spectroscopy (Figure 2.22) it is possible to appreciate that for the Silane HT180 sample, an intense Si-O-Si peak (1080 cm^{-1}) and a small Si-OH peak (3373 cm^{-1}) are present [107].
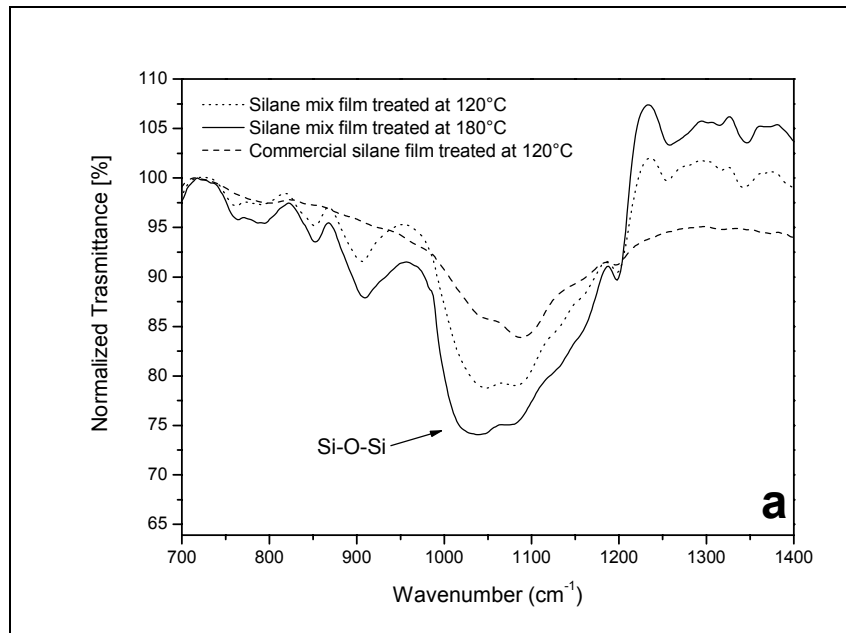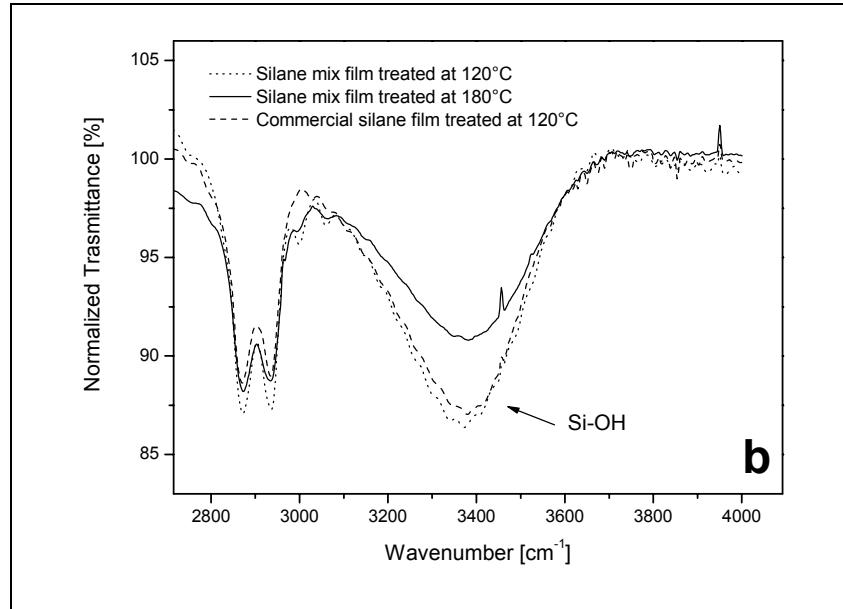
Figure 2.22 Portions (a,b) of the infra-red spectra of the different sol-gel coatings

Comparing the same peaks showed at these wave–numbers by Silane HT120 and Commercial silane samples, the silane mixture sol-gel film treated at 180°C shows the higher density of Si-O-Si bonds and the lower of Si-OH bonds among the different samples.

The chemical properties of the films were analyzed measuring the contact angle of the treated samples with water (θ_{water}). In addition, from measurements of contact angles θ of three different liquids (water, formamide and diiodomethane) with the silane layers, the dispersive σ_S^D and polar σ_S^P components of the surface energy of the layers were determined by using the Owens-Wendt model [108]. The surface energy is the sum of dispersive and

polar components. These components are connected by the equation of the liquid adhesion work W_A on the solid, given by (Eq. 1.2):

$$W_A = \sigma_L \left(1 + \cos \Theta\right) = 2\sqrt{\left(\sigma_S^d \cdot \sigma_L^d\right)} + 2\sqrt{\left(\sigma_S^p \cdot \sigma_L^p\right)} \qquad \text{(Eq. 1.2)}$$

Table 2.6 shows the values of σ_S, σ_S^D, σ_S^P and the contact angle of each film with water (θ_{water}).

Table 2.6 Contact angles of the different sol-gel coatings

Sample	σ_S (mJ/m²)	σ_S^P (mJ/m²)	σ_S^D (mJ/m²)	Θ_{water} (°)
Silane HT120	44.9	13.8	31.1	61
Silane HT180	43.4	10.3	33.1	67
Commercial silane	57.6	24.6	33.0	17

The experimental data highlight that the Commercial silane film is very hydrophilic, with a contact angle of 17°, while both the silane mixture treated at different temperatures have a higher value. Between them, the silane mix treated at lower temperature is slightly more hydrophilic compared to the film treated at higher temperature. The differences are mainly due to the polar component of the surface (σ_S^P) that changes markedly between the samples. It seems that the increase of the reticulation causes a decrease of the amount of Si-OH groups as observed by FT-IR and, consequently, leads to an increasing surface hydrophobicity.

Electrochemical impedance measurements were carried out to electrochemically characterize the hybrid films. A classical three electrodes arrangement was used: an Ag/AgCl (+0.207 V vs. SHE) electrode and a platinum ring were used as reference and counter electrode, respectively. The frequency range used for these measurements was from 100 kHz to 10 mHz while the signal amplitude was 5 mV. The immersed area was 7.1 cm². The electrolyte solution was 0.1 M NaCl.

Figure 2.23 and Figure 2.24 show the impedance modulus and phase after 1 and 7 days of immersion in the electrolyte solution, respectively.
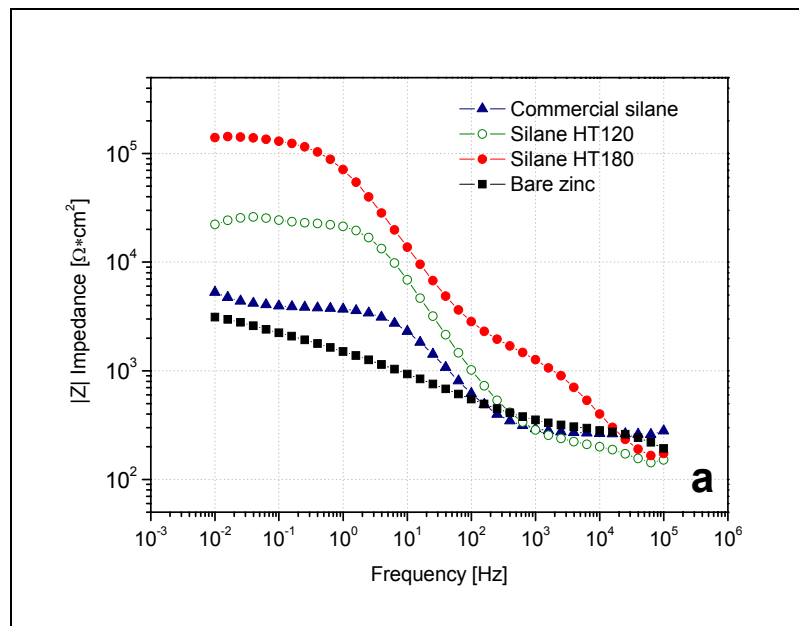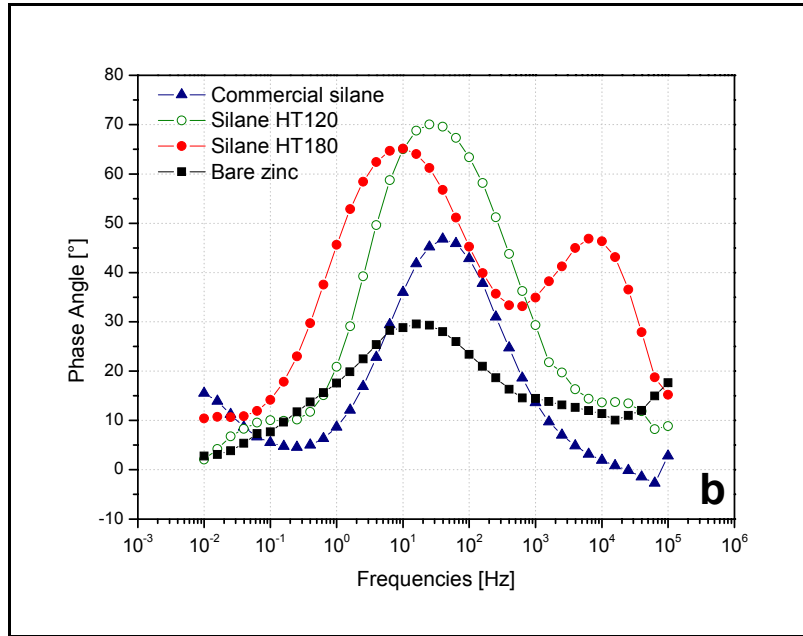
Figure 2.23 Impedance modulus (a) and phase (b) after 1 day of immersion in 0.1M NaCl solution
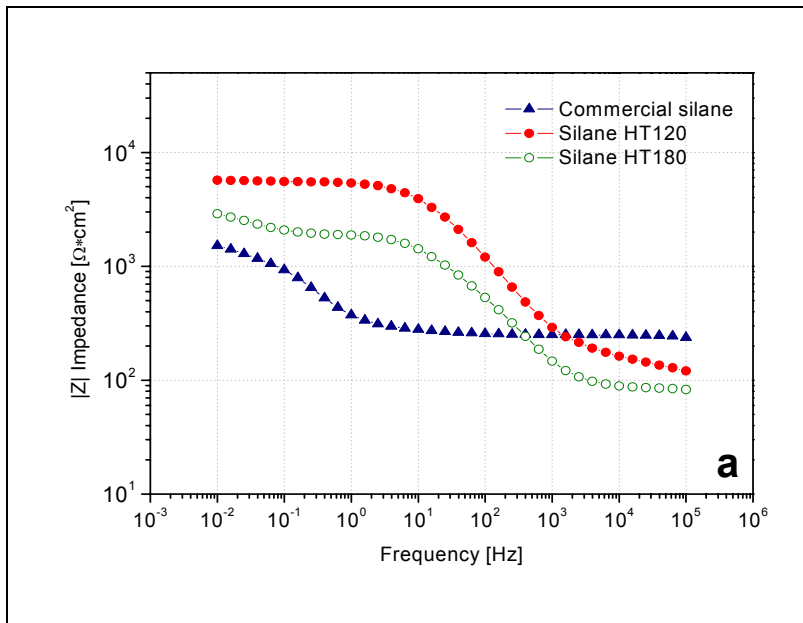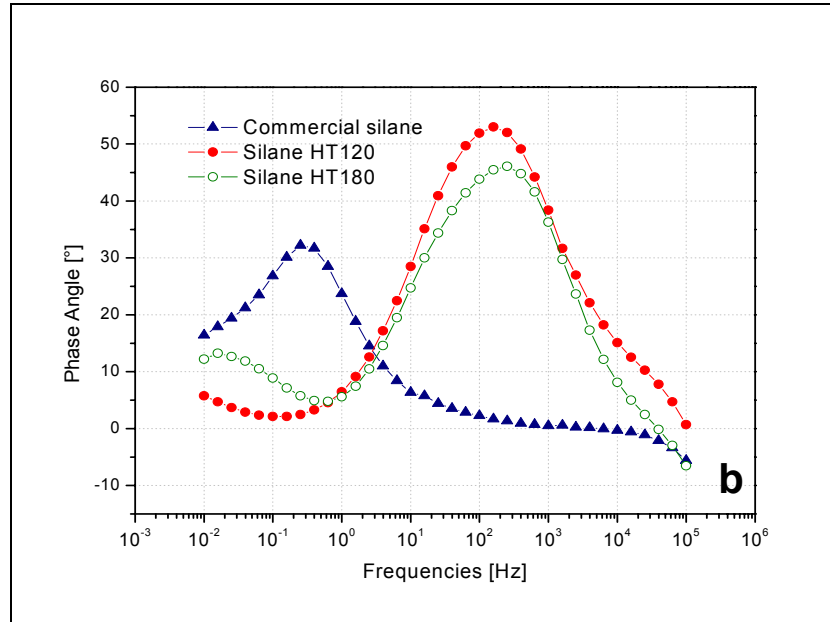
Figure 2.24 Impedance modulus (a) and phase (b) after 7 days of immersion in 0.1M NaCl solution

The sample Silane HT180 maintains a high value of the total impedance also after 7 days of continuous immersion in the conductive solution. The barrier properties of this film seem to be good and probably correlated with the dense and stable network of Si-O-Si bonds. Instead of this, the sample treated with the same silane solution, but cured at lower temperature, shows a decrease of the low frequency impedance modulus. However, the value of the total impedance after 1 day of immersion and the value of the phase angle at intermediate frequencies indicates that the film ensures a slight protection of the substrate. Figure 2.25 shows the absolute values of the low frequency impedance modulus

(about 10^{-2} Hz) for the different treated samples and for the untreated galvanized steel as a function of the immersion time in the electrolyte.
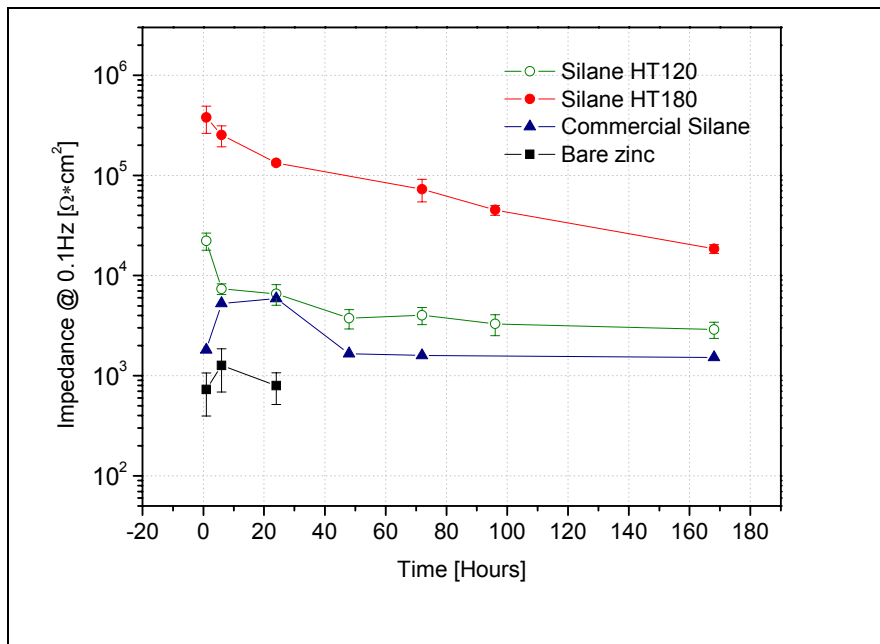
Figure 2.25 Absolute values of the low frequency impedance modulus vs. immersion time in 0.1M NaCl solution

The impedance data of the uncoated samples only refer to the first hours of immersion because of the formation of corrosion products that affects the measurements.

It is important to underline that silane hybrid films are not designed to interact directly with a corrosive solution, but to be actually a coupling agent. Thus even if a good initial barrier effect is observed, this barrier will be more or less rapidly degraded by the electrolyte resulting in the initiation of metallic

corrosion. The commercial silane shows the lowest performances. It was demonstrated by means of contact angle measurements that the film is very hydrophilic. Thus, the electrolytic solution probably swells easily the commercial film and the barrier properties decrease immediately after the first hours of immersion. Considering the impedance phase in Figure 2.23b, it is interesting to note that the silane sol-gel treated samples show two clearly visible time constants, even if localized at different frequencies. The first time constant (observable in the high-medium frequencies domain) is commonly related to the sol-gel film itself, while the meaning of the second time constant (observable in the low frequencies domain) is not clear at all. The presence of this low frequencies time constant was observed with measurements performed on similar samples and it has been the object of several studies [109]. However, the correct physical meaning is still unknown but it may be related to differently reticulated layers of the film itself.

The electrochemical properties of the film were also investigated by means of anodic and cathodic polarization measurements. Figure 2.26 shows the polarization curves collected after 1 hour of immersion in the aggressive solution (3.5 w/w% NaCl). To collect the experimental data, the same electrodes arrangement used for the impedance measurements was employed.

Great differences are observable between the cathodic polarization measurements performed on different samples. In fact, there are about 3 orders of magnitude between the cathodic currents of the sample HT180 and the bare galvanized surface. Observe that all the silane coated samples have a lower cathodic current than the sample without any conversion film.
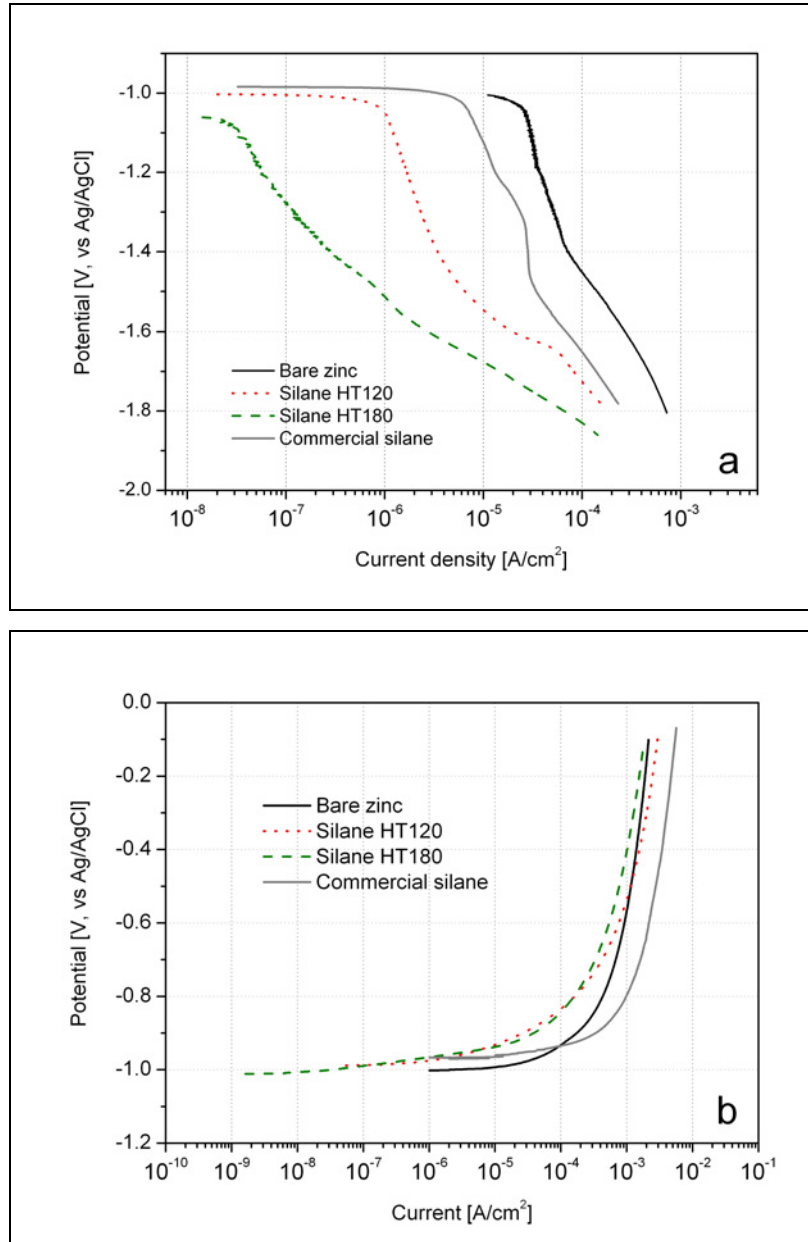
Figure 2.26 Cathodic (a) and anodic (b) polarization curves collected after 1 hour of immersion in the aggressive solution

The high degree of reticulation of sample Silane HT180 leads to very good barrier properties, underlined by the very low current density. Sample Silane HT120 shows a good inhibition of the oxygen reduction, even if not as effective as the sample cured at higher temperature. The commercial silane seems again to present the lowest protection properties. Despite the great differences in cathodic polarization, the anodic curves look very similar. In this last case, no evident differences are noticeable between the different samples. The commercial film has a slightly higher current density respect to the other samples, but the differences are negligible. Probably the protection ensured by the silane film against corrosion is related to the good oxygen barrier properties of the studied sol-gel films which lead to low cathodic current densities of all the investigated samples.

The properties of the coupling films were also checked using an industrial and qualitative test such as the exposure to the salt spray chamber. Figure 2.27 and Figure 2.28 depict the experimental results after 24 and 72 hours of exposure, respectively.

Figure 2.27 Appeareance of the samples after 24 hours of exposure in the salt spray chamber
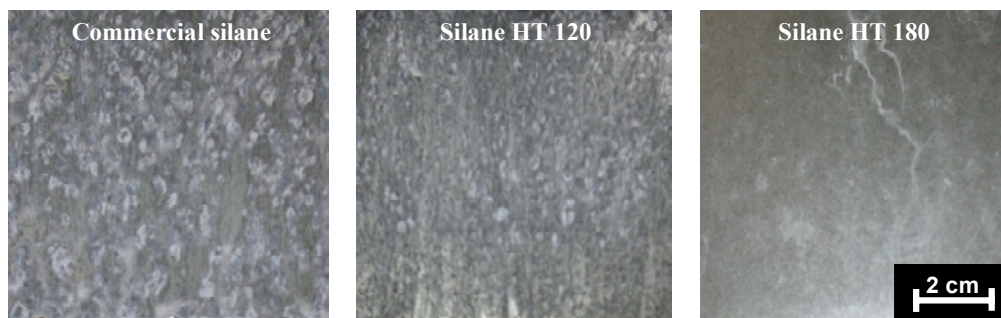
Figure 2.28 Appeareance of the samples after 72 hours of exposure in the salt spray chamber

This test confirms the results of the electrochemical measurements. Considering Figure 2.27, it is evident that after 24 hours of exposure the commercial silane treatment is completely deteriorated and huge amount of white rust (zinc corrosion products) is present on the sample surface. On sample Silane HT120 little quantity of white rust is present, while the coating of Silane HT180 looks undamaged and no white rust is observable.

After 72 hours of exposure the sample coated with the commercial silane is completely covered by corrosion products. On the Silane HT120 covered sample white rust is easily visible. The sample covered with Silane HT180 film begins to show a small amount of corrosion products. Despite silanes sol-gel films are coupling agents and, therefore, they are not designed to face directly an aggressive environment, the sample treated with the experimental mix ensures relatively very good barrier protection when exposed in the salt spray chamber. The network formed by the TEOS and MTES molecules probably lead to the formation of a reticulated film on the surface of the metal. The high

degree of intermolecular bonds (Si-O-Si) lead to the formation of a film with considerable barrier properties, in particular for a pre-treatment.

The sample treated with the silane sol-gel film shows good corrosion resistance in the very first days of immersion or exposure in salt spray chamber. Despite the very low thickness, silane sol-gel films ensure a very good inhibition of the cathodic reaction, up to 3 orders of magnitude respect to the bare HDG.

The curing treatment performed at 180°C improves noticeably the barrier properties of the sol-gel coating, enhancing the resistance against corrosion both in the salt spray chamber and in immersion in the sodium chloride solution. The commercial silane treatment shows worse performances than the experimental mixture silane sol-gel films. However, these kinds of pre-treatment are actually coupling agents. Thus, the performances of the complete protection system has to be investigated, in order to compare the potential of the different treatments as coupling agent between the inorganic substrate and organic coating. For this purpose, in the following paragraphs, the interaction between silane sol-gel films and two different kind of organic coating were investigated, in order to check the overall properties of the complete duplex system.

Interaction between the pre-treatments and powder coating

Powder coating is a widely used organic coating application technique. This technique allows obtaining homogeneous paint film with high impedance values. In addition, this is a solvent-free application technique, which does not imply the production of VOCs, dangerous for both human health and the environment.

By applying a powder coating onto the pre-treated samples it is possible to check the effect of the silane coupling film on the properties of the complete protection system. It is also possible to investigate if the heat treatment at high temperature affects the coupling potential of the silane molecules. In fact, it was proved in the previous paragraph that the curing at high temperature provides a high reticulation of the silane sol-gel film leading to the formation of a dense interconnection of Si-O-Si bonds. It is not obvious that this curing treatment is also convenient for the compatibility between the film itself and the organic coating.

As previously specified, an epoxy-polyester powder coating has been applied on the pre-treated samples. For comparison, the organic coating has been also applied on the untreated galvanized steel and on a fluozirconated galvanized steel sample, in order to characterise the interfacial stability, and thus the ability of the pre-treatment to assure coating adhesion even in the presence of defects, two different experimental approaches were used.

The samples with an artificial scratch were characterised using electrochemical impedance spectroscopy (EIS) measurements in order to monitor the loss of

adhesion. In addition, three different cathodic delamination tests were performed on scratched samples in order to measure the susceptibility to coating disbonding of each sample. The first cathodic disbonding test was carried out at constant potential, -1.2 V vs. Ag/AgCl for 5 days, in order to verify if it is possible to reduce the testing time while a second set of cathodic delamination tests was done using cyclic procedures, described in Table 2.7.

Table 2.7 Parameters of the cathodic delamination tests (OCP: open circuit potential)

Cycle 1 (x5)	OCP: 1 hour	DC: -1.6 V Vs Ag/AgCl during 30 min
Cycle 2 (x10)	OCP: 1 hour	DC: -1.3 V vs. Ag/AgCl during 5 hours

The EIS measurements were carried out on scratched samples. The performed scratches had a standard length of 20 mm and the thickness of the cutter (about 0.1 mm). The samples were immersed in a 0.3 w/w% Na_2SO_4 solution for 1 week. The progress of the corrosion phenomena was regularly monitored. Figure 2.29 and Figure 2.30 show, for example, the impedance modulus and phase after 1 hour and 48 hours of immersion, respectively.
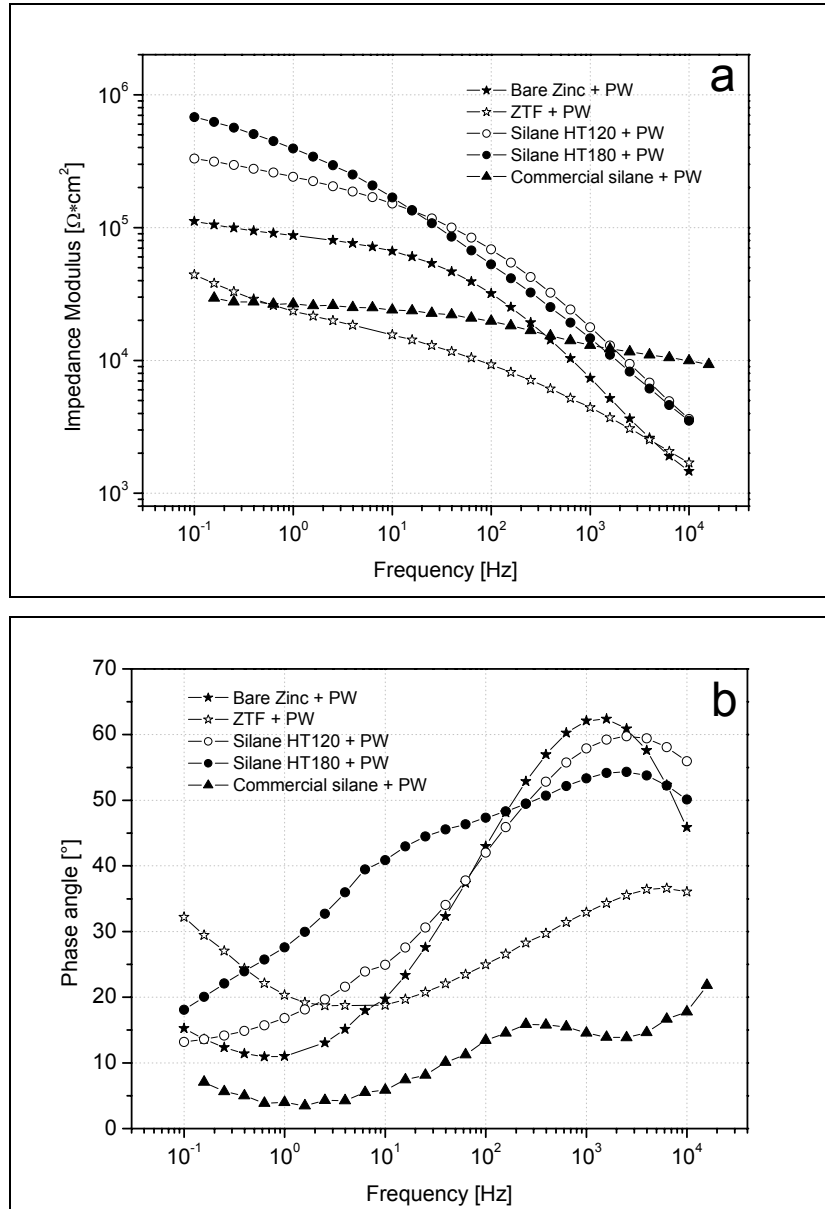
Figure 2.29 Impedance modulus (a) and phase (b) for the scratched samples after 1 hour of immersion in the electrolityc solution
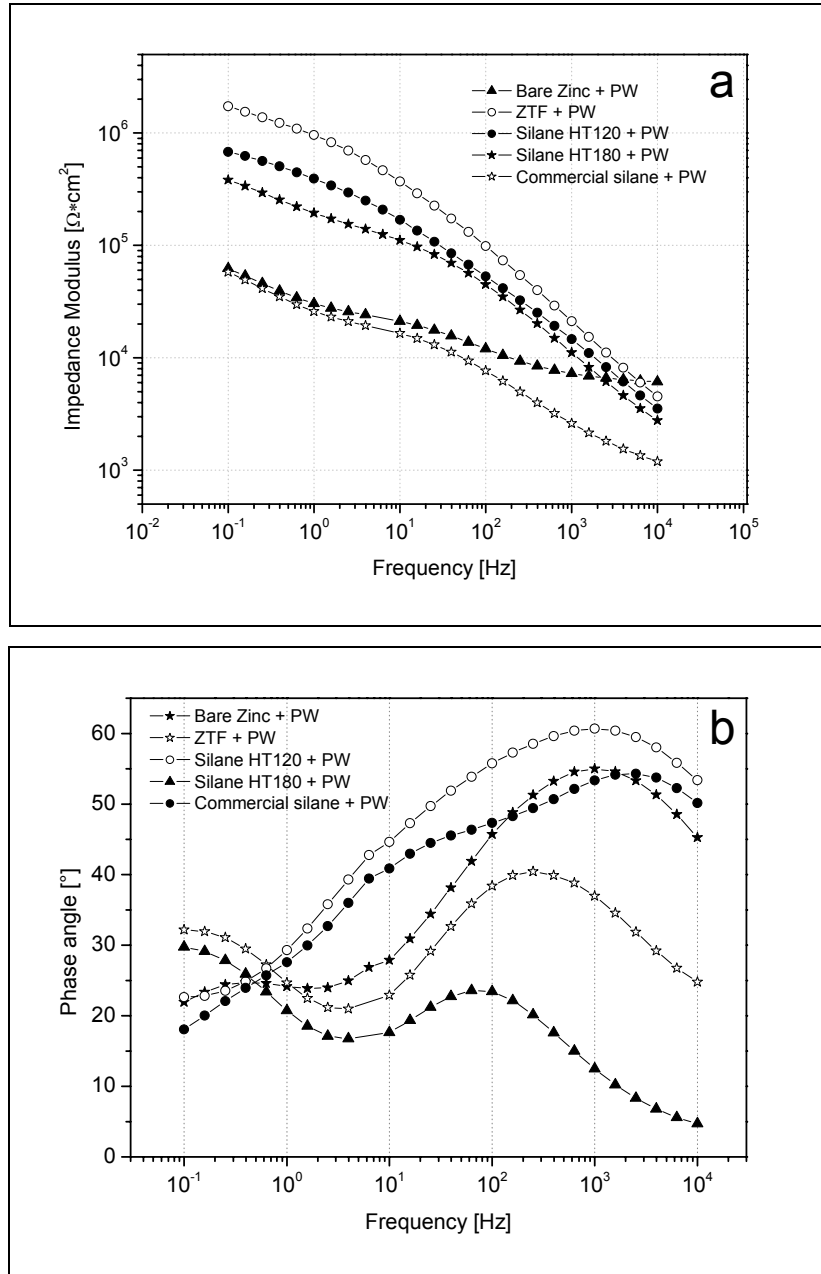
Figure 2.30 Impedance modulus (a) and phase (b) for the scratched samples after 1 hour of immersion in the electrolityc solution

The samples treated with the silane mix seem to ensure a better resistance against the penetration of the electrolyte between the metal and the coating. This fact is proved by the limited decrease of the values of impedance of these samples from 1 hour to 48 hours of immersion. In order to analyse in depth the behaviour of the silane mix treated samples, several parameters were extracted from the experimental impedance data modelling the impedance spectra with suitable equivalent electrical circuits. In addition to the electrical parameters describing the contribution to the impedance of the organic coatings (the pore resistance of the coating, R_p and the coating capacitance, C_c), generally not observed experimentally because of the macroscopic defect, two times constants are generally visible: one related to the presence of oxides and one related to the bare metal/electrolyte interface. To monitor the delamination process, the evolution of the high frequency time constant was analysed [110]. The capacitance value obtained is proportional to the exposed metal surface area. As a consequence, higher the capacitance value, higher the extent of the detachment between the coating and the substrate.

Figure 2.31 shows, as an example, the tendency of the capacitance at high frequency, C_{hf} (related, as previously described to the delamination process) for the sample without pre-treatments (bare galvanized steel coated with the organic coating).
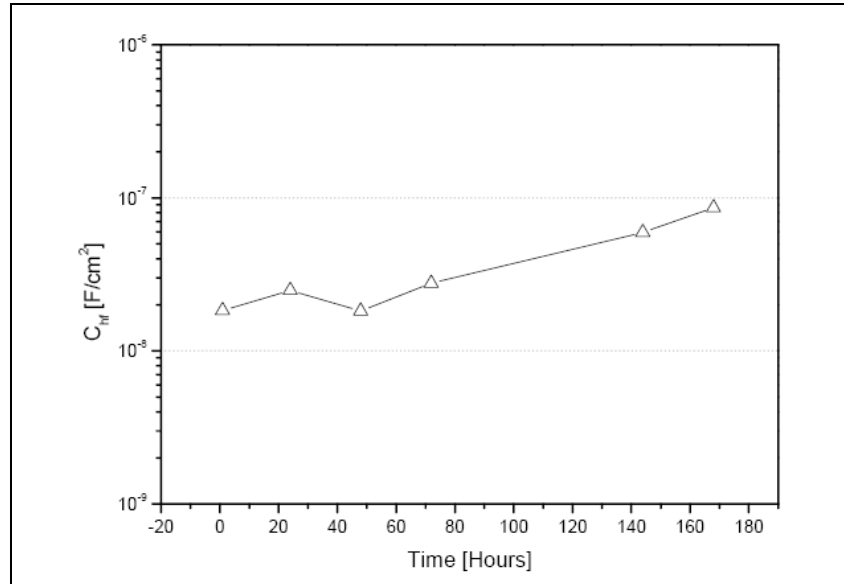
Figure 2.31 High frequencies capacitance of the bare galvanized steel coated with the powder coating vs. immersion time

It is clear that there is a continuous trend showing an increase of the capacitance related to the delamination process, which is common for all the materials. At the end of the test (120 hours of immersion), in order to compare the different silane pre-treatments, we calculated the ratio between the final C_{hf} value (after 120 hours) and the initial value (see Figure 2.32). This ratio is an indication of the enlargement of delamination, and smaller is the value, more stable is the interface.
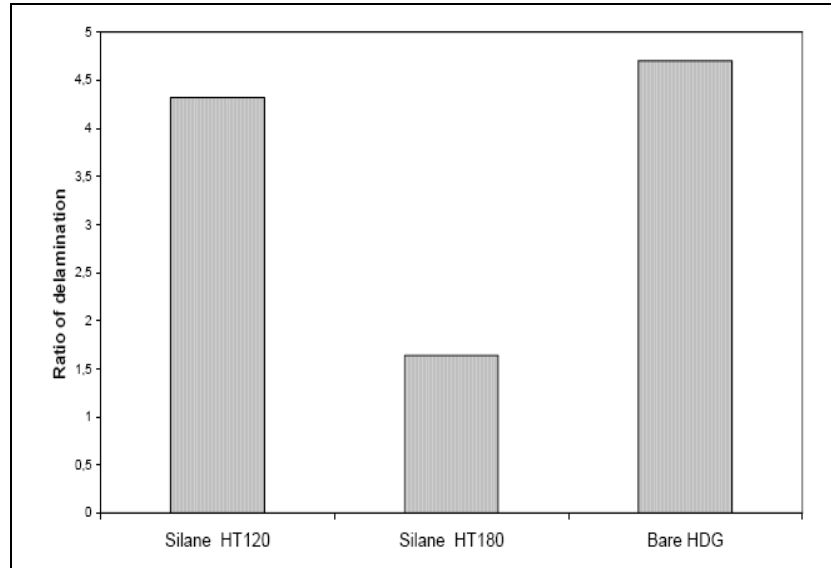
Figure 2.32 Extent of delamination (normalized) after the end of the immersion in the aggressive solution

From the data in Figure 2.32 it is clear that the stability of the silane mix cured at 180°C (Silane HT 180) is higher.

In order to better highlight the different resistances against the disbonding of the coating of the differently pre-treated samples, cathodic disbonding tests were performed. For this purpose, also in this case scratched samples were used. This experimental test was carried out with an arrangement similar to the one used for the EIS measurements, with the same electrolytic solution. However, differently from the previous test, an external voltage was imposed. In particular, a cathodic potential (with respect to zinc) was applied to the samples, in order to force the oxygen reduction on the metal surface and to consequently induce a strong increase of the local value of the pH. In fact, it is

well known [111] that alkaline pH strongly affects the stability of the metal/polymer interface. Moreover, in the case of the sol-gel pre-treated samples, the local increase of the pH, related to the production of OH⁻ groups from the cathodic reaction, can affect also the inorganic silica domains of the hybrid film.

The first delamination test was performed at constant potential (-1.2 V, vs. Ag/AgCl). The results, obtained after 5 days of conditioning are shown in Figure 2.33.
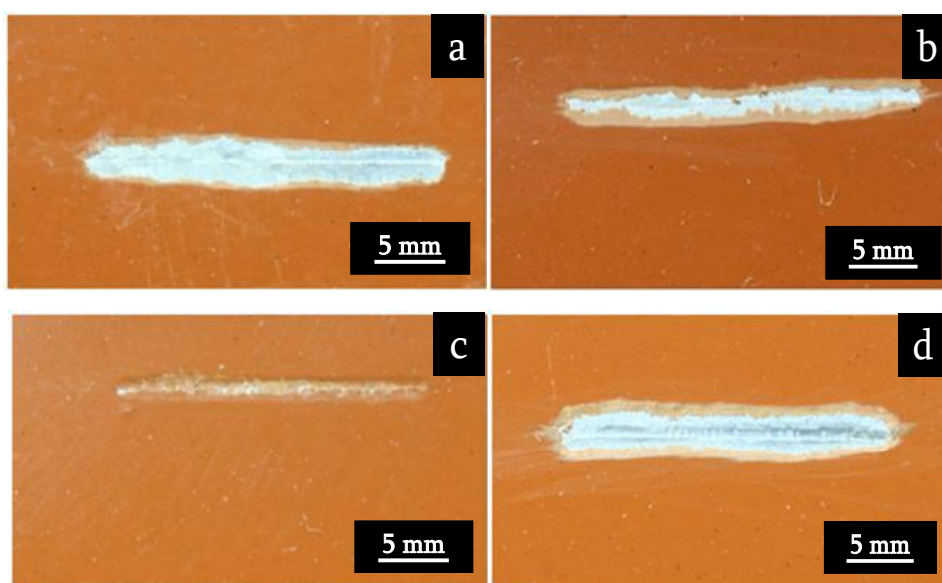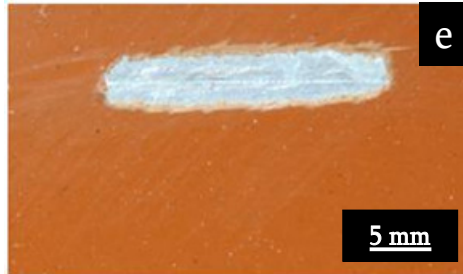
Figure 2.33 Appeareance of the different samples after 5 days os immersion @ -1.2 V (vs Ag/AgCl): untreated galvanized steel (a), Silane HT120 (b), Silane HT180 (c), Commercial Silane (d), ZTF (e)

In this case, the experimental results were analyzed qualitatively, owing to the ranking is evident: the silane mix samples (Silane HT120, Figure 2.33b, and HT 180, Figure 2.33c) show a limited delaminated area, while the samples fluozirconated (Figure 2.33e) and pre-treated with the Commercial silanes (Figure 2.33d) show a delaminated area very similar to the delaminated area of the samples without pre-treatment (Figure 2.33a).

In order to try to reduce the testing time, some cyclic cathodic delamination tests were performed following the parameters described in Table 2.7.

After the end of every complete cycle of the accelerated test the detachment of the coating has been evaluated by measuring the degree of linear delamination for each sample starting from the artificial defects. Table 2.8 (PW stands for powder coating) shows the linear extent of the detachment of the coatings at the end of each complete cycle. The extent is expressed as linear extent of the detached area from the artificial scratch.

Table 2.8 Linear extents of the detachment after the two different polarization tests

Sample	Linear extent of the detachment (mm)	
	Cycle 1	Cycle 2
Galvanized steel + PW	1.5 - 2.0	5.0 - 8.0
ZTF + PW	2.0	3.0
Silane HT120 + PW	0.0 -1.0	4.0 - 5.0
Silane HT180 + PW	0.0	1.0 - 3.0
Commercial silane + PW	1.5 -2.0	8.0 - 10.0

The data of Table 2.8 indicate the interval between the higher and the lower extent of the detachment among the three measurements performed. If only one number is present, it means that the three measurements overlap. Sample Silane HT180+PW shows the best performance in every experimental condition. The linear detachment for this sample is the lowest regardless of the cycle. The treatment with the experimental mix cured at 180°C ensures good adhesion between the metallic substrate and the coating. The clearest results are obtained with Cycle 2 (60 hours total testing time) where the different behaviour of the samples can be easily measured, proving the unsatisfactory behaviour of the commercial silane and the galvanized steel samples. Remark that these results are consistent with the electrochemical measurements and the delamination tests performed at constant potential, but the testing time is reduced by a factor at least two.

The adhesion between the organic coating and the pre-treated substrate was investigated also without forcing any electrochemical reaction on the metal

surface. In this sense, the adhesion was evaluated using a swelling solvent such as n-methyl-pyrrolidone (schematically reported in Figure 2.34).
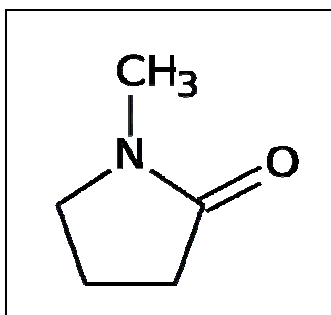

Figure 2.34 Schematic representation of n-methyl-pyrrolidone molecules

This molecule is able to swell the paint and to induce stresses between the polymer and the metallic substrate. With this procedure, in principle no corrosion reaction occurs on the metal surface during the time of the test. The lower the adhesion between the powder coating and the substrate, the earlier the detachment occurs. Figure 2.35 (a, b, c, d and e) shows the experimental results after 6 hours of immersion in the swelling solution at 50°C.
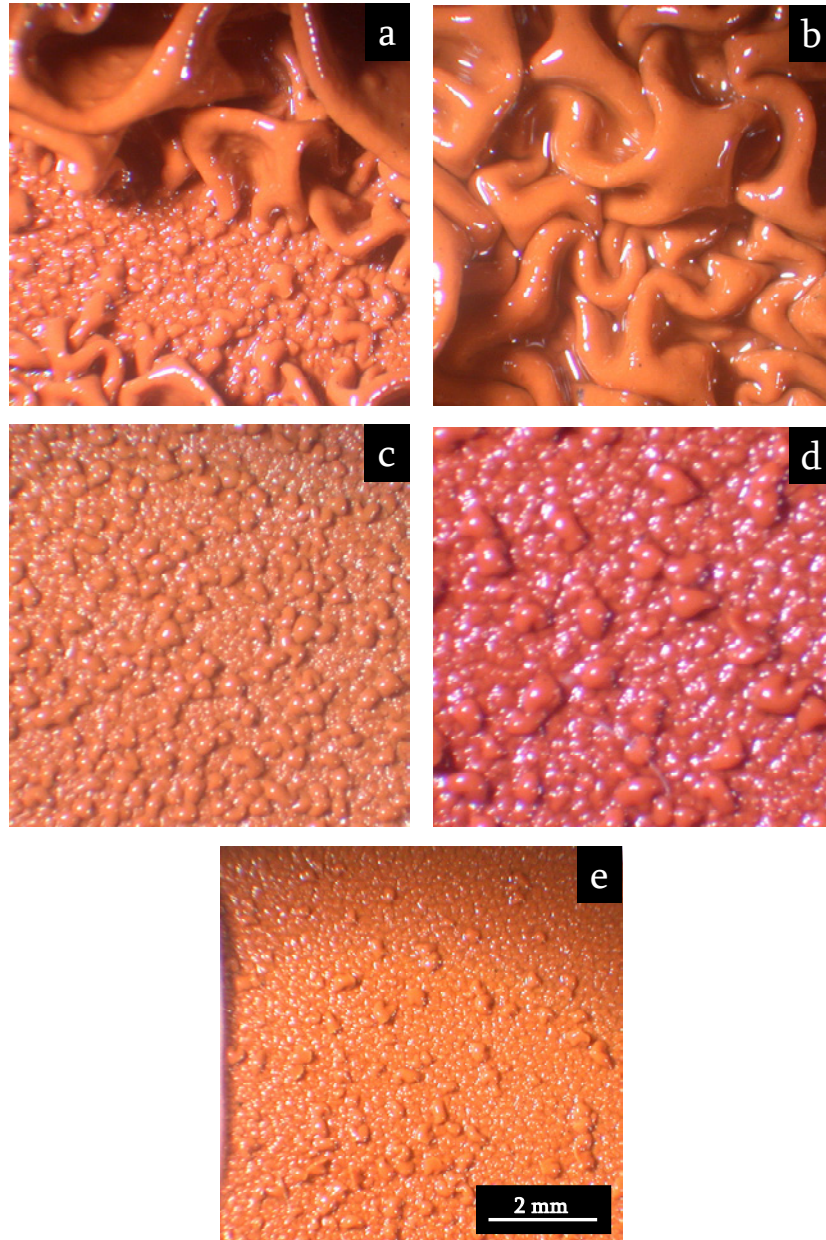
Figure 2.35 The appearance of the samples after 6 hours of immersion in n-methyl-pyrrolidone @ 50°C: untreated galvanized steel (a), ZTF (b), Commercial Silane (c), Silane HT120 (d), Silane HT180 (e).

The untreated sample and the sample with the ZTF conversion treatment (Figure 2.35a and Figure 2.35b, respectively) show a clearly visible detachment of the coating. Concerning the other samples, the detachment of the organic coating is not complete but a huge number of blisters are observable. Since this test is purely qualitative, sample Silane HT180+PW (Figure 2.35e) seems to ensure the highest adhesion between the substrate and the coating. This fact is highlighted by the lower density of blisters. Sample Silane HT120+PW (Figure 2.35d) and Commercial silane+PW (Figure 2.35c) are quite similar, even if the blisters of the sample treated with the experimental mix look bigger than the blisters on the commercial silane treated sample. The good results obtained with a curing temperature of 180°C must consider the fact that this temperature has not to be exceeded, because it is very close to the temperature at which the epoxy ring opens. This event has to be avoided because the premature opening of the epoxy ring can affect negatively the adhesion between the polymer and the hybrid film. This technological test partially corroborates the results of the other experiments. In particular it confirms the low adhesion between the samples treated with no silane coupling films. In addition, it confirms the very good performance of sample Silane HT180+PW. Note that, in this case, the sample treated with the Commercial silane does not behave as bad as demonstrated with other experimental tests (i.e. cathodic disbanding measurements). This fact can be explained by the assumption that the Commercial silane treatment ensures a rather good dry adhesion between the polymer and the substrate. Despite of this, when a scratch is performed on the surface, the silane film is directly in contact with the environment (or

83

aggressive solution, as in the experimental test) and it can be easily attacked. The test performed on the uncoated pre-treated samples proved the low resistance of this coupling film against a corrosive environment. In the cathodic disbonding test, the electrolyte is directly in contact with the cut edge of the coupling film and, thus, the conductive solution probably hydrolyzes it and penetrates through the interface between the polymer and the metal accelerating the detachment of the powder coating.

The characterization was completed by means of exposure of the scratched samples in the salt spray chamber. The experimental procedure was carried out in compliance with the ASTM B117 standard, performing an artificial "X-shaped" scratch on the painted samples using a cutting tool. The experimental results after 500 hours of exposure confirmed the different performances among the different samples (see Figure 2.36).
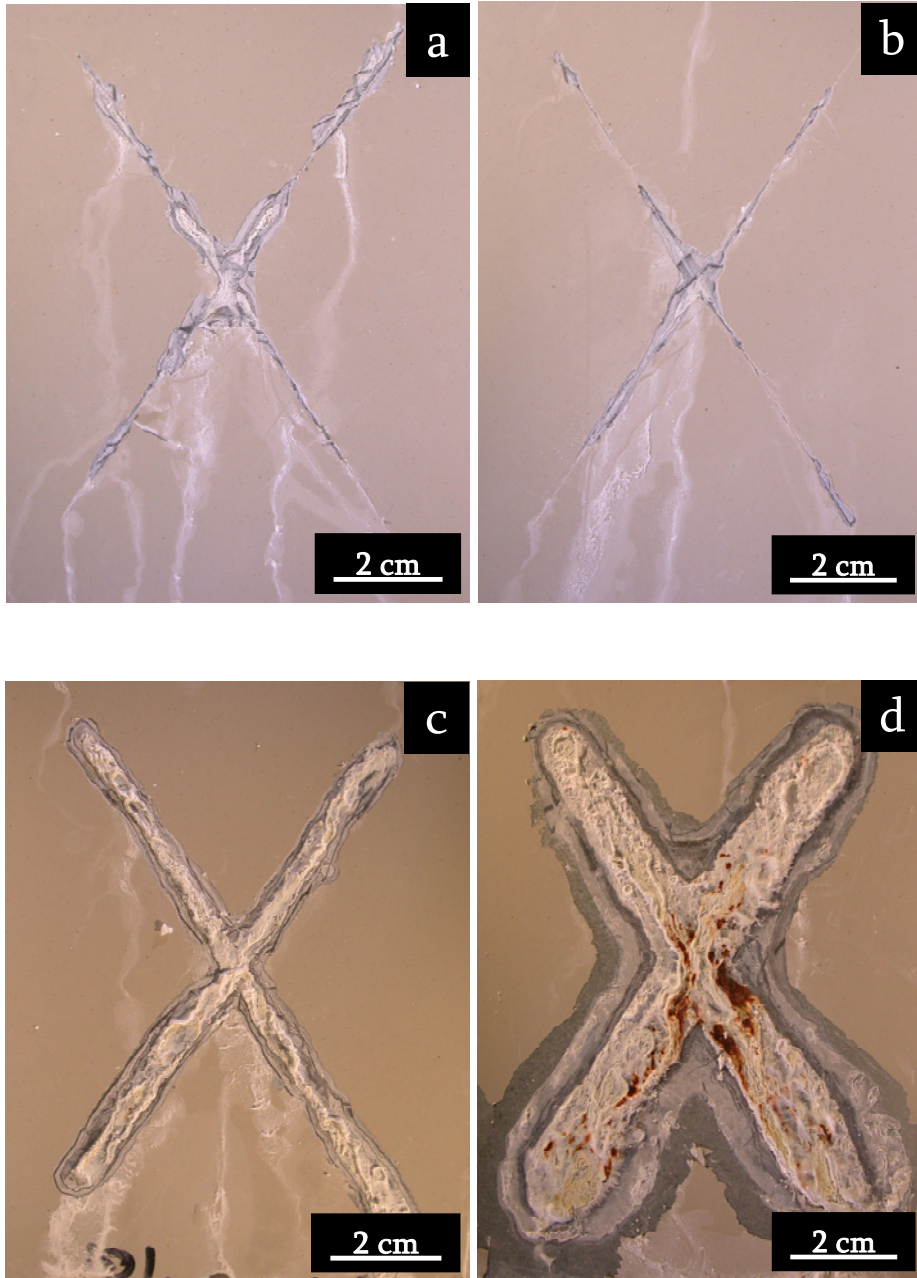
Figure 2.36 Scratched samples after: Silane HT120+PW (a), Silane HT180+PW (b), untreated galvanized steel+PW (c), Commercial silane+PW (d), ZTF+PW (e).

The sample pre-treated with the silane experimental mix and than cured at 180°C (Figure 2.36b) shows again the best corrosion protection performances. The extent of the detachment after 500 hours of exposure is very limited. Similar but quite lower is the corrosion resistance showed by the sample treated with the same sol-gel mixture but cured at lower temperature. The extent of detachment after the exposure to the aggressive environment was properly quantified in order to better highlight the difference in corrosion protection performances of the differently pre-treated samples. Figure 2.37 summarizes the extent of coating detachment for all the studied samples.
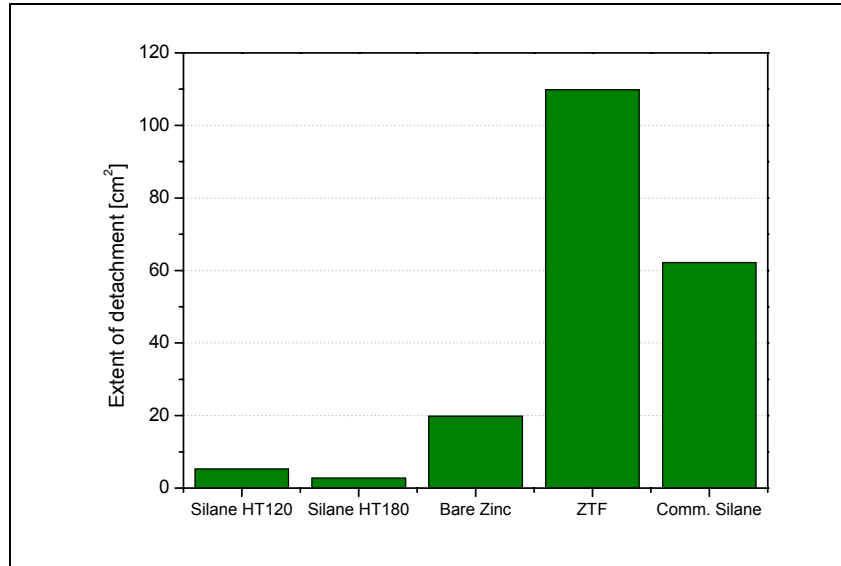
Figure 2.37 Extimation of the extent of coating detachment for all the studied samples after 500h in the salt spray chamber

The ZTF pre-treatment as well as the commercial silane shows a negative effect on the adhesion between the polymer and the substrate, leading to very bad results after the exposure in the salt spray chamber. In fact, the extent of the detachment of the organic coating for the uncoated sample is even lower.

Interaction between the pre-treatments and cataphoretic coating

Nowadays, cathodic electro-coating is a widely used technique for the application of primer layers for the protection against corrosion [112]. The cataphoretic electro-deposition is a widespread technique used in many fields, in particular in the automotive industry, for the protection of the automobile

bodywork [113,114]. This deposition method has numerous advantages, such as high protection against corrosion of the coating and high material utilization, but it is also an environmentally friendly technique, owing to the absence of organic solvents (it is an aqueous system) [115]. This last statement is growing of importance, in the light of the recent legislation restriction in the use of organic solvents containing VOCs (volatile organic carbon) [116].

Differently from the previous paragraph, first of all a simulation of the deposition conditions of the cataphoretic coating on the silane pre-treated galvanized steel samples was carried out. The aim is to determine if the electro-coat conditions destroy or not the silane pre-treatment. Indeed, the electro-coat is accompanied by a hydrogen release on the surface on the galvanized steel samples (the cathode) [117]. This release can generate degradation or destruction of the pre-treatment. The estimation of the produced damage was investigated by means of electrochemical impedance spectroscopy (EIS), comparing the impedance spectra before and after the simulation. In order to deeply investigate the effect of electro-coating conditions on the silane sol-gel film, two different thickness of the sol-gel coating were investigated, both cured at two different temperatures. The second part of the paragraph deals with the analysis of the performances of the cataphoretic coating applied on the different silane films. The characterization of the corrosion protection cycles was accomplished by EIS measurements and exposures in salt spray chamber. In this case the characterization of the protection system is not as detailed as in the case of the powder coating. In fact, as previously evidenced, the cataphoretic film is a primer and is not a final coating, as the powder coating investigated in

the previous paragraph. For this reason, the investigation was mainly focused on the compatibility between the powder electro-coating and the pre-treatments with respect to the complete protection system containing the powder coating [118]. In addition, in this part of the work, the pre-treatments performed in the acid zirconium compounds solution, as well as the silane SIVO® commercial treatment, were not analyzed any more. In fact, the first is not commonly used as pre-treatment prior a cataphoretic deposition, while the commercial treatment is no more investigated because the supplier do not considered it a suitable product for this kind of application. The compatibility between the electro-coat and the experimental silane sol-gel films treated at two different temperatures (120 and 180°C) were compared only to the uncoated galvanized steel substrate.

Prior to the application of the cataphoretic coating, the effect of a simulation of the electro-coat conditions on silane layer properties was investigated. The main goal of this simulation was to determine if the electro-coat conditions destroy or not the silane pre-treatment. The simulation of the electro-coat was performed in a Na_2SO_4 aqueous solution, modifying its pH to 6 and the conductivity to 1600μS. This solution simulates the most important parameters of the cataphoretic paint bath during electrocoating process. A stainless steel panel was used as anode, while the sol-gel coated samples were used as cathode. In the cataphoretic process the cathode corresponds to the target to coat with the paint. In this study, a current of 2 mA/cm² was applied on the sample during 10s and 20s. These conditions are slightly more drastic than the conditions used to study the building layer mechanisms (around 1 mA/cm2). A

time between10s and 20s is representative of induction time before organic coating formation at constant current. After this induction period, the film forms and the risk of pre-treatment degradation becomes limited.

The effect of the electro-coat conditions were investigated prior the deposition of the electro-coating. The highly alkaline environment and the consequent hydrogen release on the cathode can affect the properties of silane sol-gel film and can lead, eventually, to the complete degradation of the layer. The destruction of the silane sol-gel film not only affects the adhesion with the polymer, but it also leads to the formation of a heterogeneous deposition of the organic coating. The distance between the anode and the cathode was maintained constant for all the simulations.

Following the Ohm law, at constant current the film resistance is directly proportional to the applied voltage. Figure 2.38 shows the evolution of voltage as a function of time at constant current (less than 1 mA/cm^2). This graph illustrates the kinetics of film formation: the resistance increases with the thickness of the film.
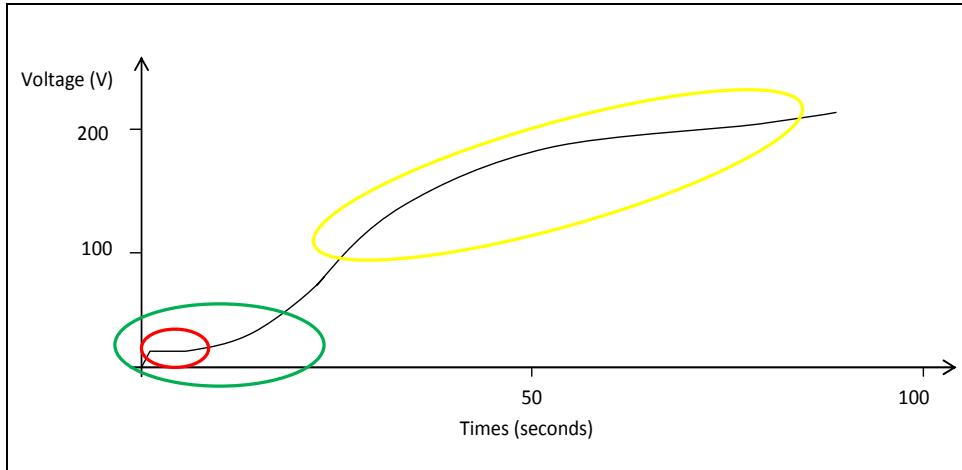
Figure 2.38 Simulation of film formation: voltage vs. time at constant current (about 1 mA/cm²)

Considering the graph depicted in Figure 2.38, three parts can be distinguished:

- in red, a first part corresponding to water electrolysis at the cathode. This part represents the time to reach the pH corresponding to electro-coagulation. Film resistance is practically zero.

- in green: electro-deposition begins. The film resistance slightly increases.

- in yellow: the increase of the resistance corresponding to film formation. The rate of the film formation progressively decreases as the coating thickness increases due to the high resistance of electro-coating.

In this study, a current of 2 mA/cm² was applied on the sample during 10 s and 20 s. These conditions represent the mean real application conditions just before the coating formation. After this induction period, the film forms and the risk of pre-treatment degradation becomes limited.

In addition to the effect of the curing temperature, different thicknesses of the silane sol-gel film were investigated. In fact, conveniently modifying the deposition and curing conditions it is possible to obtain silane film with different thicknesses and, consequently, different electrochemical properties. In particular, four different silane pre-treatments obtained by modifying the sol-gel deposition conditions and the curing temperature were tested. A VG Escalab 220iXL X-rays photoelectron spectrometer (monochromatic AlK radiation at 1486.6 eV) was used to measure the thickness of the silane sol-gel film. The samples were eroded using a 3keV Argon beam operated at a target current of 1 μA, and rastered over an area of 3·3 mm². Table 2.9 reports the different silane sol-gel film applied onto galvanized steel and their respective thickness, measured by means of XPS.

The experimental results obtained by means of XPS proved that the samples named "A" are thinner than the samples "named" B. In fact the thickcness corresponding to the "A" samples is about 120 nm while the thickness corresponding to the "B" samples is about 300 nm.

Table 2.9 Mean thickness of the different silane sol-gel films

	Silane sol-gel films	
Sample	Curing temperature (°C)	Thickness (nm)
A 120	120	~ 120
A 180	180	
B 120	120	~ 300
B 180	180	

In addition, the atomic percentage as a function of the depth profile for sample A120 is reported in Figure 2.39 for example. The zinc can already be detected at 20 nm: this is due to the high roughness of the galvanized substrate.
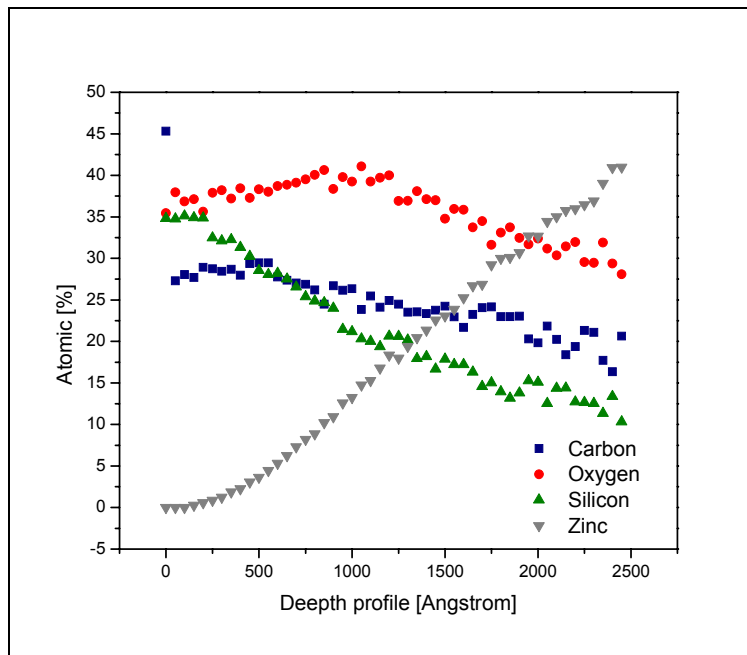

Figure 2.39 XPS profile of the silane film A120

It is likely that the two different curing temperatures lead to a different degree of densification of the silane sol-gel network.

The simulation of the electro-coating process was carried out following the previously described procedure. The silane sol-gel coated samples were conditioned for 10s and 20s applying 2 mA/cm². According to the cathodic electro-deposition the silane treated sample was used as the cathode for the simulation of the deposition conditions.

The effect of the simulation on the properties of the sol-gel layer are reported in Figure 2.40 and Figure 2.41 for the samples A120 and A180 , and in Figure 2.42 and Figure 2.43 for the thicker samples, B120 and B180. In these Figures it is possible to appreciate the extent of the degradation of the silane sol-gel layers do to the effect of the hydrogen bubbling and alkaline environment occurring at the cathode during the electro-deposition simulation.
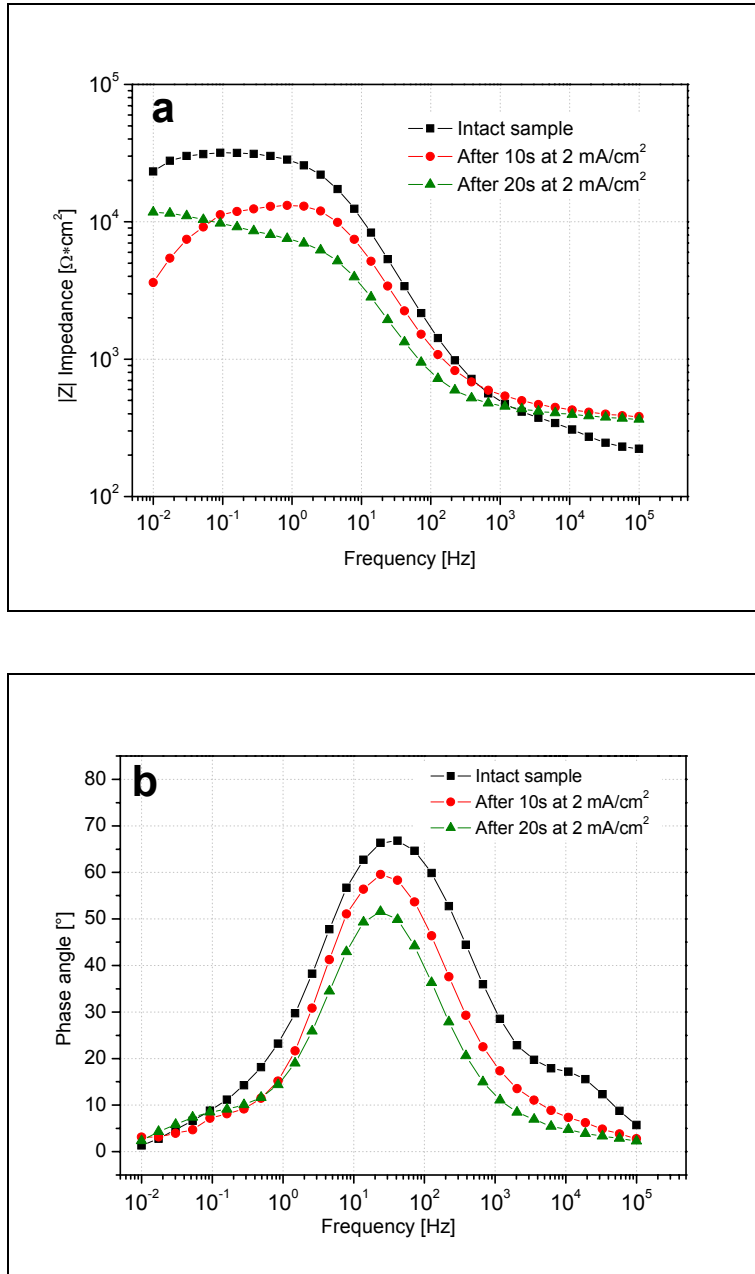
Figure 2.40 Impedance modulus (a) and phase (b) for sample A120 after 1 hour of immersion in the electrolytic solution
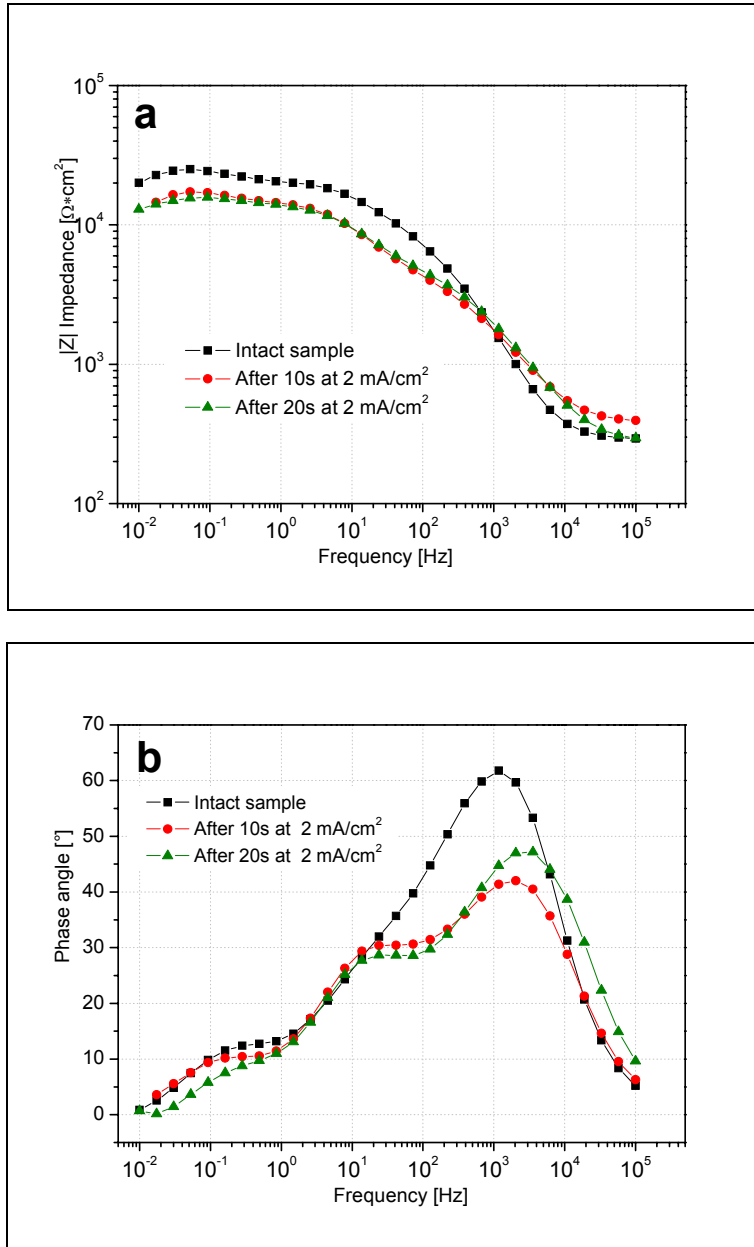
Figure 2.41 Impedance modulus (a) and phase (b) for sample A180 after 1 hour of immersion in the electrolytic solution
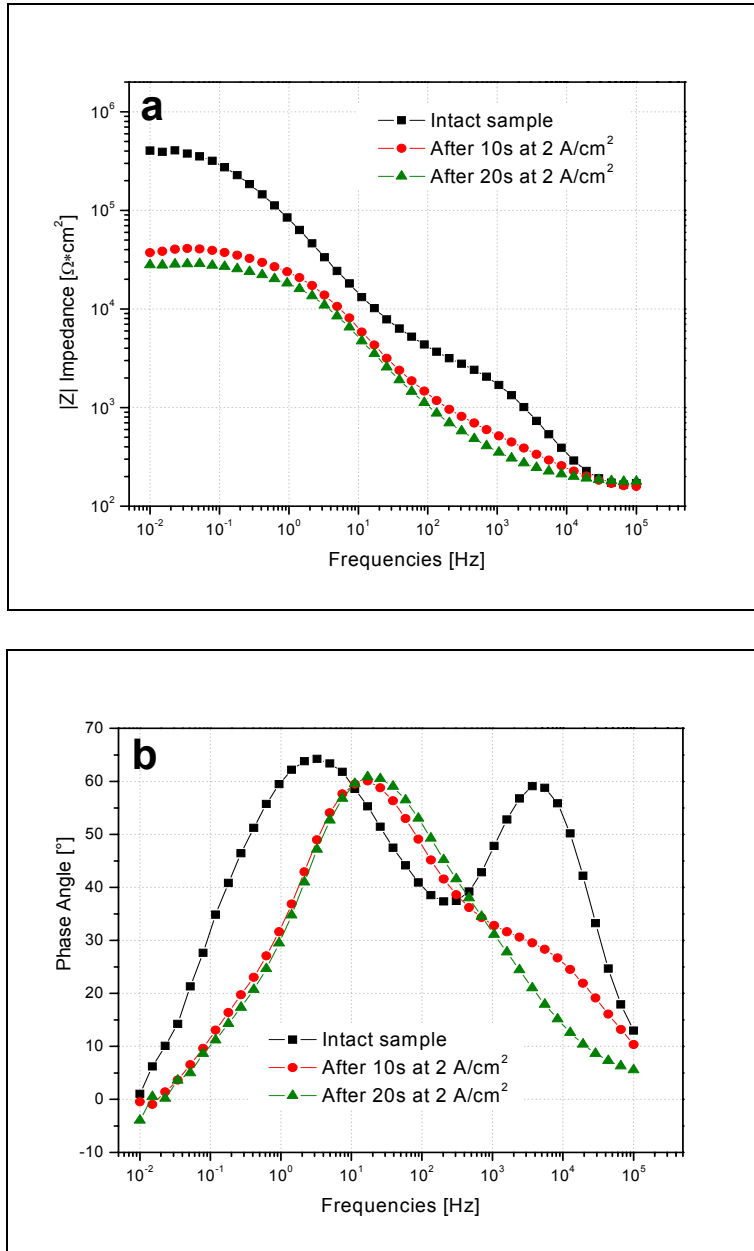
Figure 2.42 Impedance modulus (a) and phase (b) for sample B120 after 1 hour of immersion in the electrolytic solution
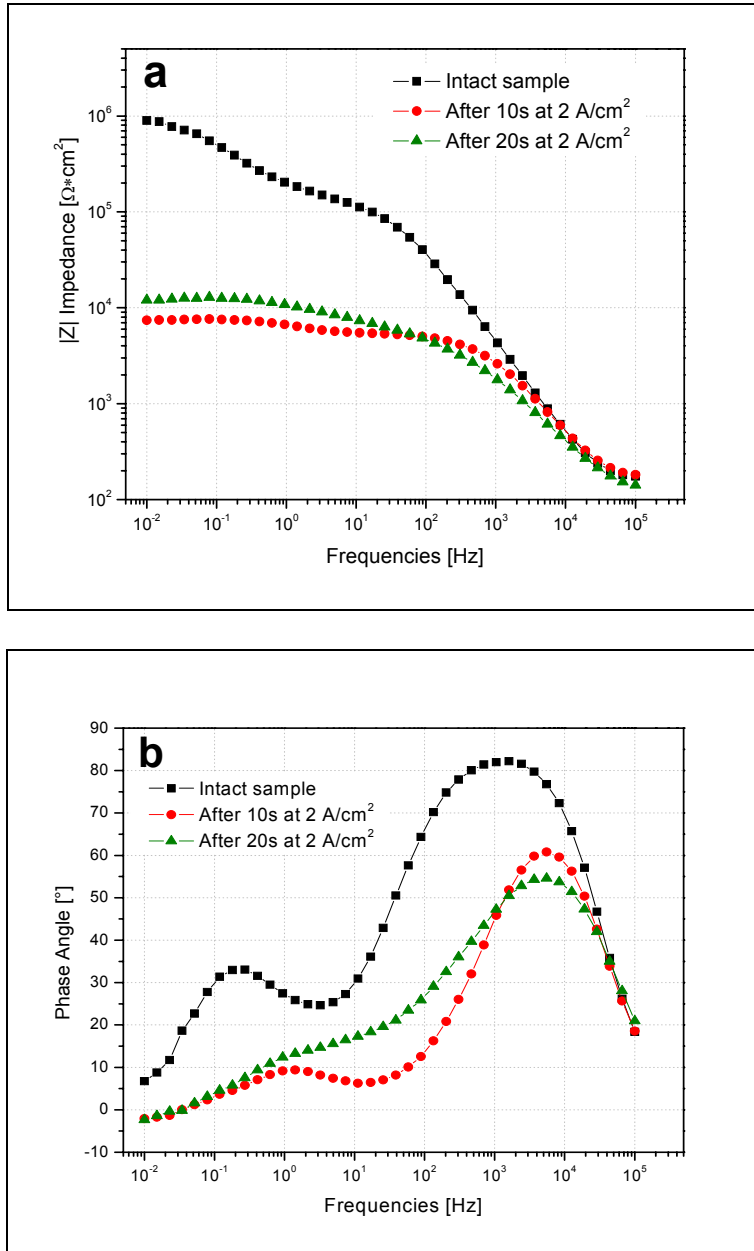
Figure 2.43 Impedance modulus (a) and phase (b) for sample B180 after 1 hour of immersion in the electrolytic solution

First of all, notice the great differences between the impedance at low frequencies of the two different kinds of samples. The samples with the thinner sol-gel film are characterized by values of the low frequencies impedance in the order of 10^4 $\Omega \cdot cm^2$, while in the order of 10^6 $\Omega \cdot cm^2$ the other samples. This difference is directly related to the different thickness of the samples. A higher thickness leads to higher barrier properties of the silane sol-gel film but also to an increasing electrical resistance during the electrodeposition. By considering the impedance modulus in Figures 2.43, 2.41, 2.42 and 2.43, it seems that the simulation leads to a considerable degradation of the properties of the thicker films. On the other hand, the thinner silane sol-gel layers show little decrease of the low frequencies impedance. In particular, sample A180 has very comparable values of the low frequencies impedance before and after the simulation. It is likely that the highest conductivity and lowest impedance of the low barrier samples lead to a lower extent of deterioration. This could be explained by a more uniform distribution of the current and hydrogen evolution on the entire surface. Indeed, the samples with high initial impedance does not allow the hydrogen evolution and the forced bubbling could be responsible of the decrease of the properties.

It is possible to evaluate the influence of the simulated deposition conditions by considering the phase diagrams of Figures 2.40, 2.41, 2.42 and 2.43. The high frequencies time constant (around 10^3 -10^4 Hz) is commonly related to the silane sol-gel film [119]. Thus, by monitoring the evolution of the maximum value of the phase angle of the first time constant, it is possible to detect the degradation of the silane sol-gel layer. For the sample A120 the first time

constant shows a very low phase angle even before the simulation. After the 20 seconds of simulation, the high frequency time constant is no more noticeable. The B120 silane behaves similarly. In fact, even if it shows an easily detectable high frequency time constant, the application of the 2 mA/cm^2 leads to a quick decrease of the silane sol-gel properties. The maximum value of the phase angle of the time constant at around 10^3-10^4 Hz shows a great decrease after 10 seconds of simulation, and eventually, it disappears completely after 20 seconds. The silane sol-gel films designed with high thickness show a huge decrease of the low frequencies impedance, up to two orders of magnitude. It is likely that this kind of pre-treatments have too high barrier properties, they are thick and, maybe, brittle. In spite of the correct reason, it is evident that the synergic effect of the hydrogen evolution and the local increase of the pH affect strongly the properties of this kind of films.

After the different simulations the low frequencies impedance are approximately the same for all the samples, in the order of 10^4 $\Omega \cdot cm^2$. Regarding the different conditioning time, there is a slightly different behaviour after 10 or 20 seconds of simulation. In general, the longest the application of the current, the highest is the damage of the silane sol-gel film.

Coating the silane pre-treated samples with the electro-coat paint will allow to verify if the degradation induced by the deposition conditions affects the final properties of the complete protection system.

According to the previously explained parameters, the electro-coat was applied on the different silane sol-gel treated samples and, for comparison, on bare

galvanized steel. The mean thickness of the coatings after curing is reported in Table 2.10.

Table 2.10 Mean thickness of the electro-coatings after the curing treatment

Samples	Thickness (μm)	
	Mean value	Standard deviation
A 120	19.9	1.4
A 180	21.6	2.2
B 120	19.9	1.5
B 180	18.8	1.7
Bare substrate	15.8	1.2

All the samples have a thickness around 20 μm, except for the bare galvanized steel sample, whose value is lower (about 15 μm). This fact is probably related to the high hydrogen activation overvoltage on zinc which requires a higher applied voltage or a longer time to obtain the alkaline pH inducing the coating electrocoagulation.

Electrochemical impedance spectroscopy measurements were carried out on the intact samples, in order to assay the properties of the applied coating. This technique highlights the presence of macroscopic defects by means of a drop of the value of the low frequencies impedance in the first hours of immersion. By means of impedance spectroscopy it is possible to check if the presence of the silane sol-gel layer promotes the deposition of an uniform and homogeneous polymer film. In fact, the degradation induced by the previously discussed

deposition conditions can affect the film formation and thus, the quality of the electro-coating and this can lead to the formation of a defective coating lacking in corrosion protection.

Figure 2.44 shows the impedance modulus and phase for the electro-coated galvanized steel. Notice that since the first hours of immersion the coating shows a relatively low value of the impedance modulus in the low frequency range (around 10^{-2} Hz) and a drop of the phase angle in the medium-low frequencies domain ($10^2 - 10^{-2}$ Hz).
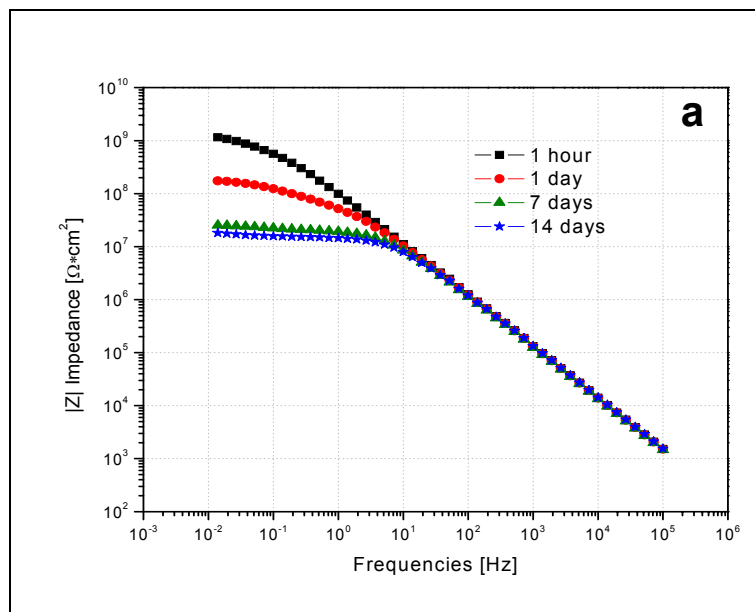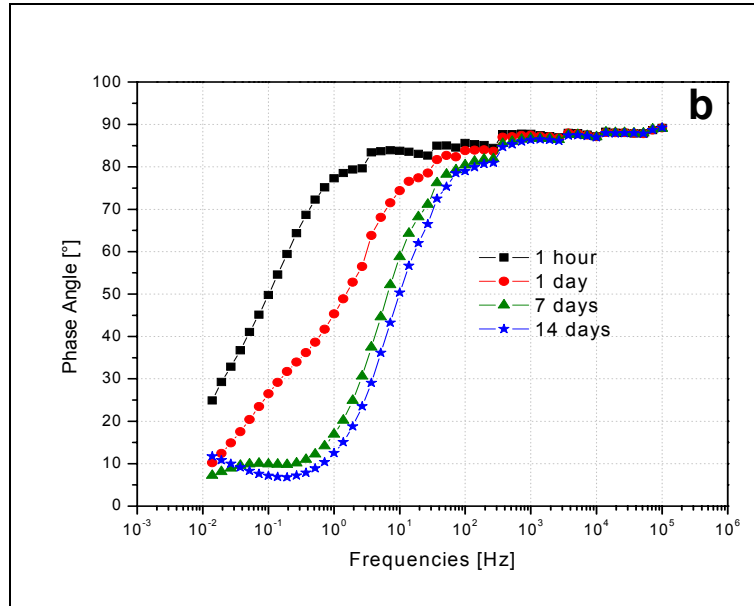
Figure 2.44 Impedance modulus (a) and phase (b) for the untreated electro-coated galvanized steel as a function of the time of immersion

It is commonly accepted that the total impedance in the low frequencies domain is an indicator of the protection properties of the organic coating. In this case, the electro-coating on the galvanized steel substrate is likely to be defected. Probably, one or more macroscopic defects are present in the coating and the electrolyte can easily reach the surface of the metal. In the light of the variables of the electro-coating process, the non uniform hydrogen activation overvoltage on zinc substrate can induce a non uniform hydrogen production and, locally, more intensive bubbling can be responsible of the presence of defects in the applied coating.

Figure 2.45 and Figure 2.46 show the impedance modulus and phase for the electro-coated A120 and A180 samples, respectively.
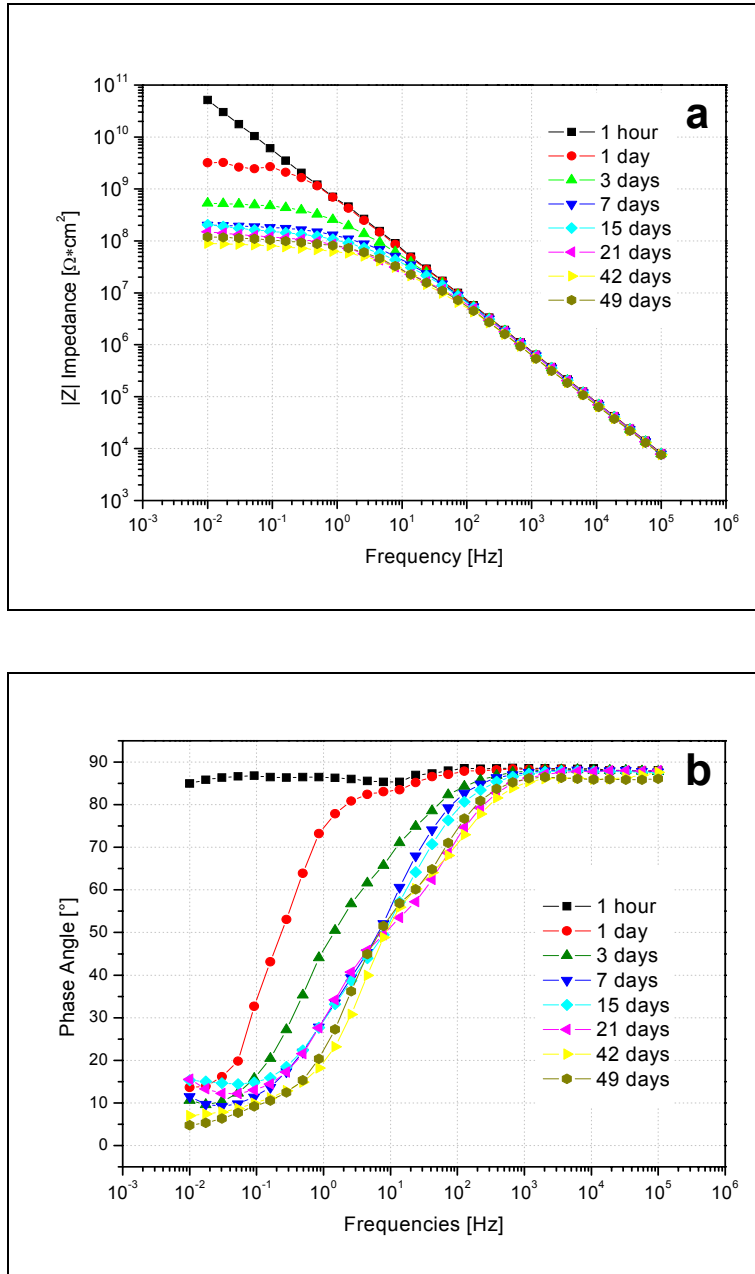
Figure 2.45 Impedance modulus (a) and phase (b) for the A120 electro-coated sample as a function of the time of immersion
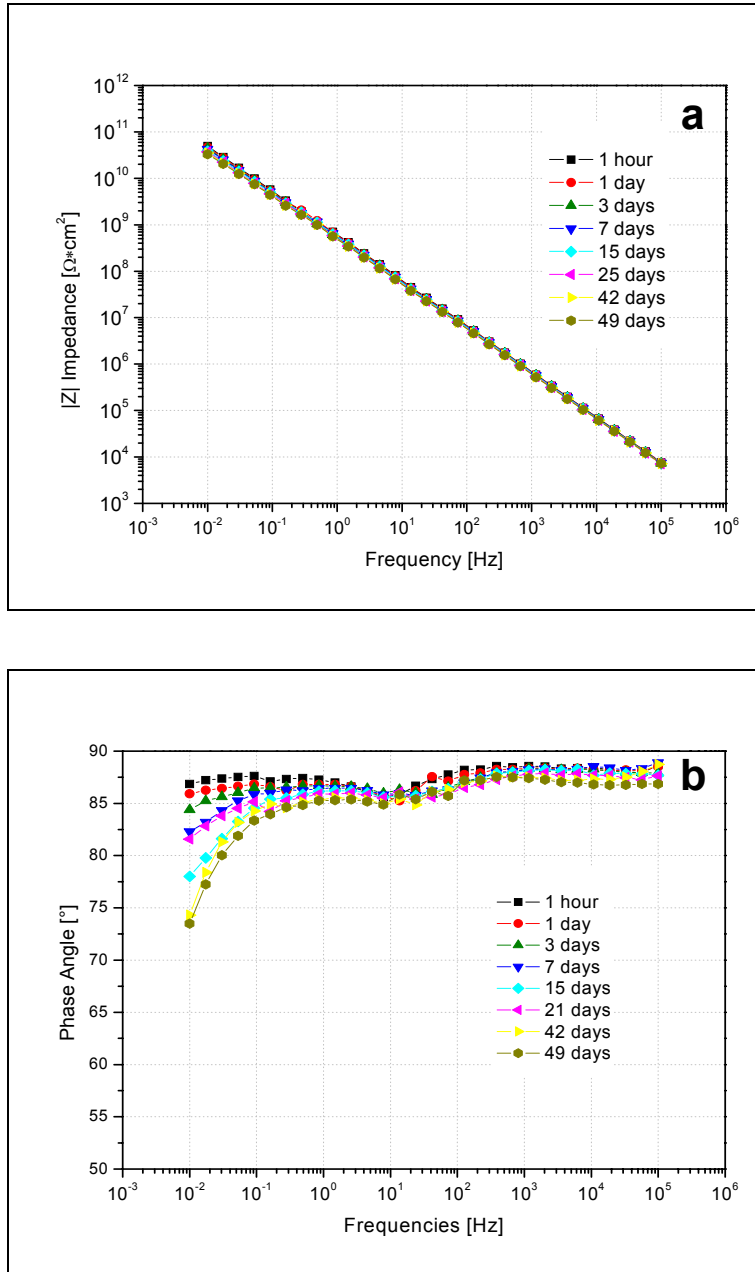
Figure 2.46 Impedance modulus (a) and phase (b) for the A180 electro-coated sample as a function of the time of immersion

The cataphoretic polymer applied onto the A120 pre-treated substrate shows a quick decrease of the low frequencies impedance. After 24 hours of immersion the total impedance drops to $2 \cdot 10^9$ $\Omega \cdot cm^2$, starting from the value of $1 \cdot 10^{11}$ $\Omega \cdot cm^2$ obtained after 1 hour of immersion. This fact indicates that, probably, also this electro-coating is defected. Instead, considering Figure 2.45, it is possible to appreciate that the electro-coat applied onto A180 silane sol-gel film does not show evidence of the presence of macro-defect. In fact, the impedance in the low frequencies domain is stable around the value of about $5 \cdot 10^{11} \Omega$ cm^2 during the 50 days of immersion. This coating seems to be free of macro-defects generated during the electro-deposition.

To better understand the behaviour of this last sample compared to the electro-coat A120, the electrochemical impedance spectra were modelled using the convenient equivalent electrical circuits [120]. For the electro-coated A180 sample a R(QR) equivalent circuit was used, where the first resistance is the electrolyte resistance (R_{el}), the second is the coating resistance (R_c) and the constant phase element (Q_c) is related to the coating capacitance. This equivalent circuit was also used for the very first hours of immersion of electro-coat A120 sample. After the initial immersion period, the spectra of this sample were fitted using a R(Q(R(QR))) equivalent circuit, adding another time constant representative of both the Faradic resistance of the metal interface (R_{ct}) and the double layer capacitance (Q_{dl}). The results of the fitting procedure are reported in Figure 2.47, which shows the values of the coating resistance (Figure 2.47a) and capacitance (Figure 2.47b) calculated from the acquired impedance spectra.

The presence of macro-defects in the coating applied on the A120 sample is evidenced by the drop of the corresponding coating resistance after about 1 hour of immersion (see Figure 2.47a). It was demonstrated [104] that the coating resistance R_c is related to the total number and the dimension of pores or capillary channels through which the aggressive solution reaches the interface. On the contrary, the electro-coating on sample A180 maintains high values of the coating resistance during the immersion time meaning that this coating is probably defect-free. Concerning the coating capacitance (see Figure 2.47b), observe that the values of the two different samples are very similar.
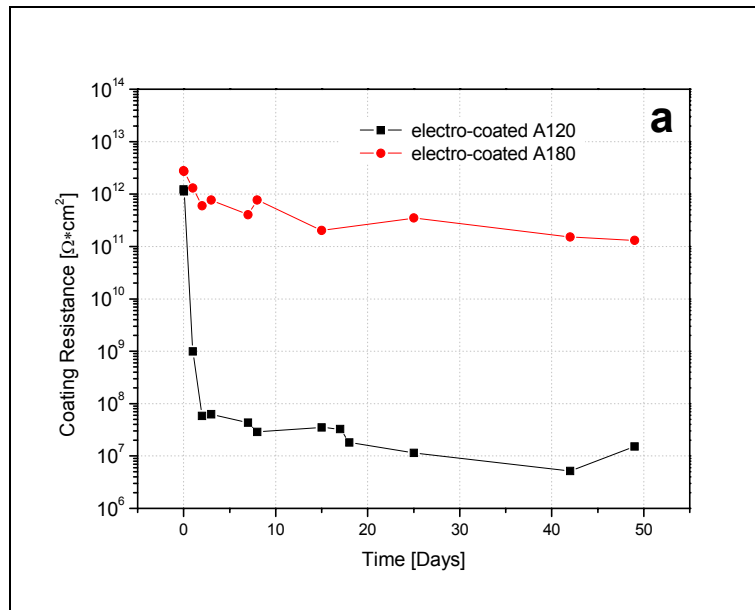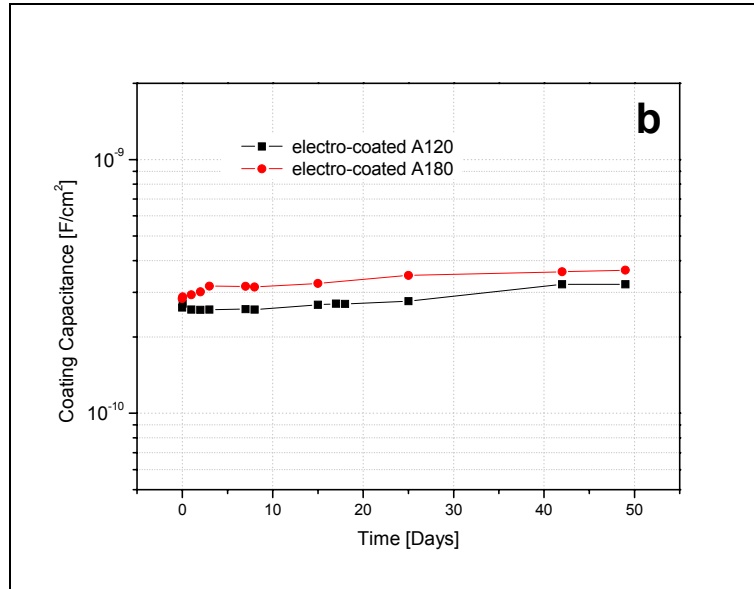
Figure 2.47 Coating resistance (a) and capacitance (b) of the electro-coat applied on samples A120 and A180 with the time of immersion in the conductive solution

It is well known that the capacitance is inversely proportional to the coating thickness. In the light of this statement, the capacitance values can be considered essentially the same, considering that the electro-coated A180 sample has a slightly higher average thickness. The experimental results summarized in Figure 2.47 suggest that there are probably a few macro-defects on the coated A120 sample, big enough to allow the electrolyte to pass through very quickly and to reach easily the surface of the metal, but not so many to influence dramatically the water absorption.

The impedance modulus and phase of the electro-coated B120 and B180 samples are reported in Figure 2.48 and Figure 2.49, respectively.
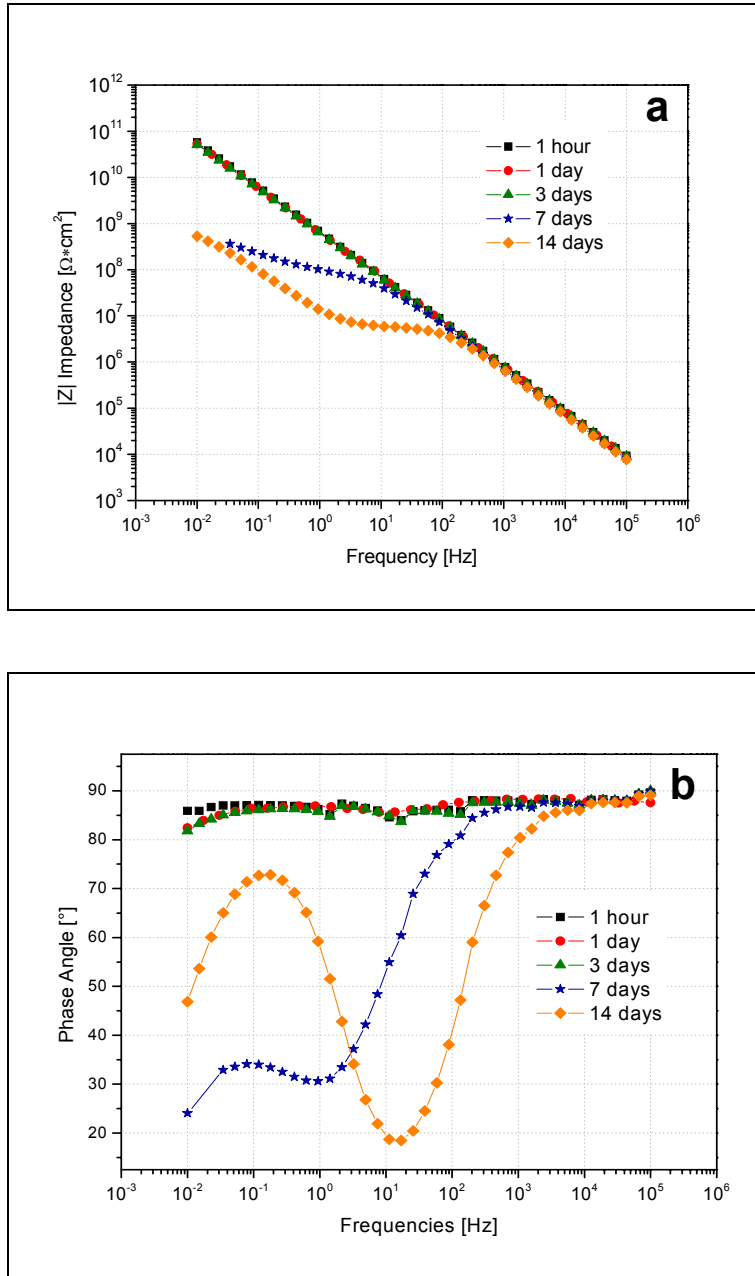
Figure 2.48 Impedance modulus (a) and phase (b) for the B120 electro-coated sample as a function of the time of immersion
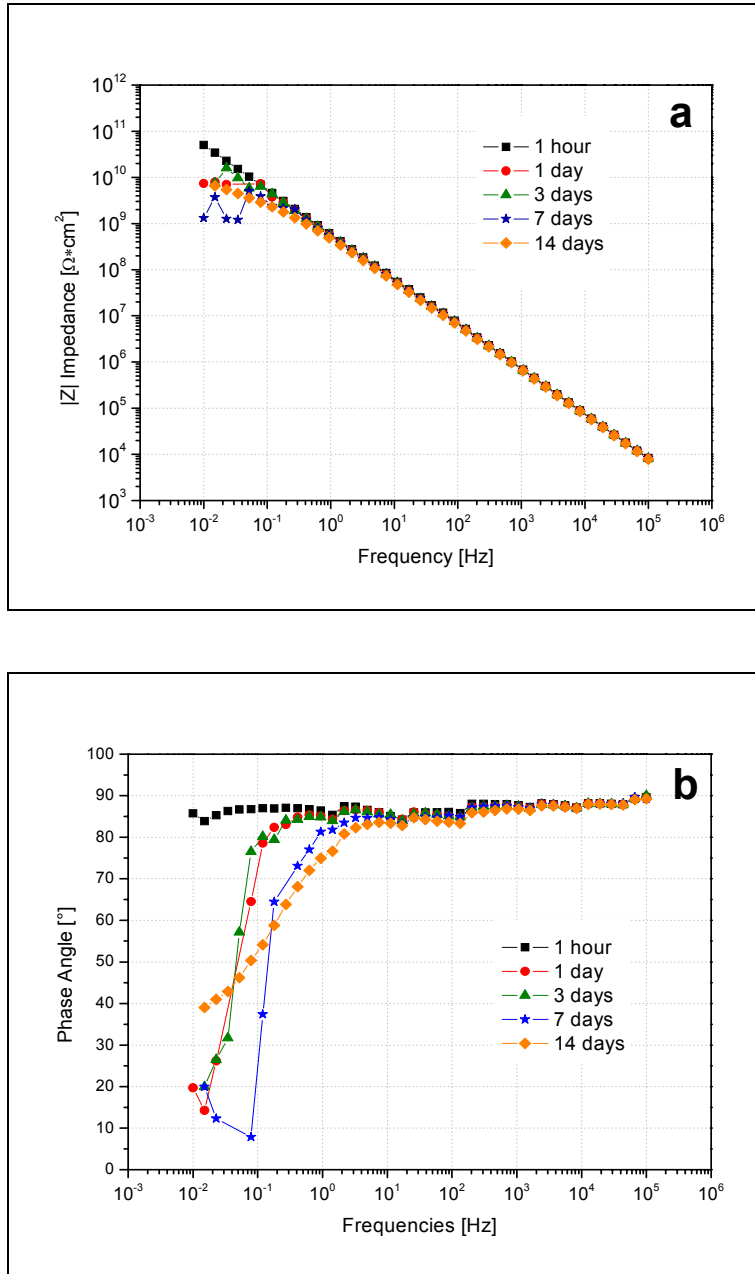
Figure 2.49 Impedance modulus (a) and phase (b) for the B180 electro-coated sample as a function of the time of immersion

Observe that for both samples the low frequencies impedance decreases very quickly. In particular, the drop of the total impedance occurs after a few hours of immersion for the electro-coated B120 sample, while the other sample maintains high values of the total impedance for about one week. After this lapse of time a second time constant is also noticeable in the Bode phase graph of sample B120 (see Figure 2.48a). It is evidence that corrosion is occurring under-paint. Owing to the low protection properties of the electro-coat coating on sample B120 and B180 and the beginning of the corrosion processes on sample B120, the immersion in the aggressive solution was stopped after two weeks. It is likely that the electro-coatings applied on the thicker sol-gel films have a few macro-defects due to hydrogen release during the electro-coating process. It was previously highlighted that the deposition conditions have a remarkable effect on the properties of the B120 and B180 sol-gel gel layer. The results of the experimental measurements performed on the electro-coated samples confirm that the degradation of the sol-gel film caused by the chemical reactions on the cathode is more pronounced for the high resistance sol-gel layers.

The wet adhesion and the resistance to the under-paint propagation of the cathodic front were roughly estimated by means of salt spray test. Scratched samples were exposed in the salt spray chamber for about 500 hours. The comparison between the experimental results of the exposure is reported in Figure 2.50.
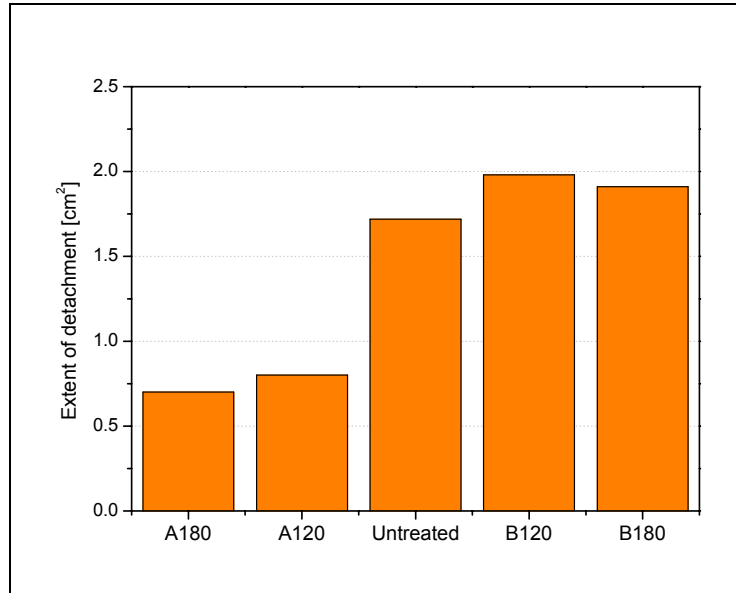
Figure 2.50 Extent of detachment for the electro-coated samples after 500 hours in the salt spray chamber

The samples pre-treated with the thicker silane sol-gel film show an extensive delamination starting from the artificial defect. Notice that the extent of delamination is higher than for the electro-coated galvanized steel. On the other hand, the samples pre-treated with the low resistance silane sol-gel film show a smaller delaminated area, related to the limited extent of the delamination process. It is likely that the A180 pre-treatment not only ensures the application of a defects free cataphoretic coating, but it also improves the resistance against the progress of the delamination front. This test also confirms the degradation of the high resistance silane pre-treatment. The resistance of these samples to the salt spray test is the worst among the different samples, and it is even worse than the electro-coated galvanized steel. This fact is probably

due to the deterioration of the silane sol-gel films, which leads to the formation of an inhomogeneous and defected cataphoretic film, characterized by poor adhesion to the substrate.

The experimental tests seems to indicate that a proper control of the barrier properties (and the thickness) of the silane sol-gel conversion layer can lead to the production of hybrid conversion film with suitable performance to improve the adhesion of a cataphoretic paint of galvanized steel. Moreover, the sol-gel film produced with the experimental mixture of silane molecules allows the formation of a defect free and homogeneous cataphoretic paint film. The final properties of the complete protection system can be explained in the light of the flexibility of the sol-gel process and the effectiveness of the experimental silane mixture.

2.4 Silane sol-gel films containing montmorillonite nanoparticles

This part of the work aims at investigating the effect of montmorillonite nanoparticles on the properties of silane mixture sol-gel films for the protection of galvanized steel. In the previous paragraph, the properties of different silane sol-gel films were analysed and compared to other traditional pre-treatment for galvanized steel. It was concluded that the experimental mixture investigated in this work improve the adhesion between the substrate and a protective organic

coating, enhancing the corrosion protection properties of the complete protection system. One step further is the improvement of the corrosion protection properties of the hybrid film itself. These kinds of sol-gel film do not provide an active protection against corrosion, but they ensure an effective temporary barrier against water and oxygen diffusion to the metal substrate. In order to improve the barrier properties of the hybrid silane sol-gel film, the idea is to embed montmorillonite nanoparticles into the silane sol-gel film. After hydrolysis, silanes molecules can graft to the montmorillonite nanoparticles, embedding the clay into the hybrid organosilane network. The mechanism of interaction between hydrolyzed silanes molecules and montmorillonite plates in schematically reported in Figure 2.51 [121].
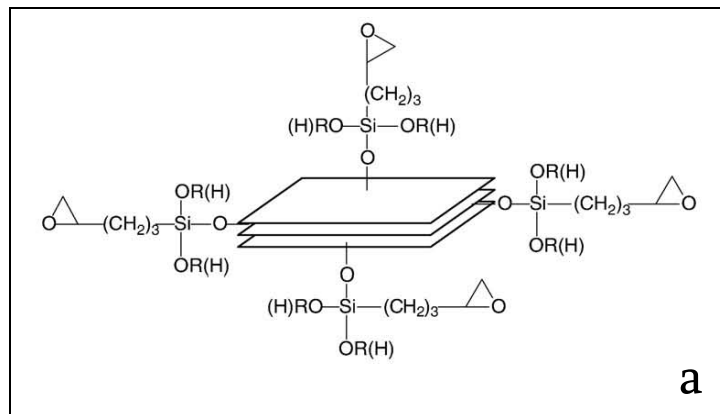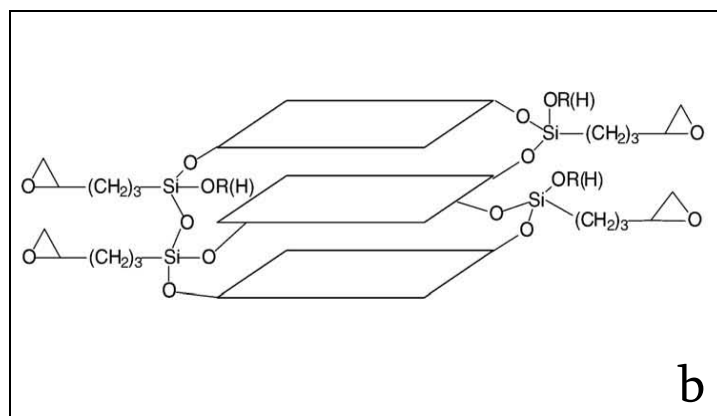
Figure 2.51 Schematic representation (a,b) of the mechanism of interaction between hydrolyzed silanes molecules and montmorillonite plates [121]

In this chapter, the interaction between the montmorillonite nanoparticles and the silanes molecules was investigated, as well as the electrochemical properties of the silane sol-gel film filled with the clay nanoparticles. In addition, clay nanoparticles containing a certain amount of cerium oxides such as CeO_2 and Ce_2O_3 were tested to check the effect of a modified clay surface on the properties of the silane sol-gel layer. The potential of rare earth compounds as environmentally friendly corrosion inhibitors embedded in the silane sol-gel layer was object of several studies [72,75,76]. Among the different rare earth compounds, the effectiveness of cerium oxides [122,123] as pigments for corrosion protection was proved. However, the combination between these kinds of oxides and the montmorillonite nanoparticles has not been investigated yet [124]. For this purpose, the experimental silane mixture was used as sol-gel matrix to embed the nanoparticles. It is expected that a convenient balance

between the different silanes molecules and the montmorillonite nanoparticles provide the sol-gel film with improved corrosion protection properties.

2.4.1 Materials and experimental procedure

The same hot dip galvanized steel sheets (Zn alloy: 0.25 w/w% Al, supplied by Arcelor Mittal, Belgium) with a mean roughness of were 1.59 μm used in the previous part were employed as substrate for the application of the montmorillonite enriched silane sol-gel films.

After the cleaning of the galvanized steel substrate, performed following the previously discussed procedure, the samples were pre-treated with the sol-gel conversion coatings.

The neat clay mineral used as fillers was a sodium montmorillonite (supplied by South Clay Products, USA), also called cloisite. The surface of the clay nanoparticles was modified by adding cerium oxides. The cerium oxides grafted to the montmorillonite nanoparticles are Ce_2O_3 and CeO_2. In particular, the amount of the different kinds of cerium oxides used to modify the nanoparticles is 5 w/w% respect to the weight of the montmorillonite particles.

The clay nanoparticles were ultrasonically dispersed in an aqueous solution. The pH of the dispersion was properly modified (pH 3.5) adding hydrochloric acid. Concentrations of 250ppm, 500ppm, 1000ppm of neat montmorillonite particles in the solution were tested.

The mixture obtained was added to 10 w/w% of silanes molecules. Silane mixture sol-gel films were applied following the standard procedure at about 20°C and 40% r.h.. The fresh films were cured in oven at 150°C for about 20 minutes.

2.4.2 Experimental results and discussion

Neat montmorillonite particles embedded into the silane sol-gel matrix

The appearance of the montmorillonite particles was observed by means of Transmission electron microscope (TEM). For this purpose, a Philips CM12 transmission electron microscope was used to collect images of the samples. The analysis and interpretation of the reported diffraction patterns was performed using the ring diffraction patterns modelling software Process Diffraction [125]. The nanopowders were ultrasonically dispersed in ethanol to facilitate the observations. Figure 2.52 shows a few examples of the appearance of the powders and their corresponding electron diffraction pattern.
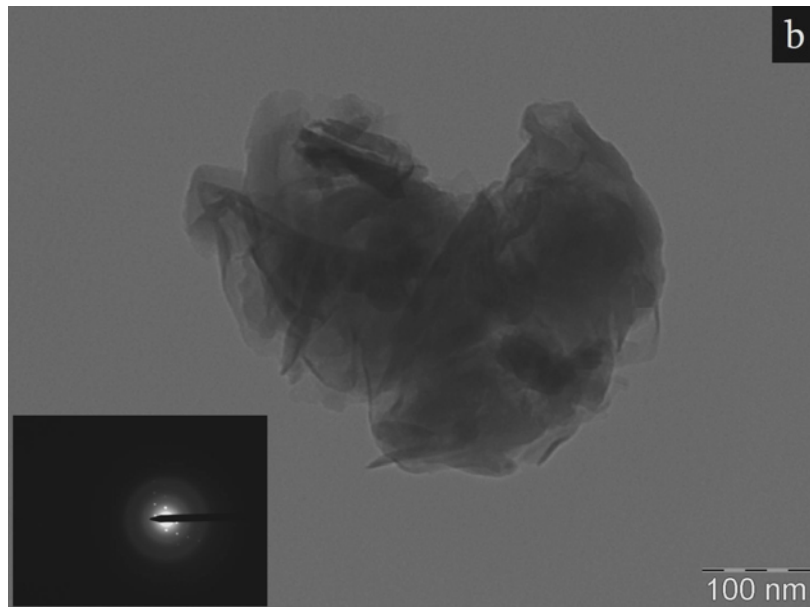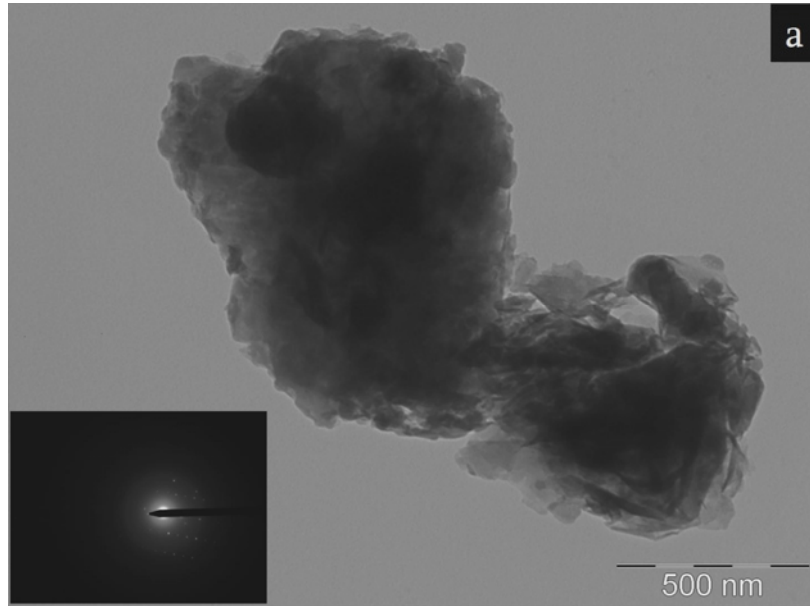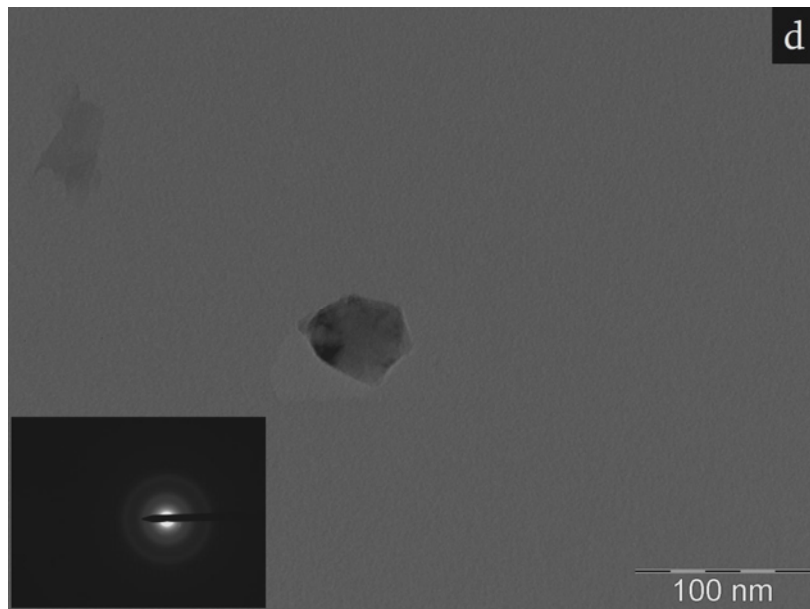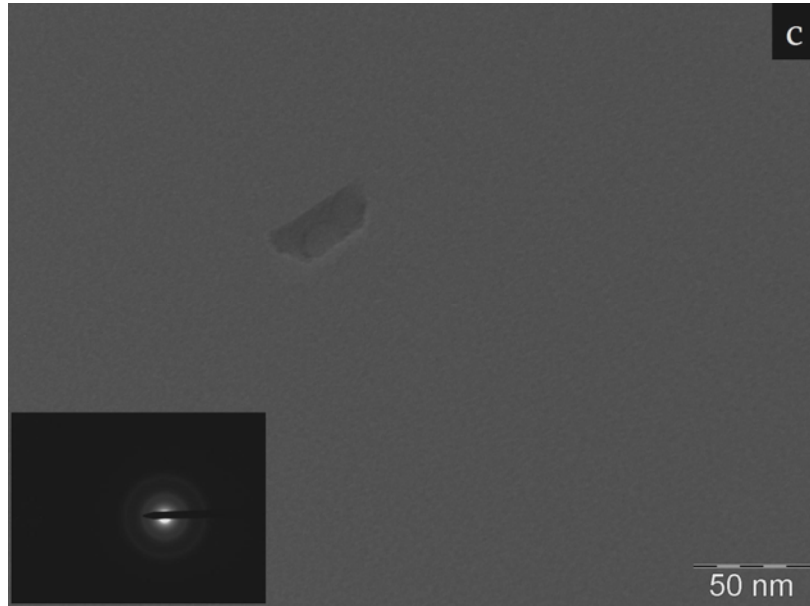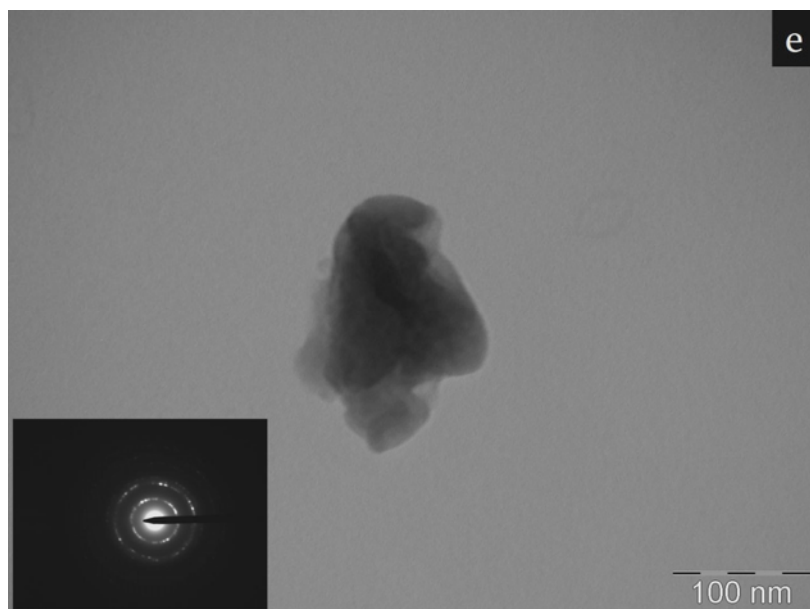
Figure 2.52 TEM images (a,b,c,d,e) of different montmorillonite nanoparticles: agglomerates of different extent

Considering the pictures depicted in Figure 2.52 it is possible to observe both single (c, d) and agglomerated (a, b, e) montmorillonite particles. It is not easy to clearly define a granulometry distribution of the montmorillonite plates because of the tendency to agglomeration of this kind of nanoparticles. However, considering the electron diffraction spectra, both spot and circle patterns are present. For example, Figure 2.52a shows a spot pattern: modelling this pattern with a suitable software (Carine 3.1) it is possible to observe that the spot pattern is related to the crystalline structure of the montmorillonite. On the other hand, all the other diffraction spectra acquired on the observed particles, are characterized by ring patterns indicating the presence of a nano-crystalline phase. The modelling of these ring patterns (carried out using the

modelling software Process diffraction) indicates that they are related to the montmorillonite. It is likely that the montmorillonite particles object of the study consist of both nano and micro crystalline particles. However, the real granulometric distribution and the degree of agglomeration of the different particles are not clear.

The particles were added to the silane solution following the procedure discussed in the previous paragraph. Table 2.11 summarizes the different samples produced for the investigation of the effect of different amounts of neat montmorillonite nanoparticles on the properties of the silane sol-gel film. The unfilled silane film was also analyzed for comparison.

Table 2.11 Summary of the different produced samples

	Silane sol-gel films	
Name of the sample	Amount of clay nanoparticles in the silane solution used for film preparation	Curing temperature
250 ppm cloisite	250ppm	
500 ppm cloisite	500ppm	150°C
1000 ppm cloisite	1000ppm	
Silane sol-gel matrix	-	

The thickness of the silane sol-gel films containing different amounts of nanoparticles was measured by means of XPS prior the electrochemical characterization.

The analysis revealed that the different films have approximately the same thickness. Figure 2.53 reports the three elements profiles acquired on the differently pre-treated samples. In particular, Figure 2.53a refers to the 250ppm cloisite sample, Figure 2.53b refers to the 500ppm cloisite sample and Figure 2.53c refers 1000ppm cloisite sample. Considering the elements profiles of Figure 2.53 it is possible to determine the thickness of the different sol-gel films.
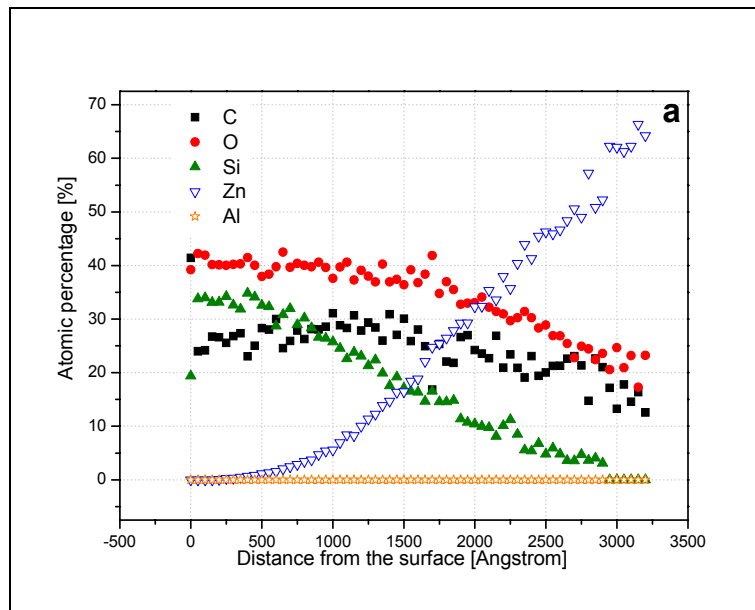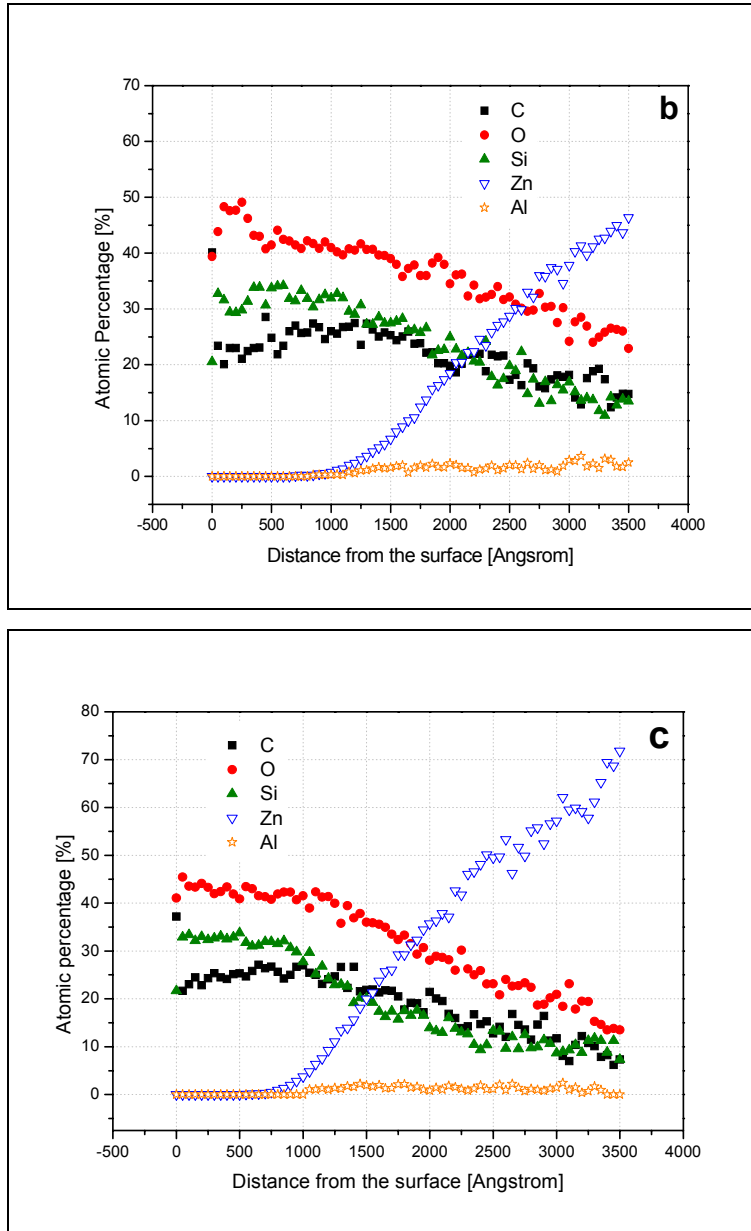
Figure 2.53 The elements profiles acquired on the differently pre-treated samples: 250ppm cloisite sample (a), 500ppm cloisite sample (b) and 1000ppm cloisite sample (c)

The different numerical values of the film thickness obtained by means of XPS are reported in Table 2.12. Observe that the thickness is not directly related to the amount of clay nanoparticles dispersed in the silane solution.

Table 2.12 Different values of the thicknesses obtained by means of XPS

Samples	Thickness
250 ppm cloisite	150 nm
500 ppm cloisite	200 nm
1000 ppm cloisite	150 nm

In fact, even if sample 500ppm cloisite is thicker than sample 250 ppm cloisite, the sample obtained starting from the silane solution richer in nanoparticles is as thick as sample 250ppm cloisite. At this level, the different amount of montmorillonite nanoparticles into the starting silane solution seems to do not affect the average thickness of the sol-gel films.

Firs of all, the results of the electrochemical characterization are reported. Figure 2.54 shows the impedance modulus and phase diagrams for the different silane sol-gel films containing 250ppm, 500ppm and 1000ppm of cloisite nanoparticles, respectively. The experimental measurements were performed after 1 hour of immersion in the testing solution. As specified before, also the spectra of the silane sol-gel film without nanoparticles is reported for comparison.
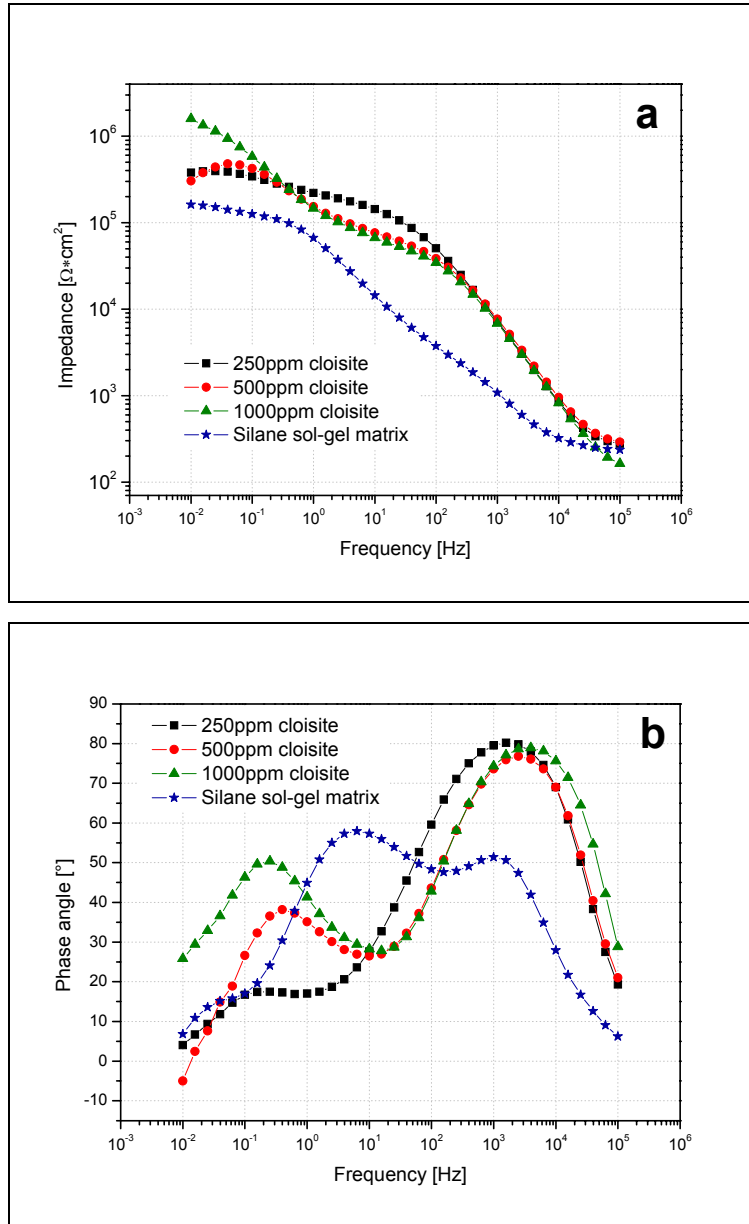
Figure 2.54 Impedance modulus and phase diagrams after 1 hour of immersion for the different silane sol-gel films obtained adding 250ppm, 500ppm and 1000ppm of cloisite nanoparticles , to the silane solution

Considering the Impedance Phase of the nanoparticles enriched sol gel films in Figure 2.54b, two time constants are clearly detectable: the high frequencies time constant is probably related to the sol-gel film [126] while the second time constant likely corresponds to the response of the substrate. The values of the low frequencies impedance are between $4 \cdot 10^5$ and $2 \cdot 10^6$ $\Omega \cdot cm^2$ for all the sol-gel films containing nanoparticles. Every different amount of montmorillonite nanoparticles improves the electrochemical properties of the sol-gel films. In fact, in the first hour of immersion, the low frequency impedance for the silane sol-gel matrix is around 10^5 $\Omega \cdot cm^2$, significantly lower than the best value of the montmorillonite filled sol-gel film. In the first hours of immersion all the sol-gel films filled with different amounts of nanoparticles have very similar protection properties. Another difference is noticeable: the silane sol-gel matrix shows three different time constants, while the silane sol-gel film filled with the nanoparticles just two. The third time constant has been investigated in several studies [127] and it is likely related to the condition of the sol-gel film/metal interface. Probably, the presence of the nanoparticles leads to strong changes in the structure of the hybrid films.

After a few days of immersion in the aggressive solution, the differences among the sol-gel films become remarkable. Considering Figure 2.55 it is possible to appreciate the different EIS spectra after one week of immersion in the electrolyte.
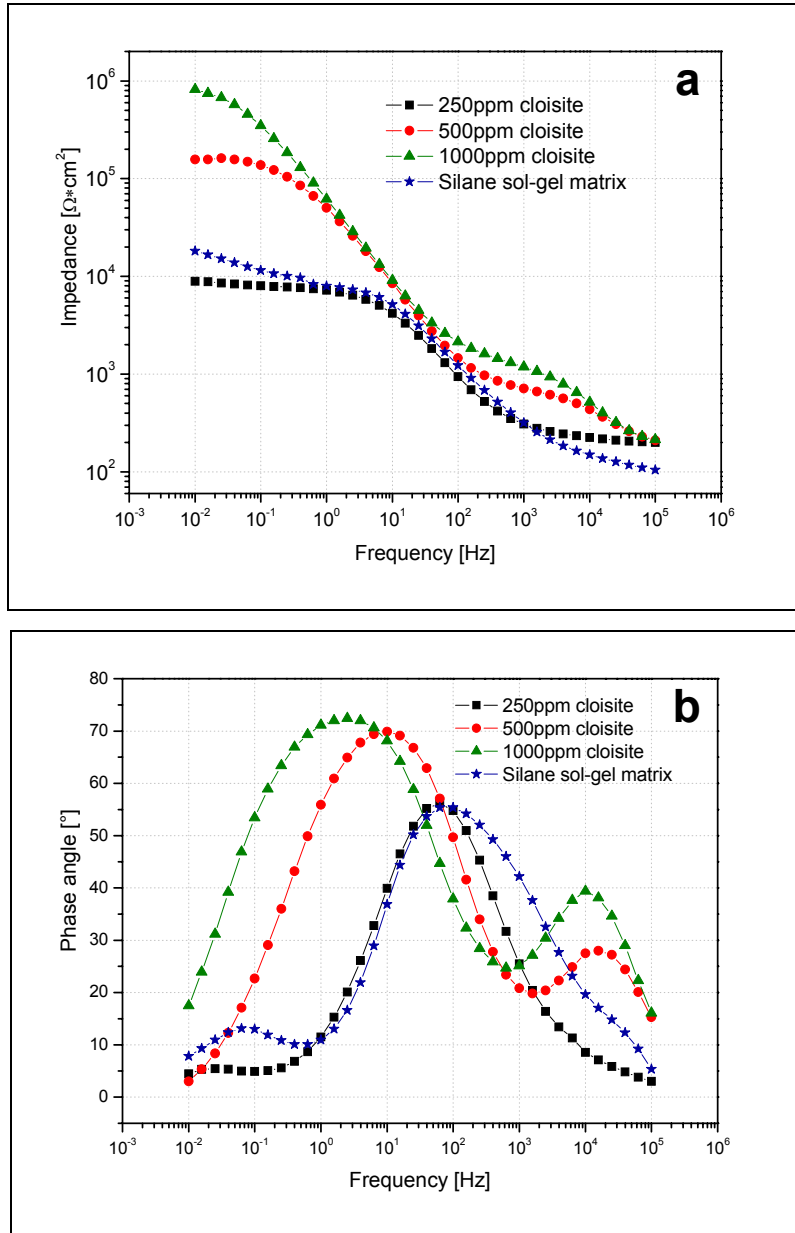
Figure 2.55 Bode modulus and phase diagrams after 7 days of immersion for the different silane sol-gel films obtained adding 250ppm, 500ppm and 1000ppm of cloisite nanoparticles, respectively, to the silane solution

The film obtained from a solution containing 1000ppm of nanoparticles maintains the value of the low frequencies impedance (corresponding approximatively to 10^{-2} Hz) very close to the value measured in the first hours of immersion. The film obtained starting from a solution containing 500ppm of nanoparticles shows a slightly decrease of the impedance in the low frequency domain, while the sample obtained from a solution containing 250ppm of nanoparticles shows an evident drop (about two orders of magnitude) of the low frequency impedance, reaching values close to the sample without nanoparticles. Notice that for this last sample the time constant related to the presence of the sol-gel film is no more observable (see Figure 2.55b). In order to better understand the electrochemical properties of the montmorillonite filled sol-gel films, the impedance spectra were fitted using a convenient equivalent circuit model. For the fitting procedure a R(R(Q(RQ))) equivalent circuit (see Figure 2.56) was used [128].
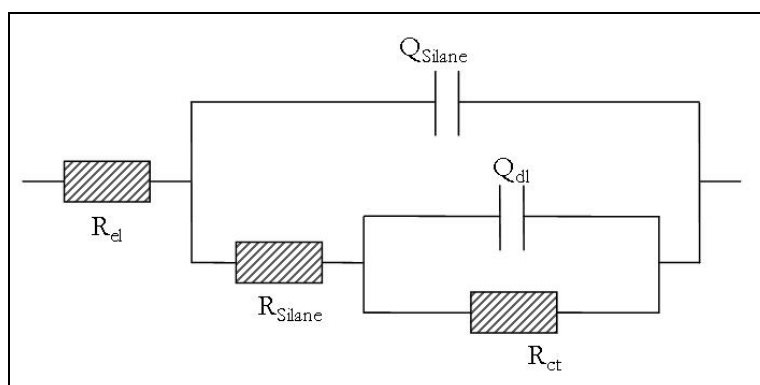
Figure 2.56 Equivalent circuit model used for the fitting procedure

The first resistance is the electrolyte resistance, the second corresponds to silane sol-gel film resistance (R_{silane}), the first constant phase element is related to the silane sol-gel film capacitance (Q_{silane}), while the other time constant is representative of both the Faradic resistance of the metal interface (R_{ct}) and the double layer capacitance (Q_{dl})

The results of the fitting procedure are reported in Figure 2.57, which shows the values of the silane sol-gel resistance (a) and capacitance (b) calculated from the acquired impedance spectra.
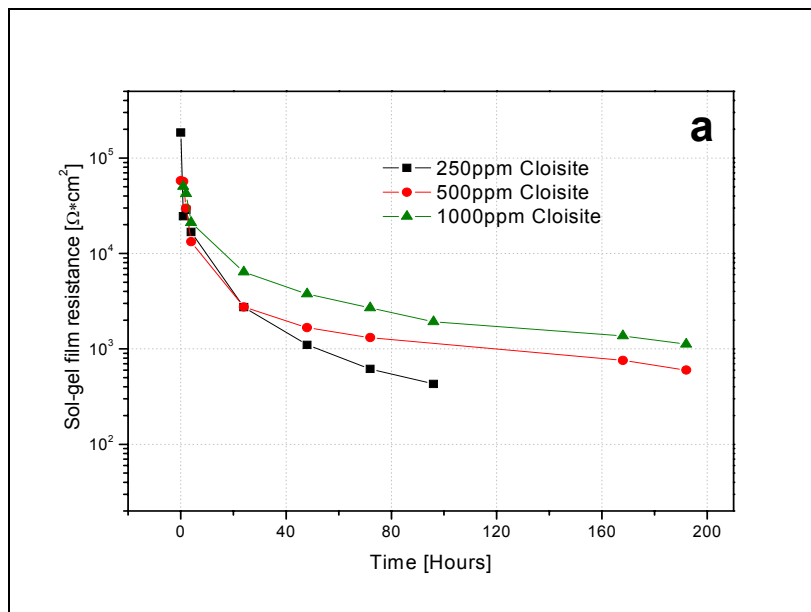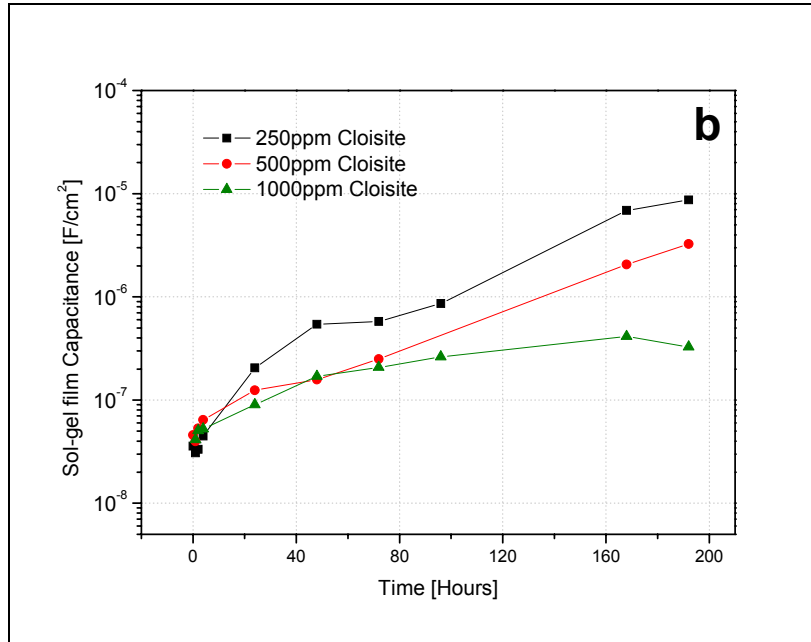
Figure 2.57 Silane sol-gel film resistance (a) and capacitance (b) with the time of immersion in the electrolyte

Notice that after 100 hours of immersion it is no more possible to appreciate the value of the silane sol-gel film resistance of the 250ppm cloisite sample, because it becomes too low and the fitting model hardly find out a correct value for this parameter. It is likely due to the formation of corrosion products at the interface between the silane sol-gel film and the metal which influences the impedance signal. It is clear that sample 1000ppm cloisite provides the best corrosion protection among the different samples. In fact, the values of the coating resistance are the highest during the immersion time in the aggressive solution. In addition, as shown in Figure 2.58, the charge transfer resistance on

the surface of this sample is mainly stable for all the immersion time in the sodium chloride solution.
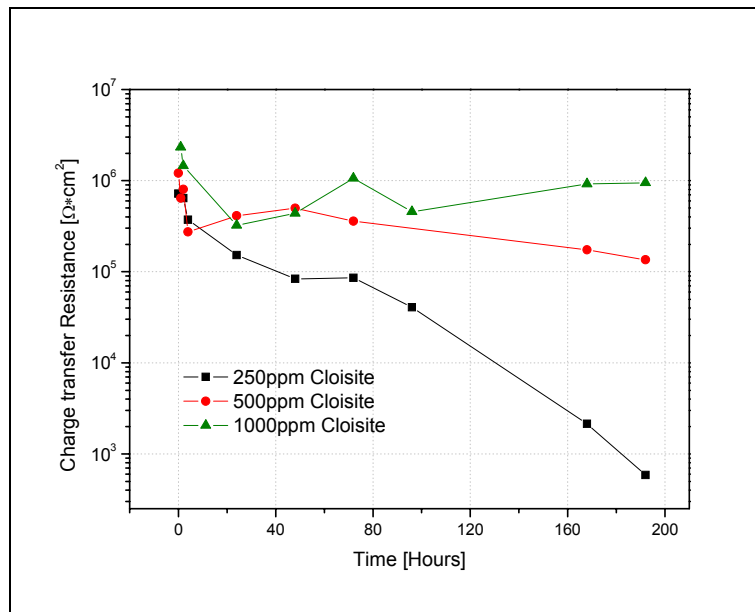
Figure 2.58 Charge transfer resistance with the time of immersion

It is commonly accepted [129] that the charge transfer resistance is inversely proportional to the corrosion rate (depending on the reactive area). Thus, sample 1000ppm cloisite is able to protect the galvanized steel substrate against corrosion phenomena. Sample 500ppm cloisite shows values of the charge transfer resistance which, even if lower, is comparable with the values of sample 1000ppm cloisite. On the other hand, the sample obtained from a solution containing 250ppm of nanoparticles shows a continuous decrease of the charge transfer resistance. This is indicative of the progression of a

corrosion process. After the 240 hours of immersion in the aggressive solution, the area of each sample affected by the electrolyte was observed by means of environmental scanning electron microscopy (ESEM). Figure 2.59 depicts the appearance of the area of the three different samples affected by the electrolyte.
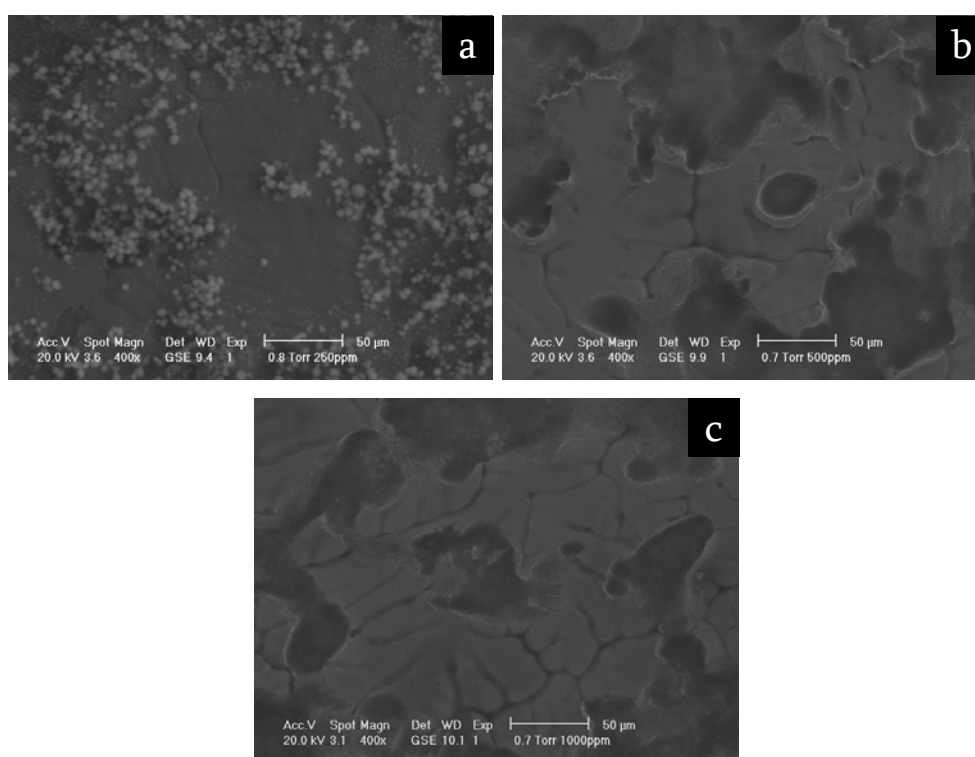
Figure 2.59 Appearance of the area of the three different samples affected by the electrolyte for 240 hours: 250ppm cloisite sample (a), 500ppm cloisite sample (b), 1000ppm cloisite sample (c)

Zinc corrosion products (lighter particles in Figure 2.59a) are observable on the surface of sample 250ppm cloisite. According to the electrochemical measurements, this is evidence of an advanced corrosion process occurring on

the surface of this sample. The surface of the other two samples does not show any accumulation of zinc corrosion products and the sol-gel film surface seems to be intact.

In order to complete the electrochemical characterization, also potentiodynamic curves were acquired. Figure 2.60 shows the anodic and cathodic polarization curves for the samples object of the study. For comparison, the behaviour of the alkaline degreased bare zinc and the unfilled silane sol-gel matrix were also reported.
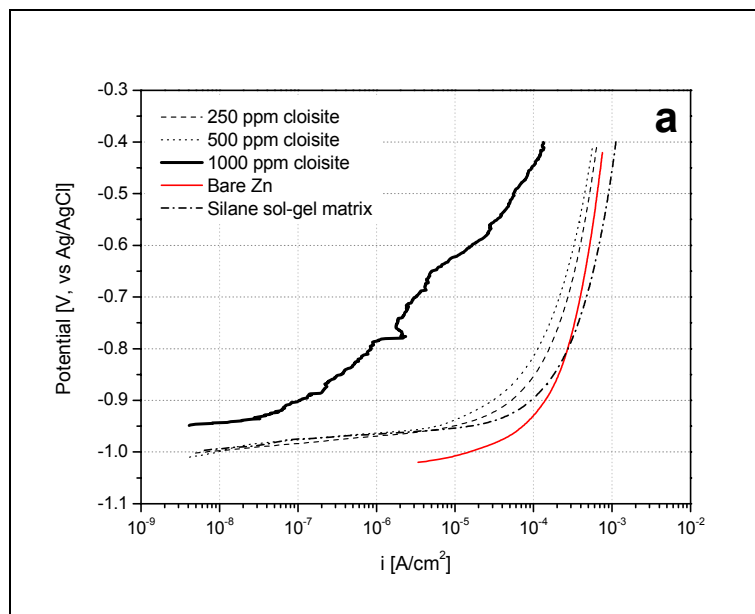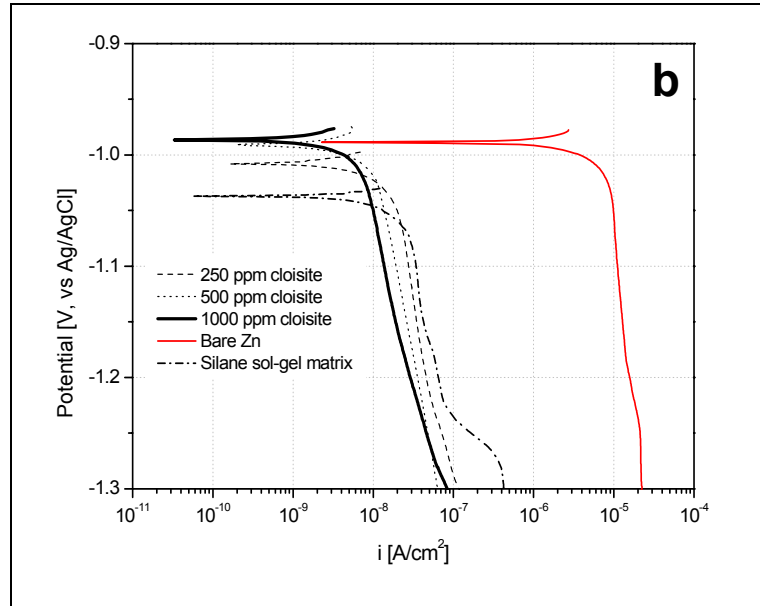
Figure 2.60 Anodic (a) and cathodic (b) polarization curves for the samples object of the study

Considering the anodic polarization curves, the main difference regards the particularly low anodic current of 1000ppm cloisite sample. All the silane sol-gel film show a higher resistance both in anodic and cathodic polarization respect to the bare galvanized steel. This difference is huge for all the samples (two or three orders of magnitude) for the cathodic polarization, while, except for the sample 1000ppm cloisite, it is slight for the anodic polarization. Among the silane sol-gel covered samples, the 1000ppm cloisite sample shows the lowest value of the cathodic current density, even if the values of the other samples are very comparable. All the montmorillonite filled samples show lower cathodic and anodic currents than the silane sol-gel matrix.

In the light of this characterization it is likely that the different amounts of montmorillonite particles lead to strong changes in the structure of the hybrid films. This statement is proved by the remarkably different electrochemical properties of the studied sol-gel film as a function of the different amount of montmorillonite nanoparticles into the starting silane solution. Previously, it was also demonstrated (by means of XPS measurement) that the silane sol-gel coatings have more or less the same thickness and that the amount of clay nanoparticles into the silane solution do not lead to an increase of the thickness of the hybrid films. Probably, the presence of the nanoparticles induces structural changes in the hybrid matrix, enhancing the barrier properties of the silane sol-gel film. An increase of the quantity of nanoparticles in the starting silane solution (from 250 ppm to 1000 ppm) seems to improve the final properties of the sol-gel film. It is likely that the higher the amount of montmorillonite nanoparticles into the silane solution, the more noticeable the structural changes of the hybrid film. In order to better understand the effect of the clay nanoparticles on the structure of the silane sol-gel film a deeper investigation of the inner structure of 1000ppm cloisite sample was carried out.

The concentration of 1000ppm of clay nanoparticles into the diluted silane solution leads to the formation of a sol-gel film with improved protection properties highlighted by high impedance values. Indeed, this sol-gel film protects the substrate against corrosion even after relatively long immersion time. The properties of the 1000ppm cloisite samples were deeply investigated by means of TEM observation.

The aim of these observations is to investigate the effect of the nanoparticles on the structure of the silane sol-gel film. Also in this case, the analysis and interpretation of the acquired diffraction patterns was performed using the modelling software Process Diffraction [125].

Figure 2.61a depicts the appearance of the silane sol-gel film observed in *bright field* while Figure 2.61b shows approximately the same portion of the sample observed in *dark field*, using a convenient angle of diffraction corresponding to a specific crystallographic plane of crystalline montmorillonite. It was possible to detect and localize the montmorillonite nanoparticles selecting a convenient diffraction angle (which undergoes Bragg scattering related to the crystallographic structure of the montmorillonite particles) and observing the sample in *dark field* where the particles appears bright.
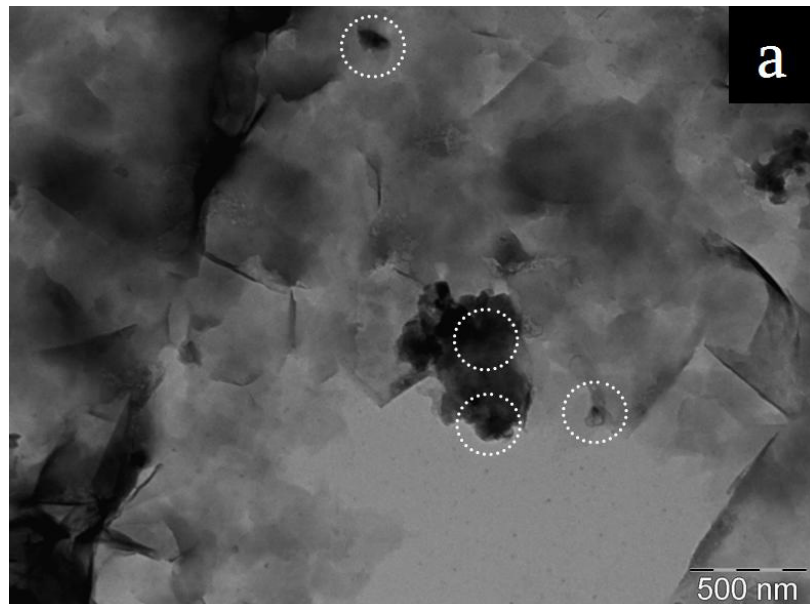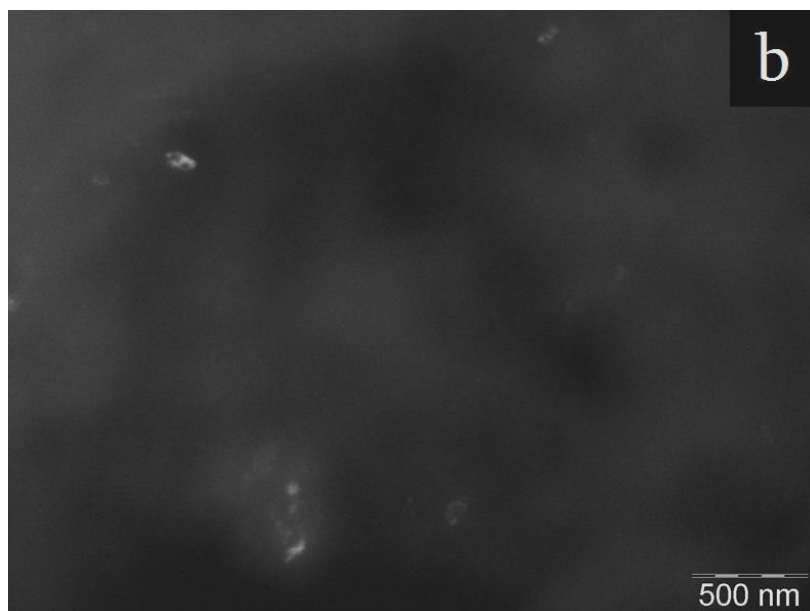
Figure 2.61 Appearance of a portion the silane sol-gel film (a) approximately the same portion of the sample observed in *dark field* (b)

The bright particles observable in the *dark field* images (Figure 2.61b) correspond to crystalline domains. The bright particles, detected and localized selecting a convenient diffraction angle and observing the sample in *dark field* were proved to be montmorillonite nanoparticles performing an electron diffraction spectrum on them, The electron diffraction pattern in Figure 2.62 was acquired all over the area of the sample depicted in Figure 2.61. Considering the diffraction pattern of Figure 2.62 it is possible to notice that both a ring and a spot pattern are visible. By analysing the spot pattern using the modelling software Carine 3.1 and Process Diffraction, it seems that the spot pattern refers to montmorillonite crystalline domains, while the ring pattern is related to the presence of a nano-crystalline phase.
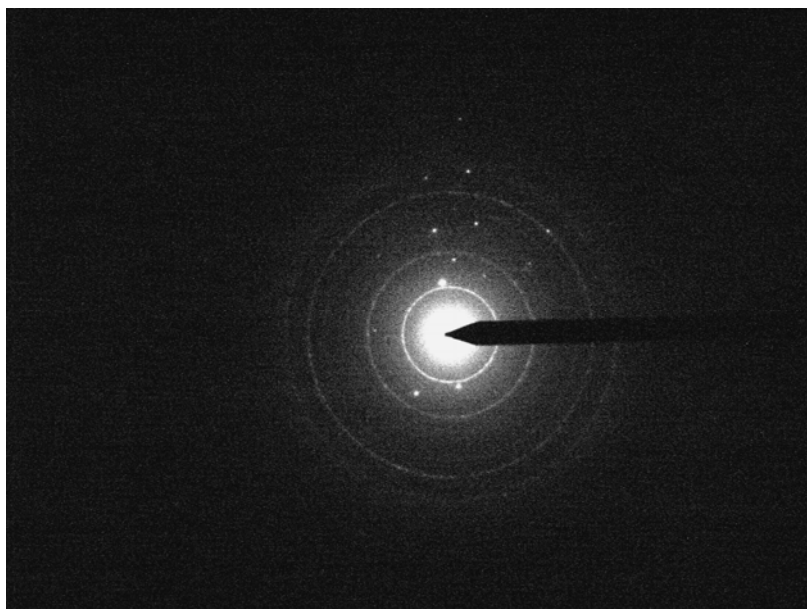
Figure 2.62 Electron diffraction pattern acquired all over the portion of the sample depicted in Figure 2.61

The solution of the ring pattern leads to the conclusion that the nano-crystalline phase consists of a hexagonal structure of silicon oxide. It is likely that the inorganic fraction of the hybrid molecules arranges itself in a nano-crystalline phase.

Consider Figure 2.63, which shows the TEM images of the silane sol-gel film containing 1000ppm of cloisite nanoparticles: by analysing the ring diffraction patterns corresponding to the dark dots dispersed into the film (highlighted by the arrows in Figure 2.63b and also observable in Figure 2.63c and d), it is possible to demonstrate that they match with the structure of silica nano-crystalline domains.
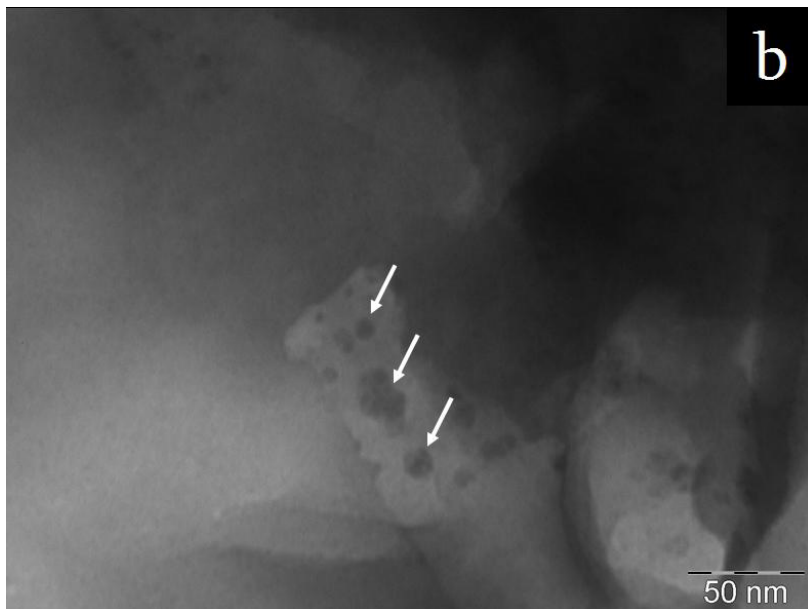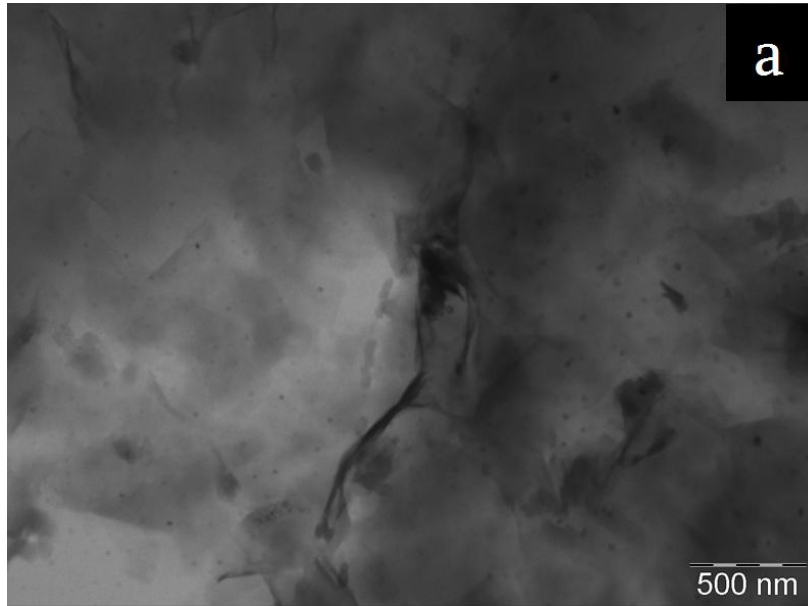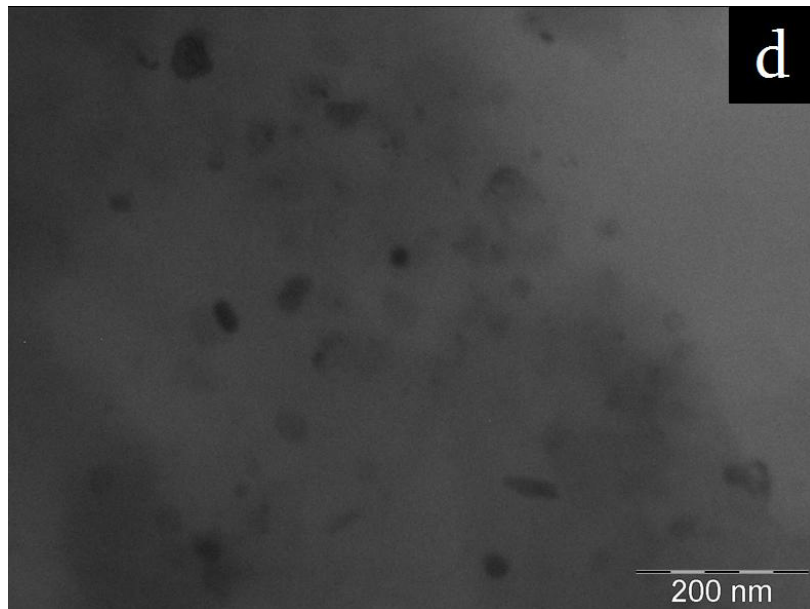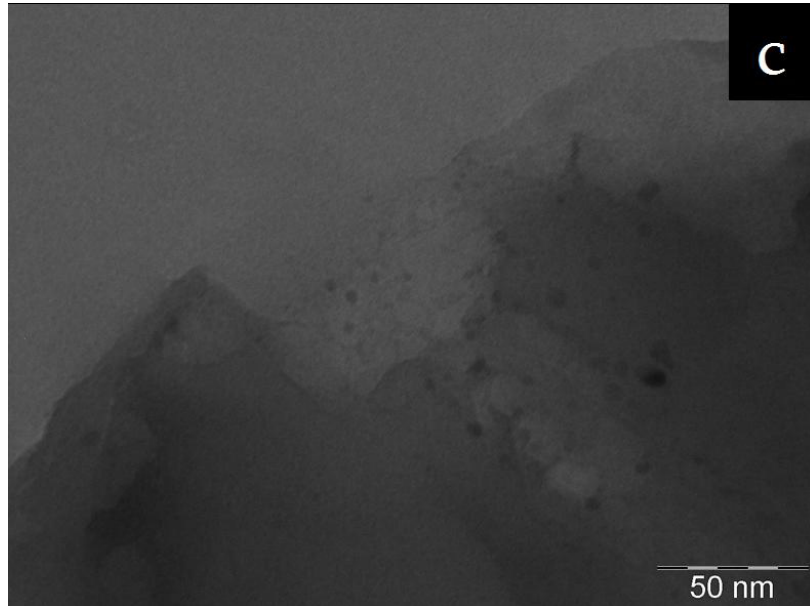
Figure 2.63 TEM images (a,b,c,d) structure and nano-crystalline domains of the hybrid sol-gel films

The presence of the nano-crystalline domains corresponding to hexagonal silica nano-crystals was investigated more in depth. Figure 2.64 reports other crystalline phases observed by means of TEM. For both the two crystalline phases depicted in Figure 2.64a and Figure 2.64c the corresponding electron diffraction pattern are reported in Figure 2.64b and Figure 2.64d, respectively. The analysis of the diffraction patterns leads to the conclusion that the nano-crystalline phase (highlighted by the arrows in Figure 2.64a and c) is, also in this case, silica arranged in a hexagonal crystalline habit.
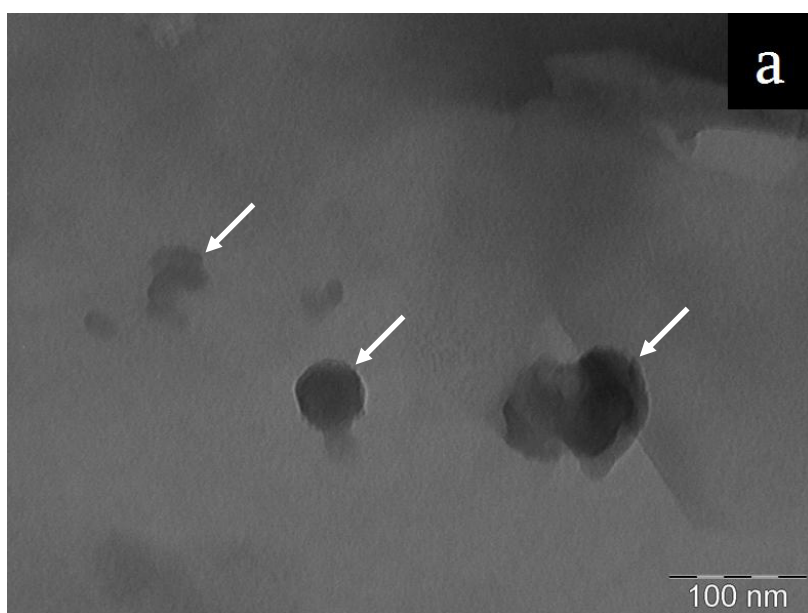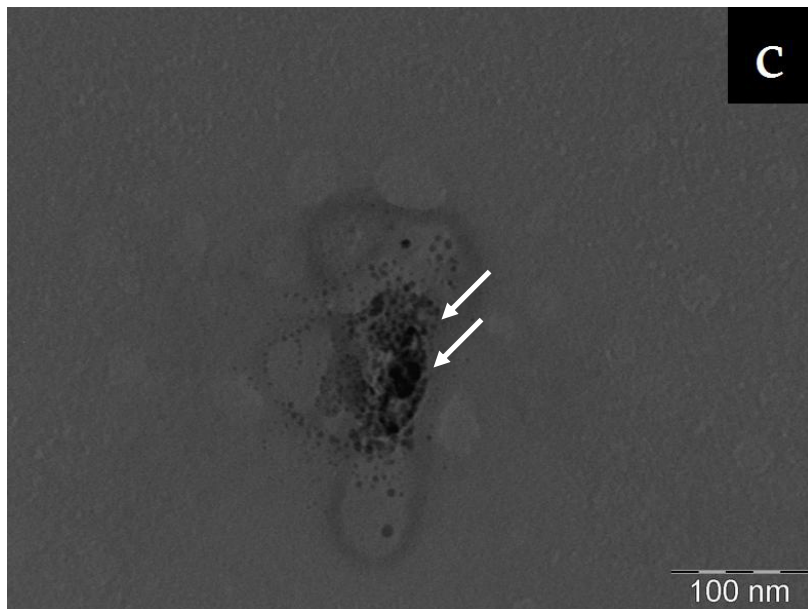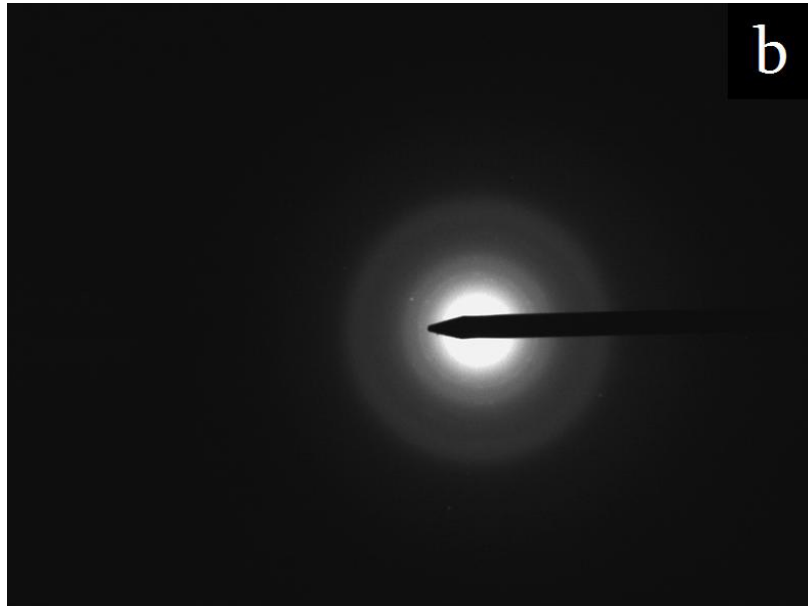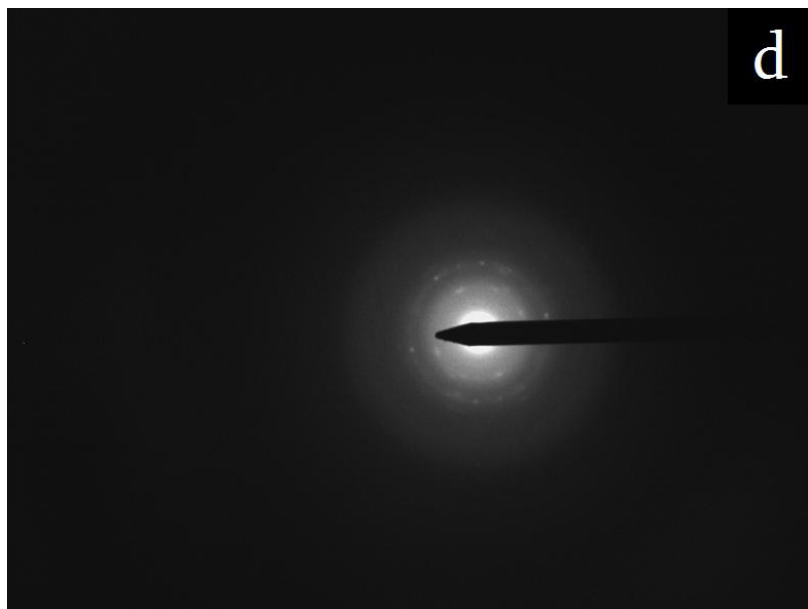
Figure 2.64 Crystalline phases observed by means of TEM: acquired images (a, c) and corresponding diffraction pattern (b, d)

Considering the pictures depicted in Figure 2.64, it is possible to appreciate nano-crystalline domains of different extent and appearance. It is likely that some of these domains are self-arranged during the curing, while other grows surrounding a montmorillonite particle. It is not clear if the silane sol-gel film properties are more affected by the *in situ* formation of nano-crystalline silica domains or by the heterogeneous nucleation of nano-crystalline domains of silica starting from a montmorillonite particle or, finally, by the embedding of agglomerations of montmorillonite nanoparticles into the matrix. However, the clay nanoparticles seem to introduce a strong modification in the silane sol-gel film structure, evidenced by the improved barrier properties of the film itself.

The montmorillonite induces a local arrangement of the molecules which lead to a lower permeability of the sol-gel film and the consequent higher resistance to the penetration of to water and oxygen.

Concerning the silica domain self arranged in the hexagonal crystalline habit, it is likely that it consist of hydrolyzed TEOS condensed during the curing in the in a crystal structure. In fact, among the studied molecules, only the TEOS can form, after hydrolysis and condensation reactions, a pure silica structure.

Cerium oxides enriched montmorillonite particles embedded into the silane sol-gel matrix

In the previous section, it was evidenced that the concentration of 1000ppm of nanoparticles in the starting diluted solution enhances the corrosion protection of the sol-gel film. Next step is to try to embed into the silane sol-gel film clay nanoparticles modified adding a corrosion inhibitor, in order to try to functionalize the inorganic particles. The final aim is to produce sol-gel films improved by means of an active corrosion protection potential. The inhibitors used in this study consist of different cerium oxides. Cerium oxides can act as corrosion inhibitors [73-76], even if the mechanism through which they act is not completely understood.

In particular, two different nanoparticles were studied: montmorillonite tailored with two different cerium oxides. The study aims also to test the effect of a surface modification on final properties of the silane sol-gel film containing

clay nanoparticles and if the inhibitors improve the corrosion protection performances of the sol-gel coatings.

Silane sol-gel layers containing the montmorillonite particles enriched with the cerium oxides were applied on the galvanized steel plates, in order to compare the performances of this pre-treatment with the sol-gel film containing the neat nanoparticles. For this purpose, 1000ppm of, respectively, neat montmorillonite, 5 w/w% Ce_2O_3 enriched montmorillonite and 5 w/w% CeO_2 enriched montmorillonite were dispersed in the diluted silanes solution to obtain three different sol-gel films (the procedure to graft the cerium oxides to the clay is protected by patent). The films were obtained following the procedure previously discussed in the experimental part. The corrosion protection properties of these sol-gel films were evaluated, as before, by means of electrochemical impedance spectroscopy. Figure 2.65 shows the silane sol-gel resistance (a) and the charge transfer resistance (b) for the different sol-gel films with the time of immersion in the aggressive solution.
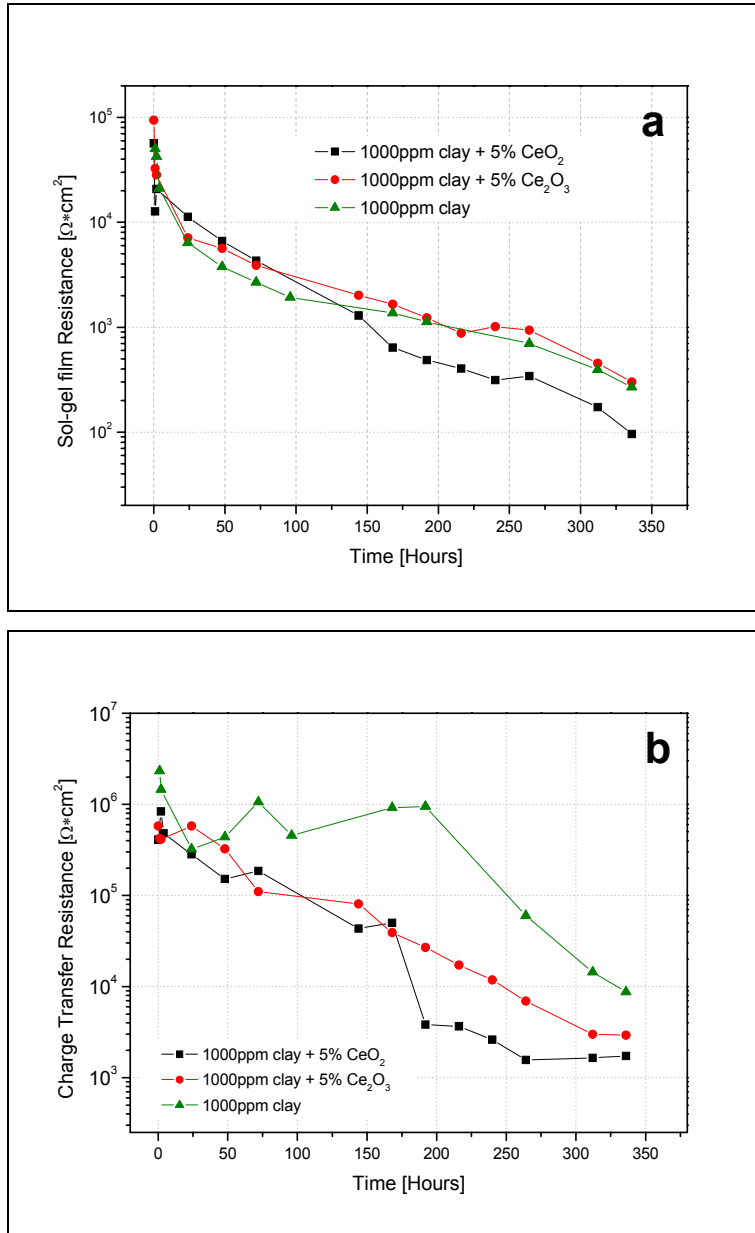
Figure 2.65 Silane sol-gel resistance (a) and the charge transfer resistance (b) for the different sol-gel films with the time of immersion in the aggressive solution

The numerical values reported in Figure 2.65 were obtained using the previously discussed equivalent electrical circuit (Figure 2.56).

The resistance values of the different clay nanoparticles filled sol-gel films are comparable. The decreasing of the resistance properties follows the same trend for each sample, with little differences only in the very last days of immersion. This is evidence that also the clay nanoparticles tailored with cerium oxides improve the barrier properties of the silane sol-gel film. However, considering Figure 2.65b, it seems that the film with neat montmorillonite embedded ensures a slightly better corrosion protection respect to the films with the cerium oxides on the clay nanoparticles. Concerning Figure 2.65a, no remarkable differences between the effects of the two different cerium oxides. In fact, the charge transfer resistance trends of both samples over immersion time are more or less the same, showing a progressive decrease of the corrosion resistance. Instead, the sol-gel film filled with neat montmorillonite shows stable values of the charge transfer resistance up to 200 hours of immersion. Only after this period of exposure time a decrease of the charge transfer resistance is appreciable. However, despite the initial differences, the final values of the resistance after 336 hours of immersion are similar.

The potential of the cerium oxides as surface modifiers was checked by means of both anodic and cathodic polarization measurements. Figure 2.66 shows the anodic (a) and cathodic (b) polarization curves for the experimental sol-gel films and, for comparison, for the bare galvanized steel.
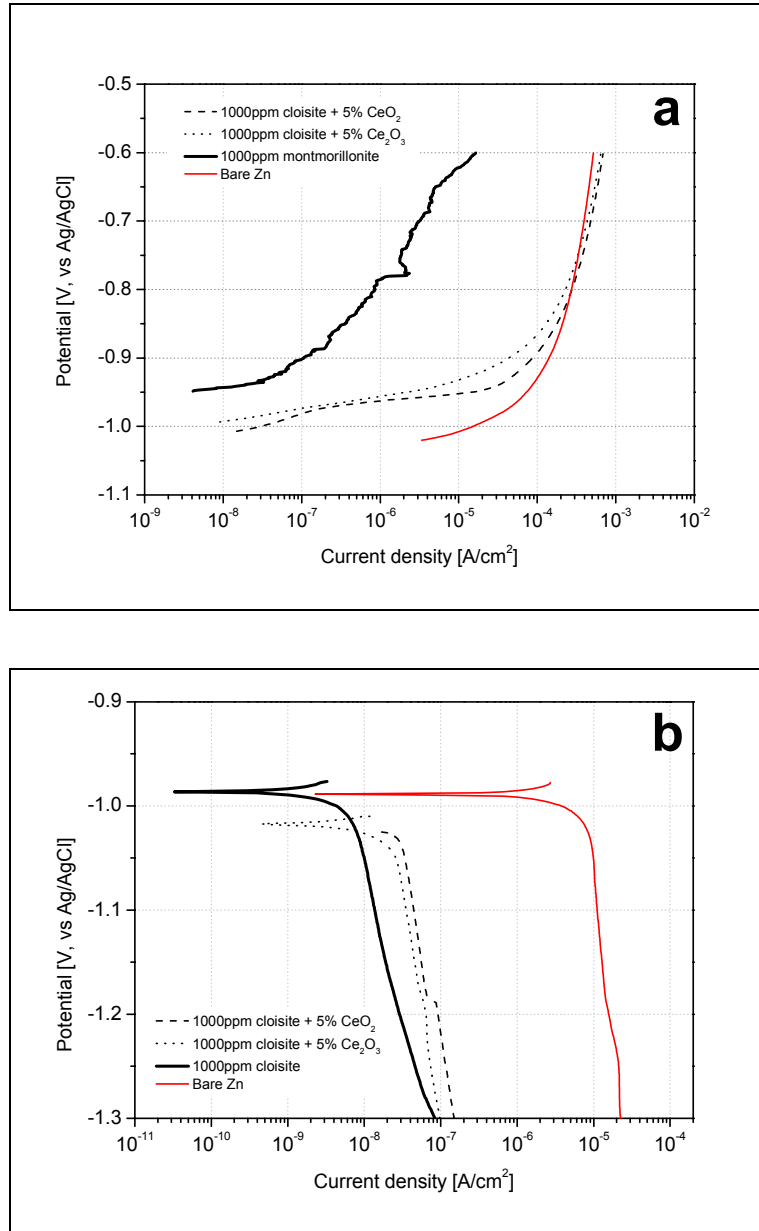
Figure 2.66 Anodic (a) and cathodic (b) polarization curves for the experimental sol-gel films with the time of immersion in the aggressive solution

Considering Figure 2.66 there is no evidence of a beneficial effect on either the cathodic or anodic reaction kinetics related to the presence of the cerium oxides on the surface of the particles. In addition, concerning the samples containing the cerium oxides enriched nanoparticles, the anodic currents are very similar to the one of the unfilled sol-gel matrix. There is just a slight decrease of the anodic current for low overvoltage, until -0.9 V (vs. Ag/AgCl) for the samples containing the modified nanoparticles. The silane sol-gel matrix filled with neat montmorillonite shows again the best performance, underlined by the lowest cathodic and anodic currents. To highlight appreciable differences among the differently filled sol-gel films, salt spray test was performed. Figure 2.67 reports the qualitative results after one week of continuous exposure in the salt spray chamber for the bare galvanized steel (a), the sol-gel matrix with the neat clay (b), the sol-gel matrix with Ce_2O_3 grafted to the clay (c) and the sol-gel matrix with CeO_2 grafted to the clay (d).
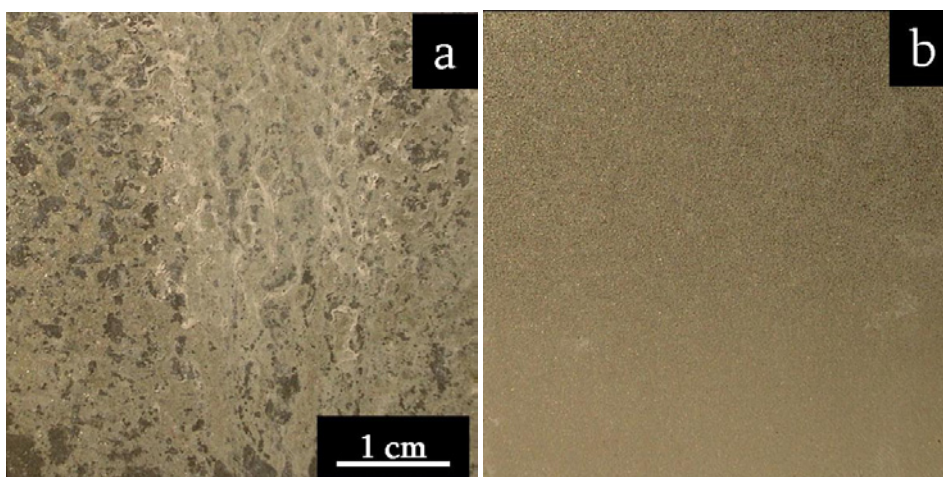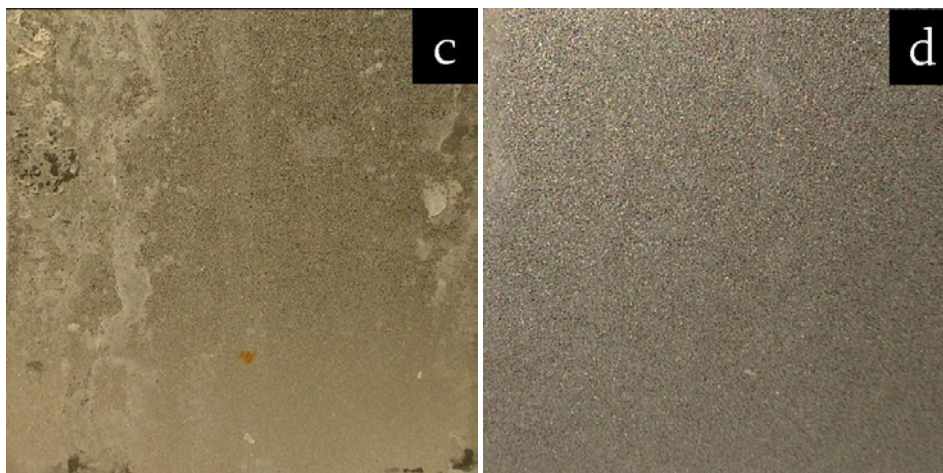
Figure 2.67 Appearance of the samples after one week of continuous exposure in the salt spray chamber: bare galvanized steel (a), sol-gel matrix with the neat clay (b), sol-gel matrix with Ce_2O_3 grafted to the clay (c) and sol-gel matrix with CeO_2 grafted to the clay (d)

The bare galvanized steel samples shows a huge amount of zinc corrosion products on its surface, while the samples covered with the sol-gel films filled with neat montmorillonite and CeO_2 enriched montmorillonite are still protective and no zinc corrosion products are observable. Instead, the presence of zinc corrosion products is appreciable on the surface of the sample covered with the silane sol-gel film filled with clay nanoparticles enriched with Ce_2O_3.

The surface modification of montmorillonite nanoparticles with cerium oxides does not improve the protection properties of the sol-gel film. In fact, the properties of the sol-gel films obtained using montmorillonite modified with cerium oxides are the same, or even worse, than the sol-gel layer obtained using neat montmorillonite.

Maybe the cerium oxides modify the clay particles interfering with the embedding procedure. Indeed, the surface modification of montmorillonite nanoparticles, due to the presence of the oxides, may negatively affect the performances of the silane films, by influencing the silane – clay interaction. In any case, it is not possible to appreciate an evidence of an inhibition of the corrosion processes carried out by the cerium oxides.

2.5 Final comments

Hybrid silicon alkoxides molecules were used for the production of sol-gel coatings to protect aluminium and HDG steel. These sol-gel pre-treatments were tested as adhesion promoters in combination with both powder and cataphoretic coatings for the development of environmentally friendly protection cycles to prevent corrosion and degradation of the studied metals. The same experimental mixture of silicon alkoxides was tested both on an aluminium alloy and on HDG steel. The results on aluminium proved that the silane treatment provides the substrate with an effective barrier against corrosion. In addition, it acts as a coupling agent improving the adhesion with the epoxy-polyester organic coating and, in general, the corrosion protection properties. The comparison with other pre-treatment technologies highlighted that the experimental silane sol-gel pre-treatment ensures good performance, comparable or higher than the other surface conversion treatments tested in

this work. Considering the application onto galvanized steel, an effective combination of silicon alkoxides, deposition procedure and curing temperature has been carried out to optimize the corrosion protection properties of the sol-gel film itself and the interaction with both powder coating and cataphoretic paints. The test carried out on HDG steel proved that covered with an organic coating and cured at high temperatures, the produced silanes sol-gel pre-treatments act both as an efficient barrier against moisture and oxygen permeation (relatively to their thickness) and also as a coupling agent improving the corrosion resistance of the complete protection system. Concerning the cataphoretic coating the experimental sol-gel treatment can be properly designed to inhibit the hydrogen release leading to the formation of a continuous and defect-free electrodeposited coating. As a further result, the barrier properties of the sol-gel coating itself were improved adding montmorillonite nanoparticles to the silane mixtures. The preliminary analysis demonstrated that the nanoparticles modify the film formation mechanism leading to the formation of sol-gel coating with enhanced resistance to water uptake and oxygen permeation.

3 Ultra violet cured nanocomposite coatings

Generally speaking, at present waterborne coatings offer the advantage of an environmentally friendly technology, but still show some drawbacks with respect to conventional solventborne systems: poorer film forming properties onto low surface energy substrates, low viscosity, non Newtonian rheological behaviour and sagging, difficult formation of defect free films with constant thickness and poor control of stoichiometry during cross-linking. As a consequence, unsatisfactory substrate adhesion, weatherability, barrier and mechanical properties can be expected. Aqueous dispersions which can be cross-linked by UV exposure are an alternative promising approach.

The UV curing technique is an efficient and environmentally friendly technology for the production of protective coatings for wood, metals, paper, plastics and glass. The technique is based on the bulk polymerisation of a radiation curable resin without the use of solvents. The process takes place at room temperature, upon irradiation of UV light if a suitable photoinitiator is used: in a very short time (from milliseconds to seconds) the coating is cross-linked [130]. The curable formulation can contain different monomers and resins, depending on the application. Water, as the non-toxic diluent thinner, already largely used for traditional paints and varnishes, has been introduced in

UV curable formulation very recently and few products of this type are available [83,131,132].

In this chapter, the design, application and characterisation of well defined model structures of waterborne UV curing coatings as neat and modified on purpose in order to obtain nano-structured waterborne films with improved corrosion resistance and thermo-mechanical properties are described. The modification of the waterborne matrix was performed adding silicon based hybrid molecules, such as TEOS and GPTS (already used in the previous chapter to form hybrid sol-gel coupling films on different metals), to the polymeric matrix. The aim is to enhance the corrosion protection properties of the UV curable organic coating using the silicon alkoxides molecules. For this purpose, two approaches were used:

- to use the silicon alkoxides to promote the formation of inorganic domains directly into the polymeric matrix (in situ);
- to use the silicon alkoxides as coupling agents between inorganic nanoparticles and the organic matrix of the polymer:

The corrosion protection properties of this new coatings materials are not well known, but the possible application in the field of corrosion protection of metallic substrates are very interesting because of the environmental compatibility of the protecting system [133].

3.1   Urethane acrylic coatings

In this section the synthesis and characterization of UV curable anionomeric polyurethane resins having polyether backbones of different molecular weight and acrylic functional groups were carried out [134]. In this case no modification of the matrix with silicon alkoxides was carried out because of this was a preliminary study on the properties of the neat polymeric matrix. The results obtained in this section were used for comparison with the silicon alkoxides modified organic coatings.

Thus, in this section the design, application and characterisation of well defined model structures of polyurethane waterborne UV curing coatings are presented. Polyurethane aqueous dispersions are widely accepted owing to their better durability, adhesion and mechanical properties [135,136]. These products basically consist of ionomeric structures [137] where the polymeric backbones bear salified groups like carboxyls $-COO^-M^+$ or quaternary ammonium salts $-NR_4^+X^-$. Basically, these ionic groups act like internal emulsifiers of the hydrophobic polymer allowing its dispersion in water as stabilised particles (macromolecular aggregates of 10^3 nm size as an average). Both monocomponent and bicomponent waterborne polyurethanes [138–140] are known in the literature. In particular, monocomponent systems are substantially thermoplastics, which can be eventually crosslinked after film formation and physical drying. Bicomponent systems [141–145] are made of functionalised polyurethanes, for example with hydroxyl groups, and are

formulated with suitable cross-linkers, such as water dispersible polyisocyanates. In this case the formulation has a limited pot life: beyond a limit time, gelling occurs and the polymeric system shows poor, if any, film forming properties. The aqueous dispersion used in this study contains a polyurethane ionomeric structure with acrylic end groups and after water removal are easily cured.

In this section, the synthesis of new anionomeric polyurethane resins having polyether backbones of different molecular weight and acrylic functional groups will be discussed. The thermo-mechanical properties of the coatings were investigated by means of both Thermal gravimetric analysis (TGA), performed on the cured coatings, DSC measurements and dynamic-mechanical analyses (DMA) on self-supported films.

Moreover a complete electrochemical characterisation of the corrosion protection properties of the UV curable waterborne urethane acrylic coatings was carried out by means of electrochemical impedance spectroscopy [EIS].

3.1.1 Preparation of the UV curable urethane acrylic coatings

The waterborne resins considered in this section are segmented anionomeric polyurethanes functionalized with acrylic end groups. They were prepared starting from polytetramethylene glycol (PTMG, see Figure 3.1), isophorone diisocyanate (IPDI, see Figure 3.2), dimethylol propionic acid (DMPA, see Figure 3.3), and hydroxyethylacrylate (HEA, see Figure 3.4), according to

general synthesis and dispersion procedures described elsewhere in literature [144,146].

No more details about the synthesis procedure are reported in this work, because it is not strictly related to the topic of this chapter.
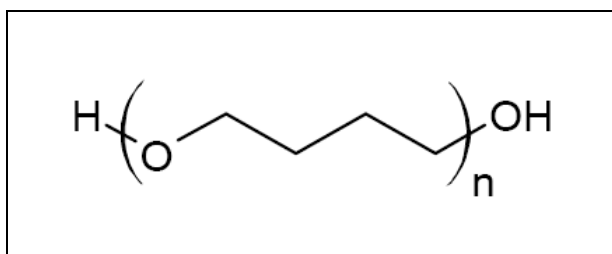
Figure 3.1 Schematic representation of polytetramethylene glycol
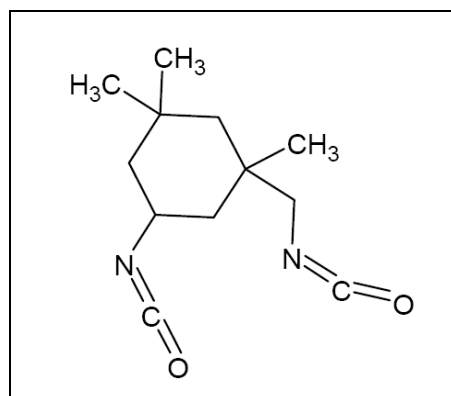
Figure 3.2 Schematic representation of isophorone diisocyanate
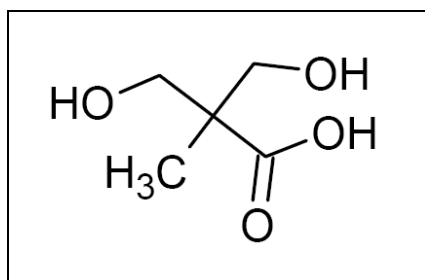
Figure 3.3 Schematic representation of dimethylol propionic acid
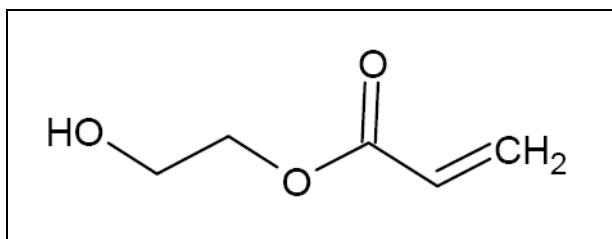
Figure 3.4 Schematic representation of hydroxyethylacrylate

Segmented anionomeric polyurethanes based on polyethers with different molecular weight (PTMG 2000 or 1000) and cycloaliphatic diisocyanates (IPDI) were synthesized following the two-step process shown in Figure 3.5 [145].

Two different lengths, 1000 or 2000, of the polytetramethylene glycol were tested in order to investigate the effect of this parameter on the properties of the coatings.
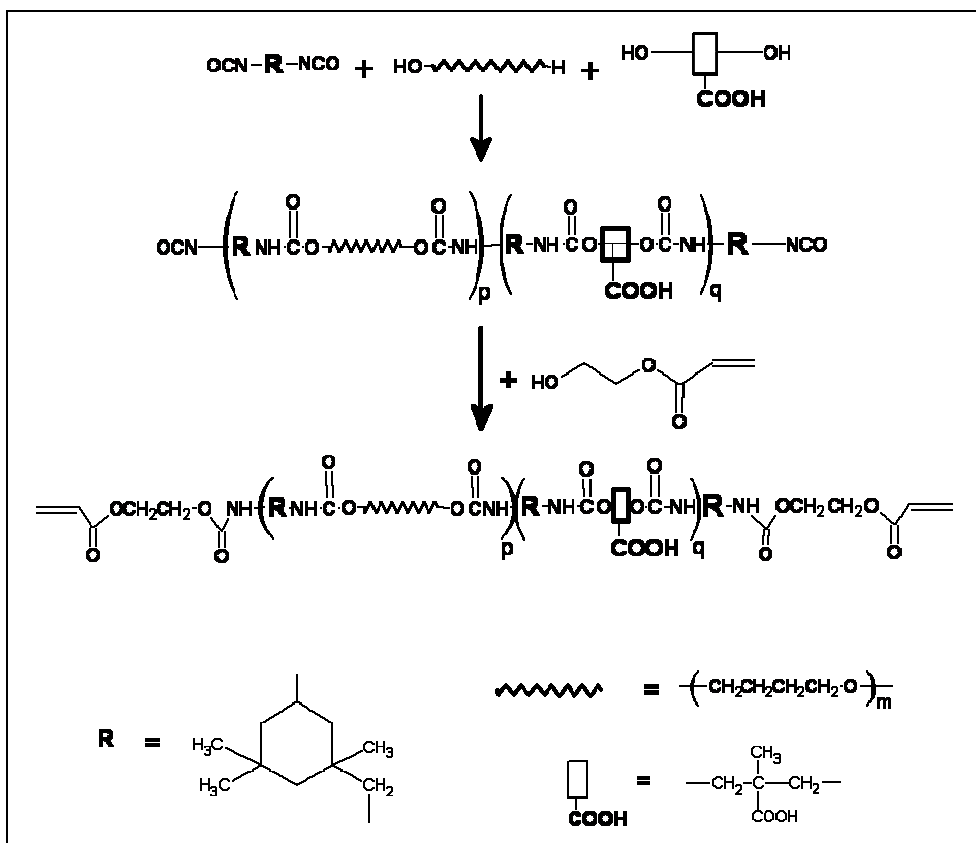
Figure 3.5 Schematic representation of the two-steps synthesis process

In addition, the efficiency of two different photoinitiators was checked. In particular, the effect of 2-Hydroxy-2-methyl-1-phenylpropan-1-one (Darocur 1173[®], supplied by Ciba, see Figure 3.6) and benzophenone (see Figure 3.7) were compared. They were added into the aqueous curable mixtures at a concentration equal to 3w/w% with respect to the solid content. Their dispersion was obtained by the aid of an ultrasound bath.
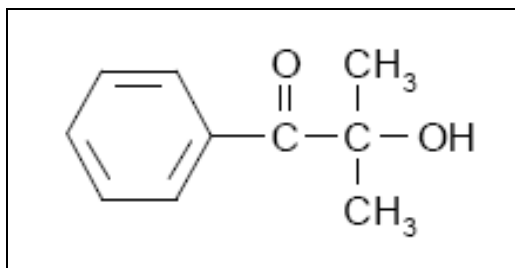
Figure 3.6 Schematic representation of Hydroxy-2-methyl-1-phenylpropan-1-one
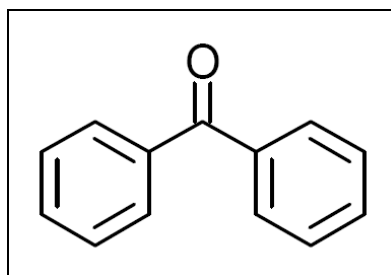
Figure 3.7 Schematic representation of benzophenone

The aqueous dispersions were cast onto well cleaned glass for mechanical testing and mild steel substrates (supplied by Q-Lab) for the electrochemical characterization. The samples were heat treated in a oven at 70°C for 1 h in order to remove water, then they were cured by UV irradiation with a 500 W medium pressure Hg lamp (light intensity on the film surface: 25 mW/cm^2). The irradiation time was 60 seconds under nitrogen atmosphere. The final coating thickness was 100 ± 20 μm.

3.1.2 Characterization of the UV curable urethane acrylic coatings

As stated beforehand, the influence of two different lengths of the chain of the polytetramethylene glycol and the effect of two sorts of photoinitiator (2-Hydroxy-2-methyl-1-phenylpropan-1-one and benzophenone) were investigated. Table 3.1 indicates the different properties of the two resins obtained starting from a 1000 Mn or a 2000 Mn PTMG macromolecule, indicated as PUD-A and PUD-B, respectively. The molecular characterization of resins was made by chemical titration according to ASTM D2572, by FTIR spectroscopy with a Nicolet Nexus spectrometer, and by GPC with a Waters instrument calibrated with polystyrene narrow standards and equipped with a refractive index detector. During the first step a NCO terminated prepolymer was formed and its isocyanate content was checked by dibutylamine/HCl backtitration. Then the prepolymer was endcapped with HEA after dilution with N-methyl Pyrrolidone (NMP, 10% on solid). FTIR spectroscopy and Gel Permeation Chromatography (GPC) were used to control conversion (disappearance of NCO stretching band at 2260 cm^{-1}) and molecular weight of the resin obtained. The structures synthesized are indicated as anionomers since they contain DMPA which can be neutralized with triethylamine allowing its dispersion in water. Consequently, once formed, the anionomer was poured in water under high speed stirring obtaining the final aqueous dispersion at solid 30%.

Table 3.1 Properties of the two resins: PUD-A and PUD-B

	PUD-A	PUD-B
PTMG Mn	2000	1000
[COOH], eq/Kg	0.30	0.30
[C=C], eq/Kg	0.69	0.91
Anionomer Mn and Mw	12200, 24500	5250, 10500
pH of the dispersion	7.0	6.8
Solid content (w/w%)	30	30

Following the previously described UV-curing procedure, it is possible to obtain free-standing, non tacky films, with both the photoinitiator chosen for the curing reaction. After the UV irradiation the coatings are highly crosslinked and insoluble. The gel content of the films was determined by measuring the weight loss of the sample after extraction with $CHCl_3$ for 16 hours at room temperature. According to the gel percentage values reported in Table 3.2, well crosslinked films could be obtained in presence of both photoinitiators.

Table 3.2 Gel content percentage with the two different photoinitiator

	Gel content [%]	
Sample	Benzophenone	Darocur 1173
PUD-A	99.7%	99.5%
PUD-B	98.3%	99.7%

Thermal gravimetric analysis (TGA) was performed on the cured coatings using a LECO TGA-601 apparatus: measurements were recorded in air, in a temperature range of 0°C - 700°C, 10°C/min heating rate. DSC measurements were made with a Mettler Toledo 30 calorimeter, temperature range: -100°C - 150°C, cooling/heating rate 20°C/min, nitrogen atmosphere. Dynamic-mechanical analyses (DMA) on self-supported films were made in shear mode with a Mettler-Toledo DMA/SDTA 861e instrument in dynamic scans from -100° to +200°C with heating rate 2°/min. The results of the dynamic mechanical and calorimetric investigations are summarized in Table 3.3.

Table 3.3 Main results of dynamic-mechanical and calorimetric analysis

Sample	Tg (DSC) [°C]	G'$_{23°C}$ [MPa]	G'$_{100°C}$ [MPa]
PUD-A	-57	0.9	0.4
PUD-B	-34	1.6	1.0

Concerning the thermal properties, the DSC analysis shows the presence of T_g lower than ambient temperature, and, therefore, the products should be considered as rubbery and flexible coatings. This statement is confirmed also by DMA analysis of films which shows that at room temperature the films are already in the rubbery plateau. Increasing the temperature, the storage shear modulus G' value doesn't vary significantly (G' of the order of 1 MPa). This is a further evidence, besides the gel content, that the coatings are well crosslinked. All coatings show an intrinsic high thermal stability. For example, the dynamic TGA curves showed in Figure 3.8 describes the thermal behaviour of PUD-A.

Notice that there is no strong weight loss up to 190-200°C. A similar trend was found for the other systems.
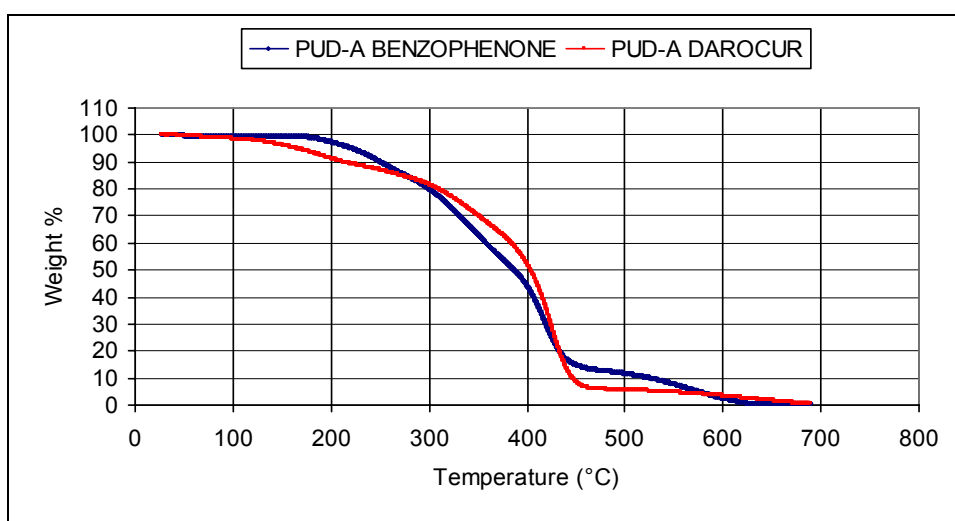
Figure 3.8 TGA curves for samples PUD-A and PUD-B

In Table 3.4 the T50 values (i.e. the temperature at which the coating loses 50% of the initial weight) are reported: they are always well above 350°C.

Table 3.4 Temperature at which the coating loses 50% of the initial weight

Sample	T_{50} (°C)
PUD-A benzophenone	389
PUD-A Darocur 1173	404
PUD-B benzophenone	368
PUD-B Darocur 1173	390

The corrosion protection properties of the coatings were evaluated by means electrochemical impedance measurements (EIS) recorded after different immersion time for 20 days of testing. The studied samples were the PUD-A and PUD-B coatings produced using Darocur 1173 as the photoinitiator. In fact, the previous experimental investigation of the thermo-mechanical properties of the coatings highlighted the better properties of the coatings UV cured using Darocur 1173 respect to the similar coatings crosslinked using benzophenone. For this reason, the electrochemical measurements were performed only on the UV cured coatings containing Darocur 1173.

To perform the EIS measurements, a classical three electrodes arrangement was used. An Ag/AgCl (+0.207 V vs. SHE) electrode and a platinum ring were used as reference and counter electrode, respectively. The frequency range used for these measurements was from 10^5 Hz to 10^{-2} Hz, while the signal amplitude was 20 mV. The immersed area was about 1.5 cm^2 and the testing solution was 0.3w/w% Na_2SO_4. This electrolyte is not very aggressive, it is just a conductive liquid media. At this level it is not important to check the corrosion resistance of the protection system, the aim of the electrochemical measurements is to investigate the properties of the coating itself. In fact, the substrate was not pre-treated to improve the adhesion of the UV cured coating e no pigments are embedded into the polymeric films.

Concerning the electrochemical measurements, Figure 3.9 shows the evolution of the free corrosion potential (E_{corr}) for the two coating materials during the 500 hours of immersion in the electrolyte solution.
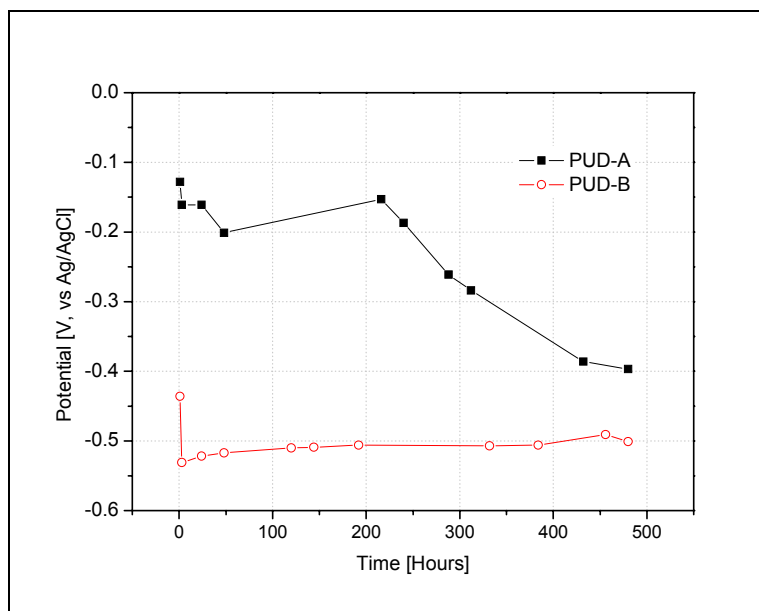
Figure 3.9 Corrosion potential with the time of immersion in the electrolyte

It is clear that the samples show a different behaviour. It is important to remember that PUD-A and PUD-B differs mainly for the molecular weight of the starting PTMG (see Table 3.1), leading to different structural properties (Table 3.3). The PUD-A sample starts with a nobler E_{corr} value, which is in general associated to higher barrier properties and lower corrosion rate [147], while the PUD-B sample shows from the beginning E_{corr} values closer to the typical free corrosion potential values of bare steel. After 500 hours of immersion the differences are remarkably reduced and both samples show corrosion potential values in the order of -0.4 ÷ -0.5 V vs. Ag/AgCl.

Figure 3.10 shows the impedance modulus (a) and the impedance phase (b) as a function of the immersion time for the sample PUD-A.
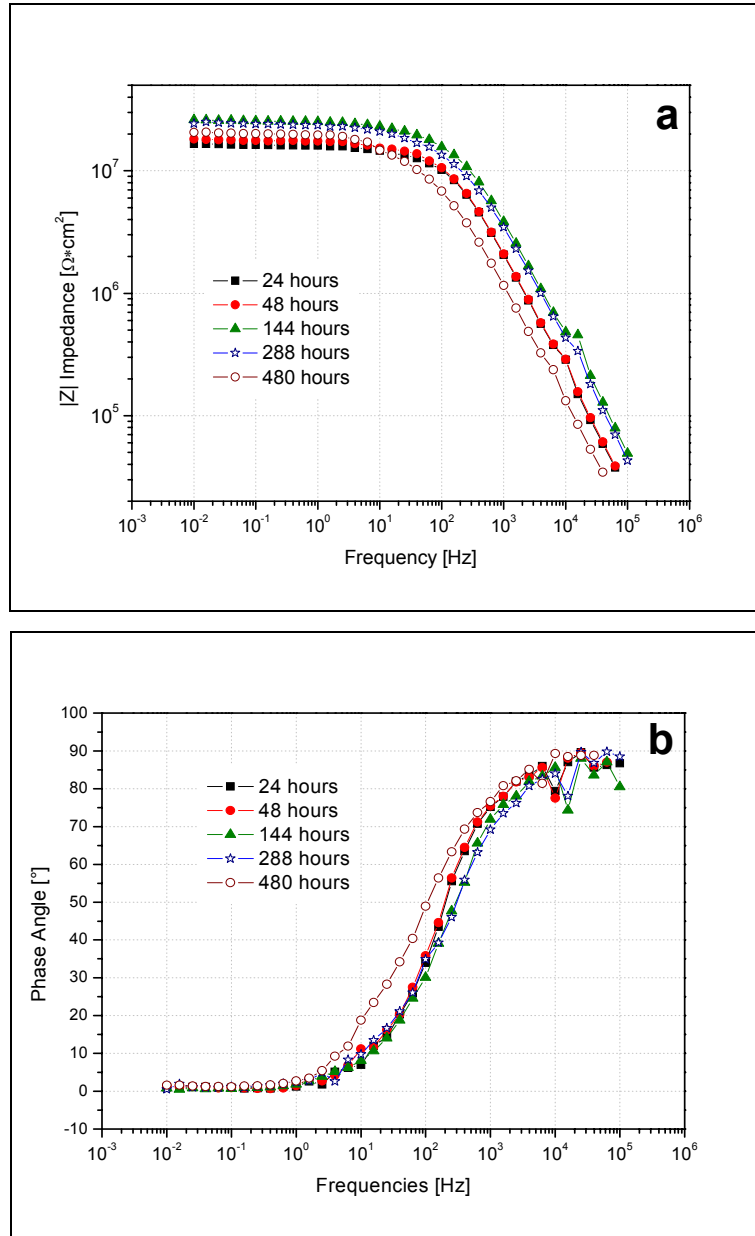
Figure 3.10 Impedance modulus (a) and phase (b) for sample PUD-A with the time of immersion in 0.3w/w% Na_2SO_4

It is interesting to note that the low frequencies impedance values, which are a rough indication of the protective properties of the coating [148], are in general high (between 10 and 30 MΩ cm^2). Therefore, these data are a first indication of interesting barrier properties. Moreover, the general trend shows an increase of the total impedance with the immersion time, at least for the first 240 hours of testing. Considering Figure 3.11, a similar but even more evident trend is shown by the sample PUD-B.
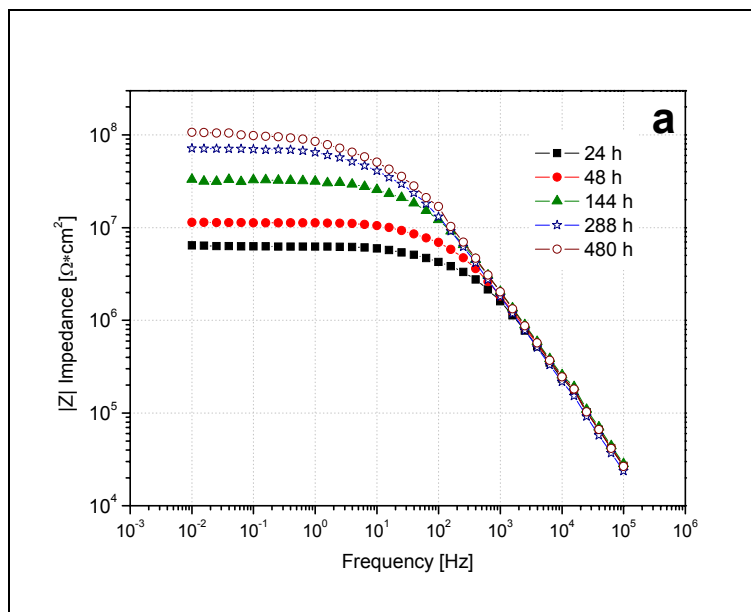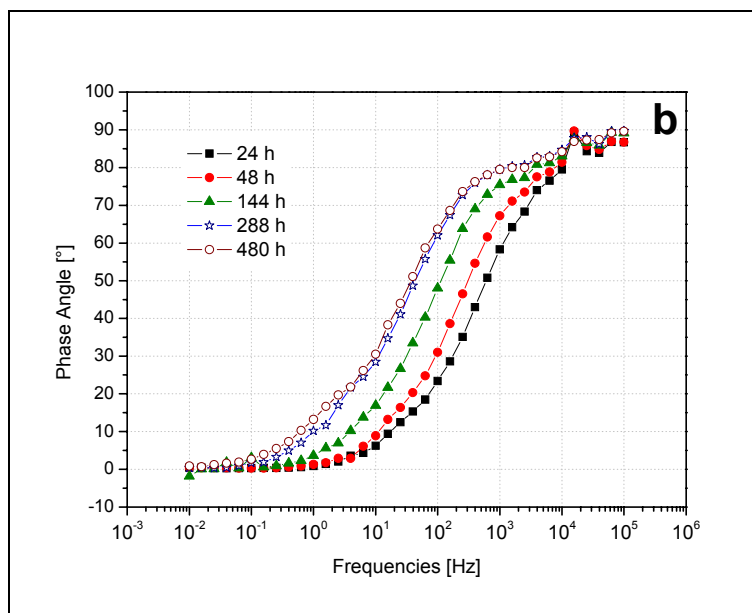
Figure 3.11 Impedance modulus (a) and phase (b) for sample PUD-B with
the time of immersion in 0.3w/w% Na_2SO_4

A clearly visible increase of the total impedance at low frequencies ($10^0 - 10^{-2}$
Hz) is observable in Figure 3.11a, where the changes of the impedance spectra
with the time of immersion are reported for sample PUD-B.

In order to obtain quantitative information from the EIS measurements, the
data were analysed using the suitable equivalent electrical circuits. Despite
apparently just one time constant was clearly visible looking to the EIS plot in
the Bode representation (Figure 3.11 a,b), only by fitting the experimental
results with two time constants it was possible to find a good correlation
between actual and simulated data. The equivalent electrical circuit adopted to
model the EIS data is therefore the circuit in Figure 3.12, where, in addition to
the electrolyte resistance R_{el}, the system is described by the coating capacitance

169

and resistance Q_c and R_c, related to the electrical properties of the waterborne coating, and the charge transfer resistance R_{ct} and double layer capacitance Q_{dl} related to the electrochemical reaction at the metal-coating interface (corrosion reactions) [149].
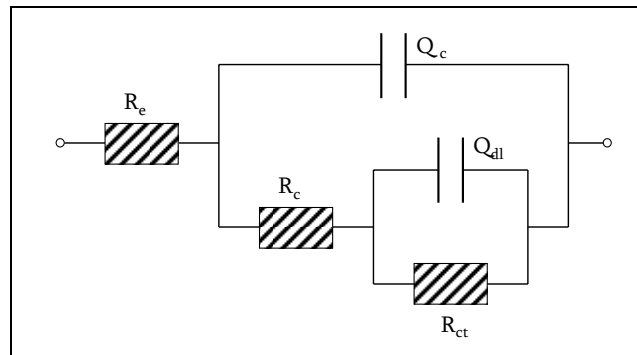
Figure 3.12 Equivalent electrical circuit used for the modelling of the experimental data

The trend of the coating resistance R_c is shown in Figure 3.13. At the beginning the sample PUD-A shows quite high value of coating resistance (in the order of 10 M$\Omega \cdot$cm^2) being an unpigmented thin coating. Moreover, this value is maintained almost constant for all the testing time. Instead, completely different is the behaviour of the sample PUD-B, which shows quite low R_c values at the beginning of the immersion (0.2 MΩ cm^2), but the values increase with the immersion time, reaching, for long immersion time, the same values of sample PUD-A.
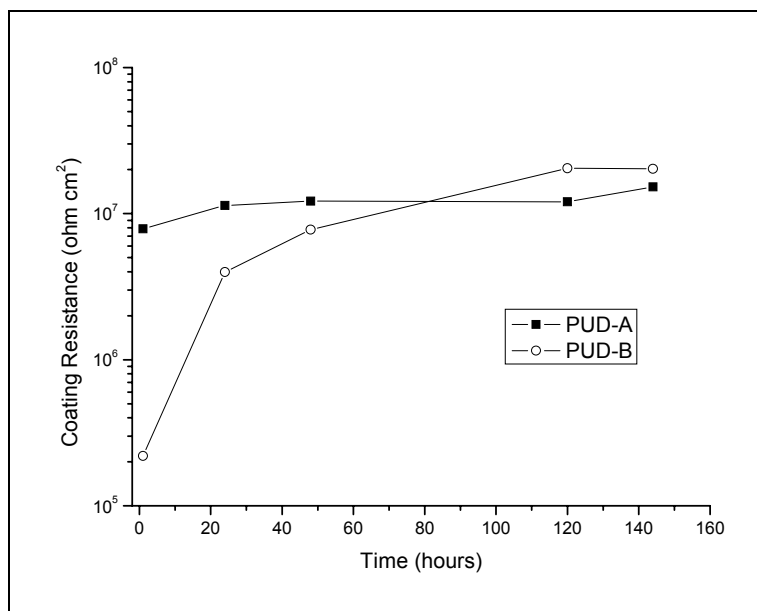
Figure 3.13 Coating resistance with the time of immersion in 0.3w/w% Na_2SO_4

Generally it is unusual to measure an increase of the R_c values with the immersion time. A decrease of the value of the coating resistance with the immersion time in an electrolyte solution is usually expected [150,151]. This fact is generally related to the water uptake processes which can induce swelling in the coating and cause an increase of the ionic barrier properties [152].

In order to verify this hypothesis, the water uptake in the two coatings was measured by analysing the C_c values and applying the Brasher Kingsbury equation (Eq. 3.1) [153]:

$$\Phi = \frac{\log\left(\dfrac{Q_t}{Q_0}\right)}{\log \varepsilon_w} \qquad \text{(Eq. 3.1)}$$

where Φ is the water volume fraction in the coating, Q_t is the coating capacitance after the time t, Q_0 is the initial capacitance of the coating and ε_w is the dielectric permittivity of water at 25°C. The results are reported in Table 3.5 where it is possible to note the higher water uptake in the PUD-B coating.

Table 3.5 Water uptake after about 500 hours of immersion in 0.3w/w% Na_2SO_4

Sample	Water uptake
PUD-A	8.0%
PUD-B	12.6%

The coating PUD-B, produced starting from lower molecular weight polyols, shows lower water barrier properties. For this reason, in a short time water can reach the metal-coating interface and, as a consequence, the free corrosion potential is lower than in the case of sample PUD-A (see Figure 3.9). Ions diffusion is easier and, therefore, R_c values are lower (Figure 3.13). However, the high water uptake can cause coating swelling, increasing with time the values of R_c [154].

This mechanism is confirmed by the evolution of the charge transfer resistance parameter (R_{ct}) shown in Figure 3.14.
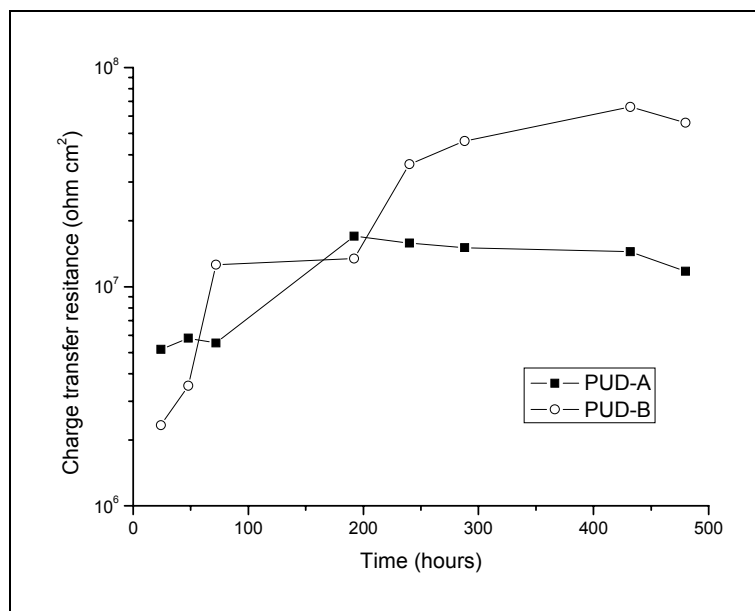
Figure 3.14 Charge transfer resistance with the time of immersion in 0.3w/w% Na_2SO_4

The R_{ct} value is around 10^7 $\Omega \cdot cm^2$ in the case of PUD-A samples, slightly increasing with the immersion time, probably because of the formation of corrosion products partially reducing the corrosion rate. For PUD-B coatings this trend is more stressed: the initial value is lower, because of the lower coating barrier properties and faster water uptake causing higher corrosion degradation, but the R_{ct} increase is more evident, reaching values higher than $5 \cdot 10^7$ $\Omega \cdot cm^2$ after 250-300 hours of immersion, when the initial corrosion products start to be visible under coating.

The overall protection properties ensured by these coatings are not very good. In particular, the barrier properties of the coatings (evidenced by the coating resistance values, see Figure 3.13) are not very high.

In order to improve the corrosion protection level of these coatings, silicon alkoxides molecules were added to the uncured polymeric mixture, as explained in the next section.

3.2 Modified urethane acrylic coatings

The properties of the previously described UV curable coatings can be improved by embedding into the polymer organic or inorganic pigments. The presence of a properly dispersed second phase can, in principle, improve both the mechanical and corrosion resistance properties of the coating. The improved physical properties, such as surface smoothness and barrier properties cannot be achieved by using conventional micro-sized particles; furthermore, the presence of nanostructured fillers in organic coatings can improve the corrosion resistance of the coated metal substrates [154-156].

In this section, the potential of the chemical route of the *in situ* formation of nanostructured inorganic pigments was investigated. In particular, TEOS (tetraetoxysilane) molecules were used to induce, after hydrolysis, the formation of inorganic silica particles into the polymeric matrix. To promote the intercalation of these particles into the UV curable matrix, MEMO (methacryloxypropyltrimethoxysilane) molecules were used. The effect of the modifications on the electrochemical properties of the UV curable waterborne

urethane acrylic coatings was deeply investigated by means of electrochemical impedance spectroscopy.

3.2.1 Preparation of the modified UV curable urethane acrylic coatings

In this section the electrochemical characterization of modified UV curable anionomeric polyurethane resins having polyether backbones of different molecular weight and acrylic functional groups were carried out. The coatings were prepared following approximately the steps described in the previous section (see 3.1.1). In addition, some new elements were added to the waterborne resins composed of segmented anionomeric polyurethanes functionalized with acrylic end groups. Tetraetoxysilane (TEOS, see Figure 3.15) and methacryloxypropyltrimethoxysilane (MEMO, see Figure 3.16) were added to the waterborne resins.
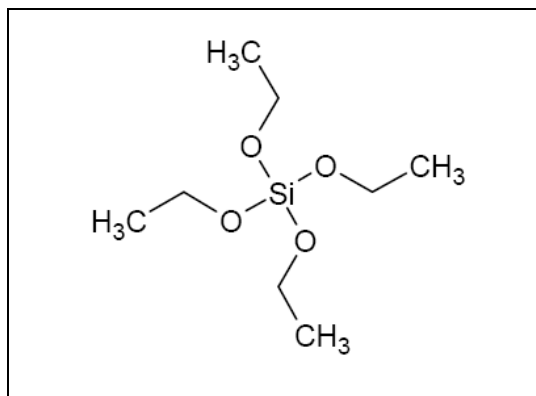
Figure 3.15 Schematic representation of TEOS
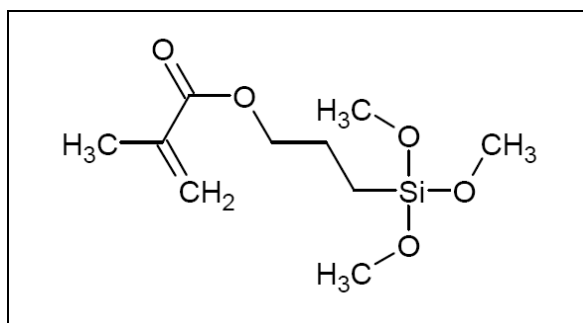
Figure 3.16 Schematic representation of MEMO

TEOS molecules are able, after hydrolysis, to arrange themselves in colloidal silica domains, while MEMO is a sort of coupling agent, able to interact with both organic and inorganic materials. The properties of TEOS molecule were previously discussed in chapter 2. Considering the picture of the MEMO molecule depicted in Figure 3.16, it is possible to appreciate that three Si-O-CH₃ groups and one Si-[methacryloxypropyl] are present. The Si-O-CH₃ bond can hydrolyse. In particular, in presence of water, the Si-O-CH₃ can form Si-OH

groups and methanol (HOCH$_3$) as by-product. Hydrolysed TEOS molecules can generate *in situ* silica domains and the MEMO can graft to the silica domains by means of the Si-OH groups formed after the hydrolysis of the Si-O-CH$_3$ bonds, following approximately the processes reported in literature [157] and, for clearness, showed schematically in Figure 3.17.
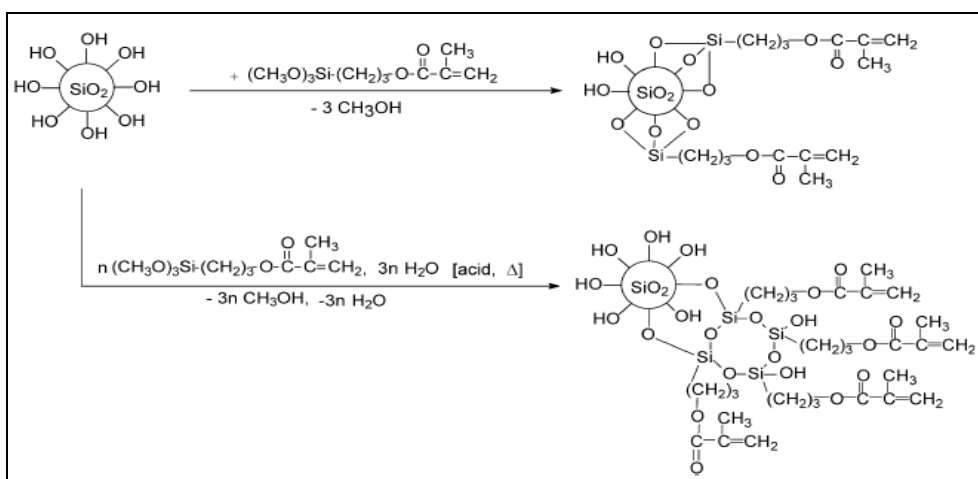
Figure 3.17 Schematic representation of the interaction between MEMO and silica domains [157]

Referring to Figure 3.17, the MEMO molecules are able to surround the silica domains and to graft to them by means of weak hydrogen bonds, at the beginning, and by means of covalent Si-O-Si bonds in a second step. The MEMO molecules can act as a coupling agent between the inorganic silica domains and the polymeric waterborne matrix. Therefore, the MEMO molecule is able, in principle, to enhance the embedding of the inorganic silica fillers into the waterborne polymeric matrix. If properly dispersed and embedded, it is

expected that the presence of an inorganic pigment into the matrix (formed *in situ* after the hydrolysis and condensation reactions) can improve the barrier properties of the UV cured coating.

In this section, the effectiveness of the modification of the waterborne coatings by adding TEOS and MEMO was investigated. In particular, 20 w/w% of TEOS and 5w/w% of MEMO were added to the original waterborne polymeric matrix. Also in this case, two different lengths, 1000 or 2000, of the polytetramethylene glycol were tested in order to investigate the effect of this parameter on the properties of the different coatings. The drying and the UV curing of the coating was carried out following approximately the previously discussed (see previous section) procedure. Also in this case, acetone degreased mild steel (supplied by Q-Lab) was used as substrate, without any surface conversion treatment.

3.2.2 Characterization of the modified UV curable urethane acrylic coatings

The samples investigated in this section are summarized in Table 3.6, which reports, for each sample, the different additives added to modify the waterborne resin.

Table 3.6 Summary of the different samples under investigation

Name	Description	
	PTMG Mn	Additives (w/w%)
PUD-1T	1000	20% TEOS
PUD-1TM	1000	20% TEOS + 5% MEMO
PUD-2T	2000	20% TEOS
PUD-2TM	2000	20% TEOS + 5% MEMO

Considering Table 3.6 it is possible to appreciate that TEOS was added both alone and in combination with MEMO for the purpose to better understand if the combination of the two different molecules improves the properties of the waterborne coating.

In this case, only an electrochemical characterization was carried out, in order to investigate more in depth the potential of these coatings for corrosion protection. The thickness of the different samples was measured before the electrochemical characterization and the results are reported in Table 3.7

Table 3.7 Thickness of the different samples

Sample	Thickness	St. Dev.
PUD-1T	75.2	20.4
PUD-1TM	95.5	49.2
PUD-2T	105.6	17.5
PUD-2TM	150.4	27.1

The thickness of the produced samples seems slightly not homogeneous. This statement is proved by the high values on the standard deviation of the thickness measurements (see Table 3.7).

The electrochemical characterization consists mainly in electrochemical impedance spectroscopy measurements. According to the measurement performed on the unfilled waterborne polymeric matrix, to acquire the experimental data a classical three electrodes arrangement was used. An Ag/AgCl (+0.207 V vs. SHE) electrode and a platinum ring were used as reference and counter electrode, respectively. The frequency range used for these measurements was from 10^5 Hz to 10^{-2} Hz while the signal amplitude was 20 mV. The immersed area was about 1.5 cm^2 and the testing solution was 0.3w/w% Na$_2$SO$_4$. First of all, Figure 3.18 shows the trend of the free corrosion potential (E$_{corr}$) with the time of immersion in the conductive solution. Also in this case (compare to Figure 3.9), the coating obtained starting from low molecular weight PTMG molecules shows lower values of E$_{corr}$, very closed to the value corresponding to the free corrosion potential of steel, than the coatings produced starting from higher PTMG molecular weight. However, these differences are remarkable only in the first 200 hours of immersion. In fact, after this lapse of time, the potential of PUD-2T and PUD-2TM decreases to potential values close to the other two samples.
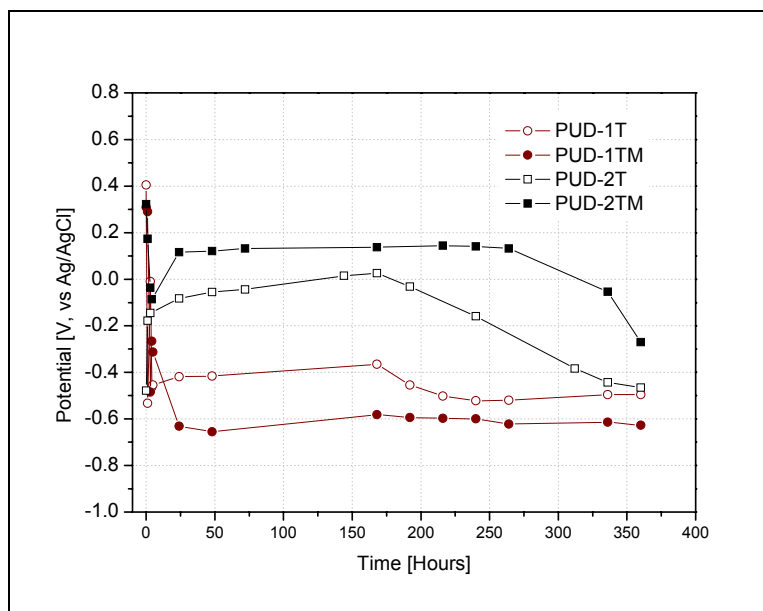
Figure 3.18 Potential vs. time of immersion in 0.3w/w% Na₂SO₄

The EIS spectra were acquired during the immersion of the samples in the conductive solution, in order to monitor the evolution of the electrochemical properties of the coatings with time. As specified in the previous section, at this level of the study the attention was mainly focused on the properties of the waterborne coating itself, not on the other aspects (such as adhesion which, actually has a dramatic effect of the corrosion protection level ensured by an organic coating) which affect the corrosion protection performances of the protection systems.

The evolution of the electrochemical impedance spectra of the different samples are reported in Figure 3.19, after 1 hour of immersion in the electrolyte, and in Figure 3.20, at the end of the test, after about 360 hours of immersion.
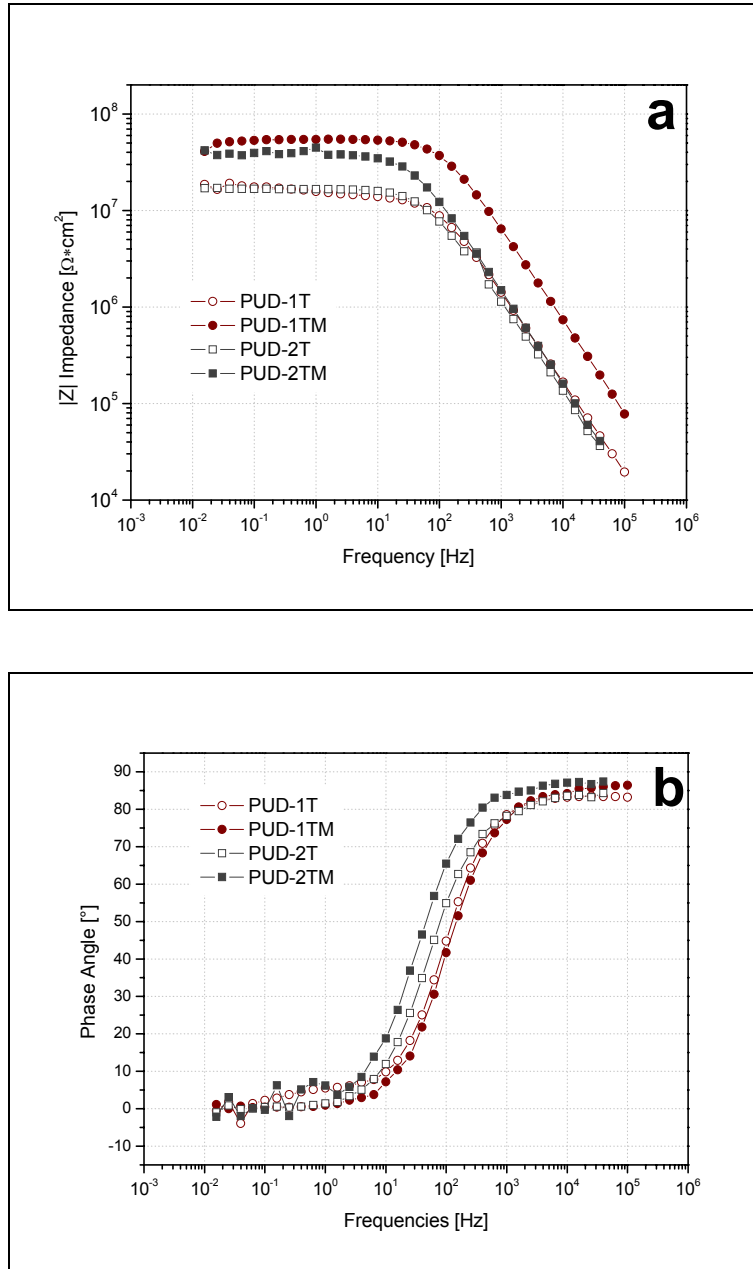
Figure 3.19 Impedance modulus (a) and phase (b) of the studied samples after 1 hour of immersion in 0.3w/w% Na_2SO_4

After 1 hour of immersion (see Figure 3.19), the EIS spectra of the different samples are quite similar. However, the samples containing only TEOS show impedance values at low frequencies around 10^7 Ω cm^2, while the coatings containing the combination of TEOS and MEMO show quite higher values of the impedance, in the order of $5 \cdot 10^7$ Ω cm^2. At this level, it seems that the presence of the MEMO enhances the performances of the waterborne coatings. Considering the shape of the Bode modulus spectra, reported in Figure 3.19b, there are not noticeable differences, except for a sort of second time constant for sample PUD-1T, appreciable in the low frequencies domain ($10^0 - 10^{-1}$ Hz).
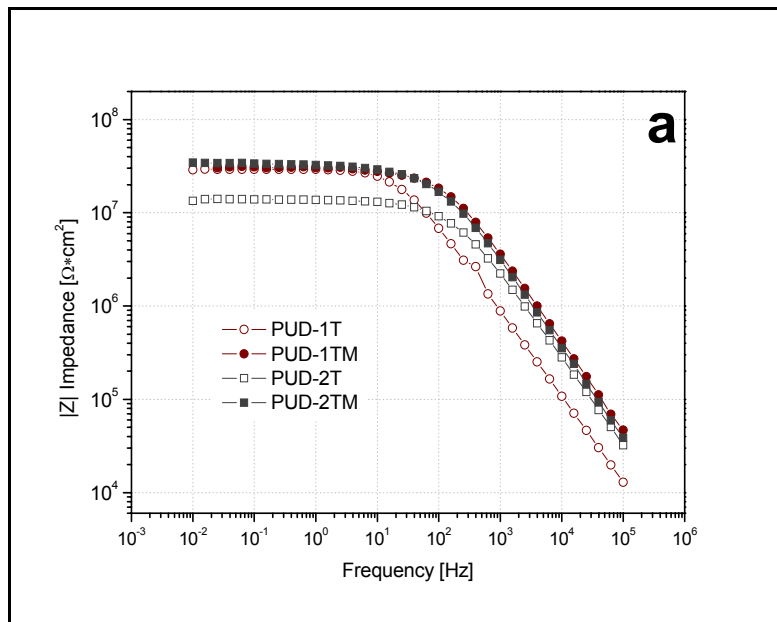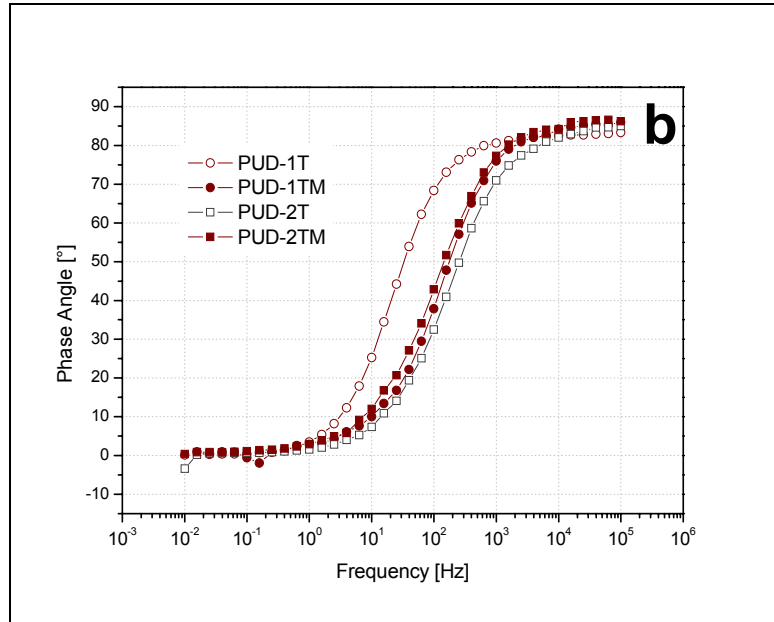
Figure 3.20 Impedance modulus (a) and phase (b) of the studied samples after 360 hours of immersion in 0.3w/w% Na_2SO_4

After 360 hours of continuous immersion (see Figure 3.20), the Bode modulus and phase spectra looks very similar. To better understand the slight differences among the samples the impedance spectra were modelled using the convenient equivalent electrical circuits. Figure 3.21 shows the two equivalent circuits used for the modelling of the experimental data [158].

The first one (Figure 3.21a), is related to the intact coating, and was used in the first hours, or days, of immersion. It contains the elements related to the capacitance (Q_c) and the resistance (R_c) of the waterborne coating.

The second one (Figure 3.21b), corresponds to a defected coating, where a corrosion process tooks place. Besides the equivalent electrical elements related

to the coating (Q_c, R_c), the terms corresponding to the corrosion process (charge transfer resistance R_{ct}, and double layer capacitance Q_{dl}) are also present [159]. After different periods it was always (for all the different samples) necessary to use the two time constant model (Figure 3.21b), due to a corrosion processes occurring under-paint. For both the models, R_e represents the resistance of the electrolyte.
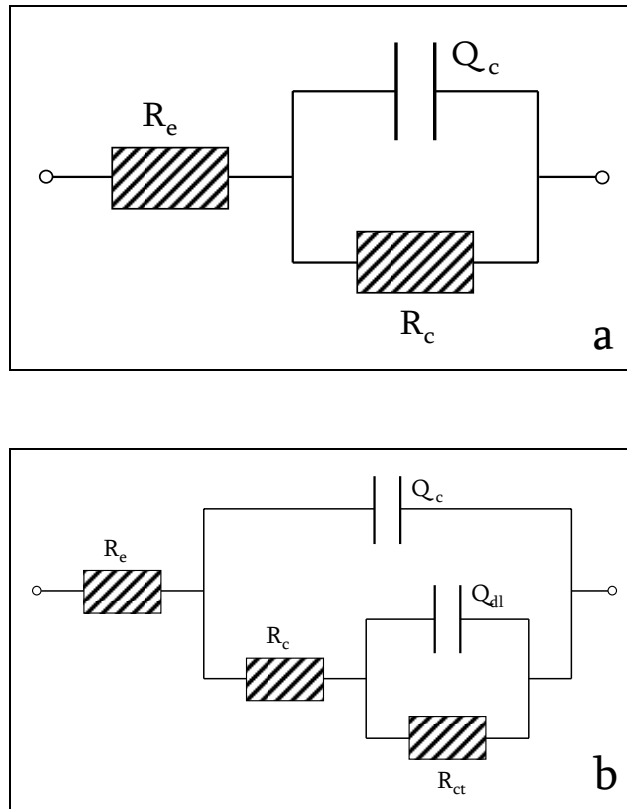
Figure 3.21 Equivalent electrical circuits used for the modelling of the experimental data

The results of the modelling of the experimental data related to the properties of the waterborne coatings are reported in Figure 3.22 (coating resistance, $R_{coating}$) and in Figure 3.23 (coating capacitance, $Q_{coating}$) as a function of the immersion time.
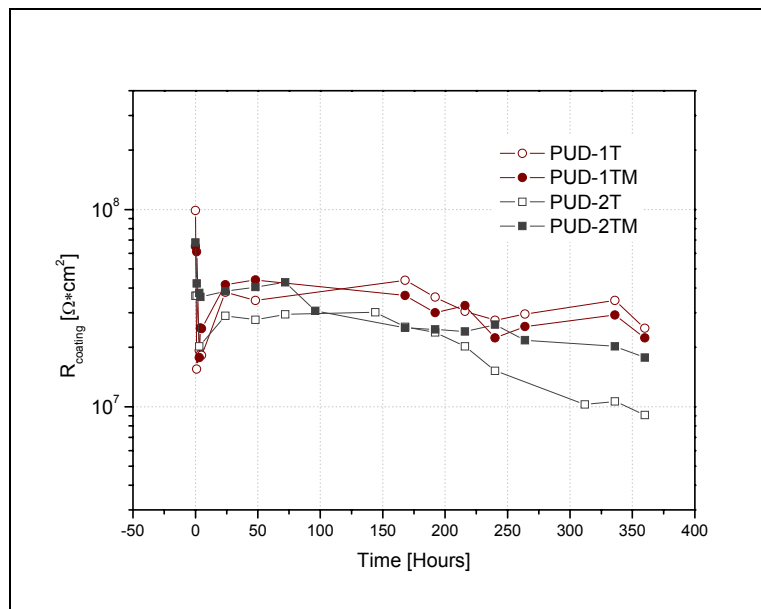
Figure 3.22 Coating resistance with immersion time in 0.3w/w% Na_2SO_4

The trends of the coating resistance are very similar. Despite the different thickness, the coatings show comparable values of the barrier properties. A certain difference is appreciable after about 200 hours of immersion, due to a higher decreasing rate of the resistance of sample PUD-2T compared to all the other samples. However, in general, the absolute values of the coating

resistance of the different samples are comparable and no remarkable differences are highlighted.

Considering Figure 3.23, it is possible to appreciate some differences among the coatings. In fact, the coating containing MEMO shows mainly stable values of the capacitance, regardless of the different length of the PTMG, even after relatively long time of immersion. On the other hand, the samples containing only TEOS shows an increase of the coating capacitance, related to noticeable water absorption during immersion [159], probably owed to the hydrophilic nature of TEOS.
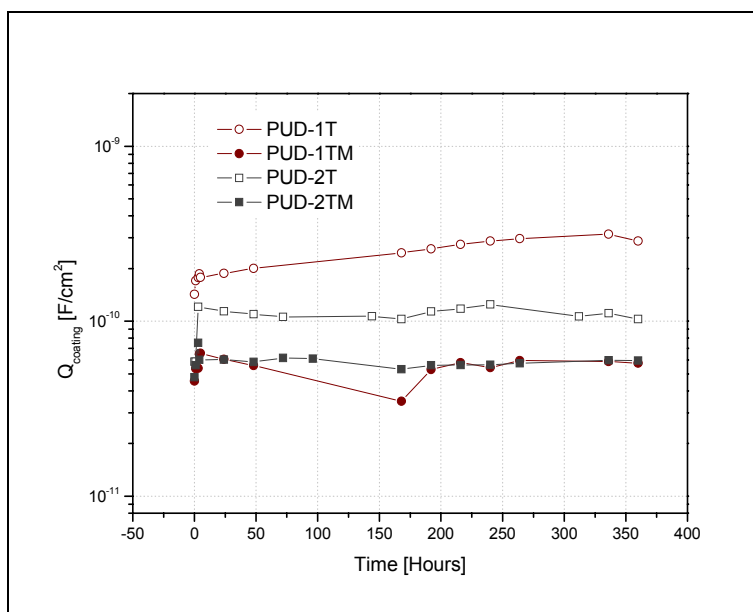
Figure 3.23 Coating capacitance with immersion time in 0.3w/w% Na$_2$SO

A finer comparison among the different samples can be carried out by considering the experimental values of the coating capacitances normalized by the values of the thickness of the different coatings. In particular, by means of a simple relation (Eq. 3.2) it is possible to determine the value of the relative dielectric permittivity at 25°C of the different coatings.

$$\varepsilon_R = \frac{Q_{coating} \cdot d}{\varepsilon_0} \qquad \text{(Eq. 3.2)}$$

Applying the above mentioned equation, it is possible to find out the values of the relative dielectric permittivity at 25°C for the different coating as a function of the time of immersion in 0.3w/w% Na_2SO_4, considering negligible the water uptake at the metal/polymer interface which affect the estimation of the relative permittivity of the coating. Actually, strictly speaking, the estimation of relative permittivity obtained applying Eq. 2 is correct only in the first 24 – 48 hours of immersion.

Figure 3.24 reports the evolution of this parameter over immersion time in the conductive solution. Figure 3.24 highlights better than the coating capacitance reported in Figure 3.23 the different performances of the waterborne coatings.
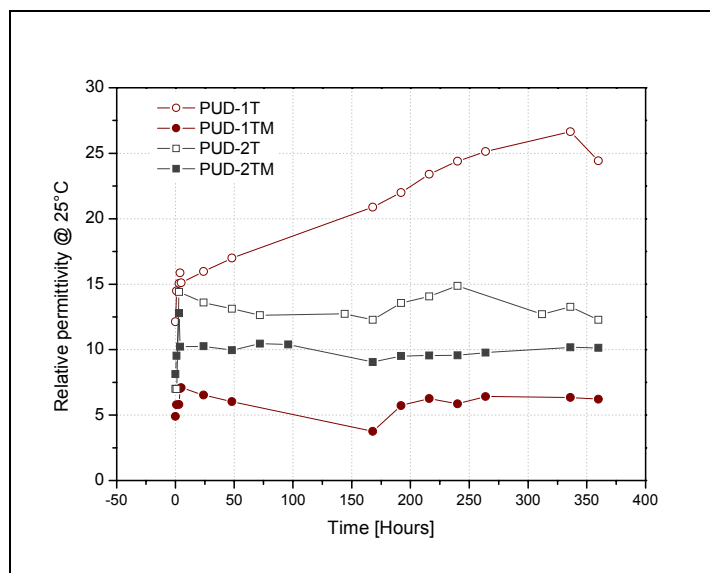
Figure 3.24 Relative dielectric permittivity at 25°C with the time of immersion in 0.3w/w% Na_2SO_4

Sample PUD-1TM is characterized by the lowest values of the relative permittivity (5-6), very close to the values of a dry polymer (3-4). In addition, these values are really stable.

Sample PUD-2TM shows higher values of ε_r, around 10, but, also in this case, a certain stability of the relative permittivity value is appreciable, except for the first hours of immersion, when an increase of ε_r is observable (starting from values around 7). Sample PUD-2T shows ε_r values around 13. Starting from the value of 7, it gets quickly higher values of the permittivity, around 13-14. However, after the very fast initial increase, the values of the relative permittivity stabilize. The values of ε_r for sample PUD-1T increases with an approximately constant rate during all the immersion time. In particular, it

starts from a value around 12 and get, at the end of the immersion test, a value higher than 25. Remark that the estimation of ε_r carried out by applying Eq. 2 is correct at all only in the firs ours of immersion (24-48). After this period, the effect of the water accumulation at the metal/polymer interface affects the calculated values of ε_r. However, this fact does not change the meaning of the discussion about the different properties of the coatings. These experimental results evidences that the presence of MEMO seems to have a positive effect on the properties of the coatings. In particular, this effect seems to be more considerable in combination with a low molecular weight PTMG in the starting polymer. It is likely that the presence of TEOS without MEMO leads to a high hydrophilic behaviour of the coating which draws in a huge amount of water molecules.

The corrosion protection properties of the coatings were investigated more in depth considering the equivalent electrical parameters related to the electrochemical processes occurring at the metal/polymer interface. In fact, when to water reaches the metal surface, corrosion reactions takes place. Figure 3.25 and Figure 3.26 show the evolution of the charge transfer resistance, R_{ct}, and the double layer capacitance, Q_{dl}, respectively.
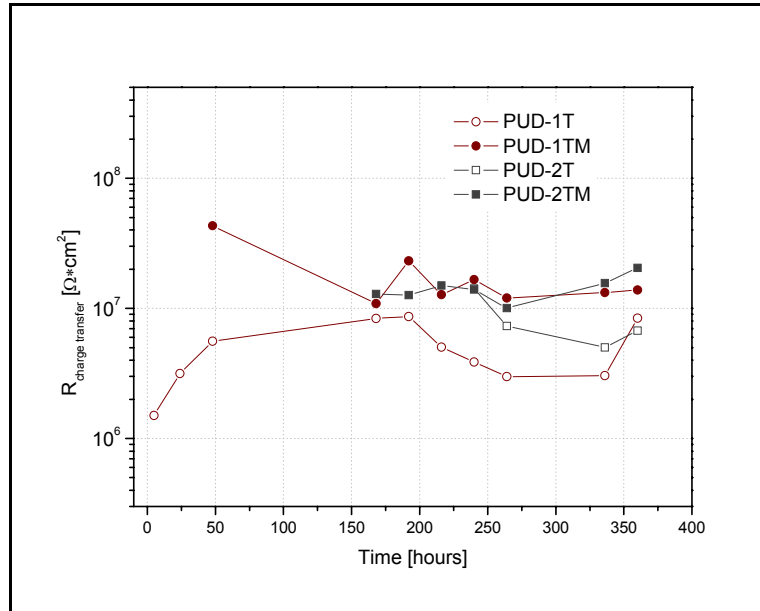
Figure 3.25 R_{ct} with the time of immersion in 0.3w/w% Na_2SO_4
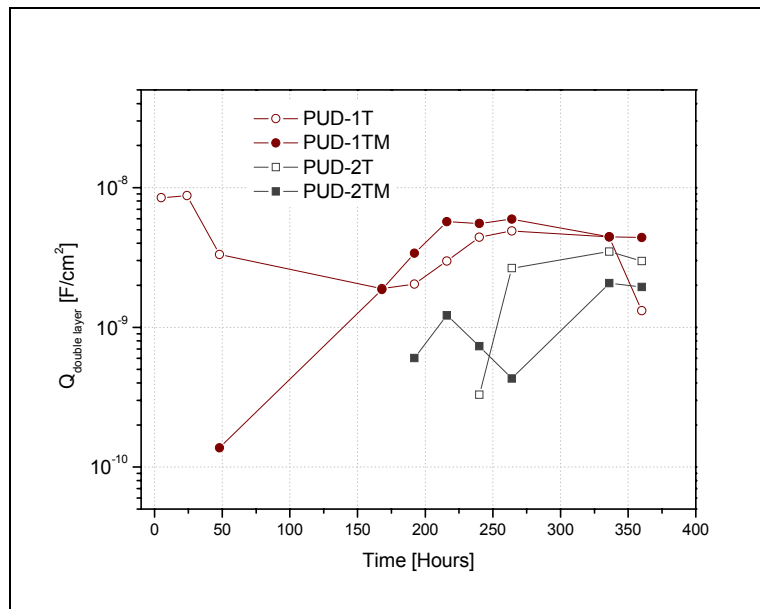
Figure 3.26 Q_{dl} with the time of immersion in 0.3w/w% Na_2SO_4

These two parameters are related to the corrosion process occurring under-paint. Q_{dl} is in an indicator of the extent of the portion of the metal surface in contact with the electrolyte, while R_{ct} is inversely proportional to the corrosion rate [110]. Considering Figure 3.26 it is evident that the parameter related to the corrosion process (Q_{dl} and R_{ct}) are detachable, for each samples, after different lapses of time. In fact, longer the time for water to reach the polymer/metal interface, longer the time to see the second time constant in the impedance spectra related to the electrochemical processes on metal surfaces. At the end of the test all the different samples reach more or less the same values of the two parameters describing the corrosion process. This is related to the low adhesion between the metal substrate and the polymeric coating, due to the absence of a convenient pre-treatment of the metal substrate.

As far as the appearance of the samples after the 400 hours of immersion is considered, Figure 3.27 (a,b,c and d) depicts PUD-1T, PUD-2T, PUD-1TM and PUD-2TM, respectively.
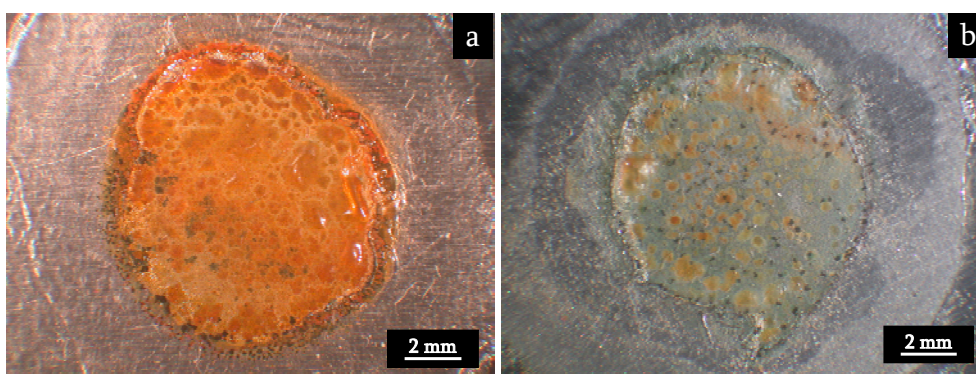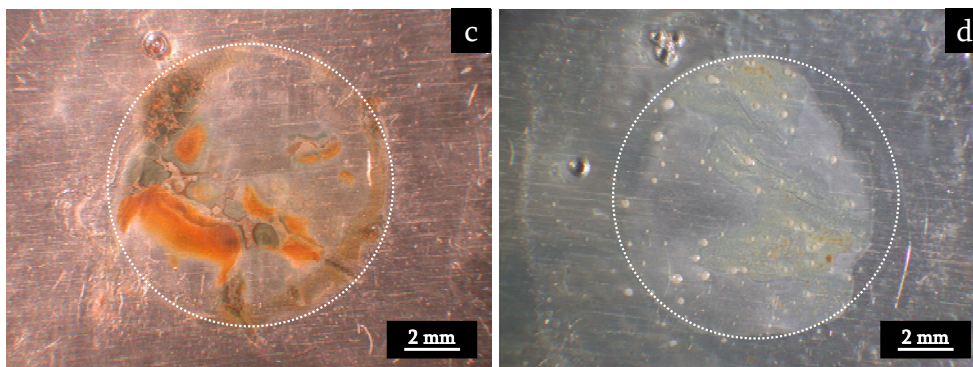
Figure 3.27 Appearance of the area affected by the electrolyte after 360 hours of continuous immersion: PUD-1T (a), PUD-2T (b), PUD-1TM (c), PUD-2TM (d)

Since Figure 3.27 gives only a qualitative representation of the extent of the corrosion process occurring under paint, it is possible to note that sample PUD-1T shows evidences of an advanced corrosion process. On the other hand, sample PUD-2TM shows a very low amount of corrosion products under paint, indicating a limited advance of the corrosion reactions.

In the light of the experimental results, it can be stated that it is possible to decrease the water absorption of a UV curable waterborne organic coating by promoting an *in situ* formation of inorganic silica particles. It is likely that the MEMO molecules act as a coupling agent between the silica particles and the polymeric matrix leading to a decrease of the susceptibility to water absorption. However, despite the modification of the polymeric structure performed adding the silicon alkoxides, the corrosion protection properties are not very high. For this reason, the a different approach was used, adding directly inorganic nanoparticles (montmorillonite nanoparticles) into the polymeric matrix and

using silicon alkoxides molecules as coupling agents to embed the particles into the polymeric matrix.

3.3 UV-cured nanostructured epoxy coatings containing modified montmorillonite nanoparticles

In the light of the experimental results obtained in the previous section a different approach was used to improve the corrosion protection properties of the UV curable water-borne coatings. Silicon alkoxides were used to graft montmorillonite nanoparticles to the polymeric matrix. For this purpose, the γGPS was employed. This molecule (as described in the previous chapter) contains an epoxy group bonded to the carbon backbone. For this reason, an epoxy based UV curable waterborne polymer was used: the chemical affinity between the γGPS molecule and the polymeric matrix can lead to the formation of strong covalent bonds

Polymer nanocoatings consist of nanosized mineral particles dispersed into a polymer matrix; among them, polymer–clay nanocomposites are within the most promising materials, since they exhibit good improvements of the aforementioned properties and their cost is quite low.

Polymer/clay mineral composite coatings can be classified in three different types: conventional microcomposites, where stacks of silicate layers are dispersed at a microscale inside the matrix, intercalated nanocomposites, in which some polymer chains are able to insert between the platelets maintaining a long-range order, exfoliated nanocomposites, in which the platelets are not ordered any more but separately and homogeneously dispersed into the matrix as single platelets. In many cases a mixture of intercalated and exfoliated structure is obtained, thus single platelets and tactoids are both present in the material. Although the best final properties are achieved when the clay mineral platelets are fully exfoliated and well dispersed, also their intercalated morphology can ensure good improvements [160].

In order to achieve a good dispersion of the clay minerals into the polymer it is often necessary to modify their surface in order to make them more organophilic and compatible with the polymer matrix. Furthermore, a suitable modification can enhance the interlayer distance of the clay mineral and, thus, facilitate a better swelling of the clay mineral itself in an organic polymer or monomer [161].

The intercalated or the exfoliated morphology of clay mineral layers after modification can be achieved by different methods [162]. Some of them need the presence of the polymer in the molten state and, therefore, can affect its stability; others are solvent-based, thus releasing large amounts of volatile compounds. In-situ intercalative polymerization is also proposed [163]: this process, which is often solvent - based, uses reactive monomers as guest species

to be intercalated. The in-situ intercalative polymerization can be performed by photopolymerizing solvent-free curable systems: the procedure, involving the use of ultra violet light (UV-curing process), guarantees the building up of polymeric thermoset matrices via a fast and environmental friendly process, which exhibits low energy consumption and no emission of volatile organic carbon (VOCs).

Epoxy resins are often used for different applications, such as coatings for metals, because of their excellent properties (high modulus, low creep, stiffness, chemical resistance and good performances at high temperature) and easy manufacturing. However, because of the crosslinking character, epoxy resins present undesirable inconvenients, such as poor resistance to crack initiation and growth, weak heat and corrosion resistance.

The incorporation of layered silicate nanofillers into epoxy resins may represent a good way in order to solve these problems including the improvement of the thermal stability and corrosion resistance. Moreover, since the viscosity of the prepolymers, curing agents and oligomers can be low, their diffusion in between the clay lamellae is not too difficult and can therefore facilitate the achievement of intercalated or exfoliated morphologies as described by many authors [164,165]. Recently the same approach was used for epoxy systems cured by UV light [166-168].

In this section, UV-cured nanostructured coatings were prepared starting from a cycloaliphatic di-epoxy monomer, namely 3, 4 - epoxycyclohexylmethyl - 3', 4'-cyclohexancarboxylate (CE), in which two different types of nanofillers, both

commercial and modified on purpose, were previously dispersed at two different concentrations (5 and 10w/w%) [169]. The nanofillers consist of montmorillonite nanparticles tailored using γGPS molecules in order to promote the chemical interaction between the inorganic nanoparticles and the polymeric epoxy matrix.

First of all, the level of compatibility between the nanoclays and the epoxy resin was investigated by performing X-ray diffraction analyses (XRD) on the liquid dispersions The same analyses were previously performed on the nanoclay powders, in order to evaluate their basal spacing and its possible increase after their modification. Moreover XRD measurements were repeated on the final UV-cured films in order to establish the intercalation/exfoliation level achieved after the UV-curing process. High intercalated or a quasi exfoliated morphologies were obtained. It was confirmed by Transmission Electron Microscopy (TEM) observations.

The kinetics of photopolymerization of the epoxy system, also in the presence of the nanofillers, was investigated by real time Fourier Transfer Infrared Spectroscopy (FT-IR) and correlated to the kind of nanoclays, its modification and its concentration in the epoxy resin.

The obtained UV-cured nanocomposite films were subjected to dynamic-mechanical analysis (DMTA), in order to evaluate their glass transition temperature (Tg); thermo gravimetric analysis (TGA) measurements in air were performed in order to check the thermo-oxidative stability of the nanocomposite coatings, with respect to the pure UV-cured epoxy resin.

Finally, the corrosion resistance of the UV-cured nanostructured coatings, previously applied onto a mild steel substrate, was investigated using Electrochemical Impedance Spectroscopy (EIS) and compared to the behaviour of the neat UV-cured epoxy resin films.

3.3.1 Preparation of the UV curable epoxy coatings containing modified montmorillonite nanoparticles

The epoxy resin, 3,4-epoxycyclohexylmethyl-3',4'-epoxycyclohexancarboxylate (CE) was kindly supplied by Dow Chemicals. Its structure is reported in Figure 3.28.
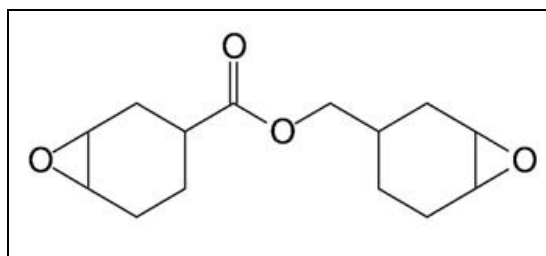
Figure 3.28 Schematic representation of CE

As photoinitiator a commercially available mixture of phosphate sulfonium salts, UVI 6990 (see Figure 3.29), also supplied by Dow Chemicals, was used as solution in propylene carbonate (50 w/w%). This solution was added to the curable mixtures at a concentration of 4 w/w%.
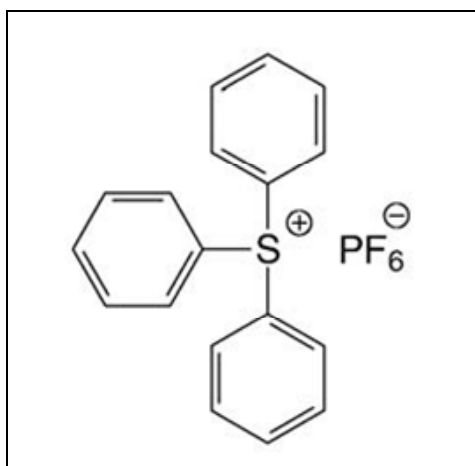
Figure 3.29 Schematic representation of phosphate sulfonium salts

Two commercially available montmorillonites, namely Cloisite Na^{+}® and Cloisite 30B® were purchased from Southern Clay Product Inc. (USA). The former is a native montmorillonite, with a cation-exchange capacity (CEC) of 92 meq/100 g. The latter contains alkyl ammonium quaternary ions (90 meq of quaternary alkyl ammonium ions per 100 g clay) bearing two hydroxyethyl groups linked to the nitrogen atom. The structure of this alkyl ammonium quaternary salt is reported in Figure 3.30, where *T* stands for *tallow* (65% C18, 30% C16 and 5% C14).
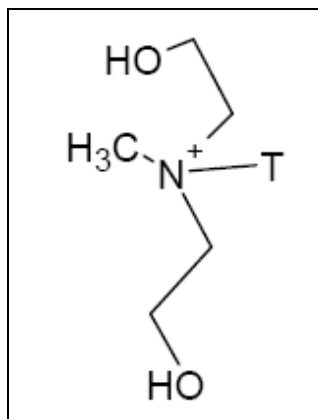
Figure 3.30 Schematic representation of alkyl ammonium quaternary salt

Since Cloisite 30B shows a basic character due to the presence of an excess of quaternary ammonium salt, such nanoclay was washed with distilled water for several times in order to optimize the UV-curing conditions. In fact the alkalinity of the nanoclay can interfere with the Brönsted acid, which is formed by the photolysis of the photoinitiator, slowing down the photopolymerization process [164]. The nanofillers containing the alkyl ammonium quaternary ions were used for comparison and, therefore, these kinds of nanoparticles have not been functionalized using γGPS.

20 g of the clay were dispersed into 300 ml of water and vigorously stirred. After a few minutes, the dispersion was decanted and filtered. The treatment was repeated three times, until the pH of water was neutral. The washed nanoclay was then dried overnight in an oven at 80°C.

In order to modify Cloisite Na⁺, 3-glycidoxypropyltriethoxysilane (γGPS) was used as received, without any further purification. Figure 3.31 schematically reports the structure of the γGPS molecule.
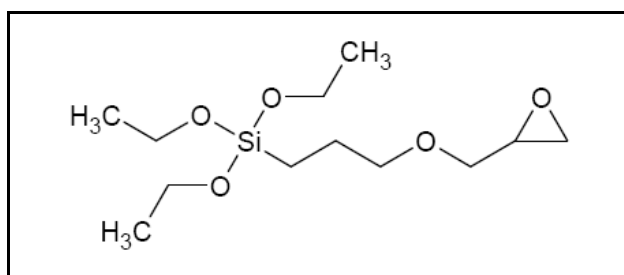
Figure 3.31 Schematic representation of GPTS

The modification of the montmorillonite particles was carried out by means of the following procedure. A 75:25 v/v solution of ethanol/water was placed in a glass flask and heated up to 80°C. Then 1.5 g of Cloisite Na⁺ were added to the solution, together with 5 g of GPTS. The dispersion was stirred at 80°C for 3 h. Then the nanoclay was filtered and washed carefully with ethanol. The resulting product was dried in oven at 80°C overnight.

It is possible to demonstrate that the Si-OH groups interact with the silicon and aluminium hydroxides of the montmorillonite particles leading to the formation of both weak and covalent bonds. The GPTS molecules linked to the montmorillonite plates are able, in principle, to bond to the polymeric matrix by means of the epoxy groups. The mechanism of interaction between the hybrid molecules and the montmorillonite lamellae is schematically reported in Figure 3.32 [121].
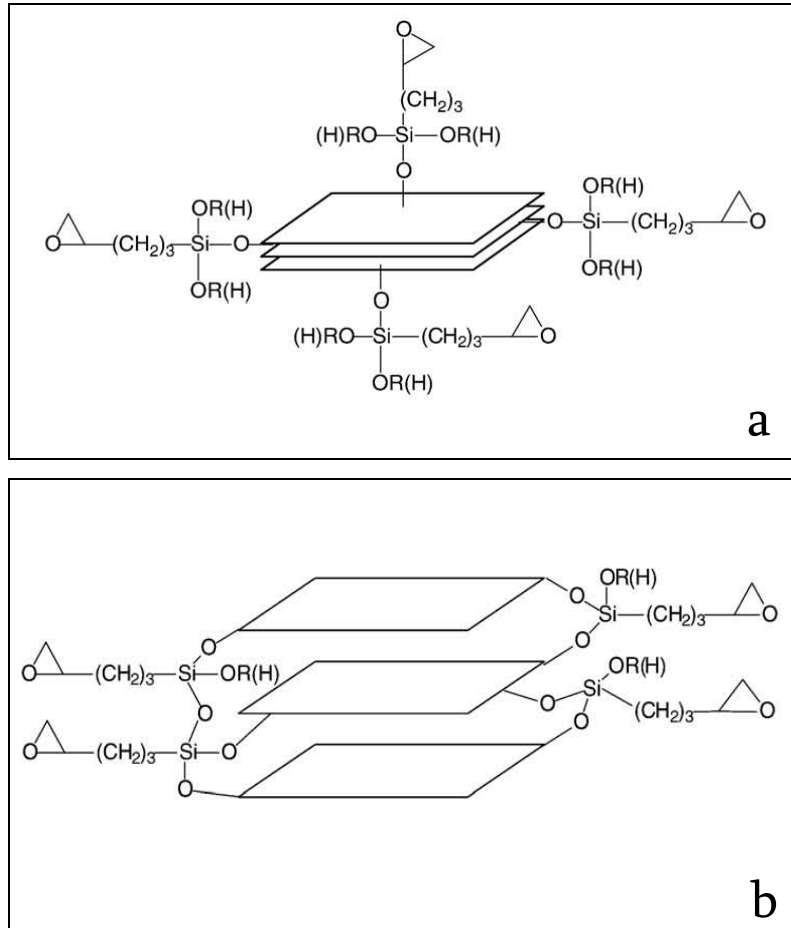
Figure 3.32 Schematic representation (a,b) of the bonding mechanism between silane molecules and montmorillonite lamellae [121]

The nanofillers were dispersed in the liquid epoxy resin by using an ultrasonic bath at room temperature for 8 hours. 4w/w% of the cationic photonitiator was added to the dispersions after sonication.

The mixtures were applied onto polypropylene sheets and on mild steel and were irradiated by using a static UV-lamp.

The steel surface was cleaned and degreased before coating deposition with an organic solvent and no specific surface pre-treatment or coupling agent was applied. The intensity of the UV light on the surface of the sample was about 35 mW/cm^2 and the samples were irradiated for 8 shots (30 s each shot). Finally, the UV-cured films were placed in an oven at 60°C overnight.

3.3.2 Characterization of the UV curable epoxy coatings containing modified montmorillonite nanoparticles

The UV-curable mixtures prepared are described in Table 3.8. The amounts of nanoclays employed are either 5 or 10w/w%.

Table 3.8 Summary of the different samples under investigation

Sample	Cloisite employed	Cloisite content (w/w%)	Cloisite modifier
CL1_5	Cloisite 30B	5%	none
CL1_10	Cloisite 30B	10%	none
CL2_5	Cloisite Na$^+$	5%	GPTS
CL2_10	Cloisite Na$^+$	10%	GPTS

The kinetics of photopolymerization was investigated by means of real-time FT-IR (Thermo-Nicolet 5700) measurements performed on both the neat epoxy

resin and on the dispersions containing the nanoclays [168]. The liquid formulations were coated onto a KBr disk. The sample was exposed simultaneously to both the UV beam, which induces polymerization, and to the IR beam which analyzes the extent of the reaction *in situ*. Since IR absorbance is proportional to monomer concentration, conversion versus irradiation time profiles can be obtained. Epoxy groups conversion was followed by monitoring the decrease of epoxy group's absorbance in the wavenumbers region 760-780 cm^{-1}. This band intensity was normalized to that of the C=O signal located at 1700 cm^{-1}. The typical kinetic profiles are reported in Figure 3.33.
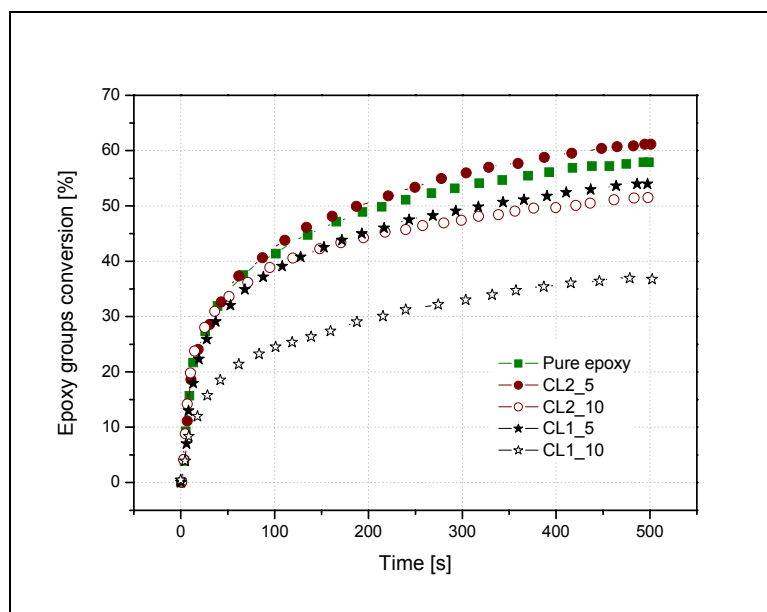
Figure 3.33 Conversion kinetic profiles for the different mixtures

First of all, by examining the kinetics profiles it is possible to appreciate that all the curves tend to an asymptotic value after 500 s of exposure. The conversion is always incomplete due to the vitrification of the reactive systems, which reduces the mobility of the cationic species during the propagation of the polymerization process [170].

As far as the systems based on CL1 clays are concerned, a decrease of both the polymerization rate (i.e. the slope of the curve) and of the final conversion occur when more than 5% of the nanofiller is added to the mixture. This behaviour can be attributed to scattering phenomena due to the presence of tactoids of Cloisite 30B [171].

In the case of CL2 systems, the influence of the nanofiller on the kinetic profile is almost modest. In general, the scattering effects are almost negligible and it is likely due to the good dispersion of the nanoclay.

XRD analyses were performed on the clay powders, on the liquid nanoclay dispersions and on the UV-cured coatings. The measured interlayer distances for both powders and liquid dispersions are collected in Table 3.9 and Table 3.10, respectively.

Table 3.9 X-Rays measurements of the interlayer distance on the clay powder

Clay powders	d (Å)
Cloisite Na+	12.0
Cloisite 30B	18.4
Cloisite Na+ modified with GPTS	29.5

Table 3.10 X-Rays measurements of the interlayer distance on liquid dispersion of modified clay powders

Clay liquid dispersion	d (Å)
CL1	34.0
CL2	n.e.[*]
Cloisite Na$^+$	12.0

It is worthy to note that after the modification with GPTS, CL2 clay exhibits a high increase of the interlayer spacing [121]. The great increase of the interlayer distance after the modification confirms the intercalation of GPTS oligomers inside the clay galleries as the only functionalization of the clay surface would produce much smaller interlayer distances as reported in literature [172,173].

Considering the dispersions of the nanoclays in the liquid epoxy resin, (Table 3.10), Cloisite Na$^+$ based dispersions show no changes in the diffraction peaks, thus indicating no interactions between the nanoclay and the epoxy resin. CL1 systems show XRD spectra where signals attributable to (001) plane reflections are present at lower 2θ values, thus only intercalation occurs. The XRD spectra of CL2-based systems show no signal related to crystalline morphology of the modified nanoclays: this behaviour could be attributed to exfoliation.

Finally, it can be mentioned that similar XRD spectra were obtained by examining the UV-cured dispersions, thus indicating that the interactions between the two phases (nanoclay and epoxy resin) take place in the liquid state and do not change after exposure to UV light, as reported in literature [168].

After the curing process, transparent and homogeneous films were obtained. They were completely tack-free for any formulation excluding CL1_10 (this was the system with lowest conversion as shown in Figure 3.33).

The gel content was determined on the cured films by measuring the weight loss after 24 h extraction with chloroform at room temperature, according to the standard test method ASTM D2765. The insoluble fraction (gel %) was very high for the systems characterized by better conversions. Comparing the gel percentage values of these systems (see Table 3.11) they are slightly lower, with respect to the pure UV-cured epoxy resin, in the presence of the nanoclays.

Table 3.11 Thermo-mechanical properties of the coatings under investigation

Sample	Gel %	Tg DMTA (℃)	T10 (℃)	T50 (℃)
Pure epoxy resin	95	150	277	358
CL1_5	87	135	276	359
CL2_5	90	150	327	377
CL2_10	90	146	310	378

Dynamic-mechanical experiments (DMTA) were performed on a MKIII Rheometrics Scientific Instrument at 1 Hz frequency in the tensile configuration, from room temperature up to 250℃, at which the rubbery plateau was attained, with a heating rate of 5℃/min. The size of the specimen was 10 x 5 x 0.15 mm. T_g was assumed as the maximum peak of E" versus temperature curve. The data obtained from the experimental test are collected in Table 3.11. It can be noticed that:

- as far as CL1 system is concerned, a slight decrease of the T_g value is observed when the nanoclay is added to the epoxy resin. This is in agreement with the reduced curing conversion.

- the addition of CL2 to the UV curable system does not affect the glass transition temperature of epoxy matrix, unless the clay concentration is 10w/w%. In this case the curing conversion was less than the neat epoxy resin.

In order to evaluate the thermo-oxidative stability of the nanocomposites investigated and to compare it with that of the pure UV-cured epoxy resin, TGA experiments were performed in air. TGA analyses were performed using a Mettler TGA-sDTA 851 Instrument in the range between 20 and 750°C, with a heating rate of 10°C/min. The collected thermograms are reported in Figure 3.34, while the numerical data corresponding to T10 and T50 are reported in Table 3.11.
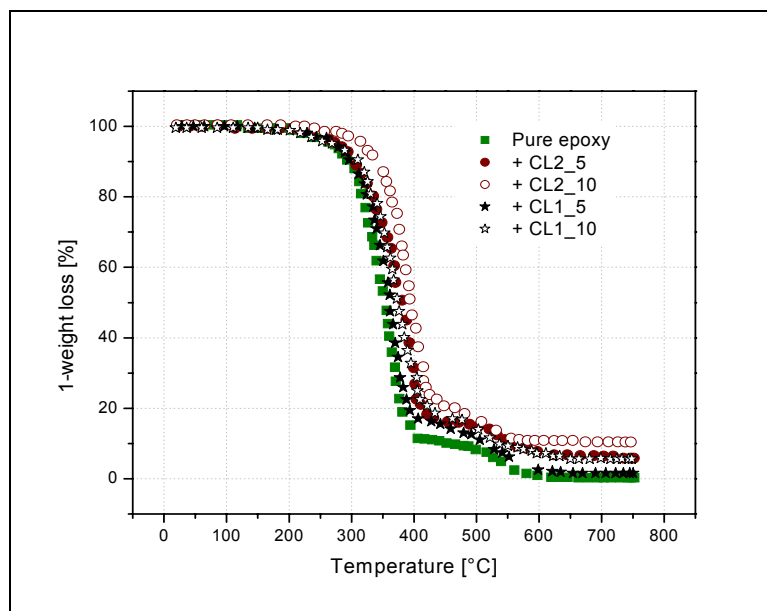
Figure 3.34 TGA curves of the samples under investigation

The experimental data clearly indicate that the presence of the nanofillers improves the thermal stability of the nanocomposites. In fact, the TGA curves shift towards higher temperatures with respect to the pure UV cured epoxy resin both for sample. Moreover, T10 and T50 values of the samples containing the modified nanofillers are found to be higher. This behaviour is due to the presence of either intercalated or exfoliated nanoclays morphologies, which lead to a decrease of the oxygen diffusion rate in the filled material.

TEM analyses (performed using of a Philips 2010 microscope) were performed on the coatings containing the different nanoclays in order to confirm the previously discussed XRD data. A typical TEM picture of the CL2 nanostructured coatings is reported in Figure 3.35.

Figure 3.35 TEM images of the exfoliated structure of sample CL2_10

While CL1 based systems likely show an intercalated structure, where the clay lamellae maintain their stacked morphology, the modification of Cloisite Na$^+$ with GPTS determines a high intercalated morphology, although some single (exfoliated) lamellae can be seen.

Prior the electrochemical characterization (carried out by means of electrochemical impedance spectroscopy), the thickness of the nanocomposite coatings applied on mild steel was measured. Table 3.12 collects the thickness of the different coatings.

Table 3.12 Thickness of the coatings under investigation

Sample	Thickness (μm)
Pure epoxy resin	186
CL1_5	358
CL2_5	261
CL2_10	255

An electrochemical characterisation was performed on coatings added of the nanoclays and coated on a metal substrate in order to evaluate the corrosion protection performances of the nanocomposite coatings. Their performances were compared to those of the pure UV-cured epoxy resin.

It is important to remember that, also for this kind of coatings, the steel surface was just cleaned and degreased before coating deposition and therefore no specific surface pre-treatment was applied. As far as EIS measurements are concerned, the electrodes arrangement, the equipment and the measurement condition was the same described in the previous section. The frequency range was 10^5 - 10^{-2} Hz and the signal amplitude 20 mV; the electrolyte used was 0.3w/w% Na_2SO_4 and the sample area 1.5 cm^2.

Figure 3.36 shows the evolution of the free corrosion potential for the different samples.
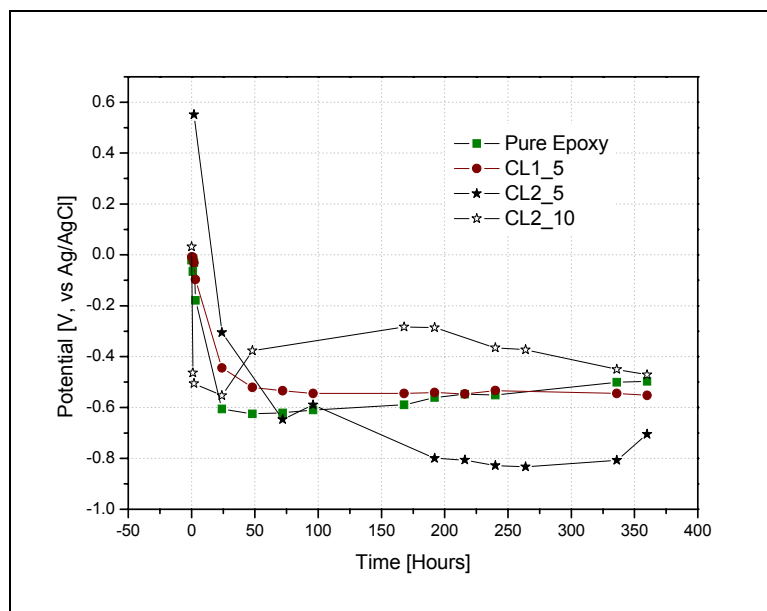
Figure 3.36 Corrosion potential versus time of immersion in 0.3w/w% Na_2SO_4

It is possible to note that after an initial decrease of the potential, during the first couple of days of immersion, due to the activation of the electrochemical reactions on the steel surface, the potential reaches quite stable values.

The potential trend of CL2 samples seems to be different from the behaviour of the other materials. Pure UV cured Epoxy and CL1 samples show the typical free corrosion potential of steel in this solution. The different behaviour of CL2 samples will be explained after the presentation of the EIS results.

Figure 3.37 shows some examples of EIS spectra (impedance modulus, Figure 3.37a and impedance phase, Figure 3.37b) obtained on the different samples after 1 hour of immersion in the aggressive solution.
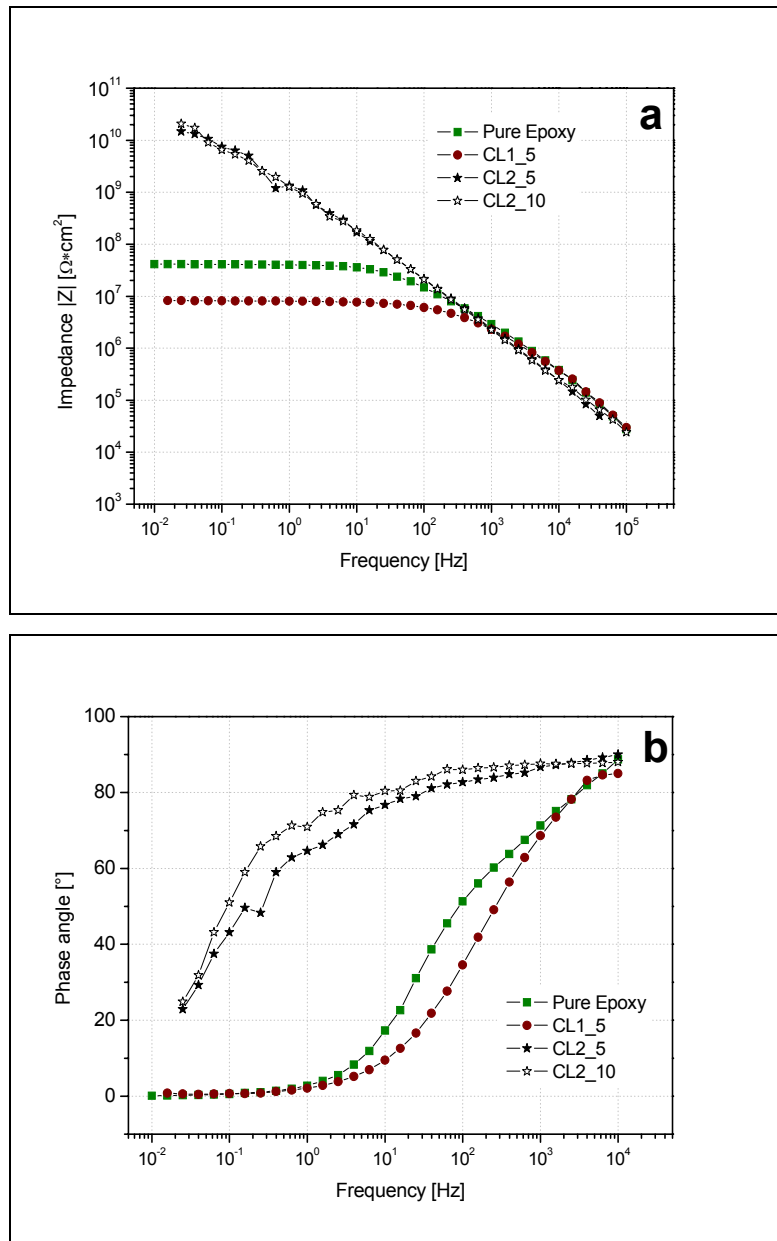
Figure 3.37 Impedance modulus (a) and phase (b) after 1 hour of immersion in 0.3w/w% Na_2SO_4

The large differences in the impedance modulus (a) comparing the different samples, are evident. The EIS data were analysed using two different equivalent electrical circuits shown in Figure 3.38 (a,b).
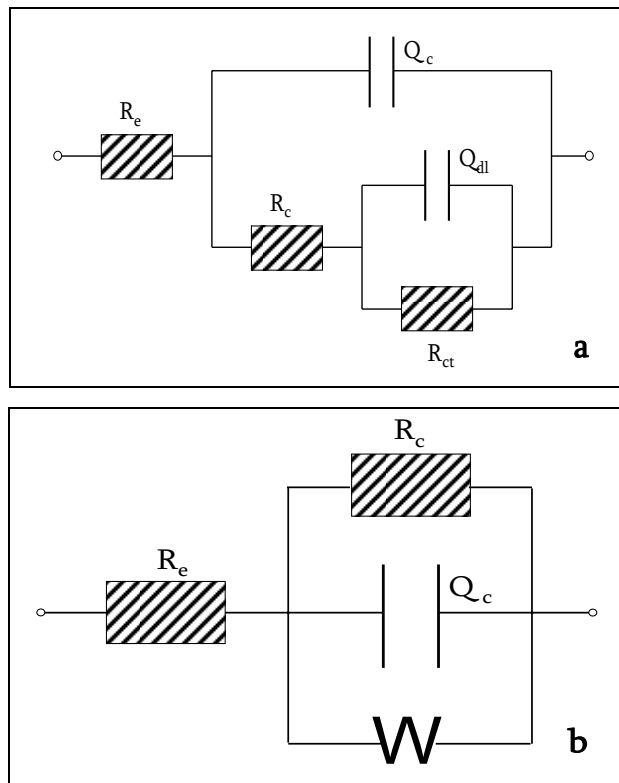
Figure 3.38 Equivalent electrical circuits (a,b) used for the modelling of the experimental data

The first one (Figure 3.38a) was used for modelling the EIS behaviour of pure UV-cured epoxy resin coated steel and sample CL1, while the second circuit (Figure 3.38b) was used for analysing samples CL2. In both the circuits we have two elements describing the coating properties: the coating resistance (R_c) and

214

the coating capacitance (Q_c) [149]. In Figure 3.38a the two typical elements describing the faradic impedance of the metal surface are also present: the double layer capacitance Q_{dl} and the charge transfer resistance R_{ct}, while in Figure 3.38b we have in parallel an element related to the diffusive control of the impedance (W) [174].

The most interesting parameter to analyze the protective properties of coatings without any active pigment is the coating resistance (R_c), describing the ability of the layer to act as an ion diffusion barrier [110]. Figure 3.39 shows the evolution of this parameter for the materials under investigation.
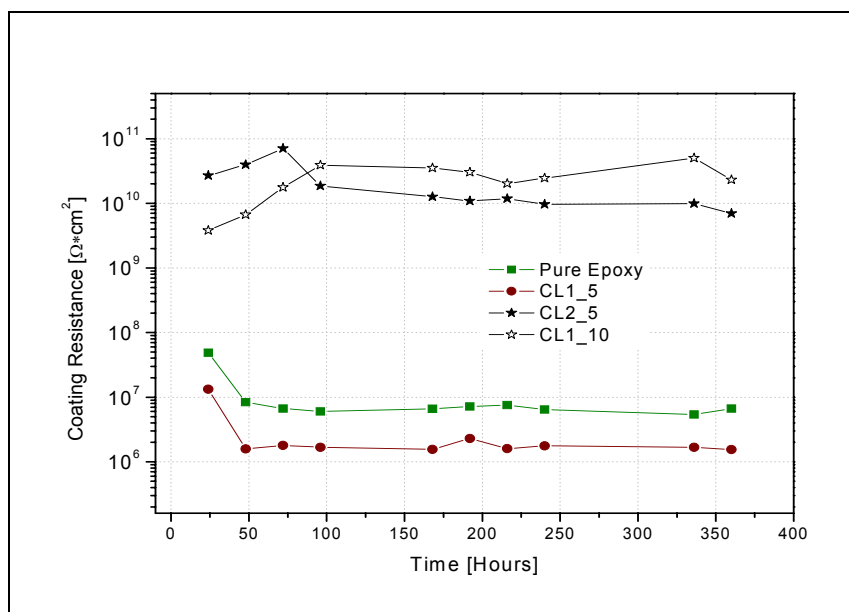
Figure 3.39 Coating resistance with the time of immersion in 0.3w/w% Na₂SO₄

The huge difference between sample CL2 and the couple sample CL1 and pure UV-cured epoxy resin is evident. These last two samples show, from the beginning of the test, resistances values which are two orders of magnitude lower than the CL2 samples, reaching later values around 10^7 $\Omega \cdot cm^2$, slightly lower for CL1 samples in comparison with pure UV-cured epoxy coating. These values are typical for unpigmented coatings with this thickness [175]. The lower values of sample CL1 can be explained by considering that without a proper interaction between nano-particles and polymeric matrix, the interface can act as preferential pathway for ions diffusion, leading to the results that the addition of nanoclays can reduce the barrier properties in comparison with pure UV cured epoxy coatings.

As far as CL2 samples are concerned, the situation is completely different. The impedance is, for both the coatings, around 10^{10} $\Omega \cdot cm^2$, which is a value exceptionally high, proving very good barrier properties. Moreover, increasing the quantity of γGPS (from 5% to 10%) their performance increases (CL2_5 and CL2_10 samples).

From these data it is evident that only with a suitable functionalization of the nanoclay, inducing a chemical interaction between the nanofiller and the polymeric matrix, it is possible to increase the barrier properties, having a beneficial effect by the presence of the composite coating, avoiding any lack of continuity at the polymer-nanoclay interface.

The trends of the relative dielectric permittivity at 25°C (ε_R) of the different coating with immersion time are shown in Figure 3.40.

Remark that the estimation of ε_r carried out by applying Eq. 2 is correct at only in the firs ours of immersion (24-48). After this period, the effect of the water accumulation at the metal/polymer interface affects the calculated values of ε_r. However, as explained in the previous section, this fact does not change the meaning of the discussion about the different properties of the coatings.
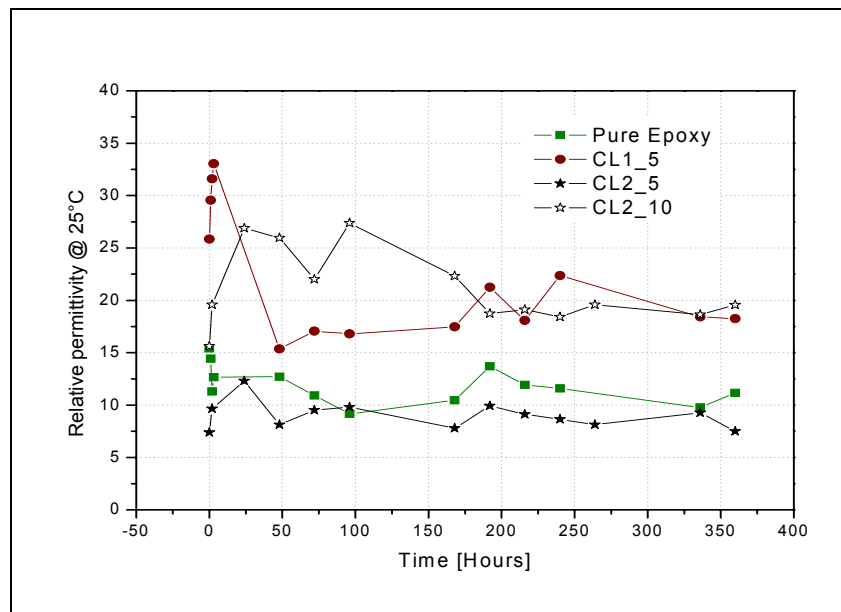
Figure 3.40 Relative dielectric permittivity at 25°C with the time of immersion in 0.3w/w% Na2SO4

The coating thickness (reported in Table 3.12) is different for the different materials and, therefore, for analysing the relative dielectric properties the normalised values were considered rather than the absolute values.

The changes in coating capacitance can be due to different processes: water uptake (the water diffusion causes an increase of the coating capacitance being

the dielectric permittivity of water higher than the dielectric permittivity of the polymeric matrix at room temperature), dissolution of polar components in the coating (causing a decrease of the coating capacitance) and the swelling of the coating due to water diffusion, which, increasing the coating thickness, causes an apparent decrease of the coating capacitance [152]. It is possible that all this processes occur at the same time.

Figure 3.40 shows two groups of samples: CL2_5 sample and pure UV-cured epoxy, and, on the other side, CL1_5 sample and. CL2_10 sample. The first couple of samples show low and quite stable values of ε_R after the first days of immersion, in the order of 7-10. The water uptake, which is possible to quantify using the Brasher-Kingsbury equation (Eq. 3.1) from the capacitance values [153], is in the order of 4-5% in volume for CL2_5 samples, thus indicating good water barrier properties. Concerning the other two samples, a different behaviour is noticeable: the coating capacitance increase after the first days of immersion and than decrease to the value of 20 during the remaining days of immersion. These results can be due to the dissolution of polar components of the coating or it can be associated to a swelling process in the coatings. In both the cases, the samples CL1_5 and CL2_10 are less stable in the aqueous solution. For all the samples, showing the lowest resistance properties (pure UV-cured epoxy coating and sample CL1), it was possible to investigate the corrosion process at the metal interface measuring the values of charge transfer resistance R_{ct} and double layer capacitance Q_{dl} using the equivalent electrical circuits depicted in Figure 3.38.

The charge transfer resistance R_{ct} is directly related to the corrosion reaction (as a first approximation lower is the R_{ct} value, higher is the corrosion rate). Figure 3.41 shows the evolution of this parameter for samples CL1_5 and pure UV cured epoxy coating.
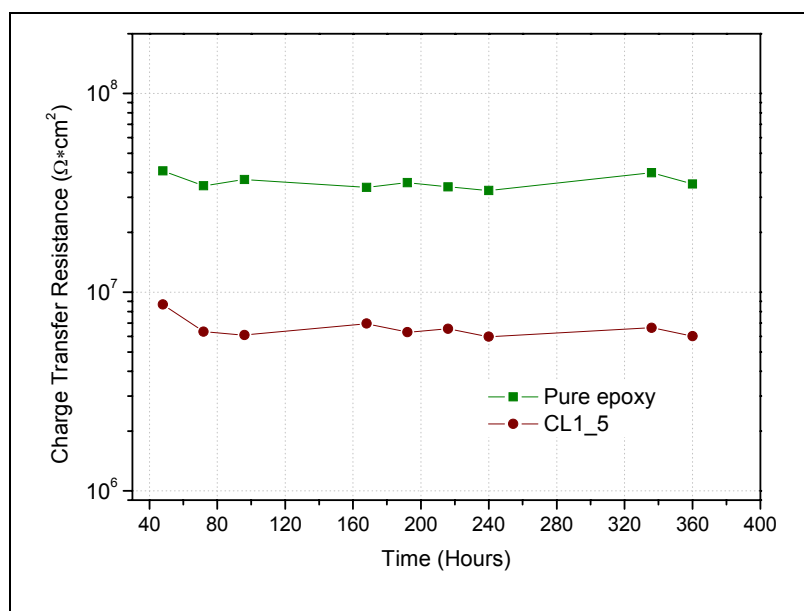
Figure 3.41 Charge transfer resistance with the time of immersion in 0.3w/w% Na_2SO_4

In agreement with the lowest barrier properties (Figure 3.39), the presence of Cloisite 30B to promote a decrease of the performances of the coating toward corrosion (i.e. it causes a high corrosion rate). The clear correlation between barrier properties (R_c) and corrosion reaction (R_{ct}) is evident, considering the fact that the coating systems do not contain any active inhibitive pigments.

The same behaviour can be noticed when the double layer capacitance (Q_{dl}) is considered (Figure 3.42).
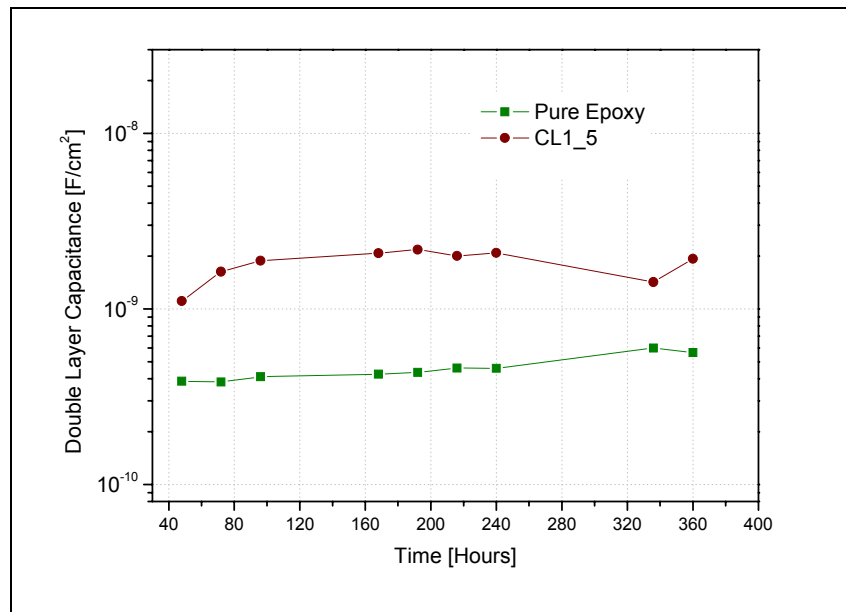
Figure 3.42 Double layer capacitance with the time of immersion in 0.3w/w% Na_2SO_4

The double layer capacitance is directly proportional to the metals surface in contact with the electrolyte and it describes the wet area, which is the corroding area. For CL1 samples, Q_{dl} was found very higher with respect to the pure epoxy coating.

For the samples CL2 it was not possible to clearly measure the corrosion reaction rate because of the very high barrier properties of the coatings. Only a diffusive element (W) was measured as shown in Figure 3.38b.

The value of the diffusive impedance is quite stable, similar for the two coatings and it is about 10^{10} $\Omega \cdot cm^2$. Now it is possible to better understand the free corrosion potential trends in Figure 3.36.

The CL2_5 sample shows a decrease of the potential (in comparison with CL1 and pure UV cured epoxy coating) which can be attributed to a limitation of the cathodic reaction, considering the increase of the total impedance (Figure 3.39 and Figure 3.41). This effect is probably due to the increased oxygen diffusion barrier properties. The sample CL2_10, on the contrary, shows an increase of the free corrosion potential. This trend can be explained considering that the decrease of the cathodic reaction is the dominant process, while the anodic reaction is not influencing in the same way the free corrosion potential. It is possible to suppose that, in addition to the oxygen barrier properties, the very high ionic barrier properties have a relevant effect in reducing the anodic reaction, causing a potential shift in the noble direction.

In Figure 3.43(a,b) the corrosion morphology of the underpaint metal surface of CL2_10 coating after 400h of immersion in 0.3w/w% Na_2SO_4 solution is depicted. The dotted line in Figure 3.43a indicates the area affected by the electrolyte for about 400 hours.
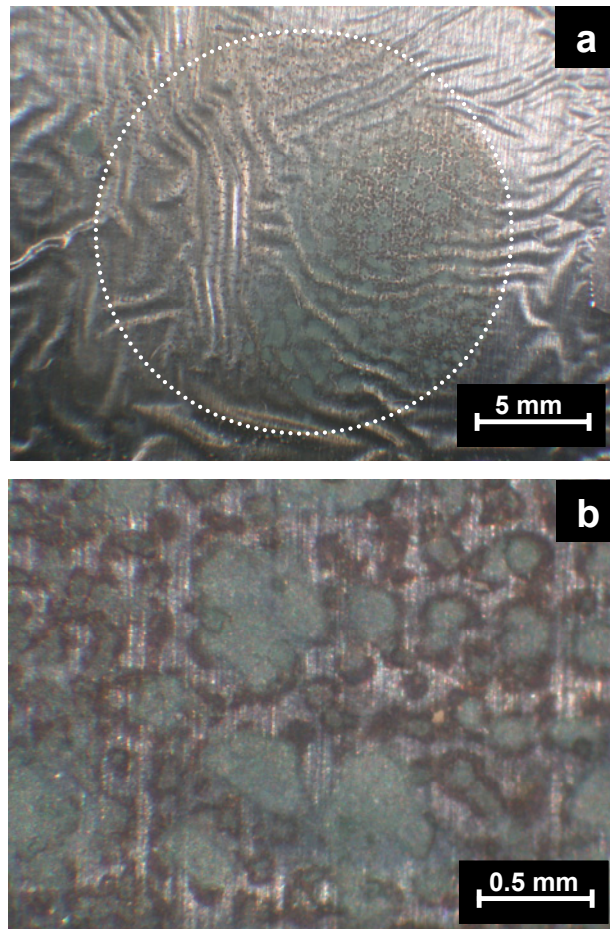
Figure 3.43 Appearance of the underpaint condition of samples CL2_10 after 360 hour of continuous immersion in 0.3w/w% Na_2SO_4: low (a) and high (b) magnification

At higher magnitudes (Figure 3.43b) some matting effects related to the oxidation phenomena can be observed. The pure UV-cured epoxy resin (Figure 3.44) shows some areas, after the treatment, where corrosive attack clearly took place. Also in this case, the dotted line in Figure 3.44 indicates the area affected

by the electrolyte for about 400 hours. The same morphology with a more homogeneous surface corrosive attack is shown by CL1_5 coating.
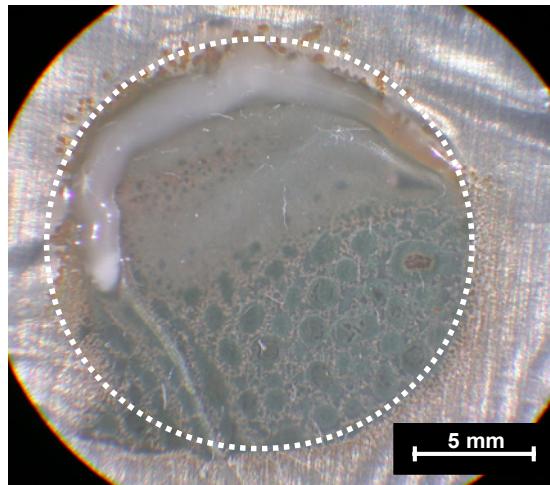
Figure 3.44 Appearance of the underpaint condition of samples CL1_5 after 360 hour of continuous immersion in 0.3w/w% Na_2SO_4

Eventually, it is possible to sustain that the coatings having exfoliated structures did not show any corrosion phenomena, with respect to the intercalated systems and to the pure epoxy resin. In particular the exfoliated coatings showed extremely high ionic barrier properties proving the importance of a correct functionalization of the nanofillers for good corrosion protection of nano-composite coatings.

3.4 Final comments

UV-cured nanostructured coatings were prepared using organo-modified nanoclays, added in different amounts to a waterborne cycloaliphatic epoxy resin (CE), and inducing an *in situ* formation of nanostructured domains in a waterborne urethane-acrylic polymeric matrix.

Depending on the modifier employed different morphologies were obtained and different corrosion protection properties as well. To better understand the effect of the modifiers on the corrosion protection properties on the UV cured matrix, the resistances and the relative dielectric permittivity of the different coatings object of investigation in this chapter were compared. This comparison is reported in terms of coating resistance (Figure 3.45) and relative dielectric permittivity of the coatings (Figure 3.46).

As far as the PUD samples are concerned, in Figures 3.45 and 3.46 only the MEMO modified samples were considered, owing to the higher affinity of these coatings with the organo-modified nanoclays enriched coatings. In fact, both these two different kinds of coatings contain inorganic particles (*in situ* formed silica domains and montmorillonite nanoparticles, respectively) and a coupling agent between the organic and inorganic phases (MEMO and GPTS, respectively). For this reasons, the above mentioned comparison can be considered consistent.
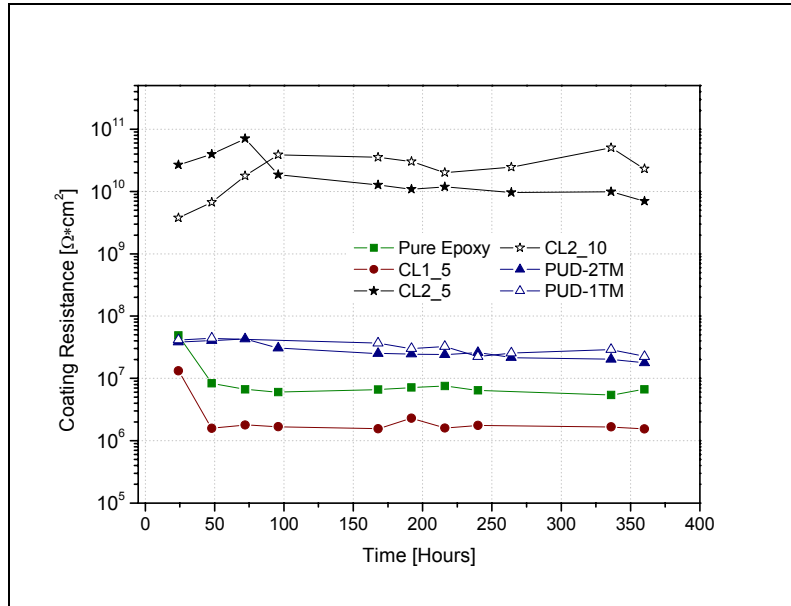
**Figure 3.45** Coating resistance with the time of immersion in 0.3w/w% Na_2SO_4
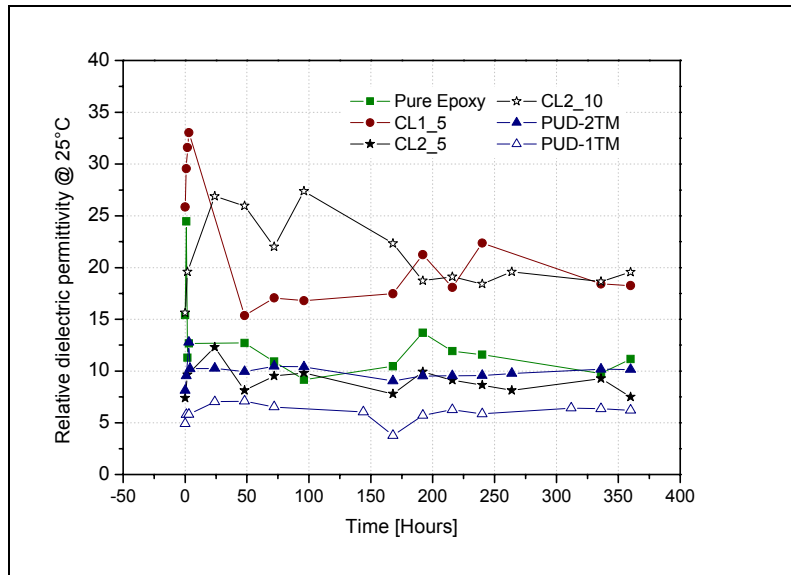
Figure 3.46 Relative dielectric permittivity at 25°C with the time of immersion in 0.3w/w% Na_2SO_4

Considering Figure 3.45 it is possible to appreciate that all the different coatings show a good stability during the 360 hours of continuous immersion. In particular, PUD samples show values of the coating resistance quite higher than the pure epoxy coating and the CL1_5 coating. However, the resistance properties of CL2 samples are noticeably higher. As far as the dielectric properties are concerned (see Figure 3.46), the PUD samples show stable and low values of the relative dielectric permittivity. CL2_5 sample and the pure epoxy resin show ε_R values comparable with PUD samples with a quite stationary trend. Instead, CL1_5 and CL2_10 samples are characterized by higher values of the relative dielectric permittivity, but it has to be underlined that the starting values of ε_R of these samples is quite high, compared to the other. In addition, the trends of the relative permittivity of CL1_5 and CL2_10 show an initial increase, followed by a decrease after a few days of continuous immersion.

Despite these differences among the differently modified waterborne coatings, the electrochemical properties of are very promising, considering that the coatings are unpigmented and with limited thickness. Moreover, the metal surface was not specifically pre-treated in order to improve the adhesion of the coating, and therefore a further increase of the protective properties could be obtained increasing the interface stability by pre-treating the metal surface.

The corrosion tests showed that the presence of MEMO and TEOS improves the properties of the coatings, reducing, in particular, the water absorption and increasing the ionic barrier properties.

In addition, the electrochemical test carried out on the waterborne resins containing the organo-modified nanoclays highlighted that the coatings having exfoliated structures did not show any corrosion phenomena, with respect to the intercalated systems and to the pure epoxy resin. In particular, the exfoliated coatings showed extremely high ionic barrier properties proving the importance of a correct functionalization of the nanofillers for good corrosion protection of nano-composite coatings.

4 Conclusions and Future Works

Nanotechnology approach for the production of effective environmentally friendly metals pre-treatments and organic coatings for the corrosion protection was investigated in this Ph.D. thesis. Multifunctional silane hybrid molecules were used to design and modify the final properties of sol-gel pre-treatments and organic coatings.

In particular, an experimental mixture of hybrid silicon alkoxides molecules was used for the production of sol-gel coating to protect aluminium and galvanized steel. These sol-gel pre-treatments were tested as adhesion promoters in combination with both powder and cataphoretic coatings for the development of ecological complete protection systems with high performances.

The results on aluminium (see 2.2.3) proved that the silane treatment provides the substrate with an effective barrier against corrosion and, in addition, it acts as a coupling agent improving the adhesion with an organic coating and, in general, the corrosion protection properties. The comparison with other surface conversion treatments/coatings highlighted that the experimental silane sol-gel pre-treatment ensures always the best performances among the tested pre-treatments. Considering the application onto galvanized steel, an effective combination of silicon alkoxides, deposition procedure and curing temperature

has been carried out to optimize the corrosion protection properties of the sol-gel film itself and the interaction with both powder coating and cataphoretic paints. On the hot dip galvanized substrate the deposition conditions were considered more critical but, in spite of this, good results have been achieved (see 2.3.2).

Covered with an organic coating and cured at high temperatures, the produced silanes sol-gel pre-treatments act both as an efficient barrier against moisture and oxygen permeation (relatively to their thickness) and also as a coupling agent improving the corrosion resistance of the complete protection system. Concerning the cataphoretic coating the experimental sol-gel treatment can be properly designed to inhibit the hydrogen release leading to the formation of a continuous and defect-free electrodeposited coating strongly bonded to the substrate. As a further result, the barrier properties of the sol-gel coating itself were improved adding montmorillonite nanoparticles to the silane mixtures (see 2.4.2). The preliminary analysis demonstrated that the nanoparticles modify the film formation mechanism leading to the formation of sol-gel coating with enhanced properties.

The same hybrid molecules used to perform the sol-gel films were used to modify UV curable water-borne coatings aiming, also in this case, to develop environmentally friendly protection systems against corrosion. Silane hybrid molecules were used to form *in situ* hybrid silica domains which were demonstrated to slightly improve the barrier properties of the water-borne coating (see 3.2.2).

In addition, it was demonstrated (see 3.3.2) that the presence of conveniently modified (with silane hybrid molecules) montmorillonite nanoparticles improves the electrochemical properties of the water-borne organic coating.

Finally, in the light of the above mentioned experimental results, it can be stated that by using an experimental mixture of hybrid silane molecules and montmorillonite nanoparticles it was possible to produce effective environmentally friendly sol-gel pre-treatments and that, by conveniently modifying the structure of UV curable water-borne coatings with the same molecules and nanoparticles it is possible to improve their corrosion protection performances.

Despite the proposed solution for processing techniques of hybrid silicon alkoxides molecules led, as proved throughout the thesis, to several interesting results, a further investigation of the potential and the properties of silane sol-gel coating as well as silicon alkoxides modified organic coatings is needed. For instance, a finer investigation of the inner structure of sol-gel coating itself and modified with montmorillonite nanoparticles can be useful to better understand effect of the nanofiller on the physical and thermal properties of the hybrid coating. In this sense, an optimization of the granulometric distribution of the nanoparticles and their morphology can remarkably increase the properties of the sol-gel coating. As far as the sol-gel pre-treatments are concerned, the addition of a convenient corrosion inhibitor in the hybrid matrix can further increase the efficiency and the performances of these materials as effective solution against corrosion.

On the other hand, the need of effective solutions for the industrialization of these kinds of materials for production on large scale of silane pre-treated manufacts can lead to different evolutions of the work, concerning the optimization and simplification of the deposition process instead of a mechanicistic study of the phenomena involved in the formation of the sol-gel film.

Considering the other main topic of the thesis, which is the modification of UV curable waterborne coatings with silicon alkoxides and nanoparticles, also in this case a lot of different developments are possible. In particular, it would be very useful to study of the mechanism of interaction between the nanoparticles and the organically modified silicon alkoxides molecules as well to investigate the properties of the polymer/nanoparticles interface, which is likely to be the critical point for the performances of the final coating. In addition, a further development of the studied materials would be the utilization of the montmorillonite nanoparticles as a cations exchange materials to dope the clay with cationic inhibitors of the corrosion reactions.

In conclusion, a combination of the experimental hybrid silane sol-gel pre-treatment with the nanoparticles or *in situ* modified UV cured water-borne coating is expected to be a very effective nanostructured environmentally friendly protection system completely designed *a priori* to ensure a high degree of protection against corrosion. And, as one would expect, it is the natural development for this work.

References

[1] F. Deflorian, S. Rossi, L. Fedrizzi, Electrochim. Acta 51 (2006) 6097

[2] O. Lunder, J.C. Walmsley, P. Mack, K. Nisancioglu, Corros. Sci. 47 (2005) 1604

[3] T. Bellezze, G. Roventi, R. Fratesi, Surf. Coat. Technol. 155 (2002) 221

[4] F. W. Eppensteiner, M. R. Jennkind, Metal Finishing, 105 (2007) 413

[5] C. M. Caruana, Metal Finishing, 104 (2006) 44

[6] "Toxicological profile for Chromium", U.S. Department of Health and Human Services, Public Health Service, Agency for Toxic Substances and Disease Registry (2008). On website: www.atsdr.cdc.gov

[7] Focus on Pigments, 2 (2008) 6. On website: www.osha.org

[8] E. Almeida, L. Fedrizzi, T.C. Diamantinio, Surf. Coat. Technol., 105 (1998) 97

[9] E. Almeida, T. C. Diamantino, M. O. Figueiredo, C. Sà, Surf. Coat. Technol., 106 (1998) 8.

[10] L. Lingjie, L. Jingle, Y. Shenghai, T. Yujing, J. Qiquan, P. Fusheng, J. Rare Earths, 26 (2008) 383

[11] F. H. Scholes, C. Soste, A. E. Hughes, S. G. Hardin, P. R. Curtis, App. Surf. Sci., 253 (2006) 1770

[12] P. Campestrini, H. Terryn, A. Hovestad, J.H.W. de Wit, Surf. Coat. Technol., 176 (2004) 365

[13] X. Zhang, C. van den Bos, W.G. Sloof, A. Hovestad, H. Terryn, J.H.W. de Wit, Surf. Coat. Technol., 199 (2005) 92

[14] J.H. Nordliena J.C. Walmsley, H. Østerberg, K. Nisancioglu, Surf. Coat. Technol., 153 (2002) 72

[15] Y. Song, D. Shan, R. Chen, F. Zhang, E.-H. Han, Surf. Coat. Technol., 203 (2009) 1107

[16] I. Van Roy, H. Terryn, G. Goeminne, Coll. Surf., 136 (1998) 89

[17] M. N. Sathyanarayana, M. Yaseen, Prog. Org. Coat., 26 (1995) 275

[18] R. L. Twite, G. P. Bierwagen, Prog. Org. Coat., 33 (1998) 91

[19] F. Deflorian, S. Rossi, L. Fedrizzi, M. Fedel, Prog. Org. Coat., 63 (2008) 338

[20] H. Neuder, C. Sizemore, M. Kolody, R. Chiang, C.-T. Lin, Prog. Org. Coat., 47 (2003) 225

[21] V. K. Gupta, N. Verma, Chem. Eng. Sci., 57 (2002) 2679

[22] H. Liebscher, Prog. Org. Coat., 40 (2000) 75

[23] M. A. Parra, D. Elustondo, R. Bermejo, J. M. Santamaría, Sci. Tot. Env., 407 (2009) 999

[24] Focus on Powder Coatings, 8 (2008) 6. On website: www.coatings.org.uk

[25] J. Lindeboom, Prog. Org. Coat., 34 (1998) 147

[26] J. A. P. Coutinho, T. Vilela, P. Pereira, P. Pessoa, M. M. M. Santos, G. M. Kontogeorgis, Chem. Eng. Res. Des., 83 (2005) 352

[27] K. Mańczyk, P. Szewczyk, Prog. Org. Coat., 44 (2002) 99

[28] S. Haseebuddin, R. Parmar, G. Waghoo, S. K. Ghosh, Prog. Org. Coat., 64 (2009) 446

[29] E. G. Belder, H. J. J. Rutten, D. Y. Perera, Prog. Org. Coat., 42 (2001) 142

[30] A. C. Rouw, Prog. Org. Coat., 34 (1998) 181

[31] F. Galliano, D. Landolt, Prog. Org. Coat., 44 (2002) 217

[32] V. Duecoffre, W. Diener, C. Flosbach, W. Schubert, Prog. Org. Coat., 34 (1998) 200

[33] H. Miao, Z. Huang, L. Cheng, W. Shi, Prog. Org. Coat., 64 (2009) 365

[34] A. Forsgren, Corrosion control through organic coatings, Taylor&Francis, Boca Raton (2006)

[35] H. Wang, J. Liu, S. Xu, W. Shi, Prog. Org. Coat., 65 (2009) 263

[36] V. Landry, B. Riedl, P. Blanchet, Prog. Org. Coat., 62 (2008) 400

[37] J. Z. Y. Wang, R. H. Bogner, Int. J. Pharm., 113 (1995) 113

[38] D. R. Baer, P. E. Burrows, A. A. El-Azab, Prog. Org. Coat., 47 (2003) 342

[39] K. L. Mittal (Ed.), Silanes and Other Coupling Agents, VSP, Utrecht (1992)

[40] K. L. Mittal (Ed.), Silanes and Other Coupling Agents, Vol. 2, VSP, Utrecht (2000)

[41] K. L. Mittal (Ed.), Silanes and Other Coupling Agents, Vol. 3, VSP, Brill (2004)

[42] K. L. Mittal (Ed.), Silanes and Other Coupling Agents, Vol. 4, VSP, Brill/Leiden (2007)

[43] K. L. Mittal (Ed.), Silanes and Other Coupling Agents, Vol. 5, VSP, Brill/Leiden (2009)

[44] S. K. Jayseelan, W. J. van Ooij, J. Adhesion Sci. Technol., 15 (2001) 967

[45] F. Deflorian, S. Rossi, L. Fedrizzi, Electrochim. Acta, 51 (2006) 6097

[46] M. G. S. Ferreira, R. G. Duarte, M. F. Montemor, A. M. P. Simoes, Electrochim. Acta, 49 (2004) 2927

[47] E. P. Pluddemann, Composites, 1 (1970) 321

[48] D. Zhu, W.J. van Ooij, Corros. Sci., 45 (2003) 2177

[49] W. J. van Ooij, D. Zhu, M. Stacy, A. Seth, T. Mugada, J. Gandhi, P. Puomi, Tsinghua Science & Technology, 10(2005) 639

[50] D. Zhu, W. J. van Ooij, Prog. Org. Coat., 49 (2004) 42

[51] E. P. Pluddemann, Silane coupling agents, 2nd ed., Plenum Press, New York (1990).

[52] Z. Pu, W. J. van Ooij, J. E. Mark, J. Adhes. Sci. Technol., 11 (1997) 29

[53] M. F. Montemor, A. M. Simões, M. G. S. Ferreira, B. Williams, H. Edwards, Prog. Org. Coat., 38 (2000) 17

[54] D. Wang, G. P. Bierwagen, Prog. Org. Coat., 64 (2009) 327

[55] M. L. Abel, R. Joannic, M. Fayos, E. Lafontaine, S. J. Shaw, J. F. Watts, Int. J. Adhes., 26 (2006) 16

[56] A. Franquet, H. Terryn, J. Vereecken, Appl. Surf. Sci., 211 (2003) 259

[57] L. Cecchetto, A. Denoyelle, D. Delabouglise, J.-P. Petit, Appl. Surf. Sci., 254 (2008) 1736

[58] J. Kron, G. Schottner, K.-J. Deichmann, Thin Solid Films, 392 (2001) 236

[59] H.-J. Kim, J. Zhang, R.-H. Yoon, R. Gandour, Surf. Coat. Technol., 188-189 (2004) 762

[60] F. J. Boerio, J. Williams, Applications Surf. Sci., 7 (1981) 19

[61] G. Li, X. Wang, A. Li, W. Wang, L. Zheng, Surf. Coat. Technol., 201 (2007) 9571

[62] J . Song, W. J. van Ooij, J. Adhesion Sci. Technol., 17 (2003) 2191

[63] J. M. Chovelon, L. E. L. Aarch, M. Charbonnier, M. Romand, J. Adhes., 50 (1995) 43

[64] M. Sheffer, A. Groysman, D. Mandler, Corros. Sci., 45 (2003) 2893

[65] K. H. Wu, C. M. Chao, T. F. Yeh, T. C. Chang, Surf. Coat. Technol., 201 (2007) 5782

[66] M. S. Donley, R. A. Mantz, A. N. Khramov, V. N. Balbyshev, L. S. Kasten, D. J. Gaspar, Prog. Org. Coat., 47 (2003) 401

[67] M. Fedel, M. Olivier, M. Poelman, F. Deflorian, S. Rossi, M.-E. Druart, Prog. Org. Coat., 66 (2009) 118

[68] P. H. Suegama, H. G. de Melo, A. A. C. Recco, A. P. Tschiptschin, I. V. Aoki, Surf. Coat. Technol., 202 (2008) 2850

[69] A. M. Cabral, R. G. Duarte, M. F. Montemor, M. L. Zheludkevich, M. G. S. Ferreira, Corros. Sci., 47 (2005) 896

[70] H. Wang, R. Akid, Corros. Sci., 50 (2007) 4491

[71] H. Wang, R. Akid, Corros. Sci., 50 (2008) 1142

[72] M. F. Montemor, M. G. S. Ferreira, Prog. Org. Coat., 63 (2008) 330

[73] M. F. Montemor, M. G. S. Ferreira, Electrochim. Acta, 52 (2007) 6976

[74] L. M. Palomino, P. H. Suegama, I. V. Aoki, M. F. Montemor, H. G. De Melo, Corros. Sci., 51 (2009) 1238

[75] N. C. Rosero-Navarro, S. A. Pellice, A. A. Durán, M. Aparicio, Corros. Sci., 50 (2008) 1283-1291

[76] M. F. Montemor, W. Trabelsi, S. V. Lamaka, K. A. Yasakau, M. L. Zheludkevich, A. C. Bastos, M. G. S. Ferreira, Electrochim. Acta, 53 (2008) 5913

[77] P. H. Suegama, H. G. De Melo, A. A. C. Recco, A. P. Tschiptschin, I. V. Aoki, Surf. Coat. Technol., 202 (2008) 2850

[78] Y. Castro, B. Ferrari, R. Moreno, A. Durán, Surf. Coat. Technol., 182 (2004) 199-203

[79] Y. Castro, B. Ferrari, R. Moreno, A. Durán, Surf. Coat. Technol., 191 (2005) 228-235

[80] M. F. Montemor, A. M. Cabral, M. L. Zheludkevich, M. G. S. Ferreira, Surf. Coat. Technol., 200 (2006) 2875

[81] Z. W. Wicks Jr, F. N. Jones, S. P. Pappas, "Organic Coatings Science and Technology", Wiley Interscience, New York (1999)

[82] N. S. Allen, J. Photochem. Photobiol. A: Chem., 100 (1996) 101

[83] F. Masson, C. Decker, T. Jaworek, R. Schwalm, Prog. Org. Coat., 39 (2000) 115

[84] C. Decker, T. Nguyen Thi Viet, D. Decker, E. Weber-Koehl, Polymer, 42 (2001) 5531

[85] T. Scherzer, A. Tauber, R. Mehnert, Vibr. Spectr., 29 (2002) 125

[86] C. Decker, C. Bianchi, D. Decker, F. Morel, Carbohydrate Polymers, 59 (2005) 57

[87] O. H. Lin, R. N. Kumar, H. D. Rozman, M. A. M. Noor, Carb. Polym., 59 (2005) 57

[88] U. Schubert, N. Hüsing, "Synthesis of inorganic materials", 2nd ed, Wiley – VCH, Weinheim (2005)

[89] U. Bexell, T. M. Grehk, Surf. Coat. Technol., 201 (2007) 4734

[90] C. J. Brinker, G. W. Scherer, "Sol-Gel Science: The Physics and Chemistry of Sol-Gel Processing", Academic Press Inc, New York, (1990)

[91] R. Krechetnikov, G. M. Homsy, J. Fluid Mech., 559 (2006) 429

[92] W. J. van Ooij, Proceedings ICEPAM 2004, Oslo, Norway, 16-18/2004, on website: http://www.sintef.no (2004)

[93] C. J. Brinker, A. J. Hurd, K. J. Ward "Ultrastructure Processing of Advanced Ceramics", (Eds. J. D. Mackenzie, D. R. Ulrich), Wiley, New York (1988)

[94] F. Deflorian, S. Rossi, M. Fedel, Corrosion Eng. Sci. Tech. (2009) In press.

[95] P. Campestrini, E. P. M. van Westing, J. H. W. de Wit, Electrochim. Acta, 46 (2001) 2631

[96] L. Fedrizzi, F. Deflorian, G. Boni, P. L. Bonora, E. Pasini, Prog. Org. Coat., 29 (1996) 89

[97] J. L. Luo, C. J. Lin, Q. Yang, S.W. Guan, Prog. Org. Coat., 31 (1997) 289

[98] F. Deflorian, S. Rossi, L. Fedrizzi, P.L. Bonora, Prog. Org. Coat., 52 (2005) 279

[99] P. Campestrini, E. P. M. van Westing, A. Hovestad, J.H.W. de Wit, Electrochim. Acta, 47 (2002) 1097

[100] I. De Graeve, J. Vereecken, A. Franquet, T. Van Schaftinghen, H. Terryn, Prog. Org. Coat., 59 (2007) 224

[101] V. Lavaert, M. De Cock, M. Moors, E. Wettink, Prog. Org. Coat., 38 (2000) 213

[102] J. H. W. de Wit, "Corrosion mechanisms in theory and practice", (Eds. P. Marcus and G. Oudar), Marcel Dekker, New York (1995)

[103] A. Amirudin and D. Thierry: Progr. Org. Coat., 26 (1995) 1

[104] F. Deflorian and L. Fedrizzi: J. Adhes. Sci. Technol., 1999, 13, 629.

[105] L. Fedrizzi, A. Bianchi, F. Deflorian, S. Rossi, P.L. Bonora, Electrochim. Acta, 47 (2002) 2159

[106] H. Asgari, M. R. Toroghinejad, M. A. Golozar, Appl. Surf. Sci., 253 (2007) 6769

[107] P. Puomi, H. M. Fagerholm, J. Adhesion Sci. Technol., 15 (2001) 869

[108] D. K. Owens, R. C. Wendt, J. Appl. Polym. Sci., 13 (1969) 1741

[109] L. M. Palomino, P. H. Suegama, I. V. Aoki, M. F. Montemor, H. G. De Melo, Corros. Sci., 50 (2008) 1258

[110] F. Deflorian, L.Fedrizzi, J. Adhesion. Sci Technol., 13 (1999) 629

[111] A. Amirudin, D. Thierry, Prog. Org. Coat., 28 (1996) 59

[112] M.-G. Olivier, A.-P. Romano, C. Vandermiers, X. Mathieu, M. Poelman, Prog. Org. Coat., 63 (2008) 323

[113] S. J. Garcia, M. T. Rodrıguez, R. Izquierdo, J. Suay, Prog. Org. Coat., 60 (2007) 303

[114] A.-P. Romano, M.-G. Olivier, C. Vandermiers, M. Poelman, Prog. Org. Coat., 57 (2006) 400

[115] M. Poelman, M.-G. Olivier, N. Gayarre, J.-P. Petitjean, Prog. Org. Coat., 54 (2005) 55

[116] S. I. Seok, J. H. Kim, K. H. Choi, Y. Y. Hwang, Surf. Coat. Technol., 200 (2006) 3468

[117] S. J. Garcıa, J. Suay, Prog. Org. Coat., 59 (2007) 251

[118] M. Fedel, M.-E. Druart, M. Olivier, M. Poelman, F. Deflorian, S. Rossi, Prog. Org. Coat., Submitted (2009)

[119] A. M. Cabral, W. Trabelsi, R. Serra, M. F. Montemor, M. L. Zheludkevich, M. G. S. Ferreira Corros. Sci., 48 (2006) 3740

[120] P. L. Bonora, F. Deflorian, L. Fedrizzi, Electrochim. Acta, 41 (1996) 1073

[121] A. Di Gianni, E. Amerio, O. Monticelli, R. Bongiovanni, App. Clay Sci., 42 (2008) 116

[122] X. Li, S. Deng, H. Fu, G. Mu, Corros. Sci., 50 (2008) 3599

[123] H. Ardelean, I. Frateur, P. Marcus, Corros. Sci., 50 (2008) 1907

[124] F. Deflorian, S. Rossi, M. Fedel, C. Motte, Prog. Org. Coat., Submitted (2009)

[125] J. L. Lábár, Microsc. Anal., 75 (2002) 9

[126] M. Bethencourt, F. J. Botana, J.J. Calvino, M. Marcos, M. A. Rodriguez-Chacon, Corros. Sci., 40 (1998) 1803

[127] A. M. Cabral, W. Trabelsi, R. Serra, M. F. Montemor, M. L. Zheludkevich, M. G. S. Ferreira, Corros. Sci., 48 (2006) 3740

[128] H. Wang, R. Akid, Corros. Sci., 50 (2008) 1142

[129] A. Di Gianni, E. Amerio, O. Monticelli, R. Bongiovanni, App. Clay Sci., 42 (2008) 116

[130] "Radiation Curing, Science And Technology", (Ed. S. P. Pappas), Plenum Press, New York (1992)

[131] Z. Wang, D. Gao, J. Yang, Y. Chen, J. Appl. Polym. Sci., 73 (1999) 2869

[132] F. Masson, C.Decker, Macromol. Mat. Eng., 288 (2003) 17

[133] A. V. Rao, D. S. Kanitkar, A. K. Parab, Progr. Org.Coat., 25 (1995) 223

[134] F. Deflorian, M. Fedel, A. DiGianni, R. Bongiovanni, S. Turri, Corrosion Eng., Sci. Tech., 43 (2008) 81

[135] M. Dahm, H. Ehlert, F. Muller, H. Toepsch, H. Traubel, W. Wieczorrek, "Polyurethane Handbook", (Ed. G. Oertel) Hanser, Munich (1994)

[136] M. Dieterich, Progr. Org. Coat., 9 (1981) 281

[137] J. W. Rosthauser, K. Natchkamp, "Waterborne polyurethanes", in "Advances in Urethane Science and Technology", (Eds. K.C. Frisch, D. Klempner), Shrewsbury: Rapra technology, Shawbury (1987)

[138] B. K. Kim, J. C Lee, J. Polym. Sci., Part A: Polym. Chem., 34 (1996) 1095

[139] S. Ramesh, K. Tharanikkarasu, G. N. Mahesh, G. Radhakrishnan, J. Macromol. Sci.; C: Reviews, 38 (1998) 481

[140] J. E.Yang, J. S. Kong, S. W. Park, D. J. Lee, H. D. Kim, J. Appl. Polym. Sci., 86 (2002) 2375

[141] C. R. Hegedus, A. G. Gilicinski, R. J. Haney, J. Coat. Technol., 68 (1996) 51

[142] R. G. Coogan, Progr. Org. Coat., 32 (1997) 51

[143] M. Melchiors, M. Sonntag, K, Kobusch, J. Eberhardt, Progr. Org. Coat., 40 (2000) 99

[144] Z. W. Wicks, D. A. Wicks, J. W. Rosthauser, Prog. Org. Coat., 44 (2002) 161

[145] R. Canteri, G. Speranza, M. Anderle, S. Turri, S. Radice, Surf. Interface Anal., 35 (2003) 318

[146] Vernici Materiali Tecnologie Proprietà, (Ed. S. Turri), CEA Edizioni, Milan (2007)

[147] J. N. Murray, Progr. Org. Coat., 31 (1997) 255

[148] P. L. Bonora, F.Deflorian, L.Fedrizzi, Mat. Sci. Forum, 192 (1995) 267

[149] F. Mansfeld, Corrosion, 44 (1988) 856

[150] E. P. M. van Westing, G. M. Ferrari, J. H. W. De Wit, Corros. Sci., 34 (1993) 1511

[151] E. P. M. van Westing, G. M. Ferrari, J. H. W. De Wit, Corros. Sci., 36 (1994) 957

[152] F. Deflorian, L. Fedrizzi, S. Rossi, P. L. Bonora, Electrochim. Acta, 44 (1999) 4243

[153] D. M. Brasher, A. H. Kingsbury, J. Appl. Chem., 4 (1954) 62

[154] O. Ali, R. Azam, Prog. Org. Coat., 62 (2008) 293

[155] G. Schottener, Chem. Mater., 13 (2001) 3422

[156] A. Di Gianni, R. Bongiovanni, S. Turri, F. Deflorian, G. Malucelli, G. Rizza, J. Coat. Technol. Res., In press, 6 (2009) 177.

[157] F. Bauer, R. Mehnert, J. Polymer. Res., 12 (2005) 483

[158] M. Kending, J. Scully, Corrosion, 46 (1990) 22

[159] G. Grundmeier, W. Schmidt, M. Stratmann, Electrochim. Acta, 45 (2000) 2415

[160] S. C. Tjong, Mat. Sci. Eng., 53 (2006) 73

[161] L. Betega de Paiva, A. R. Morales, F. R. Valenzuela Diaz, Appl. Clay Sci., 42 (2008) 8

[162] M. Kato, A. Usuki, "Polymer-clay Nanocomposite", (Eds T.J. Pinnavaia, G.W. Beall), J. Wiley, Chichester (2000)

[163] T .Lan, T.J.Pinnavaia, Chem. Mater., 6 (1994) 2216

[164] P. B. Messersmith, E. P. Giannelis, Chem. Mater., 5 (1994) 1719

[165] T. Lan, P. D. Kaviratna, T. J. Pinnavaia, Chem. Mater., 7 (1995) 2144

[166] Y. Y. Wang, T. E. Hsieh, J. Mater. Sci., 42 (2007) 4451

[167] R. Bongiovanni, E. A. Turcato, A. Di Gianni, S. Ronchetti, Prog. Org. Coat., 62 (2008) 336

[168] S. Ceccia, E. A. Turcato, P. L. Maffettone, R. Bongiovanni, Prog. Org. Coat., 63, (2008) 110

[169] G. Malucelli, A. Di Gianni, F. Deflorian, M. Fedel, R. Bongiovanni, Corros. Sci., 51, (2009) 1762

[170] J. V. Crivello, U. Valermann, J.Polym. Sci. Part A: Polym. Chem., 33 (1995) 2463.

[171] G. Malucelli, Y. Chen, A. Priola, R. Dongiovanni, M. Sangermano, Mater. Eng., 13 (2002) 99

[172] H. He, J. Duchet, J. Galy, J. F. Gerard, J. Colloid Interface Sci., 288 (2005) 171.

[173] A. M. Schanmugharaj, K.Y. Rhee, S. H. Ryu, J. Colloid Interface Sci., 298 (2006) 854.

[174] S. Skale, V. Dolecek, M. Slemnik, Prog. Org. Coat., 62 (2008) 387

[175] S. J. Garcıa, J. Suay, Corros. Sci., 49 (2007) 3256.

"Whenever a theory appears to you as the only possible one, take this as a sign that you have neither understood the theory nor the problem which it was intended to solve"

Karl Popper